HIGH STRAIN DEFORMATION OF STEELS

BY

ROBERT LESLIE AGHAN
A.R.M.I.T., M.ENG.SCI., M.I.M.

SUBMITTED IN FULFILMENT OF THE
REQUIREMENTS FOR THE DEGREE OF
DOCTOR OF PHILOSOPHY

DEPARTMENT OF METALLURGY,
HOULDSWORTH SCHOOL OF APPLIED
SCIENCE,
UNIVERSITY OF LEEDS.

FEBRUARY, 1978.

SUMMARY

The changes in mechanical properties and structure which occur when metals are deformed to high strains by cold working are summarised from the published literature, with particular emphasis on the behaviour of iron. In addition to this, the effects of second phase particles, the deformation behaviour during machining and the influence of strain history on ductile fracture are also outlined.

The results of mechanical tests, carried out at various stages of deformation, are compounded to show the overall changes in mechanical properties occurring during the process, which are then interpreted in terms of the results of structural investigations and fractography.

Investigations have included a number of different steels, which were selected and heat treated in order to investigate the fundamental changes which occur, the affect on deformation and subsequent fracture of free machining additions and the affect of a dispersion of hard particles.

It is concluded that deformation is microscopically heterogeneous, that changes in mechanical properties are associated with the formation and subsequent behaviour of an increasing number of microbands in the substructure, that ductile fracture is nucleated at pre-existing fracture centres which are formed early in the deformation process and that these play an important part in the mechanism of machine chip formation.

An important, previously unreported strengthening mechanism is seen to be operating in one of the steels.

ACKNOWLEDGEMENTS

The work described in this thesis was carried out in the Department of Metallurgy at the University of Leeds.

The author is greatly indebted to Professor J. Nutting for making research facilities available within the department and also for his supervision of the project, during which many helpful discussions were held and much encouragement received.

The author also wishes to express gratitude to his colleagues in the metallurgy department for helpful discussions, to the secretarial and technical staff for their valuable assistance, to the staff of the high voltage electron microscope section at the British Steel Corporation's Swinden Laboratories for their assistance and for provision of the two free machining steels and to Professor M. Hatherly of the University of New South Wales for valuable discussions during his visits to Leeds.

Finally the two major factors, without which this study would not have been possible, are gratefully acknowledged. The provision of an Australian Public Service Board Post Graduate Scholarship and the encouragement and support of my wife Francine and our three children.

To the best of my knowledge, the results presented in this dissertation and the deductions made from them are original, except where reference is made to the work of others. No part of this thesis has been submitted for the award of a degree at any other University.

Robert L Ayhan

Department of Metallurgy
University of Leeds.

February, 1978.

Before I began the study of electricity, I resolved to read no mathematics on the subject till I had first read through Faraday's experimental researches on electricity.

For instance, Faraday, in his minds eye, saw lines of force traversing all space where the mathematicians saw centres of force attracting at a distance: Faraday saw a medium where they saw nothing but distance: Faraday sought the seat of the phenomena in real actions going on in the medium, while they were satisfied that they had found it in a power of action at a distance impressed on the electric fluids.

Maxwell J. Clark,
Preface, Treatise on Electricity & Magnetism
Vol. 5 3rd Ed. 1892.

TABLE OF CONTENTS

CHAPTER 1

INTRODUCTION

Metallurgical operations involving plastic deformation as the basic processing vehicle generally share two objectives. One is shape change and the other property control. The latter usually comes from structure regulation.

The basic deformation may occur under steady state, or non steady state conditions, in times ranging from minutes to milli seconds, at temperatures from cryogenic to near melting and under stresses ranging from a few pascals to many mega pascals. The scope is so great that it is impossible to treat every aspect in a single project.

There is no question about the need for fundamental understanding of structural changes occuring, as technological advances depend to a large degree on awareness of the interplay between structure, composition and properties. In order to achieve desirable properties in an appropriate shape, it must be recognised that processing has structural effects. These may be unspecified or unexpected, but they ought to be understood and possibly exploited.

The structural changes may assume additional importance, because whether or not there is a fracture in a given engineering situation, may actually be determined by the processing history.

This thesis describes the results of a study of the property changes and structural changes which occur when selected steels are deformed to various degrees of strain by cold rolling. It summarises the principal findings of previous work and compares the current results with various theoretical models of plastic deformation.

The work began with a plain carbon steel, as a study of the deformation behaviour of a body-centred cubic material. Following work by Clough (1) Nuttall (2) and Nourbakhsh(3). On face-centred cubic metals, indicating anomalies in the deformation behaviour and properties after deformation to high strains

The observation of heterogeneous unstable shearing in bands within the material led to a series of experiments to compare the results with a steel containing manganese sulphide inclusions and also one containing manganese sulphide plus lead. This was because metals are known to deform by heterogeneous unstable shearing during machining, with little understanding of the mechanism and the fact that manganese sulphide inclusions and lead have long been added to steels to promote this behaviour in the so called "free machining steels".

The fact that these soft inclusions deformed and permitted shearing to occur at the particle metal interface, led to a similar investigation into the behaviour of a low Carbon steel, heat treated to give a structure of harder carbide particles in a soft matrix, in an attempt to shed more light on the mechanism of high strain deformation by inhomogeneous shear.

In each case the effect of the deformation on subsequent fracture has also been studied.

CHAPTER 2

REVIEW OF PREVIOUS WORK

2.1 Introduction

A complete coverage of all work published in this very complex field is obviously beyond the scope of this dissertation. Therefore, this review of the work of other researchers will be limited as much as possible to experimental results which are relevant to this study, trying to give as accurately as possible a current picture of the situation.

The results reviewed will naturally be mostly for steels, but where relevant to the understanding of the results of this study, results for other metals will be included.

The mechanisms of deformation will be reviewed and a summary made of results for iron and steel in terms of the dislocation movements taking place at low strains. The development of sub structures, the influence of grain boundaries, the deformation behaviour of alloys containing second phase particles and changes in mechanical properties with strain will also be summarised.

The underlying theme which will emerge from the results is local plastic instability. In the past, most work on this has been in studies of machine chip formation, where it occurs through the whole volume of the metal being studied and is therefore more easily recognised. Because of this, a review of the mechanisms of chip formation will also be included, along with surveys of the effects of manganese sulphide particles, lead addititions and the deformation behaviour of manganese sulphide.

Because of the intimate connection between deformation and the ductile fracture process, this will also be reviewed, with particular emphasis on the influence of stress state, deformation pattern, strain history and the presence of other phases.

2.2 Mechanisms of deformation of metals

2.2.1 Slip

Introduction - Metals undergo permanent deformation when stressed beyond their elastic limit, accompanied by changes in their physical and mechanical properties.

Numerous early investigations of the nature of this plastic deformation, mainly using single crystals, have been described in books by Elam (4) and Schmid and Boas (5). The most important conclusions were that deformation occurs by translational slip. One part of the crystal sliding as a unit across another part. The deformation was shown to be inhomogeneous, with intense plastic strain on certain slip surfaces, while the layers of crystal between these are almost undeformed.

A discrepancy of several orders of magnitude between Frenkel's classical estimation of the theoretical shear strength (6) and the much lower strength at which crystals were observed to slip led Taylor, (7), Orowan (8) and Polanyi (9) at about the same time to independently postulate that slip occured consecutively over the shear planes by motion of dislocations.

This was followed by countless papers on the basic structure of dislocations, and their formation and motion, which have been reviewed many times in journals (10-21) and in books (22-26) to mention just a few. The work on direct observation of dislocations by optical methods, as well as by X-ray techniques and electron microscopy has also been adequately reviewed (27) (28) and also the general properties of dislocations and applications of dislocation theory in the book by Friedel. (27) In addition There have been some beautiful mathematical studies by Nye (29), Bilby et.al. (30) and many others.

Directions and planes of slip.

Slip is anisotropic, occuring more readily along certain crystal planes and directions. It has been established (4) (5) that the slip direction is that along which the atoms are most closely packed. Thus body centred cubic metals slip along {III} in {110}planes which are the highest density planes. These are not greatly superior to {112}, and {123}planes, which are also high density planes. There is thus a total of 48 possible slip systems.

Iron has also been shown to slip frequently on a corrugated surface like a bundle of pencils sheared along their length, termed pencil glide. (31) The slip surface is regarded as a prismatic cylinder, made up of strips of slip planes intersecting in the common <111> direction.

Edge dislocations

Dislocations are generally able to glide in a slip plane containing both dislocation line and its Burgers vector. Since these are perpendicular for edge dislocations, an edge dislocation is confined to one plane. They may move in a direction normal to the slip plane into parallel slip planes in some circumstances, by a non conservative process called climb (32). Because this is dependent on the migration of vacancies, it is often non uniform, with the dislocation line partly in its original plane and partly in an adjacent parallel one. The line segment between these two planes is termed a jog. Such jogs do not impede the motion of the dislocation as they are themselves edge dislocations which can glide in the same direction on an intersecting slip plane.

For appreciable climb, large numbers of vacancies are required. Conversely, dislocations forced out of their slip plane will create sheets of vacancies (or interstitial atoms).

Any line, straight or otherwise which has the Burgers vector for its normal, qualifies as an edge dislocation. Thus the pencil glide referred to above could be possible in the case of an edge dislocation having an irregular shaped boundary in its extra half sheet of atoms. Smaller sheets are also possible which are totally enclosed in the crystal. Seitz (33) has called this a prismatic dislocation.

Screw dislocations

The definition of a screw dislocation, requiring the dislocation line to be parallel to its Burgers vector, means that its line must either be straight and parallel to the slip direction, or contain an edge dislocation segment. Thus there is no irregular screw dislocation. However, there is no non conservative motion (22), the dislocations being free to move on any cylindrical surface having the slip direction for its axis. Thus screw dislocations are able to generate the wavy slip surface observed in practice (31) by cross slip. They may also cross slip to go around an obstacle and then cross slip a second time back onto a plane parallel to the original one. This being termed double cross slip (34). If part of a screw dislocation undergoes double cross slip the resulting multiple jogs are edge dislocations which pin the remaining parts of the screw dislocation during further glide. This creates dislocation dipoles and eventually loops. This can be the beginning of a Frank Read scource to help increase the dislocation density (35).

Interaction of dislocations

The processes described above are not the only methods of jog formation. Jogs may also be formed by the interactions of gliding dislocations, (22) or by the interaction of a gliding dislocation with a forest of dislocations. As noted already, jogs on edge dislocations do not in general impede their motion, while those formed on screw dislocations may pin them. The interaction of two screw dislocations (23) creates jogs equal to the Burgers' vector. These can glide along the dislocation, and attach themselves to an edge component before the screw begins to glide, or alternatively they may be towed along non conservatively, creating vacancies or interstitial atoms in their wake. This requires a higher stress and thus contributes to hardening.

2.2.2 Twinning

The second important mechanism by which a metal can deform is twinning. A good review of this topic has been published by Hall (36) and another more recently by Mahajan and Williams. (37)

Unlike slip, the lattice is not identical before and after the deformation. During twinning, the planes of atoms shear in such a way that the twinned portion is related to the parent crystal by a mirror reflection across a plane of symmetry called a twin plane. Also, slip occurs in discrete multiples of atomic spacing on relatively widespread planes, but in the twinned region, every atomic plane is involved in the deformation.

The strain accompanying twin formation is small compared to that which results from continuous slip (38) The importance of twinning in plastic deformation therefore, comes from the fact that orientation changes accompanying twin formation may place new slip systems in favourable orientation for more slip to take place.

When slip is difficult twinning a nd fine slip may take place concurrently. (37) This behaviour is promoted by low temperatures, increasing strain rate and in the case of face-centred cubic, by low stacking fault energy. Thus iron may be twinned by impact at room temperature or by slower deformation at low temperatures to form narrow lamellar twins known as Neumann bands.

Twins can form in about 3 micro seconds (39) whereas there is a delay of several milliseconds before a slip band is formed. If twinning occurs during a tensile test, it generally produces serrations in the stress strain curve.

It has been demonstrated in columbium (BCC) that processes that cause tangled dislocation cell walls inhibit twinning. (40) Cox (41) et.al. also showed this for iron, demonstrating that 4% prestrain at room temperature increased the resolved shear stress for twinning at -196°, and that higher prestrains suppressed twinning altogether. That the disruption of long range order suppresses twinning was first suggested by Laves, (42) and has now been verified in most cases..

The exact mechanism of twinning is not yet known, although many ingenious models have been proposed. Cottrell and Bilby (43) first proposed a so called pole mechanism, involving the rotation of a partial dislocation around a dislocation which has a component of its Burgers vector normal to the twin plane, generating a twin layer at each successive revolution.

A number of others models proposed are similar to this (44-47), while some authors claim that twins grow by repeated nucleation at obstacles to dislocation motion. (48-49) A more detailed description may be found elsewhere. (36) (37)

2.2.3 Microcrack mechanism of deformation.

A microcrack mechanism of high strain deformation has recently been suggested by Walker and Shaw (50) who determined the stress-strain characteristics of a number of steels while using variable normal stress on the shear plane. They found that the strain hardening became negative at high strains prior to gross fracture, and suggest from this and from associated acoustic measurements, that microcracks are responsible. They believe that these form, re-weld and re-form several times as strain proceeds and that normal stress on the shear plane shifts the equilibrium in the direction of crack disappearance, postponing ; gross fracture.

In an earlier paper, (51) Usui, Cujral & Shaw sheared a projection from a ductile block of metal. They concluded in this case, that the large strain obtained before separation could not be the result of dislocation motion in a homogeneous solid and that such strains are the result of 'Walking' of microcracks

of small lateral extent across the shear surface by rupture-welding-rupture cyclic process.

Walker and Shaw believe that this concept of deformation by microcrack appearance, and disappearance is important in most high strain processing operations and in metal cutting.

2.3 The structure of cold worked iron.

2.3.1 Introduction.

Considerable progress has been made, in our understanding metallic structures since Hirsch et.al. (52) first used transmision electron microscopy to study dislocation structures in aluminium. Body centered cubic metals have not been quite as extensively studied as face centered cubic metals, but the main features of the deformed structures are similar for high stacking fault energy materials. An excellent review of deformation structures for both FCC and BCC materials, has been compiled by Nuttall. (2)

A summary of the principal findings related to dislocation substructure in BCC metals at strains up to 30% has been made by Keh and Weissmann (53), who concluded that the deformed structure of iron and the BCC refractory metals are very similar.

This survey will be limited to the structure observed in Iron and steel, beginning with a broad description of the general features, followed by a discussion of the processes occuring at each stage of the deformation.

2.3.2 The structure developed in Iron with increasing strain.

The deformation structure of polycrystalline iron or steel depends on the type and level of deformation. For example, the strain after stretching in tension is macroscopically homogeneous, whereas small amounts of strain by rolling, produces a series of deformed and undeformed blocks which merge into each other as the deformation is increased. (54) With increasing strain the grains become distorted and the dislocation density is increased, (55) but their distribution is far from uniform.

For less than 1% strain the dislocations produced are relatively straight and distributed uniformly throughout each grain. (53),(55). From 1%-3% strain jogs begin to appear on the dislocations isolated dislocation loops appear and dislocations of different Burgers Vectors begin to interact, forming clusters within the grains. After about 3% strain the clusters join together to form a cell structure.

Beyond 9-10% strain, most grains are subdivided into well defined cells, the walls of which are tangled dislocation networks, while the dislocation density in the interior is reported to be low. With further increase in deformation the cell walls become more sharply defined, and aligned in certain crystallographic directions, and the overall dislocation density increases. (55)

Some workers still speak of cells at very high levels of strain, but as the cell walls become sharper and misorientation across them increases they are often termed sub-grains.

A sub-grain is normally associated with the development of a cell, the difference lying in the degree of mis-orientation, this being 2° for a cell (56),(57),(58),(59), and up to 10°-15° for a sub-grain (60) (61), which is regarded as a small grain, of the order of microns in size, the boundary is of the complex low angle type. The sharpening of the boundaries is thought to be a thermal process of polygonisation during which cross slip and climb take place, lowering the lattice strain energy (62)

Relatively scant attention has been given to structural development of material strained above 30%. In recent years, electron microscope observations have been carried out both on foils produced parallel to the rolled sheet surface and perpendicular to the rolling plane but parallel to the rolling direction. For rolling plane foils, the structures have been poorly defined, commonly reported as 'A cellular structure with a high density of dislocations.' (63) Observations perpendicular to the rolling plane, were in contrast well defined, being made up of numerous elongated cells. (64) Smith (65) and Dunn (64) have reported that regions with high misorientations showed a well defined small sub-grain structure.

It was observed by Goodenow (66) that cell structures differ on approaching grain boundaries, cell size becoming smaller and mis-orientations becoming larger than in the grain centres.

Some studies (64)(65) (67) (68) have included measurements of cell size and mis-orientation angle as a function of cell sub-grain orientation, indication an isotropic stored energy of deformation, which has since been shown to be important in the development of texture (63).

The shape changes of the initial equiaxed cells during deformation are not yet understood. They do not as expected, undergo the same shape change as the bulk material in order to form the elongated sub-grains, since the observed sub-grain size is always greater than expected, indicating complicated sub-boundary formation effects and sub-grain growth must occur (67) (68). Langford and Cohen (67) observed considerable shape modifications, by subdivision, and also by coalescence. Embury et.al. found that only the edge dimension of the substructure gave any meaningful information regarding the changes of structure occuring during the rolling process.
Keh and Weissmann (3) noted the sharpening of cells into sub-grains, and a relatively constant sub-grain size beyond 30%. They also found even at high deformations, some areas existed where the dislocation density was high and the cell structure poorly developed, but did not develop this idea any further.

2.3.3 Band Structure

The structure of metals after deformation has not been found to consist entirely of dislocation cells or of elongated sub-grains. Since the early years of metallography, it has been observed that a series of bands form in the structure, indicating that the structure is far from homogeneous. Barrett and others (69-73) first showed that as deformation increased, there was a progressive growth in the mis-orientation between bands, distinguishing these deformation bands (as they called them) from mechanical twins. Deformation bands have been observed in many metals and Barrett (73) considers it not unlikely that they occur in all FCC and BCC metals. A thorough review of early observations has been given my Müller. (74)

The tendency for crystals or grains to form deformation bands has been seen to depend on the orientation of the crystal relative to the flow direction. For example iron having a {110} or {111} axis parallel to the compression axis does not form deformation bands, but all other orientations become banded. (75)

Walter and Koch (59) (76) and also Hu (77) observed deformed, oriented single crystals of Silicon-Iron by transmission electron microscopy. They showed that the boundaries between the mutually mis-oriented deformation bands, which form in certain directions relative to the rolling direction, are actually composed of a number of almost parallel elongated sub-grains constituting a micro-band.

Electron diffraction revealed rotations across the micro-bands of up to 30°, but mis-orientations across neighbouring segments were only a few degrees. These micro-bands were termed transition bands by Walter and Koch. The importance of transition bands as sites for nucleation of recrystallised grains was clearly demonstrated, but at this stage there was no systematic examination of the conditions under which such regions of lattice curvature could be created during deformation, or of their behaviour during further deformation.

The most important conclusions of the most recent reviews (78) (79) are the observations that:-

1. Transition bands are an important mechanism whereby high lattice curvature and high stored energy may develop within a material.
2. Transition bands are important as sites for nucleation of recrystallised grains, and in the development of recrystallisation texture.
3. That further work is needed before there full significance is appreciated.

Another observation of bands of deformation which may be relevant, (80) although not observed in iron yet, is the reporting by Mitchell Chevrier, Hockey and Monaghan of a previously unreported type of deformation band in Cu-Al alloys, which appeared as units by an abrupt process without time resolution. They suggested a dislocation avalanche mechanism of formation in a glide plane or group of planes as a continuation of the mechanism by which slip lines first appear. Large numbers of dislocation scources along a slip line concentrate the applied stress sufficiently to generate an avalanche involving many hundreds of dislocations, moving at high velocity and the intense stress field associated with them propagated with a velocity close to that of sound.

Dislocation avalanche mechanisms have been discussed by Orowan. (81)

Brown (82) has also carried out some interesting work on band structure. He showed that in Aluminium sheet after high strains, deformation bands inclined at 35° to the sheet surface caused marked displacement of the grain boundaries. These bands became more numerous with increasing strain and passed right through the grain boundaries.

At this stage Brown called them shear bands (83) (84). The material within the bands was highly deformed and to fine too be examined by electron diffraction.

2.3.4 The formation of deformation structures.

Large jogs and loops.

As described in section 2.3.2 large jogs on screw dislocations and isolated loops occur in the early stages of deformation, as is common to all BCC materials which have been studied. The most widely accepted theory of their formation is that first postulated by Johnston & Gillman (83) who suggested that double cross slip left jogs on moving screw dislocations which retarded their motion. These left either trails of point defects, or dipoles of positive-negative edge dislocations behind them. The portions of the screw dislocations which underwent cross slip can act as Frank-Read sources on a new slip plane.

Fourie and Wilsdorf (84) in the absence of visible barriers to cause cross slip, considered their formation to be due to the condensation of point defects on gliding screw dislocations. It has been suggested by Nott (85) and accepted by others (53) (86) that cross slip can be initiated to by-pass another locked paralled screw dislocation.

The large jogs are not considered to be the results of dislocation cutting as described in section 2.2.1 (53) as this mechanism results only in unit jogs, whereas the jogs observed are often many hundred angstroms.

Dislocation Tangles.

The mechanism of formation of dislocation tangles is not fully understood. Wilsdorf et.al. (87) thought that the large jogs and elongated loops lying outside the slip plane were the nuclei of dislocation tangles, proposing a mechanism based on vacancy condensation, but Keh and Weissman(53) conclude that a secondary slip system is necessary to interact with these jogs, since single crystals of silicon iron oriented for single slip did not show cell formation.

Cell Structure

There are several views of the formation of cell structure in the literature. Gay & Kelly (88)(89) suggested that the cell structure could be identified with deformation bands and that the cell size was probably equal to the minimum distance between slip bands. Keh and Weissman however, point out (53) that cell formation precedes the appearance of slip bands, and the average size of cells is smaller than the average

spacing of surface slip bands, so the structural interconnection is not yet proven.

Seeger (90) thought that screw dislocations piled up against some kind of barrier to produce cell walls which he identified as tilt boundaries. But piled up groups are rarely if ever observed in BCC metals, and the nature of the boundaries (91) in iron is asymetric boundaries with predominantly twist components so the Seeger model at least needs modifying.

Changes in cell structure with strain.

It has been shown (53)(92) that the cell size decreases sharply with increasing strain and then levels off. Keh and Weissman conclude that once an ultimate cell size has been established for a given temperature and strain rate, no additional dislocation tangles can be formed within the cells. To explain the accommodation of additional strain, they favour a mechanism first suggested by Li(93) that dislocations in the cell walls may move co-operatively without generating any new dislocations. Although this has not been observed, except in Zinc (94), the fact that cell walls tend to align themselves in crystallographic directions, identified as the traces of slip planes on the foil surface, indicates that this is a reasonable assumption.

Langford and Cohen (67) found that dynamic recovery was occuring at high strains during wire drawing with both cellular refinement and cell coalescence occuring, involving cell wall migration and the migration of 'h junctions' along the elongated cells

Transition bands

An analysis of the origin of transition bands has been made recently by Dillamore et.al. (78) who suggested that they may arise in 4 ways:-

1. Some relative rotation will generally follow if as a result of local differences in stress state, different parts of the crystal undergo different strains. Bands forming by this mechanism will invariably form in polycrystals and the rate of formation of bands by this mechanism should diminish with strain.

2. When strain throughout the crystal is homogeneous and specified in all its components, it is still possible that different combinations of slip systems may separately yield the imposed strain in different parts of the crystal, giving different slip rotations and causing relative rotation. The likelihood of such banding will depend on the number of independent slip systems.
3. A macroscopically imposed shape change is achieved for lower energy expenditure, if the total strain is sub-divided such that different regions of the crystal undergo different strains and again rotate relative to each other. This should occur in polycrystals similarly to category 1.
4. A crystal may be orientated in such a way that it does not rotate when subjected to a specific strain, but small displacements in opposite sense from the initial orientation cause the two orientations to continue to diverge.

They also analyse the development of transition bands by rotation due to slip and describe the possibility of predicting deformation and transition bands from orientation considerations.

Richards and Ormay (95) have shown that during rolling of polycrystalline iron, rotation from (001) [10] towards (112) [110] occurs. Dillamore and Roberts (96) have also shown that local curvature about the transverse direction occurs during the rolling process, due to dislocation storage during deformation.

2.4 The behaviour of grain boundaries during deformation.

2.4.1 The deformation of polycrystalline aggregates

Probably the most obvious feature of a deformed metal is the distorted grain shape. The early theories of deformation of polycrystalline metals by Taylor (97) and subsequent workers (98-100) assumed that continuity of the metal across the grain boundaries was maintained by each grain undergoing the same shape change as the overall material in which it was embedded. To produce this they emphasised the importance of multiple slip.

Some striking exceptions to this behaviour have been noticed (101)(102). The assumption on which this theory is based is that the deformation is homogeneous, but observations suggest that this is not true. To avoid the complications of multiple slip, Dillamore and Roberts (103) used the concept that grain continuity is maintained not by imposing a fixed shape change, but by inhomogeneous deformation.

They suggest that while there may be some multiple slip in the region of the grain boundaries, the interior of the grains deforms on single or duplex slip systems.

Peck and Thomas (101) found that during wire drawing of iron, tungsten and niobium grains do not become cigar shaped, but ribbon shaped and curled about the wire. Hosford (102) found similar curled grain shapes in compressed aluminium specimens, and in both cases has given calculations explaining the tendency of individual crystals of suitable orientation to deform by plane strain, with grain continuity being maintained by the bending of grains about one another.

2.4.2 High angle boundaries.

High angle boundaries are now considered to consist of an arrangement of dislocations, (103)(104) but as their arrangement is very complex (105) they are generally regarded as a free surface. The importance of grain boundary barriers to dislocation movement and scources of stress concentration is pointed out by Clareborough & Hargreaves. (106) Dislocation pile ups at boundaries havefrequently been observed, for example in austenitic stainless steel by Whelan et.al. (107), but have not been seen in body centred cubic metals. Brandon and Nutting (108) and Keh and Weisman (53) have shown that points of high stress concentration such as local weak spots or grain corners, can act as profuse dislocation scources.

In the early stages of plastic flow only certain grains are favorably orientated for slip and this must be accommodated in neighbouring grains. Ogilvie (109) has studied the continuity of slip across grain boundaries. Livington and Chalmers (110) alternatively studied the discontinuity of slip across boundaries, showing local nucleation of slip in adjoining grains.

Aust and Chen (111) have shown that slip is more effectively inhibited as the orientation difference increases, thus resulting in additional planes being stressed above the critical shear stress. Umeno and Shinoda (112) have also proposed that grain boundary distortion depends on the orientation difference and the shape of the boundary.

For materials such as iron, Hook and Hirth (113) consider that local stress concentrations at grain boundaries aid the nucleation of secondary slip across the boundary, but that this may only propagate a short distance into the next grain if the applied shear stress is less than the local flow stress.

More uniform distribution of dislocations is reported for lower misorientations (114)(115).

2.4.3 Low angle boundaries.

Low angle boundaries are described in many texts (116) (117). They are much less complex than high angle boundaries, the simplest types being a line of edge dislocations forming a tilt boundary and a line of screw dislocations, which form a twist boundary. The angular misorientations are only 1-2°.

They are produced during slip and create misorientation between adjoining parts of the crystals. They may be of mixed type but can still be pure tilt if all the edge dislocations are of one sign and all the screw components alternate in sign. They do not present as great an obstacle to gliding dislocations as do high angle boundaries.

Interaction between gliding dislocations and various boundary arrays has been studied by Li (118) who concludes among other things that they have long range stresses which contribute to work hardening and that simple tilt boundaries resist penetration by parellel dislocations of different Burger's vector, by slip or climb, not much more strongly than the nearest single dislocations in the boundary.
In their latest work, Langford and Cohen (119) suggest that at low strains, the average cell misorientation is small, so glide dislocations cut through nearly all cell walls, which behave like dislocation forests, while at high strains, most of the cell walls become impenetrable and behave like grain boundaries. They postulate a critical misorientation somewhere between 2° and 10° for their Fe wire below which the cells are penetrable and above which they are not.

Low angle boundaries may be glissile or sessile. Boundary motion was first observed by Parker and Washburn (120). A simple tilt boundary may move by glide with all the dislocations remaining in their planes in the boundary. Resistance to this is due to the force between dislocations.

A boundary with two sets of dislocations may split as one set moves to the right and the other to the left. Similarly with three or more sets, there being a pressure for separating any two sets.

For all dislocations to move along the boundary normal so that the boundary moves as a whole, requires both slip and climb, (therefore mass transport). In addition the motion is resisted by the forces between dislocations tending to hold them in minimum energy configuration. (121).

As mentioned earlier, sub-grain boundaries are also regarded as dislocation configurations, defining regions with misorientations up to 10°, but their constitution and behaviour during deformation is not understood at this time.

2.4.4 Deformation textures

The development of texture does not play an important part in this work, but is never the less an important aspect of deformation to high strains. The numerous early papers on the texture developed during rolling of iron and steel, have been adequately reviewed by Dillamore and Roberts (122) and more recently by Hu et.al. (123) and also by Grewen (124).

Comparison of observed and predicted rolling textures by different theories has been carried out by Dillamore and Katoh (125), who show that the main features of experimentally observed texture are best predicted by a homogeneous strain theory based on the Taylor theory of plasticity, with rotation of the slip direction toward the axis of extension until a stable orientation is approached.

The differences that still exist have their origin in the assumption that the strain is a homogeneous plane strain and recent modifications (125) have been made based on changes in the nature of the applied strain and allowing for interaction between grains. Grains with soft orientations yield first undergo. some hardening and developing stress concentrations before their harder neighbours begin to deform.

Analysis predicts the stablilisation in BCC metals of orientations near {111} <110> and {111} <112> which is what is observed.

A full analysis of orientation behaviour during rolling has been carried out by Dillamore and Katoh (126) for BCC metals and for FCC metals which deform by simple glide.

2.5 The relationship of properties to structure.

2.5.1 Changes in mechanical properties with strain.

Dramatic increases in the yield stress and ultimate tensile strength of metals after deformation, along with a corresponding decrease in ductility, have been known for many years. This phenomenon of work hardening has been used industrially to harden metals which do not respond to heat treatment.

In a tensile test, work hardening is manifested in the rising of the stress strain curve in the plastic region. Up to the UTS the stress needed to produce further plastic strain increases with strain. At the UTS the deformation becomes unstable and is concentrated in the neck of the specimen until failure occurs.

That the effect of unrelieved plastic strain is additive is shown by unloading a specimen in the stable plastic region and then re-testing. The elastic strain is recovered during unloading, but the plastic strain remains. The yield stress in the second test is then the same as the plastic stress before unloading.

Many theories of work hardening have emerged and have been the subject of critical reviews. (22)(127)(128). Most of the work has been concerned with the development of a description of plastic behaviour in terms of dislocation theory, with very little attention given to the strengthening mechanism operating during mechanical working processes such as rolling or wire drawing, where the large plastic strains involved make it difficult to correlate the observations with any elementary dislocation theory. Many workers feel that at large plastic strains, any treatment must be in terms of the behaviour of complex groups of dislocations, and although Li (118) has done valuable theoretical work calculating the elastic properties of dislocation groups, a self consistent model for large plastic strains seems as yet impossible.

The overall work hardening behaviour of iron during continuous deformation, has been studied by Langford and Cohen (67) who carried out tensile tests on wires drawn to specific strains. Assuming that wire drawing strains and tensile strains are additive they drew an overall stress strain curve for the wire drawing process showing a linear hardening rate for strains from 1 to 7.

Similar results were obtained by Clough (1) (129) who tested a range of FCC materials after cold rolling, showing approximately linear hardening rates for copper & Aluminium. One material (70/30Brass) showed a distinct change in the hardening rate after a true strain of 2. Henderson et.al. (130) did similar work to Longford and Cohen testing chromium wires after various deformations. It can be shown from their results that Chromium also has a linear hardening rate, very close to that of iron.

In a comprehensive study of a FCC metals and dilute alloys Nuttall (2) found linear hardening rates during deformation by cold rolling for all the materials in his study at low strains. For large strains some materials (Ni, Cu-10%Ni, and Ag) showed discontinuities in the curves or plateaus, which Nuttall showed were identifiable with the onset of dynamic recrystallisation. This was not seen in the microstructures of the metals which showed linear hardening rates right up to the highest strains investigated.

2.5.2 The strain hardening coefficient

Tensile stress strain curves have been used more than any other test results to obtain information concerning the strength, durtility and strain hardening behaviour of metals. The variation in the slope of the curve between the yield point and the ultimate tensile stress, reflects the extent of work hardening of a material. Thus the decrease in slope of the curve as the UTS is approached, indicates a decrease in the work hardening rate with increasing strain.

Actually a metal continues to strain harden all the way up to fracture. This may be seen using the true stress-true strain curve, based on the actual cross sectional area of the specimen at any instant. The true stress is the load at any instant P, divided by the cross sectional area at that instant A_i

$$\sigma = \frac{P}{A_i}$$

and the true strain is defined (131) from the change in length referred to the instantaneous gauge length as

$$\varepsilon = \ln \frac{L}{L_o}$$

This curve is also known as a flow curve, as it gives the stress required for plastic flow at any given strain.

Many attempts have been made to quantify the work hardening behaviour of a metal, by fitting a mathematical expression to the flow curve.

The most common being a power expression similar to that developed by Hollomon (132)

$$\sigma = K\varepsilon^{n}$$

where K is the strength coefficient (the stress at $\varepsilon = 1$) and n is the strain hardening coefficient.

It has been shown (131) the strain hardening coefficient n is numerically equal to the strain at which necking occurs

$$\varepsilon_u = n$$

and since the strain at which deformation becomes localised constitutes the tensile limit of the material, n has been used as a measure of formability (133) and in evaluation of residual ductility. Values of n are given by various workers (131)(134) (135) for different materials.

Values of n are normally found from the slope of a log-log plot of true stress against true strain, but Carreker and Hibbard (136)(137) have shown for both copper and aluminium that this does not give a straight line and hence gives ambiguous results. The use of the Hollomon equation therefore does not seem to be adequate for all materials, but it has been shown to be satisfactory for steel. (138)

Other empirical equations by Ludwik, Swift and Voce have been compared with the Hollomon equation by Kleemola and Nieminen (138) who conclude that deriving values of n from $n = \varepsilon_u$ is often misleading, and that for most cases the Voce equation (139) fits the stress strain data more accurately. Bowen and Partridge (134) also cast doubt on the reliability of n and K values and suggest the use of the proof stress-tensile stress ratio as a better strain hardening parameter.

2.5.3 Strengthening due to substructure

It has been shown (135) that the Hall Petch relationship (136)(137) for the change in flow stress σ_f due to a change in grain size d,

$$\sigma_f = \sigma_o + kd^{-\frac{1}{2}}$$

where σ_o is the friction stress opposing slip and k is a constant, is valid for most polycrystalline materials, suggesting that the $kd^{-\frac{1}{2}}$ term is an expression of the resistance of the grain boundaries to the propagation of slip.

A number of workers have applied this to the strengthening effects of sub-grain boundaries, but confusion exists as to the value of the subgrain diameter exponent.

Embury et.al. (68), for ferrous materials in which the sub-grain size decreased with drawing strain, found agreement using an exponent of $-\frac{1}{2}$, while Langford and Cohen (67) in similar experiments on Fe wire found it necessary to use an exponent of -1

Argument as to the correct value of the exponent has been considered by Hutchinson and Pascoe (138). For FCC metals there is considerable confusion, some workers suggesting that the approach works for Cu (139) and Al (140) and others (141) indicating for the same materials, that strengthening mechanisms involving sub-grains may not obey a Hall Petch type relationship at all. In view of this confusion the strengthening effect of sub-grains will not be considered in terms of a Hall Petch analysis.

A comprehensive review of substructural strengthening has been given by McElroy and Szkopiak (142).

2.5.4 Dynamic recovery

Dynamic recovery and recrystallisation, although usually associated with hot deformation, has been found to occur during cold working also. Bullen and Hutchinson (143) working on copper and aluminium, found a recovery process superimposed on the basic strain hardening mechanism, so that hardening and recovery were occuring simultaneously at high strains. They found that recovery co-incided with a stabilisation of the cell size. Nuttall (2) suggests that as their strains were only up to 30%, Bullen and Hutchinsons results may simply be a change in flow stress from that due to gliding dislocations forming cells, to that due to a Hall Petch type relationship once the cells have formed.

Weissman et.al. (144) found for aluminium that sub-grain boundaries attained a constant dimension and sharpened without further increase in interior dislocations. This same phenomenon was later found by Embury et.al. to be occuring in other FCC metals (68), but not in BCC metals to the same extent. They attributed the greater work hardening of iron than copper differences in the extent of dynamic recovery.

They concluded that the cell walls formed during deformation act analogously to grain boundaries and suggested that the stable cell size was a balance between barriers created and those destroyed by dynamic recovery.

Dynamic recovery has also been studied in FCC metals by other workers and has been very well reviewed by Nuttall (2).

In their investigations of cold drawn iron wire Langford and Cohen (67) deduced that the almost constant sub-grain size at high strains was a result of the production of cell walls by polygonization being almost balanced by strain induced recovery. They proposed a mechanism for recovery in which low angle boundaries migrate along higher angle boundaries in the form of 'h junctures' until annihilation of these occurs.

In later papers Langford and Cohen (145)(146) have shown that sub-grain mis-orientation increases with strain, as does the spread of orientation, with misorientations of 10° being found for strains in excess of 2 and as high as 15° for strains of 5. They confirmed that dynamic recovery takes place (146) but is slower than the refinement caused by cell formation for BCC metals, and suggest that at high strains the high misorientation sub-grain boundaries are acting as grain boundaries.

2.6 Deformation of alloys containing second phase particles.

2.6.1 Introduction.

There are three basic possibilities for the behaviour of particles during deformation (147).

1. Matrix dislocations can run through the particles, causing them to be split at high strains and eventually dissolved.
2. Particles can deform the matrix without being dissolved.
3. They may possess mechanical properties such that they cannot be deformed.

Of these types of behaviour, only categories 2 and 3 are relevant to this work. Manganese sulphide inclusions fall into the second category and their behaviour will be reviewed first. This will be followed by a review of relevant work carried out for alloys in category 3.

2.6.2 The deformation of MnS.

Early observations of the deformation of MnS were undertaken because of the relevance to the machinability of steels and have been recently reviewed by Segal (148). Van Vlack et.al. proposed (149) that the deformability of MnS inclusions was increased by increasing silicon content, suggesting that the inclusions were enveloped by silicious material during rolling and that this allowed the development of hydrostatic pressure as well as shear stresses around the inclusions, thus increasing the plastic slip within them. This was later discounted because of the work of Yeo, (150)(151) who showed that the Si simply reduced the Oxygen concentration in the inclusions, reducing their hardness and increasing their deformation relative to the steel.

A detailed study of the deformation of pure MnS was then undertaken by Van Vlack and co workers (152) who observed that at room temperature, the ductility was limited but increased when the sulphide was completely surrounded by a steel matrix. In favourably oriented inclusions they found slip lines on the polished surface of inclusions, with the ferrite matrix slip lines bending to coincide with the slip planes in the inclusions. In a detailed study, Chao et.al (153), used both single crystal and polycrystalline specimens to study dislocation mechanisms in manganese sulphide. He found that the primary glide system was {110} <110> with a secondary glide system developing on {111} Cleavage occured on {100} and also secondary cleavage on {110} These findings being consistent with other materials having a sodium chloride structure. Further work (154)(155) on deformation of oriented single crystals of Mns and hardness studies concluded that the deformation of manganese sulphide relative to steel is related to the relative hardness of the two materials under any given conditions.

Boniszewski and Baker (156) extracted rolled inclusions from a fracture surface parallel to the rolling direction and found some of these sufficiently thin to be transparent to the electron beam. Their observations of very mobile dislocations moving in the electron beam confirmed the observations of Wood and Van Vlack (152) that manganese sulphide does behave plastically at room temperature.

They specifically explain the fact that MnS inclusions do not affect the fatigue properties of steel, claiming that stress concentrations are not generated at the interface and cracks are therefore not nucleated, because the MnS can accommodate the strain.

Much of the work on high temperature deformation is not relevant to this project, and for this the reader is referred to the excellent review by Segal (148). However Gove and Charles who studied manganese sulphide at high temperatures also investigated the relative plasticity,(157)(158) studying in detail the decrease in relative plasticity with increasing deformation previously observed by others (159(160)(161)(162). The reasons for this are complex, but Gove suggests four important contributing factors.

1. The inclusion becomes surrounded by a shell of harder material because of different rates of work hardening in the inclusion and the matrix.
2. Friction at the inclusion matrix interface impedes deformation.
3. The matrix is constrained in trying to flow over the inclusion
4. The surface energy of the particle opposes increasing deformation when the surface to volume ratio becomes large.

He showed that the last factor is effected by the size of the inclusion as would be expected, and that this is a significant effect when the surface to volume ratio becomes large. Baker (159) has estimated the energies involved, showing that the importance of this increaces rapidly as the inclusions get smaller. He showed that for a 20 μm diameter inclusion reduced 94%, the interfacial energy is 2% of the deformation energy, while for a 2μm diameter inclusion under the same reduction, it is 20%

2.6.3 The formation of voids around MnS particles.

The nucleation of voids around particles of MnS has been studies by several workers. Brooksbank and Andrews (163) suggest that because the strength of the sulphide/matrix bond is low, separation of the interface occurs during cooling from the hot working temperature, due to difference in thermal expansion of the two phases. Baker (159) however found that inclusions were in contact with the matrix when he examined the material ahead of the crack in a fracture toughness specimen.

This was indicated by cracks within the particles even though extensive void formation was associated with the failure. Hozasu and Kubota (164) also observed both sulphide fracture and interface decohesion and noted that the interface separated more easily at low temperatures. They postulated that the interface was weaker in this case, but it could also be due to unrelieved stress in the matrix. Cox and Low (165) tested rolled sheets in tension and noticed that voids form first on the larger particles.

2.6.4 Deformation in alloys containing hard particles.

According to Ashby (166) when alloys in the third category are plastically deformed, the particles cannot deform with the matrix and some dislocations become 'Geometrically necessary' around them to maintain continuity. These are said to form secondary shear arrays at large particles (above 300 nm) involving local lattice bending. While for particles less than 100 nm. (166)(167) prismatic dislocation loop arrays are formed with no bending of the lattice.

The main features of the deformation of the matrix (147) (168)(169)(170)(171) are high dislocation density at relatively low strains, because of the fact that the particles act as dislocation sources and barriers to motion. The normal cell structure does not form so easily for fine particles and once it does form (at higher strains) it is finer. For coarser distribution, cell structures similar to those of pure metals are produced, but the mis-orientation across the boundaries seems less than for the pure metals.

An excellent review of all these points has recently been written by Onel. (172)

2.6.5 The formation of voids in systems containing hard particles.

A comprehensive review of this topic has been published by Argon, Im, and Safoglu (173) so it is only intended to summarise the work in current literature for systems containing undeformed particles. Edelson and Baldwin (174) suggested that the ductility of a two phase alloy of this sort, depended only on the volume fraction of inclusions and was independent of particle size and spacing. But this is now disproved. Palmer and Smith (175) studied internally oxidised Cu-SiO2, in which they could easily control the dispersion of silica particles. They found that voids formed first at larger particles by decohesion of the particle matrix interface.

By their calculations the interface failed at such lower strengths than it theoretically should have, so their conclusion was that stress concentration occurs by dislocation interaction around the particles. They found a strong temperature dependence of the effect of particle size on void nucleation and thought that this was due to a change in stress concentration rather than to increasing surface tension pressure around smaller particles..

Void initiation around spheroidised carbides in steels was studied by Tsuyoshi, Inove, Shushi and Kinoshita (176), who found that void initiation occured in the late stages of deformation when stresses were large and that as the interparticle spacing increased, so did the strain to initiate voids. Their explanation was that stress relaxation occured around the particles. They assumed a critical dislocation density for void formation, so that for increased inter-particle spacing, the dislocation density surrounding the particles decreased, making larger strains necessary to achieve the critical density.

Broek (177) in a study of aluminium alloys concluded that voids only formed late in the deformation process, thatthe cohesive strength of the interface in these alloys is very strong and that voids only formed at high stress levels when they were able to grow in a direction perpendicular to the tensile stress and coalesce almost instantaneously. He noticed also that voids formed at lower strains on isolated large particles, altered the stress concentration and influenced the final structures.

Butcher (178) found in copper-oxygen alloys that voids formed by cracking of particles and by decohesion at the interface. The larger particles cracked and the smallest remained coherent. He favoured an explanation based on macroscopic stress concentration around the particles, rather than a dislocation model.

There are many complicated mathematical models postulated concerning the onset of void formation. It is not intended to review these in detail, as they are not really relevant to this project and they have been reviewed by Argon and Safoglu (173) and by Segal (148)

There has been confusion concerning the growth of voids, once formed, under the influence of further strain. This may possibly be illustrated by reference to papers by Gurland and Plateau (179) who assumed the crack grew perpendicularly to the applied stress, and Ashby (180) who showed that the cavity in fact elongated in the direction of the tensile stress, and that the volume increased linearly with strain.

2.7 Metal Cutting

2.7.1 Introduction

Good reviews of the mechanics of metal cuttings have been published by Ernst (181) in 1951 and by Finnie (182) in 1956. More recently much has been written on the subject, the best summary of which appears in a book by Amerago and Brown.(183) Doyle and Samuels (184) have also published a review paper, with particular emphasis on the formation of the lamellar chip structure by shearing.

2.7.2 Current mechanisms and controversies

In recent literature three types of chip formation are recognised (183).

Type 1 Discontinuous chip formation. This involves periodic rupture so that the chip forms as small seperate segments.

Type 2 Continuous chip formation, involving a plastic flow, or shear process.

Type 3 Continuous chip with a built up edge. In this case a nose of material periodically builds up and breaks away from the cutting edge of the tool.

For a type 1 chip, the clearest demonstration that the mechanism is periodic shear in well defined planes has been that of Doyle, (187) who showed by SEM that the fracture surfaces of the chip segments parellel to the shear plane showed elongation dimples, indicating failure by a ductile rupture process involving the formation and linking of voids, presumably at second phase particles within the narrow shear bands.

For the case of type 2 or continuous chips, there is little doubt that the process occurs by plastic flow (or shear). But there is considerable controversy about the actual mechanism. While all recent observations emphasise the heterogeneous nature of the plastic flow, giving rise to the characteristic lamellar formation, there seems to be little real insight into the mechanism or mechanisms which give rise to this plastic instability. Generally, published models fall into one of two shear models. A thin shear zone model similar to Piispanen, (183) Ernst (185) and Merchant (186) with simple shear on a plane running from the tool point to a point on the free surface, and no flow on either side of this plane. Or a thick shear zone model, proposed by Palmer and Oxley (188), Okushima and Hitomi (189) and others.

Type 3 chip formation models are basically similar, with consideration being given to the flow and seperation of metal around the tool nose. This normally comes under the heading of secondary shear. It has been reviewed by Doyle (184) and discussed by Trent (190) and will not be considered in detail in this review, as only the inhomogeneous primary shear is relevant to this project.

The following are some of the models which have been conceived to explain the deformation process occuring in the primary shear zone.

1. A very rigorous approach by von Turkovitch (191) considers the energy balance in chip formation and concludes that there are two distinct processes following one another. (1) A uniform compressive deformation causing work hardening and a build up of shear stress such that large numbers of dislocations are created at points of high stress concentration. (11) This leads to an adiabatic generation of heat and a falling of the shear stress, with the whole process repeating itself in a periodic manner. The detailed microscopic mechanisms involved are not well understood.

Recht (192) and Lemaire and Backofen (193) have also advanced the adiabatic shear concept to explain chip formation at high speed and at relatively low speed respectively.

The evidence advanced for adiabatic shear is that white etching bands form along the primary shear plane. However this cannot be taken as definite evidence of anathermal softening process since white etching layers can be due to a number of structural features (194)(195).

2. At very small depths of cut, the lamellar spacing is very small. Ramalingham and Black (196) suggest that this could be the result of the increased strain rate ($\dot{\gamma} \doteq \frac{v_c}{d}$) where v_c is the chip velocity and d the depth of cut and that the thermal instability model of Von Turkovitch may apply. However, Doyle and Aghan (197) in a study of chips produced by fine Grinding and polishing, suggest that the fine lamellar spacing is due to the extremely fine microstructure developed during the deformation and conclude from their observations that the fine microstructure is developed prior to plastic instability, instead of as a consequence of some adiabatic condition,

3. Komanduri and Brown (198) and Brown and Luong (199) take a different view, suggesting that microcracks are responsible for the observed plastic instability causing lamellar formation.

They examine Quickstop chip sections (199) and convincingly demonstrate that microcracks do occur, even in continuous chips. They note that the density of cracks is greatest near the tool nose and at the free surface and suggest that a fine lamellar structure may be generated by the thermal instability model. So one is still left in doubt as to the which mechanism is important.

2.7.3 The shear stress in the metal cutting.

The shearing stress during machining of metals has been found (183) to be considerably higher than the yield stress determined by tensile tests on the work material even when extraneous effects such as rubbing on the tool clearance face and pre flow, are taken into account. It seems worthwhile to briefly look at some of the proposed explanations.

Merchant (186) proposed that the yield stress was increased by high values of normal stress on the shear plane, but work by Bridgeman (200) and later by Crossland (201) has demonstrated that the shear stress is not influenced much by hydrostatic stress, although the rupture stress is.

Following the theory of size effect for single crystals, Backer, Marshall and Shaw (202) and Shaw and Finnie (203) proposed that the increase in shear stress was due to the small size of the deformation region, in the cutting process, but the evidence for this is not conclusive. Experiments have shown (204) that the most likely cause of the apparent increase in shearing forces at small depths of cut, is the greater prominence of rubbing forces on the clearance face of the tool.

A number of workers (203)(205) have claimed that the high shear stress in metal cutting was due to work hardening, but later evidence (206)(207) indicates that this is probably not the case except at very low cutting speeds.

Consideration of the mechanism of yielding at high rates of strain indicate that high strain rates may be the cause of yield stresses above the static value, even though it has been argued that in metal cutting the opposing effect of high temperature in the shearzone cancels this out (203).

Cottrell (206) has described a mechanism of yielding at high strain rates, which suggests that above a critical strain rate the yield stress is independent of both strain rate and temperature.

He represents grain boundaries and other obstacles to slip as an undulating stress field. When the applied stress is less than the internal stress the dislocations cannot pass the obstacles unless they are provided with sufficient energy from thermal vibrations of the lattice. This depends on time and temperature, so the yield stress will be influenced by both strain rate and temperature. If however the applied stress is greater than the internal stress then rapid slip will occur and the yield stress will be independent of strain rate, He predicts that at high strain rates, the yield will be higher than the static yield stress, and above a certain rate it will be independant of strain rate, with sudden and catastrophic straining at any applied stress level such that no work hardening will be observed. This can be represented by a flat topped stress strain curve as in fig.2.1

Some years before Cottrells discussion of dislocations at high strain rates Drucker (208) suggested a flat topped stress strain curve for metal cutting. More recently Kobayashi and Thomson (207) have applied Cottrells explanation to the metal cutting situation, showing that the shear stress is higher than values at low strain rates, and that its magnitude is independent of the temperature rise during deformation and also independent of work hardening.

2.7.4 The effect of manganese sulphide additions.

Improved machinability in steels has been long associated with a large volume fraction of manganese sulphide inclusions. However, the mechanisms proposed in machining literature to account for the beneficial effect, as with any particular additive, are many and varied. Division of opinion exists between investigators in attributing the major activity of the inclusions to either the primary shear zone or the secondary shear zone around the tool nose.

Shaw et.al. (209) and Rubenstien (210) suggest that manganese sulphide inclusions act as stress raisers in the primary shear region, in which case the shape size of the inclusions becomes more important. This argument is supported by the work of Kiessling (211) who increased the hardness of the inclusions by addition of selenium and tellurium and obtained further improvements in machinability.

Merchant and Zlatin (212) found that sulphide layers were formed on tool surfaces and suggested that these act to reduce the coefficient of sliding friction.

Trent (213) also observed a layer of sulphide on the tool, admitting the possibility of lubrication effects just in the region where the metal leaves the tool, but he suggests that conditions of seizure exist between the tool and the chip, which makes discussion of friction in this contact region meaningless. Shaw et.al.(209) carried out a series of friction tests, concluding that MnS was not a good lubricant in air. This appears to make the lubrication hypothesis less attractive.

Trent also suggests (213) that sulphide inclusions play a major roll in the secondary shear, being drawn out into fine stringers and acting as zones of weakness, reducing thestress in the secondary shear zone. He has recently suggested (180) that they may appear in this region and on the tool surface by extrusion out of their sockets in the metal like toothpaste from a tube.

Kiessling (211) suggests that the temperature rise with increase in cutting speed reduces the stress and therefore the inclusions cannot act as stress raisers (or zones of weakness). His suggestion is that the most important feature of sulphide inclusions (as distinct from, say oxide inclusions) is their ability to deform plastically over a wide range of temperatures so that they can participate in rather than hinder the shear process.

More direct studies of machining free machining steels have been carried out by Hazra et.al. (214) and by Iwata and Ueda (215) who observed chip formation directly, within the specimen chamber of a scanning electron microscope. They both showed cavities forming at the particle matrix interface, frequently associated with cleavage cracking of the sulphide particles. This suggests that the inclusions act as stress raisers. Hazra et.al. point out (214) that the volume percentage of sulphide particles in steel is only about 2% and hence one could only expect a very small reduction in shear force requirements in both the primary and secondary shear zones. Their conclusion is that the main explanation of the effect of MnS particles is the dissipation of thermal energy in the primary shear zone, promoting plastic flow, and precluding the possibility that they act as stress raisers.

2.7.5 The effect of lead additions.

Although it is the most widely known free machining additive, lead is not so common in steels.

When added to steels it is generally associated with a large volume fraction of MnS particles as is usually found attached to these as a tail at each end. (190)

The action of lead in promoting better machinability has been rationalised (184) in terms of its effect on both the primary and secondary shear zones. Lead particles in the primary shear zone are presumed to reduce the area capable of withstanding the applied shear strength because of their own low shear strength. With regard to the effect of lead in the secondary shear zone, several investigators (216)(217) have noticed that high concentrations of lead appear on the smooth back face of the chip and on the tool surface, suggesting that lead acts as a lubricant between the chip and the tool.

The actual mechanism by which lead achieves its purpose is still uncertain, and in some cutting conditions it is actually detrimental (190) causing rapid tool wear.

2.8 Fracture

2.8.1 Introduction

To give a detailed and comprehensive picture of such a complicated subject as fracture would require far more time, study and courage, than is available for this project. The number of books, reports and publications in recent years, devoted to some particular aspect of this general problem, staggers the imagination. No attempt will be made to review all the fracture models which have been proposed in the past. Rather the aim will be to review some of the more critical experimental results, trying to give as accurately as possible, a current picture of the situation, with particular emphasis on the influence of stress state, deformation pattern, strain history and the presence of other phases. These variables are known to be important in altering the fracture characteristics and in assessing fractures resulting from high strain deformation processes.

Fractures are frequently classified as ductile or brittle based on the gross energy absorption or shape change accompanying the process. In a polycrystalline material they are also classified by the morphology of the path, as intergranular or transcrystalline. These classifications are important, but do not really define the fracture process sufficiently to be able to predict or understand the behaviour under conditions relevant to high strain processing.

In polycrystalline materials brittle, transcrystalline fractures frequently occur at low temperatures by separation along crystallographic planes, (cleavage planes) under the action of a normal stress. With the exception of face-centred cubic metals which do not cleave, metals have one or more specific planes on which they separate. Cleavage has been extensively studied, as a result of the many catastrophic failures which have occured by this type of fracture. However, since metals are not normally processed in a temperature range in which cleavage occurs, it will not be discussed in any great detail. Extensive studies have been carried out which indicate the directions to go when attempting to remedy situations in which accidental cleavage fractures are encountered during deformation processes. Indeed, the whole science of fracture mechanics has developed from these experiments and the concept of differentiating between crack initiation and propagation. A fracture may be clearly ductile when considered as a whole; yet additional and valuable information is gained if it is known that the initiation was ductile, requiring say 30% elongation, while the propagation was brittle. The problem comes in being able to distinguish the point at which fracture can be said to have begun, and is particularly troublesome in cases such as this project, when one is thinking about the effect of prior deformation on the fracture process.

It has been shown (218)(219)(220) that for brittle fracture of polycrystalline steel, microcleavages form during the modest deformation preceding fracture, generally separating an entire grain, final separation then occurs by the extension and linkage of these cracks.

In this review, the main concern from here on will be ductile fracture, since this project is concerned with metals undergoing deformation to high strains. The very name ductile fracture indicates that it takes place after considerable plastic deformation

2.8.2 Ductile fracture mechanisms

Although there are variations in the mechanism of ductile fracture for different specimen shapes and for specific metals and alloys, it appears from the literature that there are two basic modes involved, a 'fibrous' mode and a shear mode.

Fibrous fracture is characterised by the formation and growth of voids nucleated by non metallic inclusions and second phases, leading to a fracture surface covered with equiaxed dimples. The shear mode on the other hand gives rise to fracture surfaces with strongly oriented parabolic dimples and particularly for some classes of materials, the mechanism is not so well understood. The shear mode of ductile fracture (221) occurs in many situations, including the outer-portion of a cup and cone fracture. Tensile fracture of sheet material, and the fracture of some materials under hydrostatic pressure. French and Weinrich (222) have recently published a paper collating earlier results with more recent work together with a good summary of the basic mechanisms. Basic mechanisms leading to the various types of fracture surfaces which are commonly observed in practice will now be described.

1. Cup-cone fracture.

A typical cup-cone fracture surface (fig 2.2) contains a central transverse region exhibiting large equiaxed dimples and a sloping outer region covered in shallower elongated dimples. The mechanism of this type of fracture is well understood, mainly from the work of Tipper (223) Rogers (224) and Puittick (225)(226). During initial uniform deformation, small voids form at inclusions or second phase particles. A neck forms as deformation becomes localised by plastic instability, developing tri-axial stress components and causing intense void formation, growth and coalescence in the centre of the necked region. A central cavity develops, corresponding to the equiaxed dimple part of the fracture surface. Deformation in the rim is then concentrated by the notch effect of this cavity into zones of high shear strain approximately 45° to the axis. Sheets of voids are then nucleated in these shear zones and these coalesce to form the elongated dimple part of the fracture.

No specific mechanism was proposed by Rogers (224) for the formation of the sheet voids in the shear zone. They have been shown (227)(228) to form at inclusions in materials which contain large numbers of fine inclusions. French and Weinrich, however (221) have shown that in materials without such inclusions, no sheet void formation occurs prior to fracture and the elongated dimples on the fracture surface form during the final act of fracture.

According to Rogers (224) the mechanism is modified in larger specimens, the central cavity being extended across the plane of minimum cross section in a series of zig-zag crack extensions, each occuring by the sheet void mechanism, until it finally reaches the specimen surface in one large step forming an outer lip.

11 Double-cup fracture.

Materials with fewer inclusions (229) tend to fail by a double-cup mechanism, following the sequence of events shown in fig 2.3 (222). A typical fracture surface (fig.2.4) consists of a dimpled inner region and an essentially dimple free outer region. Later in the deformation process when a well developed neck exists a zone of shear develops across the specimen neck (fig. 2.3a) and voids develop in and around this shear zone. These then coalesce to form a central cavity (fig2.3.b) corresponding to the dimpled portion of the fracture surface (2.30). For larger diameter specimens, void coalescance occurs in the central cavity on a number of intersecting shear zones, leading to the kind of zig-zag cavity described by Rogers (224). The central cavity then grows (fig. 2.3 c & d) by a process known as 'ductile cutting', the most likely explanation for which is that of Rogers, (231) who suggested that the tip of the cavity slips apart as a constrained single crystal. The next grain is thus exposed to the same conditions and a slip fracture surface is created, producing the dimple from outer region.

111 Shear fracture.

Shear type tensile fracture occurs most commonly in the tensile failure of sheet specimens (232) but also occurs in round specimens in some circumstances (233). The entire fracture surface consists of elongated dimples similar to those in the outer rim of a cup-cone fracture (fig. 2.5). Often the fracture surface may be comprised of a number of intersecting planes. Again deformation proceeds until a well developed neck is formed, without growth or coalescence of any voids which may form in the early stages. Further deformation becomes localised to one or more zones of shear extending through the neck, by the mechanism described for cup-cone fracture.

1V Chisel point fracture

This type of fracture has also been described as ductile rupture (234) and knife edge (235). The regions to the side of the chisel point consist of highly slipped original surface, rather than a genuine fracture surface, and voids appear to play no part whatever in the process. The specimen deforms uniformly until a neck begins to be established; localised shear then occurs on two well defined zones through the neck (236). Fig 2.6 shows two aspects of the specimen at different stages of the process. Localised shear zones develop, leading to the formation of new surface and distortion of the neck. Both these features progressively increase until the two halves simply slip apart after thinning down to a line of separation.

2.8.3 The effect of strain history on ductile fractures

A large number of papers on ductile fracture relate to the weakness of metals in a direction 'across the fibre' this being a well known fact for many decades. The work of Swift (237) in 1939 on the effects of tortional strain on fracture in Mild Steel stimulated a new interest in this topic with extensive work by Zener and Hollomon (238), Klinger and Sachs (239) Backofen and co-workers,(240)(241) and others, putting new emphasis on the 'micro-crack theory of fracture' and on 'Mechanical fibering.' This concept has been reviewed previously (242-245) and will only be briefly mentioned here. In essence the idea was that even relatively pure metals contain micro-cracks arising somehow during processing from the liquid stage, possibly during solidification or during some working process. Further working was then thought to align the micro-cracks in the direction of flow. Subsequent tensile stress in the direction across the plane of the micro-cracks, causes them to fail. The tensile strength and ductility in this direction is therefore much lower than in the flow direction, where the effect of the micro-cracks is almost nil.

Swift's tortional pre-straining of Mild Steel (237) was the most dramatic, completely changing the nature of the fracture from a standard cup-cone fracture to a so called wolf's ear fracture. Backofen et.al. (240)(241) studied many different materials, and showed 1. That this effect occurs even in pure single phase material. 2. The effect increases with increasing pre-strain. 3 An intermediate anneal prior to the final test does not erase the effect of the pre-strain. 4. If a twist in one direction was followed by an equal and opposite twist, the original fracture was restored.

These facts were considered to be strong evidence for the micro-crack theory, but the biggest objection to the theory is that the cracks have never been seen except when associated with inclusions or a second phase. Also, it has been demonstrated for many engineering materials, that anisotropy is unquestionably related to the fracturing and stringing out of hard second phase particles and inclusions, or the elongation of blow holes, casting defects and soft second phases by hot working processes used to shape the metal. Backofen and co-workers also studied (246)(247) the fracturing isotropy of hot rolled mild steel plate, showing that it can be substantially improved by a sufficiently long anneal at high temperatures. The improvement was related to the spheroidization of initially elongated inclusions, which act as nuclei for cracks and localized plastic deformation.

There is however much experimental evidence in the literature showing that microcracks can be produced apart from inclusions during plastic deformationin mild steel.Low (12) has made an excellent correlation between plastic deformation, microcracks and brittle fracture. They have also been found in steels by many others (249-251) and Hahn has studied the conditions for their formation. The many dislocation models postulated for their initiation have been reviewed elsewhere. (27)

In relation to ductile fracture Rogers (224) has shown the initiation of voids within grains, in regions of high strain where the inhomogeneous deformation is particularly intense.

The newer work of Walker and Shaw (50) who believe that microcracks form, reweld and reform several times during high strain deformation processes as discussed in section (2.2.3) may also be relevant as this would have a pronounced effect on the subsequent fracture.

CHAPTER 3

OUTLINE OF INTENTIONS

3.1 Introduction.

This project began with a fairly broad aim using material which was readily available and developed by choosing different steels and conditions of heat treatment to verify ideas arising from the initial results. This chapter will briefly outline the reasons for carrying out this research, outline the sequence of experiments which have been carried out and discuss the reasons for choosing the materials and techniques.

3.2 Aims of Project.

The basic intention of this project has been to study the changes in mechanical properties and structure which occur in a body centred cubic metal during deformation to high strains.

Although high strains are regularly encountered during mechanical processing, little is known about the deformation mechanisms occuring within a metal as strain is increased, because most studies of basic deformation have been carried out at strains less than 30% reduction in thickness. Following recent work at Leeds on the structure and properties of face centred cubic metals tested in tension after rolling to high strains, it was decided to carry out similar studies of the structure of cold rolled steel in order to gain as much information as possible about the fundimental mechanism of deformation occuring and changes in the mechanism as strain is increased.

3.3 Choice of Materials.

Experiments have been carried out using four different steels in order to study different aspects of the deformation behaviour. The materials used were as follows:-

Steel 1. Low C steel (EN8)

Steel 2. Free machining steel (High Sulphur)

Steel 3. Free machining steel (High Sulphur plus lead)

Steel 4. Low Carbon steel (EN3B) (Heat treated to a special structure).

Each material was heat treated to the required structure, after which samples were rolled to various strains and made into tensile specimens. Samples at each stage of rolling were also examined in an optical microscope and in a transmission electron microscope.

Two series of tests were carried out on the first steel in different conditions of heat treatment. For the first series, the heat treatment was designed to produce a ferrite structure with carbide particles in the grain boundaries. The intention was that carbide particles would delineate the grain boundaries and help in showing their behaviour during increasing strain. The second series was carried out with the steel in the normalised condition, because this is the condition in which it is commonly used.

The structural observations suggested that the material was deforming by a heterogeneous, unstable, shearing process. This led to a series of experiments in which rolled material was strained in tension within the high voltage electron microscope. Also, because it is known that metals deform by heterogeneous unstable shearing during machining and because manganese sulphide inclusions and lead additions have been used for many years to improve machinability, it was decided to study the effects of these additions on the bulk deformation behaviour and on the resulting structure and properties.

The final steel was selected because it could be heat treated to give a structure of hard carbide particles in coarse grained ferrite matrix, in order to see if the unstable shearing was enhanced by stress concentration at hard particles. This steel in the same condition has previously been shown (172) to have anomalously low mechanical properties.

3.4 Choice of Techniques.

3.4.1 Straining: The strained material in this study was produced by cold rolling. It was decided to try to roll the material in an isothermal manner, to avoid the possibility of changes in the structure due to heating. Details of the technique will be given in the next chapter.

3.42 Microstructural Examination.

Although the optical microscope has been used in some cases where low magnification was required, and for grain size determinations, the bulk of the structural observations have been carried out using the transmission electron microscope. This is because the basic deformation structures cannot be resolved in an optical microscope. The T.E.M. also has the advantage of being able to distinguish changes in orientation between areas in the microstructure by electron diffraction.

The Photo emmission electron microscope has also been used a little to try to resolve structures at low magnification, which could not be seen optically. The examination of fracture has been carried out both in a Scanning electron microscope (S.E.M) and by replica techniques in the T.E.M. where higher resolution was required. Replicas were also used for the examination of polished surfaces to study the distribution of fine particles in relation to grain boundaries and deformation bands.

For the examination of strained material by T.E.M. foils made from both rolling plane sections and sections perpendicular to the rolling plane were studied in the first series of tests. For later steels only sections perpendicular to the rolling plane were used, because the structures of the rolling plane foils were not clear. One factor contributing to this was the fact that there were many dislocation cells through the thickness, causing the introduction of Moiré fringes, as well as complicating the interpretation of the dislocation structures.

The production of foils in the perpendicular direction from the samples which had been rolled very thin, involved electro plating before sectioning and then thinning by ion bombardment. This technique will be described in the next chapter.

3.43 Determination of mechanical properties.

The mechanical properties of the material in various states of strain were determined by tensile testing because of the wide use of this test by previous workers, enabling comparisons to be made with similar work on other materials..

The first tests were done using specimens of different thickness, each specimen being the thickness of the rolled strip after the various amounts of rolling strain had been imposed from a constant starting thickness. Some tests were carried out on specimens of the same material in the same condition, but at different thicknesses, to see if the results were influenced by a specimen size effect.

Because of long delays in getting specimens made, it was decided to make all specimens for the later series the same size, choosing 1mm thickness so that a specimen punch could be used to cut out the large number of specimens involved relatively quickly. Naturally, the very highly strained material has to be thinner than this. A few specimens were cut with their thickness direction in the rolling plane in order to check that the results were not influenced by the direction of the structure relative to the thickness of the specimen. The tensile axis was always along the rolling direction.

Some hardness tests were also carried out, but the results showed considerable differences depending on the plane of the test, and also considerable scatter due to the inhomogeneity of the deformation.

3.4.4 Other experimental observations

The anomalous features of the stress strain curves and visual differences in the fracture surfaces after different amounts of rolling strain, led to the examination of the fractures by SEM and to the comparison of fracture surfaces with fractures of machining chips made from the same materials.

Some electron probe micro analysis was also carried out on optical samples and fracture surfaces of the high Sulphur and Sulphur plus Lead steels in order to help understand the effects of these inclusions on the deformation and fracture behaviour.

CHAPTER 4

EXPERIMENTAL METHODS

4.1 Introduction

The previous chapters have shown the work relevant to this study done by other workers, and outlined the aims of the project and the methods chosen to achieve them. In this chapter the experimental techniques are described. It covers the preparation of the material, the preparation of thin foils and replicas for electron microscopy, specimen preparation and extration of data from the tensile tests and details of other experimental techniques used to confirm ideas arising from the results.

4.2 Materials and their heat treatments

All the materials were supplied in the form of extruded bars, the size and chemical analysis being shown in table 1.

Heat treatments were carried out in each case in a normal atmospheric muffle furnace. This was possible because the samples of each material were to be ground to a constant starting thickness after heat treatment and this removed any scale formed or decarburisation which occured during the treatments.

Each material was treated to the required condition by the treatments shown below.

The first steel was used in two different conditions as explained in the last chapter. The first structure consisting of ferrite with carbide particles in the grain boundaries was produced by holding for 2 hours at 950° quenching into brine and then tempering for 1 hour at 650°. The second structure was produced by cooling the samples in air after 2 hours at 950°, to give a ferrite grain structure with some small pearlite areas.

Both of the free cutting steels were used in the normalised condition, the treatment being 2 hours at 950° and cooling in air.

TABLE 1

CHEMICAL ANALYSIS WT. %

STEEL	BAR SIZE	C	Si	Mn	S	P	Cr	Mo	Ni	Al	Cu	Pb	Sn
1 EN8	1" squ.	0.12	0.5	0.80	0.027	0.025							
2 Free cut S	$\frac{3}{4}$" Dia	0.055	0.001	1.01	0.333	0.068	0.01	0.03	0.18	.003	0.18	0.02	0.019
3 Free cut S + Pb	$\frac{3}{4}$" Dia	0.067	0.001	0.91	0.362	0.068	0.03	0.04	0.15	.003	0.16	0.25	0.017
3 EN 3B	$\frac{3}{4}$" Dia	0.12	0.22	0.695	0.054	0.039	0.06	0.05	0.09	0.014	0.23		

The final steel was treated using a combination of tempering and mechanical working, as recommended by Onel(1) to give a structure of very fine carbide particles in a coarse grained ferrite matrix. To ensure that the structure was the same throughout the cross section, it was necessary to use sections not greater than $\frac{1}{2}$" thick and to quench into a 10% NaOH solution. The treatment consisted of holding for 1 hour at 950° and quenching into the NaOH solution, tempering for 1 hour at 650°, reducing 20% in thickness by cold rolling and finally tempering for 15 hours at 650°.

The grain sizes of the materials in the heat treated condition are shown in table 5.1. These were determined by the line intercept method. The mean intersept length $\bar{L}$ was first found from:-

$$\bar{L} = \frac{L}{M\,N}$$

where L is the total length of line used for the total number of fields, M is the magnification and N the total number of intersections. The mean intercept was then converted to average grain diameter (assuming tetrakaidecahedral grains) by multiplying by 1.776 (252)

Steel	Average grain diameter
1 EN8 Quenched and tempered	19 μm
1 EN8 Normalised	49.5 "
2 Free cut (High sulphur)	42 "
3 Free cut (sulphur + lead)	38 "
4 EN3B (with fine carbides)	56.5 "

4.3 Straining the material

Various amounts of strain from 2% to 99% reduction in thickness were introduced into the samples using a two high Marshall Richards rolling mill, at a rolling speed of ms^{-1}. In order to keep the deformation approximately isothermal, the deformation of each sample was carried out using many passes.

It was not possible to achieve constant strain increments, particularly at high strain levels, as the roll gaps could not be controlled accurately enough and the plastic strain in the material and in the rolling mill varied with strain. As a very rough attempt to keep the strain increments similar, the reduction in roll gap per pass was 0.2mm at the beginning and this was progressively reduced as the thickness was reduced, down to less than 0.02mm at the highest strains.

It was noticed that although the temperature did not rise more than a few degrees above room temperature at any stage, that from 40% to 60% reduction in thickness, temperature rised were higher than at other stages and the samples tended to buckle. At higher strains, samples remained flat and temperature rises were not detectable. No quantitative work was done on this aspect.

To keep temperature rises to an absolute minimum, samples were cooled in ice for a short time between passes.

For each steel all specimens were rolled simultaneously with one strip being taken out as each required stage of strain was reached, the remainder undergoing further deformation according to the previously calculated reduction schedule.

The true rolling strain T was calculated for each sample by the equation

$$\varepsilon_t = \ln \frac{T}{T_o}$$

where T is the final thickness and T_o is the starting thickness.

4.4 Electron microscopy and specimen preparation

4.4.1 Transmission electron microscopy

The microstructure of the deformed samples was mostly obtained using a Philips EM300 transmission electron microscope operating at 100 kV. Tensile straining of samples was also carried out in this machine, but since it was not possible to record these dynamic experiments and also because of the need to use thicker specimens, in situ straining experiments were mostly undertaken in the high voltage electron microscope at the

British Steel Corporations Swinden Laboratories in Rotherham, where they could be recorded on video tape. Early experiments were recorded on a Sony ½" recorder. Later recordings were of improved quality when a 1" I.V.C. recorder became available and later in the project further improvement was obtained by the purchase of a Dainbridge image intensifier system at the laboratories.

4.4.2 Thin foil preparation

In order to minimise the magnetic disturbance of the electron beam by the steel samples, it was decided to use the smallest possible samples in all cases. Therefore most of the foils examined were small foils cut out from thinned strip and placed between copper grids, except for foils made perpendicular to the rolling plane from the thinnest samples and for straining specimens. The preparation of these types of specimen will be described later.

Strips were first cut in the required section approximately ½ mm thick using a fine jewellers saw. These were then ground parallel and to about 0.125mm thick using an Excel Swing Grinder. Very fine depths of cut were used and slow swing speeds in order to avoid temperature rises which could alter the structure.

Further thinning was then accomplished by chemical polishing until samples were beginning to perforate. The thickness at this stage was less than 0.02mm. The chemical polishing solution (25%) was a stock solution of 5 ml of concentrated sulphuric acid, 8g of oxalic acid to 100 ml of distilled water. This was mixed with equal volumes of hydrogen peroxide just prior to using.

Final thinning was by a short electropolish in 5% perchloric acid in acetic acid cooled to below room temperature. The voltage used was 34V and the cathode was stainless steel.

When suitable areas were produced the specimens were washed in three separate baths of ethyl alcohol and areas cut out with a scalpel while the sample was supported between layers of cellophane to avoid bending. Foils were stored in ethyl alcohol until used.

Rolling plane sections of the thinner strips could of course be commenced at the chemical polishing stage. Window techniques (255) were tried at first but found to be unnecessary

as the above technique was found to produce foils very quickly, with no masking being necessary. Thus the large number of foils involved were able to be processed fairly rapidly.

4.4.3 Foils from very thin samples.

The foils made perpendicular to the rolling plane from specimens less than ½mm thick were made by first plating thickly with Nickel in a Watts type Nickel plating bath (256), consisting of 290 g/l nickel sulphate, 45g/l nickel chloride, and 35g/l boric acid, made up with distilled water. The solution was kept at 55°. The current density was 0.06 A cm^{-2} and the time taken to achieve a thick enough deposit was 3 days. The specimens were then sectioned with a jewellers saw and ground down to about 0.125mm thick as for the other foils. Discs were then punched out using a 3mm diameter punch set and these were thinned by ion bombardment to perforation and placed in the electron microscope for examination. The ion bombardment was necessary because all attempts to electropolish the samples once plated, resulted in preferential attack of the steel-nickel interface and loss of the sample. The bombardment was carried out in an Edwards type IBMA I commercial machine, at an Argon ion current of 50-60 A/gun and an accelerating voltage of 6 Kv.

4.4.4 Foils for in-situ straining

Straining specimens were 2mm wide strip specimens which were 0.025mm thick and polished to perforation in the centre by a jet technique. The first specimens were waisted in the shape of a normal tensile specimen, but this was later found to be unnecessary.

Strips were first cut and ground as for the normal foils down to 0.125mm. They were then chemically polished down to 0.025mm and held in a modified PTFE holder for jet polishing in a self made jetting device driven by a magnetic stirrer. This is shown schematically in fig 4-1. The jetting was carried out at a potential of 34V, in a 20% solution of perchloric acid in acetic acid, until perforation occured in the centre of the sample. At this stage it was taken out, washed as for the other foils, and stored in ethyl alcohol until used.

4.4.5 Production of replicas

The replicas made to study the distribution of fine particles relative to grain boundaries and micro bands, were made by a two stage plastic carbon method, modified as necessary to achieve the desired results.

One of the most important factors in enabling the required structure to be seen clearly was the initial etching of the micro-structure. In order to show both the fine carbide particles and the grain boundaries on the replicas, it was found necessary to carry out a double etching procedure , etching first with a saturated solution of picric acid in alcohol to show up the carbide particles and then in 2% nital to reveal the grain boundaries. This was unsuccessful unless used in this order, as the picral had no effect if used after the nital.

The plastic replicas were initially made using 0.003" thick cellulose acetate sheet (BX Film) softened in acetone. Then because this often breaks up during the dissolution stage when relatively smooth microstructures are being replicated, it was replaced by a viscous liquid plastic which could be run on in drop form, producing a slightly thinner plastic replica which did not have the same tendency to break up. The plastic chosen was not one designed for the purpose, but a first aid dressing called Germolene 'New Skin' which is readily available from any pharmacy very cheaply.

The second stage of the replicas were made by shadowing simultaneously with platinum/Carbon in an Edwards vacuum evaporation unit. Model 12 E6.

To show the fine particles clearly, low angle shadowing was used, rotating the sample during evaporation to fill in the replicated particles, which were in relief in the plastic. This can be seen schematically in Fig. 4.2 which shows the procedure.

Dissolution of the plastic was done by cutting out small squares of the replica and placing them on grids in a glass system designed to condense acetone vapour onto the samples. This method gave clean replicas which could be transferred into the electron microscope after about half an hour, or stored until ready to examine them. The system is shown in Fig. 4.3.

4.4.6 Scanning electron microscopy

The only preparation needed for the examination of the fracture surfaces was to cut the ends off the broken tensile specimens and mount them on a stub for insertion into the SEM. All examinations were carried out in a Cambridge Stereoscan 600 instrument at 15 kV.

For examination of microstructures of specimens in metallographic mounts, it was neccessary to coat with Carbon. This was done in order to make the plastic mounts conducting and thus prevent charging of the samples in the electron beam.

In a few cases it was decided to make taper sections through the fracture surfaces and polish half the sample so that both the microstructure and the fracture surface could be seen in one micrograph, in order to relate structural features with the fracture process. This was achieved by masking the fracture surface with Lacomitlacquer, carefully grinding the taper section, mounting in about 2mm of mounting resin so that fracture was protected during polishing and etching, but could easily be removed afterwards. The lacomit was then removed in acetone and the sample mounted on a stub for examination.

These same specimens were later used for examination in the photo emmission electron microscope. As the rough fractures were not suitable for this it was necessary to electro plate with nickel in the same way as described in specimen 4.4.3. The taper sections were then reground the samples ground to an accurate thickness for insertion into a standard holder as described in the next section, when polishing and etching were completed. The microstructure was thus examined right up to the fracture.

Scanning electron microscopy was also carried out on fracture surfaces of machine chips similarly to examinations carried out by Doyle (216). In this case chips were cut at a slow speed on a lathe using a 3mm wide square ended tool. These were fractured in liquid nitrogen so that any fracture regions other than cleavage must have been produced during the machining process. These examinations were made to compare the behaviour of the material during machining with the behaviour during bulk deformation. Some electron probe micro analysis was also carried out on these samples to study the distribution of Mns and Pb over the sheared surfaces.

4.4.7 Photo emission electron microscopy

The Balzers Photo Emission Electron microscope normally takes a standard specimen 11mm diameter and 32mm long with various flanges and grooves machined into it.

In order to examine some of the transverse sections of rolled strip, it was necessary to obtain a few standard specimens made in mild steel and cut thin slots in the polished face of the end which is normally examined. The strips for examination were carefully ground to the exact width of the slots and pressed in until flush with the surface. A tight fit was ensured by centre punching the sides of the strip in a few places before insertion. Polishing was carried out before insertion in the holders and when cutting the specimens to size, lugs were left on the ends by which the specimens could be pressed into the slots and manoeuvered into the correct position. These were sawn off flush with the sides of the standard specimens when the strips were in position, Samples were not etched, but were bombarded with Argon ions in the metioscope, which while cleaning the surface also slightly etched it.

The specimens were examined using an accelerating voltage of 40 kV.

4.5 Tensile Testing

This section will describe the production of the specimens used for tensile testing and the collection of the tensile data.

As mentioned in Chapter 3, the first batch of specimens were of varying thickness depending on the amount of rolling strain they had been given. These were made on a milling machine. The size of these specimens are given in table 2. Later specimens were all the same size and made by cutting the required section with a hacksaw and carefully grinding down to a thickness of 1mm. Rectangular blanks were cut out from this 1mm strip using a guillotine. Specimens were then stamped out using a specimen punch. The dimensions of these smaller specimens are also given in table 4.2. Heating at each stage of the process was kept to a minimum.

The tests were carried out in an Instron Tensile testing machine using a load cell capable of measuring loads of up to 2500Kg. The machine cross head speed used was 0.02 cm/min. Load extension curves were drawn on the machine using a chart speed of 1 cm/min.

The load extension curves were used to obtain values for the maximum load, the total extension and the plastic extension to the maximum load. These were then used to calculate the ultimate tensile strength, and the uniform strain.

For early samples, stress strain values were calculated for each curve and the log stress-log strain curves plotted for plastic extensions in order to find the slope, n value of n were also calculated from the equation

$$n = \ln (e_n + 1)$$

where e_n is the linear strain for the onset of necking and the value of n plotted against rolling strain.

TABLE No. 4.2

Sizes of specimens for tensile testing

	Large specimens (first batch)	Small specimens
Gauge length	35 mm	21 mm
Gauge width	5 mm	5 mm
Overall length	95 mm	62 mm
Thickness	Varied with the rolling strain	1 mm

CHAPTER 5

DEFORMATION STRUCTURES PRODUCED BY COLD ROLLING

5.1 Introduction

The results of the structural studies of the four different steel will be presented in this chapter, showing typical micrographs of the substructures developed as strain is increased. Discussion of the micrographs presented here will be presented in chapter 8.

5.2 Quenched and tempered low C steel

As already explained, the heat treatment in this case was designed to produce a structure of ferrite with carbide particles in the grain boundaries, in order to help delineate the boundaries after large strains. Examination of the heat treated structure revealed fairly coarse carbide particles in the grain boundaries as expected and some finer ones within the grains. This was best photographed using a replica technique as larger areas could be shown this way than by using thin foils but at greater resolution than the optical microscope. A typical micrograph is shown in figure 5.1. Occasional dislocations were seen in thin foils.

After rolling to 40% reduction in thickness, transmission electron micrographs of rolling plane sections were becoming difficult to interpret and no really useful information was obtained from them. They showed what could be confused with an equiaxed cell structure, but not very clearly. These broad darker regions moved as the samples were tilted, bringing up dislocation contrast in their vicinity, indicating that the dislocation density was high and fairly uniform.

The structure of foils made from sections cut perpendicular to the rolling plane and along the rolling direction was much more clearly defined, showing approximately equiaxed cell walls, (figure 5.2). Carbide particles could be seen in the grain boundaries, helping to pick them out, and occasional groups of elongated cells with sharper walls were to be found. All these features can be seen in (figure 5.3). Electron diffraction patterns, although like single crystal patterns in some areas, more generally showed splitting of the spots into rings (figure 5.4).

After a rolling reduction of 60%, foils in the rolling plane were again almost impossible to interpret. Transverse sections showed many areas of equiaxed cells approximately 1 μm across and also bands of sub micron wide, sharper walled cells elongated to more than 20 μm. Figure 5.5 shows one such band. The number of cells across these bands varied from 1 to 6. The length of the bands was difficult to determine, but several were traced in the microscope for more than 20 μm before they disappeared into thicker regions of the foils. The carbide particles are often associated with holes when they are in these bands, but these could have been formed during the thinning process. Grain boundaries (delineated by the carbide particles) often showed steps, with the elongated bands running from them as in figure 5.6.

Diffraction patterns in the banded regions were single crystal patterns but show splitting of the diffraction spots, (figure 5.7), indicating rotations across the cell boundaries. Trace analysis of the band directions showed that the sharp elongated cell walls are the traces of {100} planes which in the transverse sections are almost perpendicular to the foils. The bands are not usually parallel to the rolling direction along the length at this stage; rough determinations of the rolling direction obtained by making foils with a cut edge in the rolling direction, indicate that they occur at angles of up to 40° on either side of it. The examples shown in figure 5.6 are traces (101) planes in a $(\bar{1}\bar{1}1)$ foil with the rolling direction as indicated.

For samples reduced by 80% the rolling plane sections are again not very clear. They show cell boundaries becoming sharper, but these are not easily distinguished among Moire fringes and other complicated contrast effects due to multiple layers of cells through the foil thickness. Figure 5.8 is a typical example and its corresponding diffraction pattern is shown in figure 5.9.

Transverse sections were much more clearly defined. The bands of sub micron elongated cells tended to contain more cells across their width and at higher magnification some cases could be found (figure 5.10) in which the very long sharp cell boundaries seemed to result from the lining up of adjacent cell boundaries in crystallograpic directions.

The diffraction pattern is shown in figure 5.11. Small carbide particles, when seen, were always in the cell boundaries and never within the cell centres. Many cells were seen to have acutely pointed ends and small dislocation loops were commonly seen all along the length of the long sharp boundaries in the bands.

After 90% reduction, rolling plane sections are sharper but still not clear. They stay much the same up to 98% reduction, and although some sharper straighter boundaries appear (figure 5.12) the complicated pattern of extinction contours and fringes obscures most of the structure, forcing one to conclude that rolling plane sections are not very useful. A photograph typical of the fringe patterns obtained at higher magnification is shown in figure 5.13 and its typical spotty ring diffraction in figure 5.14.

Transverse section foils of specimens reduced from 90% to 98.5% all showed extremely long 0.1 μm wide cells but did not show twinned electron diffraction patterns. Figure 5.15 is typical of the structure. The bands of elongated cells have become more numerous with increasing strain and the number of cells across each band increased also. The bands have also rotated towards the rolling direction until at the highest strains the structure is almost entirely cells of this type all parallel to the rolling direction. No more information about the boundaries can be obtained even at very high magnifications as seen in figure 5.16. Some ion beam damage can be seen in this micrograph.

If the field is traversed across the elongated cell structures with the microscope set to show the diffraction pattern, the diffraction spots remain the same and simply rotate in their respective rings. This is shown in figure 5.17 a,b, and c, indicating that the mis-orientation across individual cell boundaries is close to pure rotation and while only of the order of 1° to 2° rotations of up to 30° can be obtained over 15 to 20 cells. Sometimes the rotations were seen to change to the reverse direction, indicating that adjacent bands may cause opposite rotations of the crystal structure.

High voltage electron microscopy carried out on samples reduced 40%, 60%, 80% showed similar features to those obtained at 100 kV. Penetration was achieved through thicker specimens as expected and slight improvement in the resolution as seen in figure 5.18, but since no new information was obtained and because of the amount of travelling involved, the increased difficulty of operation and frequent machine breakdowns, it was decided not to continue using this instrument except for the in-situ straining experiments which will be described later.

Specimens made from sections cut perpendicular to the rolling plane and across the width of the strip were also examined for some reductions. They showed elongated cells, which can be seen in figure 5.19 after 60% reduction, in which case the aspect ratio was about 1:6 . Cell walls in all cases appeared to be thicker, but this is presumably due to the fact that they are not parallel to the rolling direction, which comes out of the photograph, and therefore one sees a taper section through the walls. Bands of narrower cells were again seen,(figure 5.20) but in this direction there was no evidence for rotation of the structure across the cells, the diffraction patterns all being single crystal patterns with no splitting of the spots around rings as for the other sections (figure 5.21). The greater thickness of the cells in the bands can also be explained by the fact that they are sections through cells which are inclined to the rolling direction.

The two stage carbon replica technique as described in the last chapter was used to look at larger areas of the samples, in an attempt to trace the grain boundaries, but although the shadowing method used showed up the carbides very clearly, grain boundaries could not be traced at high strains. By 60% reduction (figure 5.22) only grain boundaries which were almost parallel to the rolling direction were still clear. Many grains (or portions of them) had acutely pointed ends and only occassional short segments of grain boundary running across the rolling direction could be found. After 80% reduction it was difficult even to pick out the boundaries which were along the rolling direction and large trails were associated with many of the larger particles and also some of the small ones. (figure 5.23). Shadowing replicas in the direction across these trails cast long shadows from tongues of plastic that had run into them (figure 5.24) showing them to be cracks. This behaviour will be studied further in later work.

Optical microscopy was tried in the early stages, but with only limited success as the microscope was being strained to its limits. Light etching bands were seen in the microscope but were very difficult to photograph. They are similar to the bands that will be shown later in the normalised steel, running right through grains in the early stages and increasing in number with strain. By 80% reduction, grain boundaries are no longer distinguishable and the bands have all rotated into the rolling direction and become very long (figure 5.25). Although not clear in the photographs there appears to be an absence of carbide particles within the bands. Figure 5.26 is an attempt to show these bands by phase contrast.

5.3 Normalised low carbon steel.

The changes in grain shape and behaviour of grain boundaries were best studied at relatively low magnification by optical microscopy. These results will be described first, followed by the detailed study of structural changes and observed in the transmission electron microscope.

After as little as 10% reduction by rolling, light etching bands were again apparent in the optical microscope. Difficulty was experienced in showing them clearly in photographs, but eventually reasonable results were obtained with the aperture closed well down after etching the samples in a fresh saturated solution of sodium bisulphate. While not in all grains they appeared in many (figure 5.27) at approximately 45° to the rolling direction but this angle varied. They were generally only in one direction in a grain, but occasionally two directions were seen. In many cases steps were seen in the grain boundaries with band continuing, but sometimes changing direction in the next grain.

As strain increased the angles of the grain corners which subtended the rolling direction became noticeably more acute, and grains became longer and thinner, with sections tending to be parallelograms as shown in figure 5.28. The bands increased in number and broadened with strain, appearing in more and more grains. By 60% reduction, bands were obvious in nearly all grains at smaller angles to the rolling direction, but still not parallel to it.

Most boundaries running across the rolling direction were now fragmented by intersection with many bands, showing that deformation by shear is associated with the bands (figure 5.29). A plot of the angles within the grains subtending the rolling direction against rolling strain is shown in figure 5.30, each angle shown being the average of 100 angles measured.

After 80% reduction, the 'micro bands' have rotated into the rolling direction and even the grain boundaries parallel to them (if they still exist) cannot be distinguished from them. The structure then remains much the same up to 98.8% reductions.

Photo emission electron microscopy was also tried, but no new information was obtained. A typical photo emission micrograph is shown in figure 5.31 after 60% reduction. It may have been worthwhile to do some dynamic straining experiments in the PEEM but as the screen intensity was low for samples examined at room temperature and the department has no facilities yet for image intensification or videotaping it was decided not to continue with this idea.

By this stage it was becoming obvious that these micro bands were forming as early as 10% rolling reduction, so although the work began as a study of high strain behaviour it was decided to begin the transmission electron studies at low strains in order to find out as much as possible about the early development of the micro bands. It was also decided that only foils transverse to the rolling direction would yield much new information, so all the micrographs from here on are for foils made from samples cut transverse to the rolling plane and along the rolling direction.

After a reduction in thickness of 2%, transmission electron micrographs showed the usual deformation structures, which have been well documented in the past, many dipoles, jogged dislocations, and small vacancy loops, (figure 5.37) and some dislocation clustering into the beginning of cell walls. (figure 5.33)

By 5% reduction the clusters had broadened and fairly large cells of 1 - 2 μm were clearly defined (figure 5.34) in some regions.

Samples reduced 10% showed increasing signs that the deformation was microscopically inhomogeneous, there being considerable differences in the structure. Some regions showed only small amounts of deformation, looking similar to the samples which had been reduced only 2% (figure 5.35), while other areas had obviously undergone further deformation because the cells had become smaller and the boundaries had sharpened a little. Grain boundaries tended to be broad and to contain complex dislocation structures and loops (figure 5.36). Superimposed on the dislocation cell structure, there was another type of boundary which appeared to be crystallographic. They were very straight and many were traced in the microscope for up to 20μm before disappearing into thicker regions of the foil. There were narrow bands of material which had obviously deformed a great deal more, in which parallel groups of these boundaries were seen, (figure 5.37). Separation varied from 0.1 to 0.3μm and after 10% reduction the number of boundaries in a group varied up to about 6. Diffraction patterns showed spots which rotated around rings as the bands were traversed in a similar way to transition bands (59)(77). Misorientations were also evident as contrast changed across the individual walls and by large displacements of extinction contours along the boundaries (figure 5.38).

Although these boundaries were often relatively thick and easy to see, there were cases where they could only be detected by the displacement of the extinction contours which show lines of equal inclination to the electron beam (252). Presumably they form as very sharp boundaries and once formed may thicken as dislocations are stopped by them or become entangled with them. Figure 5.39 shows the displacement of contours which appeared abruptly during a straining experiment in the electron microscope. The bands do not appear to be formed from the initial dislocation cell structure, but occur abruptly, without time resolution, by a shear process. This appears to be similar to the rapid deformation bands reported by Mitchel et.al. (80) in Cu-Al alloys, but may be on a finer scale as bands were observed by interference fringes in an optical microscope.

As the deformation increased, the band structure became more predominant, with bands becoming more numerous and also wider. The boundary separation remained much the same. Some regions, particularly near grain boundaries, took on a 'blocky' appearance (figure 5.40) as though bands had been displaced or kinked sideways in segments along their length. By 60% reduction bands were often 20 to 30 boundaries wide, and intersecting bands in different directions in the same grains were evident. Block shearing was occuring in the material associated with these bands as shown in figure 5.41 by the sideways displacement of one band when intersected by a more recently formed one in another direction. Near the edge of foils it was also common to see displacements in bend contours at the boundaries, helping to show them up. (figure 5.42).

Above 80% reduction the structure does not appear to change, being now almost entirely consisting of these long boundaries. By 80% reduction they all appear to have rotated into the rolling direction or very close to it. The boundaries themselves were very sharp, but close examination of them revealed numerous small dislocation loops along their length. No grain boundaries could be distinguished and may not exist by this stage of deformation.

In situ straining experiments of material rolled to 90% reduction showed the following points

1. Material deforms by boundary sliding.
2. Extinction contours run along individual segments of the structure, often in opposite directions in adjacent parts, indicating changes in relative orientation are occuring.
3. Coalescence of boundaries by the migration of 'h junctions' as seen in the top centre of figure 5.43.

5.4 HVEM Straining experiments

Many samples which had been rolled from 40% to 60% reduction to produce the elongated bands in the structure, were strained in tension within the High Voltage Electron Microscope and several reels of video tape were taken, in order to study the deformation behaviour once formed.

The results show that in addition to the phenomena described above, that frequent block shearing occurs associated with these bands. The process occurs suddenly and very rapidly. Often a band other than the one being observed shears, causing a sudden large displacement of the image, but occasionally it was possible to see the shear occuring. The bands looked the same before and after, with no evidence that a shear has occured. The only thing that shows on the video tape is a sudden rapid movement of two halves of the field of view in opposite directions along the length of the band, sometimes right off the screen. Attempts to slow this down and analyse the tapes frame by frame have failed, as the process is occuring too fast to be stopped on individual frames at the video speed of 15 frames per second. In single frame analysis one sees only the band up till the start of the shear, a very blurred image for 7 or 8 frames and then a similar looking band when the shear is over.

5.5 High sulphur steel.

Examination of this steel in the optical microscope showed that the grain structure was behaving similarly to that of the normalised steel already described, the grains becoming elongated with increasing strain, grain corner angles becoming more acute and grain boundaries showing increasing evidence of breaking up by shear associated with light etching bands. Grain boundaries were again indistinguishable above 80% reduction.

The main difference in the optical microstructures was the behaviour of the manganese sulphide particles. These were slightly elongated at the start, but although they did not change much in the first 30% reduction, by 10% it was becoming obvious that the interface was cracked. This is shown in figure 5.44 by the etching stains. The etchant seeped out of the cracked interface after drying and stained the area near the cracks. This made specimen preparation particularly difficult at higher strains when the cracks were larger and more numerous.

By 30% reduction it was becoming obvious that the manganese sulphide particles were being deformed. They appeared in transverse sections as long thin stringers (figure 5.45), becoming progressively longer and thinner with increasing strain. Above 80% reduction many were beyond the limit of resolution of the optical microscope (figure 5.46).

Etched samples at high strains revealed that there were three types of longitudinal bands as shown in figure 5.47. Long thin MnS particles, long bands of strung out pearlite and, although not very clear in the photograph, there are also numerous light etching bands of the type described earlier. The MnS stringers and pearlite stringers showed many obvious cracks.

Because the earlier electron microscope results using foils from rolling plane sections did not yield much useful information, only foils produced from sections cut perpendicular to the rolling plane and parallel to the rolling direction were studied for this steel.

In the early stages of deformation the structure of the ferrite was little different to that of the first steel. Figure 5.48 shows a typical area after 10% reduction containing the usual jogged dislocations, vacancy loops and the beginning of a cell structure. By 40% reduction occasional long straight boundaries were found similar to those described for the first steel (figure 5.49), but these appeared to be thicker. Regions like the one shown in figure 5.50 were frequently seen also containing extra spots in the diffraction patterns (figure 5.51). The microscope was calibrated using the ferrite spots as a standard and the extra spots were analysed. In each case within the limits of measuring accuracy, they corresponded to lattice spacings of manganese sulphide, the d spacings for which were obtained from an x-ray powder data file. Some d spacings calculated from spots from figure 5.5 are shown in table 5.1 overleaf, compared to the d spacings of manganese sulphide.

TABLE 5.1

calculated d spacings from figure 5.52	d spacings of manganese sulphide
3.015	3.015
2.62	2.62
1.31	1.306
1.06	1.066
0.87	0.8705
0.83	0.8260

The camera constant L was obtained from the 110 ferrite spots on the same pattern, its value is 1.206 Å cm.

Between 40% and 60% reduction there were surprisingly large areas in the foil which seemed to have deformed only a little, looking rather like figure 5.48. Some bands of up to about 8 parallel elongated cells were found (figure 5.52) and often these appeared to have thicker, more tangled boundaries. One very interesting band was found in an area of the foil which was in (113) orientation so that the $(1\bar{1}0)$and $(\bar{1}12)$ slip planes were not perpendicular to the foil but sloping through it at an angle of 65° and 60°. In this case the boundaries could be seen to consist of many hundreds of similar dislocations (fig.5.53). The diffraction pattern with the aperture over a single boundary from this band showed that the mis-orientation across these cell walls is again a small rotation (figure 5.54).

At higher strains the bands of cells became much broader as seen in figure 5.55 after 85% reduction. This micrograph may in fact be of two bands. Another interesting feature of this micrograph is that the broader 'cell' in between the two groups of narrower ones contains what could be the remains of the initial cell structure. Ultimately the structure of the ferrite regions becomes almost entirely elongated cells like the above micrograph.

Long thin manganese sulphide particles running along the boundaries as in figure 5.56 were also very commonly seen. The few in situ straining experiments tried on this steel in the 100 kV electron microscope, resulted in sudden fracture (or separation) of the manganese sulphide-steel interface soon after straining was started. Figure 5.58 shows the same manganese sulphide particle as figure 5.57 after an instability in straining.

5.6 High Sulphur steel with lead.

The structures observed in this steel were on the whole very similar to those of the high sulphur steel, so only a brief description will be given here, concentrating mainly on pointing out the differences in the behaviour of the two steels.

The first difference which was obvious in the optical microscope was the much greater prominence of cracking at the manganese sulphide-steel interface. Even after little or no strain, as in figure 5.58, it was very difficult to produce a specimen for examination which was not very badly stained by etchant seeping out of the cracks. The lead seemed to be present as small almost sub-microscopic spheres.

Unetched the manganese sulphide particles can again be seen to be deformed (figure 5.59), but in this steel they become fragmented. Small lead particles can often be seen at the points of fracture of the inclusions and one particle in the micrograph has lost some fragments during polishing, which illustrates the weakness of the interface. As the strain is increased the particles become increasingly fragmented, producing long strings of broken fragments which can be seen in figure 5.60. At highest reductions the etched structures were similar to the high sulphur steel, showing (figure 5.61) long strings of drawn out pearlite, long thin MnS particles (but not as thin or continuous as the previous case), long light etching bands and small spherical lead particles.

Transmission electron microscopy revealed little difference in the early stages. Figure 5.62 shows the general structure of the ferrite regions after 10% reduction to be the same as the other steel. The only straight band seen at this stage was across a grain corner and is shown in figure 5.63.

From 40% reduction to 60% bands were forming in the structure but the cell walls were always quite thick compared to the sharp boundaries in the normalised steel (figure 5.64). No extra spots were apparent in the diffraction patterns but a small rotation could be measured across the boundaries (fig 5.65).

Great difficulty was experienced in producing foils at higher strains in this material as the specimens kept falling apart prematurely.

Most attempts at electro-polishing generally resulted in the inclusions being polished out before the material was thin enough for examination, followed by rapid growth of the holes. Only a few small areas of specimen were successfully thinned. Figure 5.66 is one such area and appears to be similar to the high sulphur steel.

5.7 Low carbon steel with hard particles.

As mentioned in chapter 3 this steel was heat treated to produce a structure of fine carbide particles in a coarse grained ferrite matrix, in order to study the effect of hard undeformable particles on the deformation behaviour of the ferrite, and in particular, to see if unstable shearing similar to that which was occuring in the normalised steel, could be caused to occur as a result of stress concentration at hard particles.

The starting structure is shown in figure 5.67 in an optical micrograph and more clearly in the transmission electron micrograph of figure 5.68.

After 5% reduction, the optical structure did not seem to have changed very much and the transmission electron microscope revealed only the usual dislocation structures. These were beginning to form tangles and develop into a cell structure, but this was not yet very clear (figure 5.69).

By 10% reduction, although the grain structure did not look different except for slight distortion of the grains, the optical microscope revealed that many long dark streaks had developed. These looked like cracks and could be seen to be associated with the fine carbide particles (figure 5.70). They progressively increased in number with strain and at the same time the grain boundaries began to show signs of breaking up, particularly those that cut across the rolling direction. The structure is shown after 60% reduction in figure 5.71. Above 60% no grain boundaries could be recognised. The optical structure then remained the same right up to the highest strains consisting of the long crack-like streaks, and fine carbide particles in a ferrite matrix, with the streaks becoming more numerous and looking more like cracks as strain increased.

Obviously cracked areas could not be retained in thin foils so attempts were made to show them on replicas. They appeared on all specimens strained to 10% reduction or more and are shown in figure 5.72 to be the same kind of trails as those found in the quenched and tempered steel described earlier.

Scanning electron microscopy was tried also and although not really successful for this application, it did show beyond any doubt that these long streaks were cracks. Figure 5.73 shows one of these after 60% reduction.

Transmission electron microscopy revealed that by 10% reduction there were many straight bands of dislocations associated with the carbide particles (figure 5.74). These increased in number with increasing strain and sometimes appeared to be in groups of long cell-like structures similar to those described earlier (figure 5.75) but many seemed to be in pairs associated with deformation on either side of single particles and many boundaries are quite sharp, as seen in figure 5.76 after 60% reduction. Figure 5.77 shows a rather unique micrograph taken at higher magnification, in which a definite boundary has formed, appearing rather like stacking fault contrast. Displacement of the crystal seems to have occurred leaving some form of boundary sloping through the foil. Dislocations can be seen in the boundary. The diffraction pattern(figure 5.78) shows the foil to have (001) plane parallel to the surface. The direction of the trace of the boundary is [110] which seems to make the boundary in either $(1\bar{1}2)$ or $(\bar{1}12)$ as these slip planes slope through the foil at about the right angle. The $(1\bar{1}0)$ plane also has its trace in the same direction but this is perpendicular to the foil surface.

CHAPTER 6

THE INFLUENCE OF COLD ROLLING ON THE MECHANICAL PROPERTIES

6.1 Introduction

This chapter will present the results obtained from the tensile tests on the materials studied, carried out after various amounts of strain by cold rolling. Discussion of these results will not be entered into here, but will be carried out in chapter 8.

Specimens of the normalised steel tested in the same condition, with variations only in the specimen thickness, showed that there is a specimen size effect, but only for very thin specimens. Specimens of 0.3 mm thickness (the smallest tested) were the only ones to show significant variations. These showed a drop of up to 10% in the U.T.S. and the uniform strain was reduced to about half of its value in thicker specimens. But as almost all specimens were tested above this thickness, the results will not be affected except at the very extreme values of strain and should not influence any of the points discussed.

The results presented will be firstly the unusual features of the load extension curves themselves and variations between the different materials. This will be followed by the results obtained from the curves, with particular emphasis on changes in the strength, uniform strain and work hardening characteristics which occur with increasing strain.

6.2 The load extension curves

The general form of the load extension curves and their variation with strain, is shown in figures 6.1 to 6.5, which compare the curves for each material after various rolling reductions. These are meant to be a guide to differences in shape only and the number of curves included in each case was simply chosen as being sufficient to give the overall trend of the shape changes of the curves which occurred as strain increased.

The curves could in general be divided into several distinct regions, the first of which was the usual region of elastic strain, in which the curves rose steeply up to the limit of proportionality.

This was followed by a region in which the curves showed serations, indicating that heterogeneous plastic strain was occurring. In this region the load increased with a gradually decreasing slope up to the maximum load.

At the maximum load there was a region of uniform strain in which the curves remained flat, further extension occurring steadily with no further increases in load.

At the end of this region a neck usually appeared in the tensile specimen, the load began to fall off and serations appear in the curves again. The load continued to drop with increasing slope until fracture occurred.

Both the serrated region of the curve prior to the maximum load and the flat region at the maximum load, decreased in extent as the rolling strain increased except for the normalised low carbon steel (figure 6.2) in which case the strain to the maximum load and the flat region at the maximum load first decreased with rolling strain up to about 70% reduction and then increased again with further straining, finally falling off again above 90% reduction.

The strain hardening rate, as reflected by the slope of curves up to the maximum load, showed differences between materials, which were most obvious in the unstrained material and specimens rolled only small amounts. Before straining, the slope for the normalised steel decreased only slightly, continuing to rise right up to the maximum load.

Both the free machining steels showed a marked turn over in the curves at the limit of proportionality followed by a slight rise, but then became fairly constant in slope with the load rising only very slowly up to its maximum.

Both the quenched and tempered steel with particles in the grain boundaries and the steel heat treated to have particles in the matrix showed a very high initial strain hardening rate, but the curves quickly levelled out to a constant low slope rising only slowly up to the maximum load.

After about 20% reduction there seemed to be little difference in the behaviour between materials. The curves for each steel turned over and reached maximum load fairly quickly.

The two steels containing fine carbides were characterised at all stages of strain by a very slow fall off in load once necking began, with considerable extension of the specimen occurring after this before fracture occurred. On the other hand the steel containing lead always showed a very rapid drop in load with fracture occurring very quickly after the onset of necking.

6.3 Variation of ultimate tensile stress with strain.

Engineering stress values were calculated for the maximum load values of the load extension curves. Engineering strain was then calculated for the values of extension at which the maximum load occurred and the true stress calculated from the relation:-

$$\sigma = s(1 + e)$$

Where σ is the true stress

s is the engineering stress

and e is the engineering strain.

As the maximum load in most cases was maintained for considerable extensions, it was decided to use the maximum value of extension in each case for the calculation of the Ultimate Tensile Stress. (U.T.S.). From these values, curves of U.T.S. against rolling strain were plotted. These are shown in figures 6.6 - 6.10 and described in detail below.

6.3.1 Quenched and tempered steel

The curve showing the variation of U.T.S. with rolling strain for the quenched and tempered steel is shown in figure 6.6. After an initial rise with a slightly higher slope the curve seems to be linear up to the highest strain investigated with a slope of 187 MPa. There may be a slight fall off in the slope at the highest strain but if so I believe this to be a size effect due to the thinness of the specimens at this stage.

6.3.2. Normalised Steel

The curve of U.T.S. against rolling strain for the same steel in the normalised condition is shown in figure 6.7. The increase in U.T.S. with strain is again linear with a slope of 240 MPa. In this case there seems to be a plateau in the curve between strains of 1.2 - 2 where there is no increase in U.T.S.

6.3.3 High Sulphur steel

Figure 6.8 shows the U.T.S. rolling strain curve for the high sulphur steel. There is a very steep rise at the very early stages of straining but this soon decreases to a linear slope of 140 MPa. There is again a plateau at the same values of strain as for the normalised steel and this is followed by an increase in the slope of the curve to 214 MPa. remaining linear up to a strain of around 3. Above this strain the U.T.S. unexpectedly rose rapidly with further strain to very high values. The slope of the curve in this region is 1428 MPa.

6.3.4 Steel with Sulphur and Lead.

The U.T.S. rolling strain curve for this steel (figure 6.9) again shows an initial steeper rise, quickly changing slope and becoming linear with a slope of about 95 MPa, which is retained up to strains of about 2. Above this strain there is an increase in the slope, but not as steep as the previous steel and not to such high values of U.T.S. The slope in this region is 300 MPa.

6.3.5 Steel with fine carbide dispersion.

The U.T.S. rolling strain curve for this steel is shown in figure 6.10. There appears to be a very slight drop in the U.T.S. after very small strains followed by a rise similar to the other steels. The curve then remains linear up to strain of around 3 after which it levels off. The slope of the linear portion is in this case 166MPa.

The slope of the linear regions of the curves are collected together in table 6.1 for ease of comparison.

6.4 The Work Hardening Modulus

If a family of tensile curves for a given material are each drawn at their own true rolling strain and a curve drawn to envelope them, the gradient of this curve will give the rate of increase of stress with strain for the overall rolling process. This gradient is the work hardening modulus m and is given by the expression:-

$$m = \frac{d\sigma}{d\varepsilon}$$

The value of m for the various steels studied is therefore given by the gradient of the curves for U.T.S. against strain shown in figures 6.6 - 6.10.

As it is usual to rationalise values of m by dividing by the shear modulus of the material, values of $\frac{m}{G}$ have been calculated and included in table 6.1. The values of the shear modulus G used (257) were as follows:-

For EN8 $G = 8.26 \times 10^4$ MPa

For EN3B $G = 8.26 \times 10^4$ MPa

For free cutting steel with sulphur $G = 8.12$ MPa

No value was available for a steel containing sulphur plus lead so the same value was used as for the steel with sulphur only.

Steel	Range of rolling strain	Slope (MPa)	$\frac{m}{G}$
EN 8 (Quenched & tempered)	0.4 - max.	187	2.26×10^{-3}
EN 8 (Normalised)	0.3 - 1.2	240	2.90×10^{-3}
	1.2 - 2	no rise	
	2 - max.	240	2.90×10^{-3}
Free cutting (Sulphur)	0.2 - 1.2	140	1.72×10^{-3}
	1.2 - 1.6	no rise	
	1.6 - 3	214	2.63×10^{-3}
	3 - max.	1428	17.58×10^{-3}
Free cutting (Sulphur + lead)	0.5 - 2	95	1.17×10^{-3}
	2 - max.	300	3.69×10^{-3}
EN 3B (Carbide dispersion)	0.3 - 3	166	2.04×10^{-3}
	3 - max.	levels off	

TABLE 6.1

6.5 Variation of Uniform Tensile Strain.

The maximum extension to the maximum load was measured from the load extension curves. These values were then converted to true strain by the relationship:-

$$\varepsilon = \ln \frac{l_i}{l_o}$$

Where ε is the true strain

l_i is the extended gauge length at the maximum load

and l_o is the original gauge length

Curves of total strain up to the U.T.S. (uniform strain) against rolling strain were then plotted and are shown in figures 6.6 - 6.10 as detailed below.

6.5.1 Quenched and tempered steel

Figure 6.6 shows the plot of uniform strain against rolling strain for this material. Although no specimens of this material were tested at very low rolling strains, it appears that the uniform strain drops very quickly with the introduction of strain into the samples and then decreases slowly with a gentle change of slope, until it becomes fairly constant after strains of about 2.5. The value of the uniform strain after large rolling strains is quite small.

6.5.2 Normalised steel

The same steel in the normalised condition, shows the initial large drop in uniform strain as rolling strain begins. (figure 6.7). After a further slow fall to rolling strains of around 1.0 the uniform tensile strain begins to slowly rise again and peaks after a rolling strain of 2.3 before falling again to a constant low value at strains above 3.5. There may be a smaller peak between strains of 1.5 - 2 but this needs further checking.

6.5.3 High sulphur steel

The uniform tensile strain-rolling strain curve for this material is shown in figure 6.8. In this case the initial abrupt drop in uniform strain with the introduction of rolling strain is not down to quite such low values as for the normalised steel, but falls of to about the same value by a rolling strain of around 0.9. After this it is fairly constant, although there may be a slight rise in the region of the peak in the normalised steel curve. It is as though the peak in the normalised steel curve is occurring at much lower strains, appearing in this case as strains less than 0.5.

6.5.4 Steel with sulphur and lead

The curve showing the variation of uniform strain for this steel (figure 6.9) follows the form of that for the high sulphur steel, the only difference being that the slightly higher values at strains up to 0.5 are not as great in this steel.

6.5.5 Steel with fine carbide dispersion

Figure 6.10 shows the uniform strain curve for this steel. A few specimens of this steel were tested at very low rolling strains, so it can be seen just how abrupt the initial drop in uniform strain is. The values up to a rolling strain of 1 are a bit erratic but seem to fall slightly between 0.5 and 1. The values then seem to remain fairly constant up to strains of about 3, although there may be a slight rise occurring between strains of 1 and 2.3. Above strains of 3 the uniform strain seems to rise significantly.

6.6 Strain hardening exponent n and strength coefficient k

In the early stages, the tensile tests carried out on the normalised steel were analysed assuming that the Hollomon equation $\sigma = k\varepsilon^n$ was satisfied for the material. Plots of log σ against log ε taken from each curve in the uniform plastic strain region did in fact give reasonable straight lines and are shown for various rolling strains in figure 6.11.

The strain hardening exponent n as given by the gradient of these curves has been plotted against rolling strain in figure 6.12.

The strength coefficient k is the stress at a strain of 1 (log $\varepsilon = 0$). This has also been obtained from the curves by extrapolation and plotted against rolling strain in figure 6.13.

Since, as pointed out in section 2.5.2, the strain at which necking begins should be numerically equal to the strain hardening exponent, i.e. $\varepsilon_u = n$ then the uniform strain curves shown in figures 6.6 - 6.10 should also represent the variation of the value with rolling strain. Comparing figure 6.7 with figure 6.12 shows in fact that although the numerical values are a little different, the shape of the curves are the same, showing the initial sharp drop, a gentle rise turning over at strains of about 1.5 and a larger peak at higher strains, so that the trend of the behaviour can be obtained.

Also comparison of the k against rolling strain curve in figure 6.13 with the U.T.S. rolling strain curve in figure 6.7 both of which give a measure of the overall strengthening effect, the shape can again be seen to be similar, showing a rise and a plateau, followed by a further rise in strength at higher strains. The discontinuities in each case occurred at about the same strains.

Which numerical value of n is correct is hard to say, because both methods of obtaining the values contain difficulties. For the Hollomon analysis the difficulty was to get enough points from the tensile curves at high rolling strains when the tensile strains were only small and in the estimation of the line of best fit through them , since a small shift in the slope of the line drawn markedly affected the value of n. For values of n obtained from the uniform strain, the problem was that the maximum load was maintained over a range of extension, causing confusion as to which value of extension should be used for the strain calculations.

Because of recent criticism of the Hollomon approach as outlined in the literature survey, and because the most important part of this project is not in absolute values, but in comparing the trends in behaviour with the microstructure, the Hollomon analysis was not pursued further, as the trends of behaviour can be obtained more easily from the U.T.S. curves and the uniform strain curves.

CHAPTER 7

RESULTS OF FRACTOGRAPHIC ANALYSIS

7.1 Introduction.

It was noticed during the tensile testing that there were visible changes in the appearance of the fracture surfaces of some tensile specimens and that this generally coincided with changes in the mechanical properties at particular values of rolling strain. This led to the examination of all the fracture surfaces by scanning electron microscopy.

The results of these investigations will be presented in this chapter along with the results of fractography carried out on machining chips of the same materials which were broken at liquid nitrogen temperature.

The chapter will conclude with the results of electron probe micro analysis, which was carried out on the fracture surfaces.

7.2 Fractography of the quenched and tempered steel.

The as heat treated specimens and those strained to reductions of up to 45% all appeared to fracture by a cup-cone mechanism as described in section 2.8.2, exhibiting a central region normal to the tensile axis with equiaxed dimples and outer shear zones sloping at 45° to the tensile axis (figure 7.1) The nature of the fracture surface in these regions can be seen more clearly in figures 7.2 and 7.3. At higher strains the appearance of the fractures changed and the mechanism changed to the double cup mode described in section 2.8.2. Failure occurred in a shear plane at 45° across the neck with a central cavity developing as shear progressed. (figure 7.4). The central cavity portion of the fracture consisted of equiaxed dimple type fracture as in figure 7.5 and the outer shear surface is shown in figure 7.6.

Above 60% reduction although still failing by a double cup mechanism, changes are occurring in the central zone. In many places several of the dimples can be seen to be coalescing to form large cracks parallel to the rolling plane as in figure 7.7.

By 80% reduction the double cup mechanism is still in operation but the fracture now looks almost like a shear fracture.

The bulk of the fracture surface is now elongated dimples of the kind shown in the outer zones of the earlier fractures, but there is still a central cavity in which there are one or more large cracks parallel to the rolling plane (figure 7.8). The surface of these shows very long shallow dimples parallel to the rolling firection (figure 7.9) .

The fractures usually slope at about 30° across the width direction and the shear dimples in the outer zones are elongated at an angle instead of straight out towards the surface along the 45° slope.

Above 80% reduction there is no further change in the fracture behaviour. All specimens up to 98% reduction looking similar.

7.3 Fracture behaviour of the normalised steel.

Samples of the same steel in the normalised condition which had been reduced less than 60% by rolling failed by the cup-cone mechanism, which was slightly modified because of the sheet nature of the specimens.

The two halves of the specimen were generally concave and convex across the thickness direction showing relatively equiaxed dimple fracture in the centre and shallower elongated dimples in the sloping shear zones toward the edges.

Figure 7.10 is a view across the thickness of a tensile specimen which had been reduced 60% in thickness by rolling. It shows the distinct zones across the thickness. In the specimen width direction the fractures were not perpendicular to the tensile axis but sloped at around $30\text{-}35^{\circ}$. The shear component in this direction can be seen in the fact that the elongated dimples in the shear zones do not run straight out the shear face toward the specimen surface but are inclined across the width. Also, the relatively equiaxed dimples in the central zone are slightly elongated in the width direction.

All specimens which had undergone less strain than the first peak in the uniform strain-rolling strain curve (figure 6.6) showed cup-cone fracture behaviour, but from 60% to 80% reduction the size of the equiaxed dimple region decreased and the sloping shear zones increased. Around 80% reduction (corresponding to the first peak in the uniform strain curve) the central zone disappeared and the fractures exhibited the shear type mechanism described in section 2.8.2, showing only elongated shear dimples (figure 7.11).

The fracture surfaces were inclined at 45° across the thickness direction and at about 30° - 35° across the width. The shear dimples were aligned in the maximum slope direction. Sometimes the fractures consisted of several intersecting planes as in figure 7.12.

In the region of the larger peak in the uniform strain curve, after about 90% reduction, the fracture mechanism was somewhere between a shear mechanism and a double cup mechanism. Large cavities formed steps in the fracture surfaces as in figure 7.13. The areas in between the steps tended to show an approximately equiaxed dimple structure like the centre of a double cup fracture, but in some cases these were shear type fractures occurring on intersecting planes as in figure 7.14, in which case the dimples were shallower and elongated up the shear faces. The relatively smooth step faces (figure 7.15) appeared like large cracks in planes parallel to the rolling plane, the surfaces of which seemed to be made up of very shallow dimples similar to those in the central cracks of the quenched and tempered specimens. It appears as though very deep cavities have formed in the rolling direction and coalesced into cracks in the rolling plane.

Taper sections of the fractured specimens, produced as described in chapter 4 in order to relate the steps in the fracture surfaces to microstructural features such as grain boundaries were not overly successful. It was not possible to distinguish the finer features of the microstructure, but it was possible to see that the step faces were usually associated with ferrite regions (figure 7.16) and also noticeable that the cavities making up the equiaxed dimple structure were very much deeper than one imagined by looking at the fracture surface (figure 7.17).

Fractures consisting of thin regions of equiaxed cavities separated by cracks parallel to the rolling plane, persisted up to the highest strains investigated.

7.4 Fracture behaviour of the high sulphur steel.

The first difference in the fracture behaviour of the high sulphur steel, was that the low strain specimens did not fail by the same cup-cone mechanism as did the earlier steels.

The fractures consisted almost entirely of relatively equiaxed cavities, some of which were very deep and had formed around elongated manganese sulphide particles (figure 7.18). In the thickness direction, fractures were normal to the surface of the specimen and there were no shear zones at the edges. In the specimen width direction, (parallel to the rolling plane) the fracture surfaces tended to slope at 30° - 35° and in many regions the cavities could be seen to be elongated in this direction (figure 7.19).

Above 60% rolling reduction shear zones developed at the outer regions of the specimen sloping at 45° through the thickness direction. Figure 7.20 shows that rather than elongated dimples, these tended to be thin areas of equiaxed dimples separated by surfaces parallel to the rolling plane, in which many fragmented manganese sulphide particles could be seen. The fragmentation could have occurred during the fracture process. At this stage the fracture could be described as occurring by the cup-cone mechanism, but as strain increased there was a gradual change to the shear mechanism, generally beginning at one side and progressing across the width of the specimen. By 80% reduction about half of the specimen was a 45° shear fracture, and by 90% reduction the specimens were entirely shear failure, looking rather like the end of a wood chisel. (figure 7.21). Again the fracture surface was not straight up the slope, but a series of steps with the actual fracture zig-zagging from normal to the rolling plane, where it was equiaxed cavities, to parallel to the rolling plane, where the surface could be seen to result from the joining up of many long cavities as shown in figure 7.22. Much of the surface appeared to be covered with thin manganese sulphide particles, made visible by the fact that they were beginning to break up. This fracture mode continued right up to the highest levels of strain.

7.5 Fracture behaviour of the steel with sulphur and lead.

At low strains the shear zones again seemed to be suppressed by the manganese sulphide particles, but not to the same extent as when no lead was present. In the thickness direction the edges did show shear zones at least over part of the specimens. In these regions the cavities were quite long as seen in figure 7.23 and contained many fragmented particles of manganese sulphide.

Fractures generally sloped across the width direction at about 30° indicating shear components in this direction and in the centre region of the specimens the fracture surface was a mixture of equiaxed cavities and cavities elongated in the width direction as shown by figure 7.24.

By 40% reduction fractures had changed at least partly to shear at 45° through the thickness and by 60° were again like the point of a wood chisel, although some specimens had a shear component across the width direction causing a slope of the fracture surface in this direction of above 30°. Fractures were similar to this up to the highest rolling strains and in this case also, showed a series of steps made up of thin equiaxed cavity regions separated by surfaces which were parallel to the rolling plane (figure 7.25). These again appeared to be covered with thin manganese sulphide particles over a large proportion of their area, but this was much more fragmented than when no lead was present.

7.6 The steel with a fine carbide dispersion

The as heat treated specimens of this steel failed by a cup-cone mechanism, producing a fracture surface which was concave-convex through the thickness direction and inclined at about 30° in the width direction. The dimples on the surface were much smaller in this case than for the other steels, presumably because of the large number of inclusions at which they can be initiated. The central region and the sloping side regions can be seen in figures 7.26 and 7.27.

After strains as little as 5% reduction, although the fracture mechanism seemed to be the same, many of the fine cavities could be seen to be coalescing to form larger cavities as shown in figures 7.28 and 7.29, forming sheets of cavities parallel to the rolling plane.

From 10% to 20% reduction there was an increase in the amount of shear, as specimens changed gradually to the shear mode of failure, often on intersecting planes as seen in figure 7.30. The shear surfaces were again a series of steps up the slope as in figure 7.31, with equiaxed cavities normal to the rolling plane and surfaces made up of coalesced deep cavities parallel to the rolling plane.

Strangely, the shear mode changed again and by 30% reduction specimens were beginning to show a double cup fracture mode as described in section 2.8.2. Figure 7.32 shows an overall view. Many cavities could be seen to have coalesced into cracks parallel to the rolling direction as in figure 7.33.

This double cup fracture mode persisted up to the highest rolling strains. Most fractures sloped at about 30^{o} across the width showing a component of shear in this direction and across the thickness there were occasional areas of shear on intersecting planes, particularly around 60% reduction when the fractures seemed to be part shear and part double cup. Above 60% reduction the fractures were still of the double cup mode, but the central cavities had coalesced into one or more large cracks parallel to the rolling plane.

7.7 The fracture behaviour of machining chips

For all the materials, fracture surfaces of machining chips broken at liquid nitrogen temperature showed extensive regions which were not cleavage and which had therefore formed during the machining process.

The fracture surface in these regions exhibited ripples running perpendicular to the shear direction and angular changes could be seen in the surface along the shear direction giving the appearance of grain corners. A typical region from a chip of the normalised steel is shown in figure 7.34.

Such fracture surfaces have been observed before and have been termed 'stretch zones' by Doyle (258)

Both the proportion of the fracture surface which was made up of these stretch zones and the width of the individual rippled portions varied from steel to steel. In the two free machining steels, the fracture surfaces were dominated by large broad rippled regions as in figure 7.35, often looking as though the process causing them was occurring on different levels similar to a cleavage fracture, with the different levels joining up by ductile fracture. Chips of the quenched and tempered steel and the steel with a fine carbide dispersion also showed fracture surfaces with a large proportion of stretch zones, but in these two cases the individual rippled areas were much smaller and more numerous as seen in figure 7.36.

7.8 Comparison of machine chip and tensile fractures.

At first it was thought that the stretch zones were regions of intergranular fracture because of the angular, grain corner appearance of some parts of the surface, but this posed a problem as to why they should be smaller and more numerous in the steel with the fine carbide dispersion, since this had the largest grain size.

The first clue to their real origin came while looking over photographs of some of the tensile fracture surfaces, when it was noticed in many of the higher magnification photographs that the interior surface of cavities formed around inclusions was rippled. This is shown in figure 7.37 for cavities around manganese sulphide particles in the centre of a cup-cone fracture of the high sulphur steel after 10% rolling strain. It can be seen more dramatically in figure 7.38 which is a shear zone of a fracture in the same steel after a greater amount of rolling strain, in which case several cavities have coalesced to form an angular rippled surface similar in appearance to the stretch zones in the machine chip fractures. Similar features on a finer scale were seen in the steel with a fine carbide dispersion and can be seen in the photograph which appeared earlier as figure 7.29. The same thing in the quenched and tempered steel is shown in figure 7.39 which looks down a shear face in the specimen which had undergone 60% rolling strain.

Thus it appears that the stretch zones in the chip fractures may form during the planar shear by the coalescence of cavities formed around inclusions. Further discussion of this will appear in chapter 8.

7.9 Electron probe micro analysis.

Close examination of the stretch zone surfaces of the two free cutting steels indicated the possibility that like the tensile fractures after large strains, much of the surface may be covered with a thin layer of manganese sulphide (see figure 7.40).

Electron microprobe analysis was tried in order to confirm this and also check the possibility of a lead smear on the surface in the case of the steel with sulphur and lead. This was carried out within the scanning electron microscope using a Link X-ray energy analysis system.

Figure 7.42 is a chart showing the characteristic X-ray spectrum from the ferrite matrix of a polished sample of the high sulphur steel, taken for comparison with the spectrum from a stretch zone surface in the same steel. Many stretch zone surfaces were tried and each yielded spectra identical to the one shown in figure 7.43, which shows strong peaks corresponding to manganese and sulphur in addition to the iron peaks from the ferrite. A similar spectrum (figure 7.44) was also obtained from shear surfaces in the tensile fractures after high strains, such as that shown in figure 7.22, showing that both the fractured machining chips and also the tensile specimens after high rolling strains do have shear surfaces which are covered over much of their area by a thin layer of manganese sulphide.

Similar experiments were carried out for the steel with sulphur and lead additions. In this case, as can be seen in figure 7.45, there was the further addition of a lead x-ray peak which was not present in a standard spectrum taken from the matrix of that material. The scale was changed in this case in order that the lead peak could be included on the chart. It was not possible to determine by these simple experiments whether the lead in the stretch zones was present as a smear over the surface, as tiny particles, as lead sulphide or as a complex lead iron sulphide. However, spectra from manganese sulphide particles in both of the free cutting steels before straining were identical (figure 7.46) and did not contain a lead peak, so the possibility of the lead in the stretch zone spectrum being a complex sulphide seems to be ruled out.

Spectra taken from stretch zones in the steel with fine carbides, the normalised steel and the quenched and tempered steel did not show the manganese and sulphur X-ray peaks. The spectra in each of these cases were identical to the spectra of the ferrite matrix.

The fact that a large area of the shear surfaces of the two free machining steels were covered with manganese sulphide was also confirmed by deeply etching both fracture surfaces and machining chips in 20% nital. An example is given in figure 7.41, which shows many flattened manganese sulphide particles in the deeply etched front surface of a lathe turning from the high sulphur steel.

CHAPTER 8

DISCUSSION OF RESULTS

8.1 Introduction

In this chapter the effects of increasing amounts of deformation on the structure, mechanical properties and subsequent fracture behaviour of the individual steels will be discussed.

The variation of mechanical properties with strain will be interpreted for each case in terms of the changes in microstructure which have been observed and where potentially useful improvement in the properties occurred. The discussion will be more detailed.

Significant features of the progressive structural changes occurring, about which little is known, will also be discussed at greater length, with a view to obtaining a more comprehensive understanding of the mechanism by which deformation occurs and the way in which this affects subsequent fracture.

Throughout the discussion comparisons will be made of the results for the various steels, in order to glean more general information as to the affects of manganese sulphide and lead particles on deformation and fracture, both during machining and also during bulk deformation and the affect of hard particles, such as carbides, dispersed throughout the structure.

8.2 Anisotropy of cold rolled substructure.

Before beginning to relate the changes in properties which occur with increasing strain to the observed microstructures, it is necessary to mention a few points relative to the early attempts to examine the sub-structure in foils prepared from rolling plane sections.

From a simple consideration of the geometry of the rolling process it is obvious that the maximum shear stress is in planes which are parallel to the rolls and inclined to the rolling direction. If the events occurring in these planes during the early stages of rolling are to be studied, it becomes essential to use thin foils cut from sections which are perpendicular to the rolling plane and along the rolling direction, because rolling plane sections will only show the little bit of structure in the inclined

shear planes which happens to lie along the line of intersection of the shear planes and the rolling plane. The most informative structures will therefore not be seen in such sections in any great detail.

After large rolling reductions, the substructure developed has long been known to be inhomogeneous with respect to the shape, size, and alignment of the cells (64)(65)(67)(68), but information on the distribution of cell dimensions for the three principal directions in rolled steel sheet has only recently been made available for the first time. Although not for the same steel as used in the present work, Willis (259) has shown a size distribution as follows:-

In the rolling plane parallel to the rolling direction

(cell length) 0.3 to 27 μm

In the rolling plane perpendicular to the rolling direction

(cell width) 0.2 to 5 μm

Perpendicular to the rolling plane

(cell thickness) 0.05 to 1.4 μm

This suggests that after rolling, a large proportion of the cell boundary area will lie in the rolling plane and that thin foils from rolling plane sections will contain large areas of cell boundary. Looking through these cell boundaries will be confusing, because a high dislocation density in a thin boundary plane could easily be interpreted as uniform high dislocation density and also because any misorientation between the cells above and below and boundary will introduce Moire fringes to complicate the interpretation of the structure. Even worse, the very small thickness of the cells makes it possible that observations would be through multiple cell boundaries.

The present results, which will be discussed in more detail later, show that long cell like structures having sharp boundaries which lie in slip planes inclined to the rolling direction do form during deformation and that these rotate into the rolling plane as strain increases.

For the reasons given above, these most interesting results would not have been seen if, as in a considerable amount of previous work, observations had been limited to those from foils cut from rolling plane sections.

Although a lot easier to produce, such foils did not yield much in the way of useful information. The straight boundaries in figure 5.12 are examples of what could be sections through cell boundaries which are inclined through the foil and figure 5.13 shows the type of fringe patterns which confuse the interpretation of the structures when rolling plane sections are used.

For the remainder of this discussion, except where specific mention is made otherwise, the structures considered will be those observed in foils from sections perpendicular to the rolling plane and along the rolling direction.

8.3 Structure Property Relationships

8.3.1 The quenched and tempered steel

The essential changes in mechanical properties with increasing strain, as seen from figure 6.6, are that the U.T.S. increases linearly with strain with a slope of 187 MPa except in the very early stages when the rate of increase is higher, while the uniform tensile strain drops very rapidly and then decreases only slowly with a gentle change of slope, becoming constant at quite small values after higher rolling strains.

The rate of strain hardening (with respect to strain), or work hardening modulus $\frac{d\sigma}{d\varepsilon}$, given by the gradient of the U.T.S. strain curve, appears to be constant over most of the range of strains for this steel.

It is important to distinguish this from the strain hardening exponent n, since confusion often arises in discussions because of the similarity of the terms. From the definition of n (260) the two are related by

$$n = \frac{d(\log \sigma)}{d(\log \varepsilon)} = \frac{d \ln \sigma}{d \ln \varepsilon} = \frac{\varepsilon}{\sigma} \frac{d\sigma}{d\varepsilon}$$

or

$$\frac{d\sigma}{d\varepsilon} = n \frac{\sigma}{\varepsilon}$$

As seen in section 2.5.2 the value of n is used as a measure of the capacity of a material to undergo further plastic deformation because of Considere's construction (see ref.131) showing that it is numerically equal to the strain at which necking occurs.

Therefore the curve in figure 6.6 showing the variation of uniform strain with rolling strain shows that the capacity to deform further (in tension) falls to quite small values after only small amounts of deformation by rolling, then falls only slightly with increasing strain, becoming relatively constant.

This emphasises the limited usefulness of pure tension for the reduction and elongation of metals, as even at the highest value of n for a metal, which is about 0.5 (260), neck free straining could hardly exceed 60%.

Considerable detailed knowledge of the structure of iron in the early stages of plastic deformation has been obtained from thin foil electron microscopy and has been reviewed many times (53)(63), so rather than spend time discussing what is already known, I intend only to briefly compare my results and get on fairly quickly to the lesser known events occurring at higher strains.

In similar work to this on F.C.C.metals (1)(2) and much work on theories of strain hardening (261), initial rapid increases in strength and decreases in uniform strain have been attributed to the rapid multiplication of dislocations, interaction of these in different slip systems, the formation of dislocation tangles and the development of these into a cellular network. Initial strengthening then, is by an alteration of the structure to one through which dislocations can move only with increasing difficulty, moving only short distances through the cells before joining the tangles in the cell walls.

Since no specimens of the quenched and tempered steels were tested or examined at very early stages and similar ferrite structures and mechanical properties were obtained in the other steels, necessary points concerning the very early stage structures will be made later. The structures of this steel at the earliest stage which was examined (fig. 5.2) did show mostly the normal equiaxed cell structure with tangled dislocations in the walls, indicating that the initial changes in properties probably are attributable to the above structural changes.

At higher strains, it appears that the rate of strain hardening, in agreement with other work on iron and pure B.C.C. metals (67), is constant and does not diminish significantly up to the highest strains investigated.

It has been suggested that once the cellular substructure is formed, its size becomes the dominant factor contributing to the strengthening which occurs as strain continues (67)(68) (1)(2).

As mentioned in section 2.5.3, investigators have tried to relate the change in low stress to a change in cell size $\bar{d}$ by a relationship analogous to the Hall-Petch relationship (136)(137) for grain size strengthening of annealed metals:-

$$\sigma_F = \sigma_o + k\bar{d}^{-\frac{1}{2}}$$

where in this case $\bar{d}$ is the mean linear intercept between the cell walls in the transverse sections.

Although not entirely unsuccessful, confusion has arisen as to the correct value of the cell size exponent.

Since this approach was not tried in the present work and argument regarding this is given elsewhere, it is only necessary here to make a few comments because of the structures observed.

The cell size does appear to be the dominant factor contributing to the strengthening, but not by a gradual, uniform reduction in size. The final structure consists of thin ribbon like 'Cells' (figure 5.15), both in this case and also in the later steels, but these formed in small groups of 'microbands' within the more general equiaxed cell structure. The formation of these bands, the nature of the boundaries, the orientation differences across them and the behaviour during subsequent deformation will be discussed in more detail later, but as the number of bands and their width (the number of cells across them) increase as straining continues, the increase in strength may be related to the proportion of the total volume occupied by microbands of this type.

At very high strains the ribbon like cells, which now occupy almost the total volume, remain approximately constant in size and it may be that a balance between cell reduction and dynamic recovery by coalescence as discussed by Langford and Cohen (67) is taking place.

Although in some cases it looked possible that the long ribbon like cells could be forming by elongation and coalescence of the original equiaxed cells together with a sharpening of the boundaries (figure 5.10), it did not look as though this was occurring in general, since many of the thin cells were far too long to have resulted from elongation of the original cells and seemed to cut right through them.

Many of the thin cells contained carbide particles (figure 5.5) making it possible that their formation was associated with stress concentration around cabide particles. Even at quite high strains (figure 5.16) some long cells still appeared to be in small groups or even single and these could possibly be associated with carbide particles, or other points of stress concentration. This will be discussed in greater detail later when dealing with the steel having a fine carbide dispersion within the ferrite, as these experiments were designed to check this.

Original grain boundaries should also contribute to the increase in strength, since as grains are reduced the decreasing boundary separation in the thickness direction is an effective reduction in grain size.

Despite the fact that this steel was first used in this condition in order that the carbides would delineate the grain boundaries, they could be detected only with difficulty and were often stepped when intersected by bands of ribbon like cells (figure 5). Above 60% they were not detectable at all. It seems they are either completely broken up by shear, or are indistinguishable from the ribbon like cell boundaries. Langford and Cohen (146), after their misorientation measurements at high strain, suggest that the ribbon like sub-grain boundaries behave like high angle boundaries at high strains.

It was also observed in this steel, and measured in later work for the normalised condition of the same steel (figure 5.30), that grain boundaries which lie across the rolling direction rotate about the triple points during strains of up to 0.9 (60% reduction). For this case and also in the steel with dispersed carbides which will be discussed later, the carbide particles may resist this and in doing so also contribute to the strength.

So while I believe that there is a grain boundary contribution to the increasein strength at least up to strains of 60%, it is difficult to apportion and probably varies with orientation difference as the resistance to shearing will also vary with this (111)(112). For reasons that will become increasingly clear as this discussion continues, I do not believe that the original grain boundaries still exist as such above about 60% reduction.

While the impression gained from the U.T.S. curve is that the rate of strain hardening is constant, it should be emphasised that this is the overall microscopic effect.

The heterogeneous nature of the microstructures and particularly the serrations in the individual load extension curves between the beginning of plastic deformation and the U.T.S. suggest that microscopically, the deformation is far from uniform and the rate of strain hardening far from constant.

Serrations of this type appeared in all the steels tested and will therefore be considered only briefly here, their cause being taken up in a more general discussion later.

Their shape indicates that the load repeatedly stops rising, remains constant for a short time and then begins to rise again, the horizontal segments of the curve becoming progressively longer as the U.T.S. is approached.

As mentioned in section 2.2.2, serrations in stress strain curves can be caused by mechanical twinning, but no twins have been observed in the present work.

In similar work to this on an Al-5% Mg alloy, Nuttall (2) explained serrations in the stress strain curves in terms of the repeated locking and unlocking of dislocations by solute atoms, similar to the Portevin-Le Chatelier effect found in Al alloys at high temperatures.

He related the behavior to the fact that high vacancy concentrations in strained material allow rapid migration of the solute back to unlocked dislocations, similar to explanations of the Portevin-Le Chatelier effect, where rapid migration of the solute is made possible by the vacancies present at high temperatures.

While arguments similar to this could possibly explain the serrations observed in these steels, I believe these serrations to be an indication that the state of uniform strain is giving way to one in which the straining is localised.

In general, instability of plastic flow can vary widely, from necking in tension at one extreme, through some intermediate level in various kinds of shear band developement, to slip band formation at the other extreme. The origin also varies, from a purely mechanical reason in necking, to reasons much more within the material.

If the serrations are due to localised straining, then this should show up as local changes in microstructure and since localised formation of bands of ribbon like cells is observed and these become more numerous with increasing strain, it is a reasonable assumption that localised straining is associated with the formation of these bands, or is occurring within them once they are formed.

The serrations in the load extension curves can therefore be interpreted as being due to microscopic variations in strain hardening, the condition for their appearance after any amount of prior straining being that somewhere in the material the next increment of strain-induced hardening is cancelled out by a local strain-induced softening. Further straining taking place in the region where resistance to continued flow is lost.

The flats in the load extension curves (figure 6.1) at the U.T.S. could be an extension of the phenomena causing the serrations. Local unstable deformation could be becoming more general (at least in tension) once sufficient microbands are produced in the structure to allow more general deformation to occur by the same mechanism. This will also be taken up later in the discussion.

Since the more extensive deformation in this steel after on onset of necking than in the normalised steel and the free cutting steels is probably due to differences in the fracture process, this will be more conveniently dealt with after discussing the fracture behaviour, and when comparing the results of the other steels.

The fracture behaviour will also only be briefly covered at this point, concentrating on features which are different from those in the other steels.

The cup-cone mechanism operating initially and after strains of up to 45% is well documented and explained as seen in section 2.8.2. But in this case there is a noticeable difference in the depth of the cavities. In fact both the centre portion (figure 7.2) normally described as voids or equiaxed dimples and the outer shear faces (figure 7.3) normally described as elongated dimples, appear to be transverse sections and steeply inclined sections through the same deep cavities with their axis in the rolling direction.

At later stages of strain, although the appearance of the fracture changed (figures 7.4 & 7.8), the same deep cavities were evident (figures 7.5 & 7.6) and each different mode was basically a different path of separation through the same deep cavities.

The sloping shear faces were interesting in that normally the appearance of elongated dimples is explained (262) as shown in figure 8.1 in terms of the spreading out of voids in the shear direction, but in this case there was a definite resistance to sideways shearing of the cavities and separation occurred by cutting through them in the shear plane (figure 8.2).

Since after rolling, the uniform strain during tensile testing is quite small, I believe that the very deep cavities must originate during the rolling process. This idea is supported by the replica studies on deformed surfaces, as seen in figure 5.23 and many more micrographs which space would not allow me to include in this dissertation.

Thus the cup-cone fractures begin in the centre by necking down of the walls between long cavities produced during the rolling process.

A central cavity develops and deformation in the outer regions is concentrated by the notch effect of this cavity into planes at approximately 45° in the normal way. The fracture still extends by necking and separation of the cavity walls, but changes direction and develops a step like appearance between cavities (figure 8.2) as it travels in a zig-zag path along the direction of higher stress, alternately as longitudinal and transverse rupture through the cavity walls.

After higher rolling strains the central region of the fracture becomes proportionately smaller, possibly because higher shear stress (due to the increased strength of the material), causes the fracture to break out in the shear plane before the central cavity can extend far. It extends longitudinally slightly and then breaks out on a shear plane, causing a 45° fracture with a double cup in the centre (figure 8.3). The single shear plane could arise from geometric considerations, as these specimens were thinner, being more in the nature of sheet specimens.

With increasing rolling strain above 60% reduction, the cavity walls tend to neck down in the longitudinal direction causing the coalescence of sheets of cavities into large cracks in the rolling plane. Thus one or more central cavities form longitudinally rather than laterally, final fracture occurring by the same shear mechanism as before through the remainder of the material as in figure 8.4.

8.3.2 The normalised steel.

In the normalised condition, the U.T.S.-rolling strain curve (figure 6.7) again shows an initial rise, after which the U.T.S. increases linearly with strain over most of the range of straining, but in this case there is a small range of strain around 1.2-2 in which there is no apparent increase in strength, as shown by a plateau on the curve.

The uniform strain curve (figure 6.7) also varies from that of the quenched and tempered steel in that after the initial rapid fall to small values, there is a slight rise in the region of strain corresponding to the plateau of the U.T.S. curve and another larger peak at high strains. Since this curve also shows the variation of the strain hardening exponent n, the capacity of the steel to undergo further plastic strain is increasing slightly after these amounts of strain.

Clough (1) and Nuttall (2) in their work on F.C.C. materials, related the similar plateaus in U.T.S. which they observed in some alloys to dynamic recrystallisation. According to Nuttall, the plateaus correspond to the appearance of strain free grains and long boundaries, the rate of dislocation tangling being balanced by the rate of dynamic recovery. Further increases in strength after the plateau are then due to dislocation tangling and hardening in the strain free areas.

No new strain free grains were observed in the present work, but the plateau must be caused by some form of strain induced softening the balance with the strain hardening in that region of the curve, and should be evident as some change in the microstructure. I have endeavoured to set out below several changes in the microstructure which are evident after rolling strains corresponding to its appearance which could possibly be contributing to the strain softening indicated by it.

The plateau appears in the range of strain where grain boundaries are no longer detectable. Therefore softening could be due in part to the loss of the grain boundary contribution to strengthening. But this does not explain its absence in the quenched and tempered steel unless grain boundaries are contributing less in that case due to the carbides within them.

As explained in section 5.3, microbands (similar to those in the quenched and tempered steel) consisting of groups of long cell like structures with sharp boundaries, were forming at an early stage and with increasing strain were increasing in number and in width (the number of cells across each band) and were rotating into the rolling plane.

If microscopic shearing (accompanied by local softening) is associated with their formation, or occurs within them, as seems likely from the serrated stress strain curves, then it may be that once these bands begin to dominate the structure, a more general deformation begins to take place by the same mechanism, with accompanying softening to balance the strain hardening. That is, it may be similar to the behaviour suggested in the last section to explain why the stress strain curves become flat at the U.T.S. The behaviour of the microbands is to be taken up in a more general discussion later.

Alternatively, since the plateau only occurred in the normalised steel and the two free cutting steels, all of which contained areas of pearlite (about which nothing has so far been said), it is possible that a value of stress is reached at which the pearlite colonies begin to be broken up and lose their affect as a strengthening agent. This seems to be the most consistant explanation because, a/ It is at these values of rolling strain that the pearlite first appears broken up in optical micrographs and strung out in the rolling direction as in figure 5.47 (note that it still appears undeformed in figure 5.29 after 60% reduction). b/ The plateau does not appear in the steels that do not contain pearlite. c/ For each of the steels in which it does appear, the plateau appears at almost identical values of stress. d/ Once the pearlite is broken up and strung out in the rolling plane, it should have little effect on further hardening as strain is increased more.

The larger peak in the uniform strain curve is at the stage where the microstructure is predominantly ribbon like cells all aligned in the rolling plane.

It can be seen from the results of the fractography that this peak corresponds to the first appearance in the fracture surface of large cracks parallel to the rolling plane.

Since the uniform strain curve is also an n value curve, the peak represents an increase in the capacity to deform further and this shows in the load extension curves of material strained this amount as an increase in the unstable extension occurring at the U.T.S. where the curves are flat.

Since it is associated with the appearance of large cracks, the additional unstable strain may be caused by an internal necking process involving the opening of cavities from 'ductile fracture centres' (to be discussed later) produced during the rolling process, and the coalescence of sheets of these long cavities in the rolling plane, similar to the large cracks formed at high strains in the quenched and tempered steel.

More strain may be accommodated once the cracks are formed as the remaining material necks down internally.

It should be noted that the presence of large cracks parallel to the rolling plane does not seem to affect the strength (at least in the rolling direction) which continues to increase with further strain.

Thus the peak in the uniform strain curve can be seen as an indication that the fracture process has begun and is extending longitudinally, but separation cannot occur because of the compressive nature of the component of the rolling stress in thickness direction. This also explains the occasional longitudinal split which can occur during late stages of rolling.

The unstable deformation at the U.T.S. during tensile testing can be similarly explained, in that the fracture process has begun at this stage, from many sub-structural 'ductile fracture centres' produced during the rolling process, but these are extending longitudinally without separation. Ductility is increased and transverse fracture delayed, until the stress necessary for separation is supplied indirectly as the transverse stress in the neck. Final fracture occurs similarly to that described in the last section, by internal necking and rupture of the walls between the cavities opened up by the above mechanism and its path may vary between normal to the rolling direction and stepping along a shear plane (similar to figure 8.2), depending on the internal stress pattern at each stage of its propagation.

8.3.3 The high sulphur steel.

The variation of the mechanical properties with strain in this steel has developed into the most potentially useful result of this study.

Figure 6.8 shows that after an initial steep rise the U.T.S. curve is linear to rolling strains of around 1.2 and then has a plateau, followed by another linear portion with a higher slope than before the plateau and a very large increase in slope for strains above 3.0.

Perhaps with a little foresight, the portion of the curve above the plateau would have been drawn as a continuously increasing slope, but the important thing is that at high strains the strength of the material is increased by a factor of three.

The linear portion below the plateau has a lower slope than the previcus steels and this low rate of strain hardening also shows up in the lower slope of the plastic region of the load extension curves in the early stages of straining. (figure 6.3).

The structure at this stage shows a much lower proportion of microbands than the other steels for the same strains, so if as suggested earlier, the strengthening is dependent of the proportion of microbands in the structure, this could explain the lower rate of strain hardening.

The plateau, as has already been explained in section 8.2.3, could have several contributing factors, but I believe that it is basically the breaking up of the pearlite colonies and the loss of their contribution to the strength.

The higher rate of strain hardening above the plateau seems from the microstructures to be at least partly due to the more rapid increase in the number of microbands (figure 5.52) and their increasing width until they dominate the structure (figure 5.55) as in the other steels. But as the strain increases further, the dominating factor causing the very large increases in strength becomes the presence of long thin sheets of MnS as seen optically in figure 5.45. Many of these cannot be seen optically, being as thin as 0.1 μm. An example of this can be seen in figure 5.56.

This appears to be a fibre strengthening effect, which to my knowledge has not been reported in the past and could have important practical applications.

The uniform strain curve in figure 6.8 is similar to the normalised steel, showing a rapid drop to low values, but in this case the peak corresponding to the onset of longitudinal fracture, which occurred for the normalised steel at strains of around 2.3, is in this case occurring at quite low strains.

A check back through the microstructures has revealed that many of the long sheets of MnS at this stage extended in length and been reduced in thickness by much more than could be expected from the amount of rolling strain. For example the average thickness of the MnS particles was approximately 12 μm and after a rolling reduction of 30% it is only around 2 μm with correspondingly large increases in length. This means that during a 30% reduction in thickness of the steel the MnS particles have been reduced by over 83%.

This together with the observations of Iwata and Ueda (214)(215) during dynamic machining experiments in the S.E.M. causes me to believe that cracks form from the MnS and extend longitudinally, while at the same time the rolling stress intrudes the MnS into the cracks as they extend. Separation does not occur because of the compressive components of the rolling stress (see section 8.7.2).

The ductility inceases because additional strain is accommodated by shearing along the cracks.

The slight rise in the curve at high strains is an indication of the longitudinal extension of smaller 'ductile fracture centres' which later separate to form deep cavities under the action of the resolved shear stress during the tensile tests. These then neck down during the final fracture process, showing up on the load extension curves as the unstable deformation at the U.T.S.

The suppression of the cup-cone shear zones in the low strain fractures, indicates that even at an early stage, the elongated MnS inclusions strongly resist shearing through the thickness direction. This could also have important practical applications in terms of greatly improved resistance to penetration by projectiles, but more work is needed to check this out.

From the tendency of the fractures to slope in the width direction, one gathers that the resistance to shearing, naturally enough, is not so great in a direction parallel to the plane of the sheet like inclusions.

At higher strains the very high resistance of the inclusions to shearing is probably the main contributing factor to the very high strength, since without shearing, the specimens cannot neck down. Thus the stress required for separation of the longitudinal fractures in this case comes only from the 45° resolved shear stress during the tensile test. But deformation in this direction is strongly resisted by the sheet inclusions, so the material continues to extend without plastic deformation (or the accompanying softening which would result), until internal necking and rupture of the small cavity walls occurs, producing a fracture which steps along the MnS interface cracks in order to follow the 45° resolved shear stress direction.

This wood chisel shaped fracture surface is seen in figure 7.21 and the steps on the shear surface are shown at higher magnification in figure 7.22.

8.3.4 The steel with sulphur and lead.

The trends of the mechanical property changes with strain in this steel were similar to the previous one, but not so startling and could in general be explained in the same way.

The initial load extension curve (figure 6.4) showed the lowest slope of all, which was constant from the beginning of plastic deformation to the U.T.S., apart from the small serrations, indicating a very low rate of strain hardening. This also showed in a lower slope of the U.T.S. (figure 6.9) curve below strains of 2. Only the faintest suggestion of a plateau existed at strains just below 2, since as shown in figure 5.58 there is not much pearlite present in this steel.

There is a strengthening affect at high strains, but not nearly as large as the previous steel, the U.T.S. curve remaining linear with a slope not all that much greater than that of the normalised steel.

The uniform strain curve shown in figure 6.9 initially falls to values not much above the relatively constant values for the remainder of the curve, so although additional strain is accommodated by shearing along cracks caused by MnS ,this is not as great as when no lead is present. It is occurring however, and the sudden turnover of the load extension curves at the limit of proportionality in unstrained specimens,is probably because of such unstable shearing, in both this steel and the previous one(see 8.7.2-3).

There was no evidence that lead was present as 'tails' on the MnS particles as suggested by Trent(190). Instead the lead appeared to be present as small, almost sub-microscopic spheres (figure 5.58). These had the affect of breaking up the MnS inclusions, so that the long sheet like inclusions present in the high sulphur steel are in this case fragmented. This can be seen at different stages of strain in figures 5.59 and 5.60. The initial increase in strength is most likely due to dislocation tangling around the small lead particles, although the fact that the curve becomes linear more slowly than the others suggests that in this case there may be a softening associated with the MnS interface shearing, probably because the particles do not fill the cracks so well.

In the first linear region, similar microbands are forming to those in the previous steels, but they do not strengthen the material to the same degree. The only noticeable difference in their structure is the thickness of the individual boundaries. When the nature of the boundaries is being discussed later, it will be seen why they are weaker and it will also be shown later,that these weaker boundaries lead to easier ductile fracture initiation.

The decreased degree of fibre strengthening in this steel relative to the high sulphur steel (when no lead is present) is obviously due to the fragmentation of the MnS stringers, resulting in a much lower resistance to shear, although there was still a noticeable affect, as seen by the partial suppression of shear zones in the low strain cup-cone fractures and the developement of neck free, wood chisel fractures at 45° after high rolling strains.

8.3.5 The steel with a fine carbide dispersion.

The variation of mechanical properties with strain for this steel are shown in figure 6.10.

The two peaks in the uniform strain curve at strains up to 0.5 can be seen to occur at strains where there are noticeable changes in the fracture characteristics. It seems that in this case also, ductile fracture is nucleated quite early in the straining process at many sites within the structure, but extended only in the longitudinal direction because of the compressive rolling stresses.

In the quite low strains in the region around the first peak, optical micrographs show a small number of cracks (figure 5.70) and the tensile fractures show the coalescence of deep cavities in the rolling plane in both the central region and the shear regions of the cup-cone fractures (figures 7.28 and 7.29). This can be explained in the same way as for the quenched and tempered steel.

As the strain increases slightly the ductility falls as the relatively small cracks concentrate the local stress around them into the longitudinal direction. This causes a resistance to transverse shearing and the fractures tend to be of the 45° shear type, stepping along the microscopic resolved shear stress direction as in the high sulphur steel at high strains.

As rolling strain increases to 0.5, the tensile ductility increases slightly again, this time associated with the development of a neck. The transverse stresses in the neck cause the opening of the extended ductile fracture centres into deep cavities. The cavity walls neck down and rupture, producing a central void which extends laterally and opens longitudinally, to produce a double cup fracture as in figure 7.32. The unstable deformation results from the internal necking process of the cavity walls.

By 10% reduction, straight bands of tangled dislocations could be seen running tangentially to many of the carbide particles. They appear to be bands where deformation by slip has occurred due to the stress concentrating affect of the particles. They were not the same as the microbands of ribbon like cells described earlier, but may be the beginning of these.

Specimens rolled by this amount have very recently been strained in the H.V.E.M. They showed that such bands extend in length gradually out from the particles and that once formed, abrupt shearing can occur along their length. More work is needed before this can be fully understood.

Not much work was done on this material at high strains, because the structure could only be produced in relatively thin sections and this meant very thin samples at high strains.

The rolling plane cracks were increasing in number and in length with strain (figures 5.70-73) and I suspect that the unstable deformation at strains above 3.0 is caused by the coalescence of these cracks and that it would not be possible to roll this material to greater reductions without splitting occurring in the rolling plane.

8.4. The affect of large strains on grain boundaries.

As seen in section 2.4.1, much work on deformation of polycrystalline aggregates has been based on the theory (97) that grains undergo the same shape change as the overall material and that multiple slip systems are required to maintain continuity. The results of the present work however, support the suggestion (103) that while multiple slip may be occurring in some areas, the interior of the grains deform in general on single or duplex slip systems and continuity is maintained by inhomogeneous deformation.

While grains may undergo a similar shape change initially, there is with the reduction and elongation a tendancy for the grain boundaries which cut across the rolling direction, to rotate about the triple points towards the rolling plane. Also, as strain is increased many of these become fragmented by shearing (figures 5.27 & 5.29). This is associated with a band structure similar to that first seen in Al (82) and recently reported in Cu (259). Above 60% reduction, grain boundaries not parallel to the rolling direction had apparently been completely broken up, as no grain boundaries could be recognised as such in any of the steels.

One reason for the break up may be that (as suggested by Nutting (263)), for grains to undergo the same shape change as the overall material, a very large increase in surface area is required. This can be illustrated by a very simple calculation of the fractional increase in grain boundary area of a simple cubic grain while being reduced at constant volume. A plot of this increase against rolling strain is shown in figure 8.5, the conclusion from this being that the increase in surface energy required to continue such a shape change at strains greater than 2 is so great that the process becomes impossible.

8.5 The Nature and Behaviour of the Microbands produced During Deformation.

8.5.1 Introduction

As seen in chapter 5 and discussed to some extent with the structure-property relationships, microbands consisting of groups of very long ribbon like cells were formed in the microstructures, superimposed on the normal equiaxed cell structure which is formed at relatively low strains.

Numerous observations of long ribbon like cells have been made after heavy cold working, but little if anything is known about their origin or behaviour during subsequent deformation. In current literature, many observations of groups of such cells and discussions of various kinds of shear bands are appearing, as their importance in both the deformation and texture development of many materials is increasingly recognised. (3)(264)(266)(267). Similar behaviour to that observed in this work has recently been found to occur in Copper (268) and may therefore be common to many metals.

As so little is known about these bands, the discussion concerning them will be more detailed. A summary of the observations will be made first, followed by speculation as to their mature, formation, behaviour and their contribution to the increase in strength of the material.

8.5.2 Summary of observations

The microbands consist of groups of ribbon like cells the boundaries of which are generally very sharp and their length is far greater than could be expected if they formed by elongation of the original equiaxed cell structure.

They show in optical micrographs as light etching bands (figure 5.27), but are very difficult to photograph.

Large shearing deformation is associated with them, as can be seen by the steps they produce in grain boundaries. This has also been observed during straining experiments carried out in the H.V.E.M., but single frame analysis of videotapes has not been very successful and it is not clear at this stage whether the abrupt shearing which occurs corresponds to the formation of an additional cell or is simply rapid shearing along the boundaries.

The number of microbands increases with strain and the number of approximately constant thickness cells across them becomes larger, so the width increases also.

Different microbands within the same grain were normally parallel, but sometimes there were two sets at angles on either side of the rolling direction. Their angle to the rolling direction varied from grain to grain, the average angle to the rolling direction of 100 sets counted being 32°. They therefore appear to be forming in the slip plane which is most closely oriented to the maximum shear stress.

Their formation in slip planes was also confirmed by the electron diffraction results, because trace analysis of the direction of the boundaries showed them to be mostly {110} planes which in the transverse sections were perpendicular to the foils and occasionally {211} planes.

Electron diffraction patterns from the bands were single crystal patterns with splitting of the spots around rings, indicating small rotations of the structure across the individual boundaries, larger misorientations being accommodated across the bands in small stages in a similar way to the transition bands described in section 2.3.3. Misorientations across the individual boundaries were also apparent as displacements of the extinction contours in electron micrographs.

As strain increased, the microbands rotated into the rolling direction, so that after very high strains the structure was dominated by broad bands of 30-40 cells parallel to the rolling direction. Some cell coalescence is observed at these high strains similar to that suggested by Langford and Cohen (67), presumably in balance with a reduction in cell thickness since the cell thickness remains approximately constant.

From the above observations one sees that there are many unanswered questions such as:-

Are they shear bands?

How do they form and how do they contribute to the subsequent deformation?

Do they always form on the same planes throughout and if so how do they form new parallel cells once they have rotated away from their original directions?

Why do they cluster together?

What is the roll of the original equiaxed structure during subsequent deformation?

How do they contribute to the strength?

It is clear that all these questions cannot be answered without a great deal of work, but speculation on the answers to some of these will be given in the next few sections.

8.5.3 The Nature and Formation of the Boundaries.

The rotation of the diffraction patterns suggests that the boundaries may be low angle tilt boundaries made up of many hundreds of edge dislocations of the same sign. This was in fact seen to be the situation (figure 5.53) in one case, when a sample was observed in an orientation such that the slip planes were sloping through the foil.

If one imagines looking at such a structure in planes perpendicular to the foil, then it is possible that it would appear sharp and show small loop type contrast as in figure 5.43. On the other hand, it is possible that the structure of 5.53 formed because of overheating in preparation, since Walter and Koch (59)(76) saw similar structures in transition bands after a short anneal.

While much evidence suggests that the boundaries have this structure, the main problem is that the glide plane of the dislocations in such an array is perpendicular to the boundary. So while this structure allows for sideways motion of the boundaries (120), rotation and even sideways shearing as in figure 5.41, it is not consistent with shearing along the length of the boundaries, which required the dislocations to be of screw orientation.

These apparently contradictory facts can be reconciled by the following speculations as to the mechanism of formation of the bands.

Early in the straining process local differences in stress state develops, tending to cause local variations in strain in various parts of the crystals and relative rotations, which may separately yield the overall microscopic strain and maintain the grain continuity. Possible mechanisms for this have been discussed in the excellent paper by Dillamore et.al. (78) on the origin of transition bands which has been summarised in section 2.3.4.

Suppose now that under the action of these local stresses, slip occurs and continues (with local hardening) until local overstraining and fracture occurs. Cracks could propagate some distance (even right through grains), with the necessary local strain being accommodated by a rapid shear of material on either side of the instantaneous crack, which may then rapidly heal up once this is accomplished, aided by the compressive components of the rolling stress.

An additional reason for rehealing of the cracks may be that the elastic strain energy released in the shear process, which would normally supply the surface energy to maintain or propagate the crack according to the Griffith theory (269) is supplying the ever increasing surface energy of the deforming grain boundaries which is illustrated in figure 8.5.

A relatively stable array of geometrically necessary dislocations of the kind described above may be formed as a mismatch structure to accommodate the relative rotation of the two portions of the lattice which has occurred with the local strain. Since this array is required to accommodate the rotation, it will resist deformation, remaining relatively straight, and as local stresses again build up they will be concentrated in a parallel direction, causing the process to repeat and so produce a series of parallel ribbon like portions of lattice which in the past have been described as elongated cells.

8.5.4 Subsequent Deformation Behaviour of the Microbands

While the above explanation of the mechanism of formation of the microbands and the nature of the boundaries is consistent with the observations (and if assumed correct) can explain most of the peculiarities in the result chapters, as well as providing answers for some of the questions in section 8.5.2. For example:-

Arguments as to whether the microbands are shear bands or transition bands are unnecessary as they are both being shear bands during their formation and transition bands (merely accommodating lattice rotations) by the time they are viewed in the electron microscope.

The rotation into the rolling plane can be explained in terms of a graded lateral glide process (figure 8.6a), with dislocations at various distances along the boundary gliding different distances as the boundary rotates through the lattice while remaining intact. This may be forced on the bands by geometric considerations during the rolling process (figure 8.6b), or may be analogous to the way that slip planes are forced to rotate into the tensile axis during a tensile test (270).

Some points, such as how additional portions are formed once the band has rotated out of the slip plane are not yet clear, as these would have to be formed in a different plane. This requires more work. The rotation out of the {110} slip planes however, may be a means of explaining the absence of {110} components in the final texture.

The acoustic measurements of Walker and Shaw (50) leading to their microcrack deformation mechanism (section 2.2.3) can also be explained.

To keep more to the point, some of the results of this project which can be explained are as follows:-

The abrupt shearing in the H.V.E.M. straining experiments can be simply interpreted as local fracture and re-healing.

The relatively thick boundaries in the leaded steel can be explained in terms of small lead particles being smeared out along the cracks during the shearing process, preventing proper matching of the surface. This also accounts for its poor mechanical properties, as these weaker boundaries will easily open up into cavities under the action of the resolved shear stress during tensile tests. E.P.M.A. was tried in an A.E.I., EMMA 4 electron microscope, but without success, due to insufficient resolution to obtain spectra from the boundaries.

The absence of long microbands in the steel with a fine dispersion of carbides can be explained, in that even though local slip begins due to the concentration of slip by these particles, so many slip sources are operating from other particles nearby, that a much more general deformation can occur, with any large local build up of stress being quickly relieved by deformation from nearby sources.

If any localised straining does continue long enough to cause a fracture, the crack is prevented from healing by carbide particle within it preventing the faces from coming together. Hence the appearance of micro-cracks associated with particles in this steel, increasing in number with strain and also their appearance in the quenched and tempered steel in smaller numbers at later stages of deformation.

In the high sulphur steel, microbands do not form at such an early stage as local strains are accommodated by an analogous process along ready made cracks at the MnS interfaces. In this case they are filled with MnS as they propagate, as explained earlier. Microbands do form at a later stage, possibly because of concentration of the stresses into a parallel direction by long sulphide sheets.

8.5.5 The Contribution of the Microbands to Strengthening.

As seen in section 8.3.1, the dominant structural feature contributing to strengthening is the increasing number of microbands. As little has been known about them in the past, little is known about their action in increasing the strength.

Early in the project, my thinking was that the deformation is concentrated into bands, because some way or another a structure is formed through which there is an easy shear path. The strengthening affect of the microbands on the other hand seems to indicate that they are quite strong.

The following idea grew from a suggestion by Doyle (271) that shear bands might be strong.

If the stress is concentrated in local regions of the crystals and it is assumed that all strain is being accommodated where shear bands are forming, leaving the rest of the structure relatively unaffected, then allowing the overall applied load to act only on the cross sectional area of the shear bands could mean that very high strengths are involved.

Assuming a reasonable dislocation density and therefore many atomic bonds already broken, perhaps the stress could be building up to around half theoretical strength and causing a non consecutive slip (or de-cohesion) to occur in the slip planes, which heals again when the strain is accommodated and the stress relaxed as described in section 8.5.3.

If this is so, then at later stages of straining when the increasing number of shear bands means that the load is acting on a larger cross sectional area, a larger load is required to build up the necessary local high stresses for continued band formation.

This is obviously not the only mechanism operating, but superimposing this on all the normally suggested mechanisms for work hardening, could explain the dominant role that the increasing number of microbands seems to play in increasing the strength.

A further increase in strength could be obtained at higher strains when the bands have rotated into the rolling direction (by the increasing lamination of the structure). The local stress around them may be concentrated into a parallel direction, increasing the resistance to shear as in the case of the long MnS sheets, but not so greatly, so that in tension, the material continues to extend elastically until the resolved shear stress builds up to higher levels.

8.6 The Nucleation of Ductile Fracture in Deformed Materials

In comparing the mechanisms of ductile fracture reviewed in section 2.8 with the fracture behaviour of the deformed steels as discussed in section 8.3, there are some obvious differences which need explaining.

The normal mechanism is that voids nucleate at inclusions or second phase particles, grow under the action of a tensile stress and once enlarged, concentrate the strain to the point of fracture by a process of void sheet nucleation.

In section 8.3.1, it has been pointed out that during tensile testing of the strained material, the fractures showed conclusive evidence of extremely deep cavities even though the tensile strain was quite small and that when the mode of fracture changed, it remained basically a different path of separation through the same cavities. This suggests that cavities of 'ductile fracture centres' must be produced during the rolling process.

This is also indicated by the work reviewed in section 2.8.3 on the effects of strain history which emphasises several points of importance:-

1. That deformed materials are weaker in a direction 'across the fibre'.
2. That fracture always takes place in planes that have undergone extensive shearing.
3. A microcrack theory is strongly suggested by experimental results, but not observed.

In view of the results already discussed and the above suggestions from past work, I suggest that the mechanism of nucleation of ductile fracture during tensile tests on cold rolled materials, is the opening up of deep cavities in the rolling plane along the boundaries of microbands formed during rolling, under the action of the normal component of the resolved shear stress (and at a later stage, by transverse stresses in the neck).

Physical reasons aiding the initiation of such cavities are:-

1. The difficulty of maintaining compatibility during tensile deformation around a site that is stronger than its surroundings.
2. The fact that the laminated structure, although strong longitudinally, is much weaker in the transverse direction.

Depending on the changes in local stress state, the material between the cavities may neck longitudinally so that they coalesce in sheets forming large cracks in the rolling plane, or neck down and rupture laterally, producing a surface with equiaxed cavities of considerable depth.

In materials with small 2nd phase particles (such as the steel with a dispersion of carbides), while it may often happen that voids form by separation at the metal particle interface (or by cracking of the particles), and either extend under the action of a tensile force or distort under the action of a shear stress (figure 8.1), this was not observed in this study.

In deformed materials, it seems likely that cavities are more often nucleated in a similar way to the above mechanism, from the bands of intense shear, which form outwards from the particles as stress is concentrated by them during the deformation process.

8.7 Deformation and Fracture in the Machining Process

8.7.1 A Model for Primary Shear

The work reviewed in section 2.7 has emphasised that heterogeneous deformation during machining results in a characteristic lamellar structure of the chip, but the mechanism by which this occurs is still in doubt.

The comparison of tensile fractures of the deformed steels with transverse fractures of machining chips, has shown that the walls of cavities opening up during tensile testing to produce ductile fracture by the mechanism described in section 8.6, have the same rippled appearance and the same angular lines where cavities coalesce (figure 7.39) as the so called 'stretch zones' which appear in the chip fractures. This suggests that the stretch zones are formed by the coalescence of cavities formed in the material.

Micro-cracks have many times been suggested as a mechanism for primary shear, but have not been seen except in quickstop sections (199) when the tool was exploded away from the work.

Also it has been shown (273) that electron microstructures of foils cut from longitudinal sections of mild steel machine chips show the same lamellar structure of ribbon like cells as has been described in the present work after high strains.

With all this in mind, I now suggest that the mechanism for primary shear during machine chip formation of steels is identical to the localised shearing process described in section 8.5 during bulk deformation.

High localised stresses in the shear plane cause localised overstraining and fracture to occur in some areas, allowing rapid shearing along the crack faces and relative rotation of the lattice to occur, at the same time relaxing the stress.

The micro-cracks immediately re-heal, adopting the same transition band structure of edge dislocation arrays which has been described earlier.

The shearing of the chip segment allows the tool to indent further, building up the stress in a parallel shear plane and the process repeats itself in the characteristic stop-start manner.

This is very similar to the proposal of Walker and Shaw (50), but adds more detail to their idea that micro-cracks are forming and re-welding and explains the structure of the chips.

8.7.2 The Effect of MnS Additions

Having suggested consistent mechanisms for the formation of the structures and nucleation of ductile fracture in the bulk materials and for the machining process when no MnS is present, it is now possible to add more detail to the idea (discussed in section 8.3.3) that shearing occurs along cracks ahead of MnS particles and to see how this influences the machining process.

The results suggest that the MnS particles act as stress raisers in the primary shear zone, as claimed by Shaw and Rubenstien (209)(210). This causes bands of slip to occur in the shear plane ahead of the particles, as in the steel with fine carbides, only in this case the local stress is not relaxed by slip from large numbers of nearby sources and localised overstraining and fracture occurs, extending the interface cracks and allowing rapid shear of a segment of the chip. The cracks are filled with MnS as they extend, in the way discussed earlier.

It should be pointed out here that the shearing of a segment of a chip is not one single shear from a particle of MnS, but consists of a number of separate shears from particles in the shear plane, the areas in between shearing by microband formation in the same way as discussed previously.

Comparing the mechanism of shearing along cracks caused by stress concentration at MnS particles, with the mechanism proposed for the case when there was no MnS present, it is seen that the two processes are very similar.

The real benefit of MnS inclusions during machining can be more easily seen from the mechanical test results.

If figure 6.7 and figure 6.8 are compared, it is immediately seen that the peak in the uniform strain curve which occurs at a strain of 2.3 in the normalised steel curve, occurs at a strain of only about 0.3 in the high sulphur steel.

Since it has been already shown that these peaks correspond to the onset of longitudinal fracture by the coalescence of sheets of cavities in the rolling plane (section 8.3), shearing along cracks associated with MnS particles must be occurring very early in the straining process, compared to that along the shear band cracks when no MnS is present.

Thus, in the machining process for a steel containing MnS, the unstable shearing producing the chip segments occurs without the need to strain the material ahead of the tool to such a high degree and the necessary cutting force is greatly reduced.

8.7.3 The effect of Lead Additions

The structures and fractography showed that similar mechanisms of deformation occur to those in the high sulphur steel, the only difference being that the MnS particles become fragmented and do not fill the cracks so effectively. The mechanisms occurring during the machining process can therefore be expected to be much the same as the previous case.

The uniform strain curve (figure 6.9) showed a similar peak at low values of strain to the high sulphur steel and therefore this steel could be expected to be machined with similar low cutting forces.

Without more work, it is difficult to pin point any particularly significant contribution of the lead to machinability which would improve it over the plain high Sulphur steel sufficiently to warrant its inclusion, because of the poorer mechanical properties of any components made from it, but the following factors could give marginal additional reductions in cutting forces.

1. The strain hardening rate is the lowest of all the steels tested.
2. The strength is lower in the early stages of strain when the unstable shearing associated with the MnS particles is beginning to occur.
3. The lead particles appear to be smeared out in the micro-cracks preventing re-healing from taking place properly. This means that microbands and MnS interfaces are weaker.

It also means that if stress builds up again, shearing can continue without the need to re-fracture and that ductile fracture initiation is easier.

The easier chip break up brought about by this last point may also aid the machining process.

CHAPTER 9

GENERAL CONCLUSIONS

9.1 Experimental Methods

1. Because of the shape and orientation of the substructure, electron microstructures of rolled materials must be studied in foils made from sections perpendicular to the rolling direction and along the rolling direction.

   Rolling plane foils are confusing and leave the most important features of the structure undiscovered.

2. The overall changes in strength and ductility occurring during cold rolling can be successfully studied by compounding the results of tensile tests at various stages of deformation.

   For each of the steels studied, the variations in properties so shown could be explained in terms of the changes in microstructure observed.

9.2 Properties and Structures

1. The deformation during rolling is microscopically heterogeneous.
2. Grain boundaries become increasingly fragmented during rolling and do not appear to exist as such at strains greater than 60% reduction.
3. In the three steels in which they existed, pearlite colonies broke up at approximately the same value of stress and rolling strain and their contribution to the strength was lost. This was identified as the reason for a plateau in the three corresponding U.T.S. rolling strain curves.
4. The dominant microstructural contribution to the increasing strength, appears to be the formation of an increasing number of microbands in the structure, with very long sharp boundaries. Groups of these boundaries accommodate lattice rotations in small stages, Large shearing displacements are associated with them and with increasing strain they become broader and gradually rotate into the rolling plane.
5. Ductile fracture is nucleated at pre-existing fracture centres which form early in the deformation process.

Fractures in the deformed materials develop extremely deep cavities, even though the tensile strain is low and as the mode of fracture changes, separation remains basically a different path through the same cavities.

6. Anomalous peaks in the curves showing the variation of uniform strain with rolling strain can be identified with changes in the fracture behaviour.

7. The very steep change of slope in the U.T.S. rolling strain curve for the high sulphur steel can be explained in terms of a fibre strengthening effect, as the MnS particles become strung out into very long thin sheets in the rolling plane. The strength goes up by a factor of three and this could be a very important strengthening mechanism which has not previously been reported. The steel with sulphur and lead does not show this to the same degree, because the sulphide particles become fragmented.

8. The steel with a fine carbide dispersion demonstrates that stress concentration at the particles occurs at very low strains, causing slip in bands running out from them. The large microbands do not form to the same extent in this material because slip from the large number of close sources operating in this way dumps out the large shears necessary for their formation.

9.3 Speculations

1. A model is proposed for the formation of the microbands in the structure which is consistent with all the observations of their nature and behaviour. It is speculated that they are shear bands during their formation and transition bands at a later stage. The model involves the formation and re-healing of micro-cracks, along which large shear deformation can occur.

   An attempt is also made to account for their strengthening effect.

2. Based on the pronounced affect that the deformation has on the fracture behaviour, a model is proposed for the nucleation of ductile fracture in the deformed structures and with the observed fractures.

3. A model is proposed for the primary shear process occurring during metal cutting, based on the observation that the fracture behaviour of machining chips is the same as the deformed material and that deformation behaviour in both bulk material and machine chip formation is heterogeneous.

4. A model is proposed for deformation during machine chip formation when MnS inclusions are present. The action of MnS in machining is to effectively lower the cutting force required, by allowing deformation to occur by a similar mechanism at lower strains.

5. When Pb is present in addition to MnS, the mechanism is still similar. Cutting forces may or may not be marginally reduced and the chips break away more easily.

BIBLIOGRAPHY

1. J. Clough
PhD thesis University of Leeds (1972)

2. J.L. Nuttall
PhD Thesis University of Leeds (1976)

3. S. Nourbakhsh
PhD Thesis University of Leeds (1977)

4. C.F. Elam
'The Distortion of metal crystals' Oxford (1936)

5. E. Schmid & W. Boas.
'Plasticity of crystals'
F.A. Hughes London 1950
(Translation of Kristallplastizitat springer Berlin 1936)

6. J. Frenkel
Zeit. Phys. 37 572 (1926)

7. G.I. Taylor.
Proc. Roy. Soc. A 145 362 (1934)

8. E. Orowan.
Zeit. Phys. 89 605, 614, 634, (1934)

9. M. Polanyi.
Zeit. Phys. 89 660 (1934)

10. F. Seitz
Adv. Phys. 1 43 (1952)

11. F.C. Frank
Adv. Phys. 1 91 (1952)

12. A. Seeger
Handbuch der Phys. 7 383 (1955)

13. P.B. Hirsch
Progr. Met. Phys. 6 236 (1956)

14. F.R.N. Nabarrow
Adv. Phys. 1 271 (1952)

15. N.J. Petch
Progr. Met. Phys. 5 1 (1954)

16. J.D. Eshelby
Solid State Phys. 3 79 (1956)

17. A.N. Stroh
Adv. Phys 6 418 (1957)

18. A.H. Cottrell
Trans, AIME 212 192 (1958)

19. L.M. Clarebrough & M.E. Hargreaves
Prog. Met. Phys. 8 1 (1959)

20. S. Amelinckx & W. Dekeyser
Solid State Phys. 8 327 (1959)

21. B.A. Bilby
Progr. Solid Mech. 1 331 (1960)

22. A.H. Cottrell
'Dislocations and Plastic Flow in Crystals'
Oxford Univ. Press (1962)

23. W.T. Read
'Dislocations in Crystals' Wiley New York (1953)

24. H.G. Van Bueren
'Imperfections in Crystals ' North Holland
(Amsterdam) (1960)

25. D. Mclean
'Grain Boundaries in Metals'
Oxford Univ. Press (1957)

26. F. Seitz, J.S. Koehler & E. Orowan
'Dislocations in Metals' Wiley New York (1954)

27. J. Friedel
'Dislocations' Pergamon Press (1964)

28. 'The Direct Observation of Imperfections in
Crystals' Interscience Publ. New York (1962)

29. J.F. Nye
Proc. Roy. Soc. A 200 47 (1953)

30. B.A. Bilby, R. Bullough & E. Smith
Proc. Roy. Soc. A 231 263 (1955)

31. G.I. Taylor & C.F. Elam
Proc. Roy. Soc. A 112 337 (1926)

32. N.F. Mott
Proc. Phys. Soc. B 64 729 (1951)

33. F. Seitz
Phys. Rev. 79 723 (1950)

34. F.R.N. Nabarro
'Theory of Crystal Dislocations'
Oxford University Press (1967)

35. F.C. Frank & W.T. Read
Phys. Rev. 79 722 (1950)

36. E.O. Hall
'Twinning and Diffusionles Transformations in Metals'
Butterworth London (1954)

37. S. Mahajan & D.F. Williams
Int. Met. Reviews 18 43 (1973)

38. C.S. Barret & T.B. Massalski
'The Structure of Metals'
McGraw Hill (1966) P411

39. W.P. Mason, H.J. McSkimin & W. Shockley
Phys. Rev. 73 1213 (1948)

40. D.E. Dieter Jr.
'Mechanical Metallurgy' McGraw Hill (1961) P 106

41. J.J. Cox, R.F. Mehl & C.T. Horne
Trans A.S.M. 49 123 (1957)

42. R.W. Cahn & J.W. Coll
Acta Met. 9 138 (1961)

43. A.H. Cottrell & B.A. Bilby
Phil. Mag. 42 573 (1951)

44. N. Thompson & D.J. Millard
Phil. Mag. 43 442 (1952)

45. P.B. Hirsch, A. Kelly & J.W. Mentor
Proc. Phys. Soc. (London) B68 1138 (1955)

46. D.G. Westlake
Acta Met. 9 327 (1961)

47. J.A. Venables
Phil. Mag. 6 329 (1961)

48. J.T. Fourie, F. Weinberg & F.W.C. Boswell
Acta Met. 8 851 (1960)

49. P.B. Price
Proc. Roy. Soc. A260 251 (1961)

50. T.J. Walker & M.C. Shaw
Proc. 10th Conf. on Machine Tool Design and
Research P.241 Pergamon Press 1970

51. E. Usui, A. Gujral & M.C. Shaw
Int. J. Mach. Tool Design and Research 1 187 (1970)

52. P.B. Hirsch, R.W. Horne & M.J. Whelan
Phil Mag. 1 667 (1956)

53. A.S. Keh & S. Weissmann.
'Electron Microscopy and the Strength of Crystals'
(Editors G. Thomas & J. Washburn)
Interscience (1963) P231

54. R.D. Butler & D.V. Wilson
J.I.S.I. 201 16 (1963)

55. A.S. Keh
'Direct Observations of Imperfections in Crystals'
Interscience New York (1962) P213

56. J. Clough
PhD. Thesis University of Leeds (1972)

57. I.L. Dillamore, P.L. Morris, C.J.E. Smith &
W.B. Hutchinson
Proc.Roy.Soc. A329 405 (1972)

58. I.L. Dillamore, C.J.E. Smith & T.W. Watson
Met. Sci. J. 1 49 (1967)

59. J.L. Walter & E.F. Koch
Acta Met. 10 1059 (1962)

60. R.D. Doherty
Met. Sci.J. 8 132 (1974)

61. J.E. Bailey & P.B. Hirsch
Proc.Roy.Soc. A267 11 (1962)

62. R.W. Cahn
J. Inst. Met. 76 121 (1949)

63. C. Dasarathy
British Steel Corporation Report SM/668/A (1973)

64. A. Dunn
PhD Thesis University of Liverpool (1970)

65. C.J.E. Smith
PhD Thesis University of Birmingham (1968)

66. R.H. Goodenow
Trans. ASM 59 804 (1966)

67. G. Langford & M. Cohen
Trans ASM 62 623 (1969)

68. J.D. Embury, A.S. Keh & R.M. Fisher
Trans. A.I.M.E. 236 1252 (1966)

69. C.S. Barrett
Trans. A.I.M.M.E 135 296 (1939)

70. C.S. Barrett & L.H. Levison
Trans. A.I.M.M.E . . 135 327 (1939)

71. C.S. Barrett & L.H. Levison
Trans. A.I.M. M.E. 137 112 (1940)

72. C.S. Barrett & F.W. Steadman
Trans. A.I.M.M.E. 147 57 (1942)

73. C.S. Barrett
'Structure of Metals' McGraw Hill (New York) (1952)

74. H. Muller
Z. Metallk. 50 351 (1959)

75. N.K. Chen & C.H. Mathewson
Trans A.I.M.E. J.Metals 3 653 (1951)

76. J.L. Walter & E.F. Koch
Acta Met. 11 923 (1963)

77. H. Hu
'Recovery & Recrystallisation of Metals'
Ed. L. Himmel, Interscience (1963)

78. I.L. Dillamore, P.L. Morris, C.J.E. Smith &
W.B. Hutchinson
Proc.Roy.Soc. London A 329 405 (1972)

79. C. Dasarathy
British Steel Corporation Report SM/668/A.Aug.1973

80. J. W. Mitchell, J.C. Chevrier, B.J. Hockey &
J.P. Monahan Jr.
Proc.Int.Conf. on Deformation of Crystalline
Solids Ottawa (1966) Canadian J.Phys. 45 453 (1967)

81. E. Orowan
Z.Phys. 89 605, 614, 634 (1934)

82. K. Brown
J.I.M. 100 341 (1972)

83. W.G. Johnston & J.J. Gillman
J.Appl. Phys. 31 632 (1960)

84. J.T.Fourie & H.G.F. Wilsdorf
J. Appl. Phys. 31 2219 (1960)

85. N.F. Mott
Proc Phys Soc. B.64 729 (1951)

86. J.C.M. Li
J.Appl.Phys. 32 593 (1961)

87. D. Kuhlman-Wilsdorf, R. Madin & H.G.F. Wilsdorf
'Symposium on Strengthening Mechanisms in Solids'
A.S.M. P.137 (1960)

88. P. Gay & A. Kelly
Acta Cryst. 6 765 (1963)

89. P. Gay & A. Kelly
Acta Cryst. 6 172 (1963)

90. A. Seeger
'Dislocations and Mechanical Properties of Crystals'
Wiley New York (1956)

91. S. Weissman
J.Appl.Phys. 27 1335 (1956)

92. P. Gay, P.B. Hirsch & A. Kelly
Acta Cryst. 7 41 (1954)

93. J.C.M. Li
'Direct Observations of Imperfactions in Crystals'
Interscience (1962) P 238
Discussion of a paper by A.S.Keh.

94. A. Berghezan, A. Fourdeaux & S. Amelinckx
Acta Met. 9 464 (1961)

95. P.N. Richards & M.K. Ormay
Trans.Metal.Soc. A.I.M.E. 245 715 (1969)

96. I.L. Dillamore & W.J. Roberts
J.Inst.Metal. 92 193 (1963)

97. G.I. Taylor
J.Inst.Metals 62 307 (1938)

98. J.F.W. Bishop & R. Hill
Phil.Mag. XLII P 414 & P 1298 (1951)

99. U.F. Kocks
Acta Met. 6 85 (1958)

100. W.F. Hosford Jr. & W.A. Backofen
9th Sagamore Conference A.R.M.A.
Fundamentals of Deformation Processing
Syracuse Univ. Press P 259 (1962)

101. J.F. Peck & D.A. Thomas
Trans.Met.Soc. A.I.M.E. 221 1240 (1961)

102 W.F. Hosford Jr.
Trans Met.Soc. A.I.M.E. 230 12 (1964)

103. I.L. Dillamore & W.T. Roberts
Acta Met. 12 281 (1964)

104 D.G. Brandon
Acta Met. 14 1479 (1966)

104 T.Schober & R.W. Balluffi
Phil.Mag. 21 109 (1970)

105. W. Carrington, K.F. Hale & D. McLean
Proc.Roy.Soc. A259 203 (1960)

106. L.M. Clareborough & M. Hargreaves
Progress in Metal Physics 8 1 (1959)

107. M.J. Whelan, P.B. Hirsch, R.W. Horne & W. Bollman
Proc.Roy.Soc. A240 524 (1957)

108. D.G. Brandon & J. Nutting
Acta Met 7 101 (1959)

109. G.L. Ogilvie
J.Inst.Metals 81 491 (1953)

110. J.D. Livingston & B. Chalmers
Acta Met. 5 322 (1957)

111. K.T. Aust & N.K. Chen
Acta Met. 2 634 (1954)

112 M. Umeno & G. Shinoda
J.Mat.Sci. 3 120 (1968)

113 R.E. Hook J.P. Hirth
Acta Met. 15 535 (1967)

114. W.C. Leslie, J.T. Michalac & F.W. Aul
'Iron and its Dilute Solid Solutions'
Interscience New York P 119 (1963)

115. F.J. Humphreys & J.W. Martin
Phil.Mag. 16 927 (1967)

116. W.T. Read
'Dislocations and plastic flow in crystals'
Wiley New York (1953)

117. A.H. Cottrell
'Dislocations and Plastic Flow in Crystals'
Oxford University Press (1953)

118. J.C.M.Li
'Electron Microscopy and the Strength of Crystals'
Interscience (1962) P. 713

119. C. Langford & M. Cohen
Met. Trans. 6A 901 (1975)

120. E.R. Parker & J. Washburn
J.Metals 4 1076 (1952)

121. W.T. Read & W. Shockley
Phys.Rev. 78 275 (1950)

122. I.L. Dillamore & W.T. Roberts
Met.Revs. 10 271 (1965)

123. H. Hu, R.S. Cline & S.R. Goodman
'Recrystallization, Grain Growth & Textures'
Ed. H.Margolin,Metals Park Ohio (A.S.M.)
P 295 (1966)

124. J. Grewen
'Recrystallization in Metalic Materials'
Ed. F. Haessner Stuttgart (Reiderer Verlag)
P 135 (1971)

125. I.L. Dillamore & H. Katoh
Met. Sci. J. 8 219 (1974)

126. I.L. Dillamore & H. Katoh
Met.Sci.J. 8 73 (1971)

127. L.M. Clareborough & M.E. Hargreaves
Prog. in Metal Phys. 8 1 (1959)

128. F.R.N. Nabarro, Z.S. Basinski & D. Holt
Adv. in Phys. 13 193 (1964)

129. J.H. Cairns, J. Clough, M.A.P. Dewey & J. Nutting
J.Inst.Metals 99 93 (1971)

130. F. Henderson, F.P. Bullen & H.L. Wain
J.Inst.Metals 98 65 (1970)

131. G.E. Dieter
Mechanical Metallurgy, McGraw-Hill, Tokyo
(1961) p. 249

132. J.H. Hollomon
Trans.Met.Soc. A.I.M.E. 162 268 (1945)

133. W.T. Lankford & E. Saibel
Trans. A.I.M.E. 171 562 (1947)

134. A.W. Bowen & P.G. Partridge
J. Phys. D. 7 969 (1974)

135* J.Datsko
Mats. Props & Manf.Proc. Wiley New York (1966)

136* R.P. Carreker & W.R. Hibbard
Acta Met. 1 656 (1953)

137* R.P. Carreker & W.R. Hibbard
Trans A.I.M.E. Journal of metals Oct. 1157 (1957)

138* H.J. Kleemola & M.A. Nieminen
Met. Trans. 5 1863 (1974)

139* E. Voce
Metallurgica 51 219 (1955)

135 R.W. Armstrong
Advances in Materials Research 4 101 (1970)

136 E.O. Hall
Proc.Phys.Soc. 64B 747 (1951)

137 N.J. Petch
J.Iron & Steel Inst. 173 25 (1953)

138 M.M. Hutchinson & R.T. Pascoe
Met.Sci.J. 6 90 (1972)

139 C.J. Ball
Phil. Mag. 2 1011 (1957)

140 D.H. Warrington
Proc. European Conf. on Electron Microscopy
Delft Vereniging (1961)

141 A.W. Thompson & M.L. Baskes
Phil.Mag. 28 301 (1973)

142 R.J. McElroy & Z.C. Szkopiak
Int. Met. Rev. 17 75 (1972)

143. F.P. Bullen & M.M. Hutchinson
Phil.Mag. 7 557 (1962)

144 S. Weissman, T. Imura & N Hosokawa
'Recovery and recrystallisation of Metals' P 241
(Editor L. Himmel) Interscience New York (1962)

145 G. Langford & M. Cohen
Proc. 2nd conf. on strength of metals and alloys
A.S.M. Cleveland (1970) P. 475

146 G. Langford & M. Cohen
Met. Trans. 6A 901 (1975)

147 U. Koster
Met. Sci. 8 151 (1974)

148 Segal A.
Ph D Thesis University of Cambridge (1975)

149 L.H. Van Vlack, O.K. Riegger, R.J. Warrick
& J.M. Dahl.
Trans Met. Soc. A.I.M.E. 221 (1961)

150 R.G.B. Yeo
J. of Metals June (1967) 29

151 R.G.B. Yeo
J. of Metals July (1967) 23

152 L.E. Wood & L.H. Van Vlack
A.S.M. Trans. Quart. 56 (1963) 770

153 H.C. Chao, L. Thomassen & L.H. Van Vlack
Trans. A.S.M. 57 (1967) 386

154 H.C. Chao, L.H. Van Vlack, F Oberin & L. Thomassen
Trans. A.S.M. 57 (1964)

155 H.C. CHao & L.H. Van Vlack
Trans.Met.Soc. A.I.M.E. 233 (1965) 1227

156 T. Boniszewski & R.G. Baker
Acta Met. 11 (1963) 990

157 K.B. Gove & J.A. Charles
Met.Tech 1 (1974) 279

158 K.B. Gove & J.A. Charles
Met.Tech. 1 (1974) 425

159 T.J. Baker & J.A. Charles
J.I.S.I. 210 (1972) 680

160 E. Scheil & R. Schell
Stahl. U. Eisen 72 (1952) 683

161 F.B. Pickering
J.I.S.I. 189 (1958) 148

162. T. Malkiewicz & S. Rudnik
J.I.S.I. 201 (1963) 33

163 D. Brooksbank & K.W. Andrews
J.I.S.I. 206 (1968) 595

164 I. Kozasu & H. Kubota
Trans. I.S.I. Japan 11 (1971) 321

165 T.B. Cox & J.R. Low
Met. Trans 5 (1974) 1457

166 M.F. Ashby
'Strengthening Methods in Crystals' P 137
Eds. A Kelly & R.B. Nicholson
Elservier, London (1971)

167 L.M. Brown & W.M. Stobbs
Phil.Mag. 23 1201 (1971)

168 J.L. Brimhall & R.A. Huggins
Trans A.I.M.E. 233 1076 (1965)

169 N. Hanson & B.Bay
J. Met. Sci. 7 1351 (1972)

170 N.E. Ryan & S.I.M. Johnston
J. Less Common Metals 20 7 (1970)

171 N.E. Ryan
Acta Met. 17 269 (1969)

172 K. Onol
Phd Thesis University of Leeds (1977)

173 A.S. Argon, J. Im & R Safoglu
Met. Trans. 6A 1975 825

174 B.I. Edelson & W.M. Baldwin Jr.
Trans A.S.M. 55 1962 230

175 I.G. Palmer & G.C. Smith
Met.Soc. A.I.M.E. Conf.
'Oxide Dispersion Strengthening'
Bolton Landing 1966 p 253

176 Tsuyoshi, Inoue, Shushi & Kinoshita
Inst. of Metals & I.S.I. 3rd Int. Conf
'The Strength of Metals & Alloys' Cambridge (1973)p 159

177 D. Broek
Int.Met.Rev. 19 135 (1974)

178 B.R. Butcher
Atomic Energy Research Establishment Report No R.7314

179 I. Girland & J. Plateau
Trans A.S.M. 56 (1963) 442

180 M.F. Ashby
Phil. Mag. 14 (1966) 1157

181 H. Ernst
Anals of the New York Academy of Sciences
53 936 (1951)

182 I. Finnie
Mech.Engr. 78 715 (1956)

183 E.J.A. Amarego & R.H. Brown
'The machining of metals'
Prentice Hall Inc. New Jersey (1969)

184 E.D. Doyle & L.E. Samuels
J. Aust. Inst. Metals 21 11 (1976)

185 H. Ernst
'Machining of Metals'
Cleveland Ohio Amer. Soc. Met. (1938)

186. M.E. Merchant
J. Appl.Phys. 16 267 (1945)

187 Doyle E.D.
Pro.Int.Conf.Pro.Eng. Japan Part 1 P.522 (1974)

188 Palmer, W.B. & Oxley P.L.B.
Proc.Inst.Mech.Engrs. 173 623 (1959)

189 Okushima K. & Hitomi K
Trans.Amer.Soc.Mech.Engrs. Series B.J. of Eng.
for Ind. 83 545 (1961)

190 Trent E.M.
Metal cutting Butterworths London (1977)

191 von Turkovitch B.F.
Trans.A.S.M.E. Series B 92 153 (1970)

192 Recht R.F.
J. Appl.Mech. Series E 31 189 (1964)

193 Lemaire J.C. & Backofen W.A.
Met.Trans. 3 447 (1972)

194 Turley D.M.
Mat. Sci. and Eng 19 79 (1975)

195 Grozin B.D. & Tankevich.
Friction and Wear in Machinery 15 143 (1962)

196 Ramalingam S. & Black J.T.
Met.Trans. 4 1103 (1973)

197 Doyle E.D. & Aghan R.L.
Met.Trans. 6B 143 (March 1975)

198 Komanduri R. & Brown R.H.
Metals and Materials 6 531 (1972)

199 Brown R.H. & Luong H.S.
Metals Technology 2 1 (1975)

200 P.W. Bridgeman
J. Appl. Phys. 8 329 (1937)

201 B. Crossland
Proc. Inst.Mech.Engrs. 168 935 (1954)

202 W.R. Backer, E.R. Marshall & M.C. Shaw
Trans.Amer.Soc.Mech.Engrs. 74 61 (1952)

203 M.C. Shaw & I. Finnie
Trans. Amer.Soc.Mech.Engrs. 77 115 (1955)

204 E.J.A. AMarego & R.H. Brown
Int.J.Prod.Res. 1 75 (1962)

205 P.L.B. Oxley
Int.J.Mech.Sci. 3 68 (1961)

206. A.H. Cottrell
Conference on the properties of metals at high rates of strain. London Inst.Mech.Engrs. (1957)

207. S. Kobayashi & E.G. Thomson
Trans.Amer.Soc.Mech. Engrs. Series B, J.of Eng. for Ind. 81 251 (1959)

208 D.C. Drucker
J. Appl.Phys. 20 1013 (1949)

209 M.C. Shaw, N.H. Cook & P.A. Smith
Trans A.S.M. Series B 83 163 (1961)

210 C. Rubenstein
'Machinability'
Iron and Steel Inst. Special Report No. 94
P.49 (1968)

211 R. Kiessling
'Non Metalic Inclusions in Steel' Part 3
Iron and Steel Inst. Publication. (1968)

212M.E. Merchant & N. Zlatin
Trans.A.S.M. 41 647 (1949)

213 E.M. Trent
'Machinability'
Iron & Steel Inst. Special Report No. 94 P.11

214 J. Hazra, D. Caffarrelli & S. Ramalingam
Proc.Int.Conf.Prod.Eng. Japan Pt.1 P.509 (1974)

215 K. Iwata & K. Ueda
Proc.Int.Conf.Prod.Eng.Japan Pt.1 516 (1974)

216 E.D. Doyle
Proc.Int.Conf.Prod.Eng.Japan Part 1, P.522 (1974)

217 C.D.H.Stoddart, M.P. Seah, M.McLean & B. Mills
Nature 252 187 (1975)

218 J.R. Low Jr. Relation
'The Relation of Microstructure to Brittle Fracture'
'Relation of Properties to Microstructure'
Amer.Soc.Met. Cleveland Ohio (1954) P 153

219 J.R. Low Jr.
'Dislocations and Brittle Fracture in Metals'
Deformation and Flow of Solids.
IUTAM Conf. Madrid 1955, Springer Verlag,Berlin(1956)
P 60

220 W.S. Owen, B.L. Averbach, & M. Cohen
Trans. A.S.M. 50 634, (1958)

221 I.E. French & P.F. Weinrich
Met. Trans 7A 1841 (1976)

222 I.E. French & P.F. Weinrich
J.Aust Inst. of Metals 22 No.1 40 (1977)

223C.F. Tipper
Metallurgia 39 133 (1949)

224 H.C. Rogers
Trans. A.I.M.E. 218 498 (1960)

225 K.E. Puttick
Phil.Mag. 4 964 (1959)

226 K.E. Puttick
Phil.Mag. 5 759 (1960)

227 I.G. Palmer & G.C. Smith
A.I.M.E.Conf.Oxide Dispersion Strengthening
Gordon & Breach New York (1967)

228 D. Brock
Int.Metall.Reviews. 19 135 (1974)

229 G.Y. Chin, W.F. Hosford & W.A. Backofen
Trans.AIME 230 437 (1964)

230 I.E. French & P.F. Weinrich
Met.Trans.A. 6A 1165 (1975)

231 H.C. Rogers
Acta Met. 7 750 (1959)

232 P.F. Weinrich & I.E. French
Acts.Met. 24 317 (1976)

233 I.E. French & P.F. Weinrich
Acta met. 21 1533 (1973)

234 H.C. Rogers
'Fundimental aspects of deformation processing'
Eds. W.A.Backofen, J.W.Burke, L.F. Coffin Jr.,
W.L. Reed, & V. Weiss. Syracuse University Press (1964)

235 F.D. Rosi & M.S. Abrahams
Acts.Met. 8 807 (1960)

236 I.E. French & P.F. Weinrich
Met.Trans. 6A 785 (1975)

237 H.W. Swift
Journal of the Iron & Steel Inst. 140 181 (1939)

238 C. Zener & J.H. Hollomon
Trans.Amer.Soc.Metals 33 163 (1944)

239 L.J. Klinger & G. Sachs
Journal of the Aeromautical Sciences 15 731 (1948)

240 W.A. Backofen, A.J. Shaler & B.B. Hundy
Trans.of the Amer.Soc.Metals 46 655 (1954)

241 W.A. Backofen & B.B. Hundy
Journal of the Inst. of metals 81 433 (1953)

242J.H. Hollomon & C. Zener
Journal of Appl.Phys. 17 82 (1946)

243 . J.H. Hollomon
'The Problem of Fracture'
Amer. Welding Soc. (1946)

244 M. Gensamer, E. Saibel, J.T. Ransom & R.E.Lowrie
'The Fracture of metals'
Amer. Welding Soc. New York (1947)

245 J.H. Hollomon
'Fracture and the Structure of metals'
Amer.Soc.Metals, Cleveland Ohio. P262 (1948)

246 F. deKazinczy & W.A. Backofen
Trans.Amer.Soc.Metals 53 55 (1951)

247 B.M. Kapadia, A.T. English & F.A. Backofen
Trans.Amer.Soc.Metals 55 389 (1962)

248 J.R. Low
'Deformation and Flow of Solids'
Springer Verlag Berlin (1956)

249 W.S..Owen, B.L. Averbach & M. Cohen
Trans ASM 50 634 (1958)

250 A.W. Sleeswyck & C.A. Verbraak
Acta Met. 9 917 (1961)

251 R. Honda
J.Phys.Soc.Japan 16 1309 (1961)

252 P.B. Hirsch, A. Howie, R.B.Nicholson, D.W. Pashley
& M.J. Whelan
'Electron Microscopy of Thin Crystals'
London Butterworths (1965)

253 R.C. Gifkins
'Optical microscopy of metals'
Sir Issac Pitman and Sons, Ltd
London (1970) (appendix)

254 J. Iron & Steel Inst. 1145 (1966)

255 D.H. Kay
'Techniques for Electron Microscopy'
Blackwell, Oxford (1965)

256 F.A. Lowenheim
'Modern Electroplating'
J. Wiley & Sons (1974)

257 J. Woolman & R.A. Mottram
'Mechanical and Physical Properties
of the British Standard EN Steels'
Vol. 1, P.1,38,101.
Pergamon Press 1964.

258 E.D. Doyle
Proc. Int. Conf. Prod. Eng.
Japan Pt.1 (1974)

259 D.J. Willis
PhD Thesis University of N.S.W.(1976)

260 Ref. 131 2nd Ed. P. 340

261 D. McLean
'Mechanical Properties of Metals'
P.153-161
J. Wiley & Sons N.Y.(1962)

262 W.A. Backofen
'Deformation Processing'
P. 251
Addison Wesley (1972)

263 J. Nutting
Private communication.

264 W.B. Hutchinson, B.J.Duggan & M. Hatherly
To be published.

265 J. Gil Sevillano, P. Van Houtts & E. Aernoudt
Scripta Met. 11 581 (1977)

266 Texture 2 35 (1976)

267 P. Van Houtts & E. Aernoudt
Mat. Sci. Eng. 23 11 (1976)

268 M. Hatherly
To be published.

269 A.A. Griffith
Philos. Trans. R. Roc. London 221A 163 (1920)
(reprinted Trans.Am.Soc.Met. 61 871 (1968)

270 Ref. 131 2nd Ed. P.131

271 E.D. Doyle
Private discussion.

272 R.L. Aghan Unpublished Work.

FIGURE 2.1

Representation of the yield stress at high strain rates according to Cottrell.
(After ref. 183)

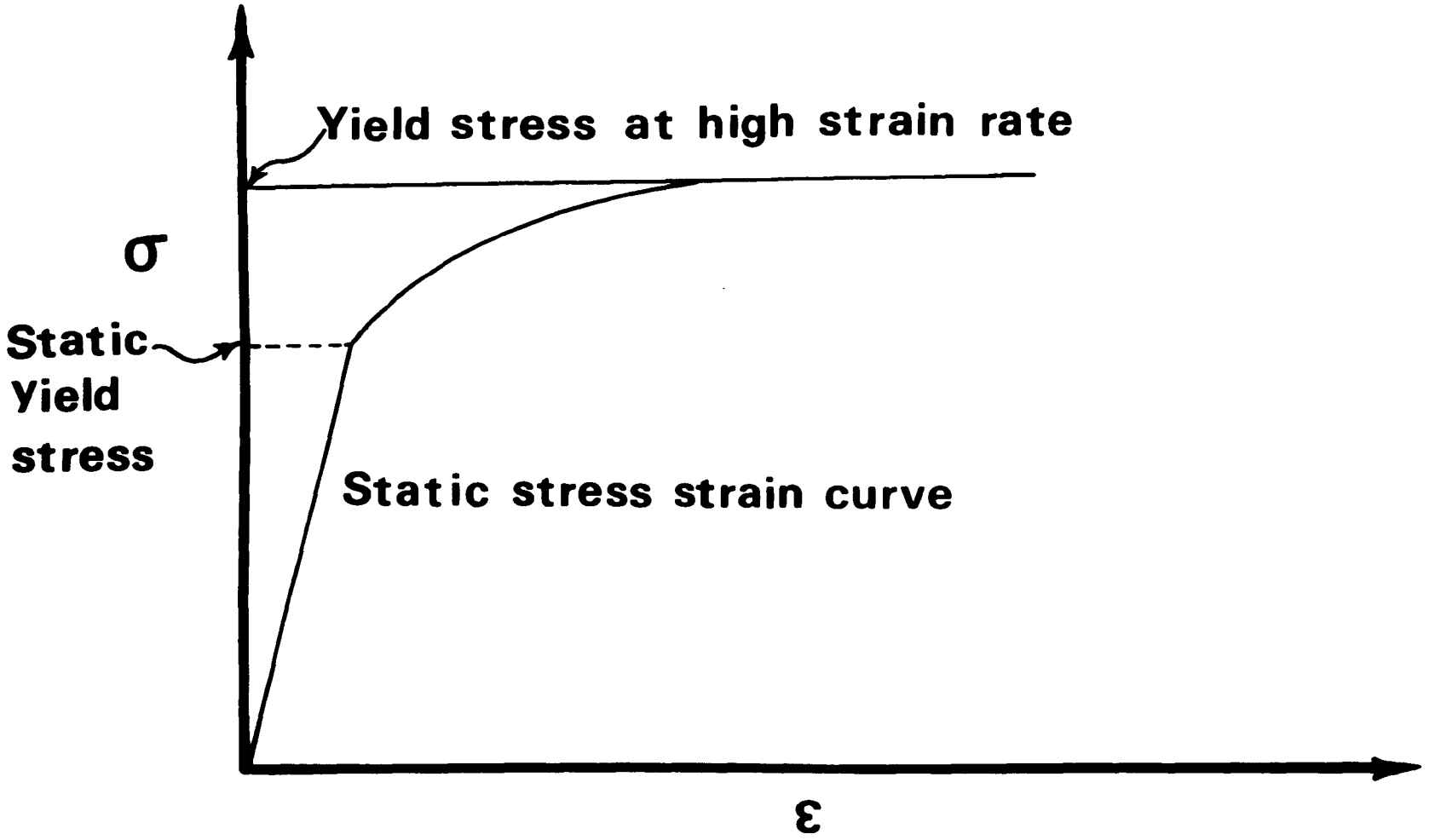
Yield stress at high strain rate
σ
Static
yield
stress
Static stress strain curve
ε

FIGURE 2.2

A typical cup-cone fracture surface showing an equiaxed dimple region in the centre and sloping outer regions.
(After French and Weinrich in ref. 222)

FIGURE 2.3

The sequence of events in the development of a double cup fracture surface.
(after ref. 222)

FIGURE 2.4

A typical double cup fracture surface.
(After ref. 222)

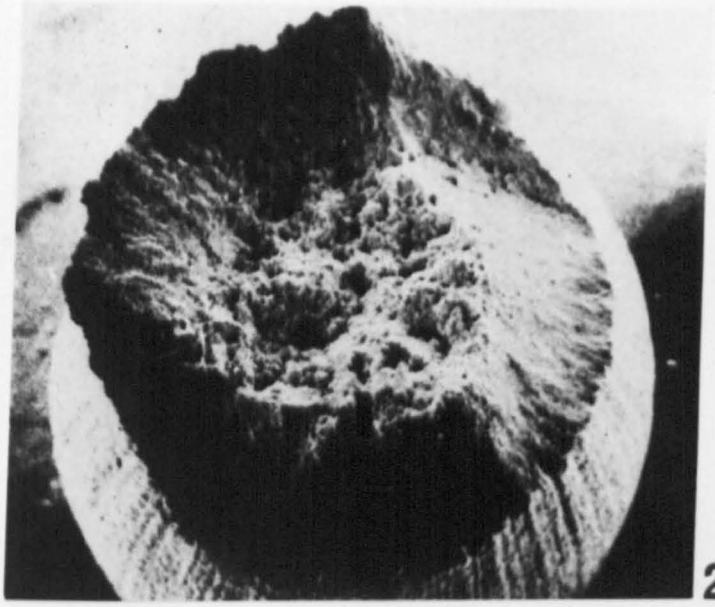

2•2

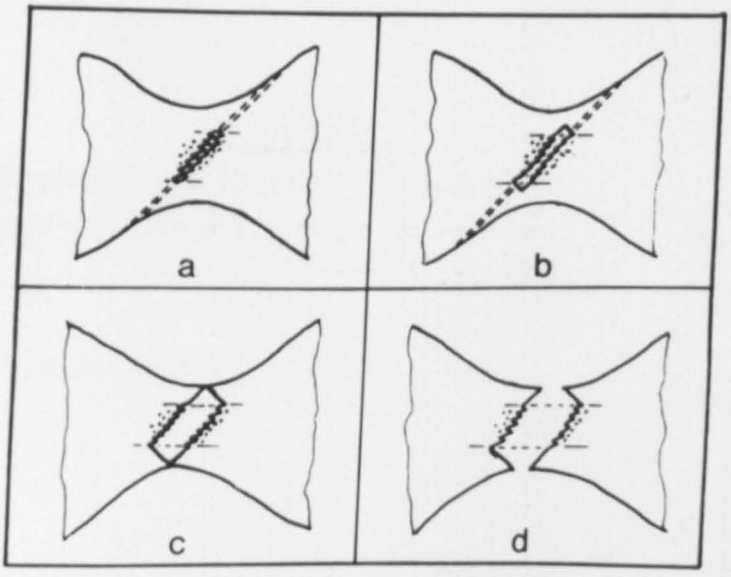

2•3

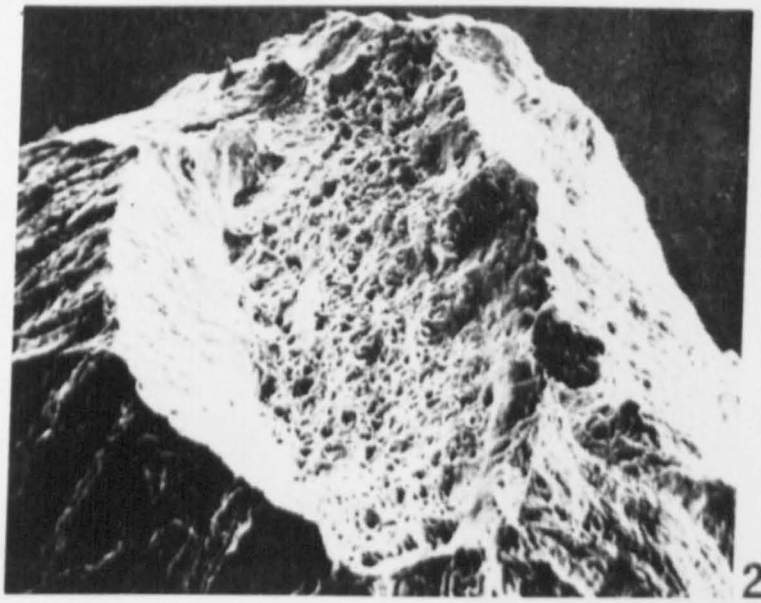

2•4

FIGURE 2.5

Typical fracture surface of a sample which has failed by a shear type tensile fracture process.
(After ref. 222)

FIGURE 2.6

Two aspects of the specimen at different stages of the ductile rupture (or chisel point fracture) process.
(After ref. 222)

A typical fracture surface is shown in figure 2.7.

FIGURE 2.7

A typical fracture surface of a sample which has failed by a ductile rupture process.
(After ref. 222)

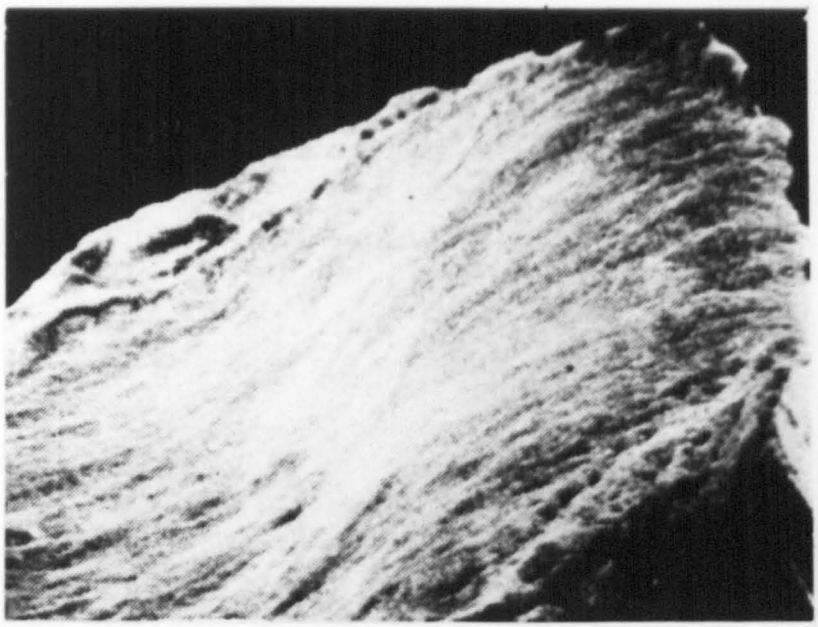

2•5

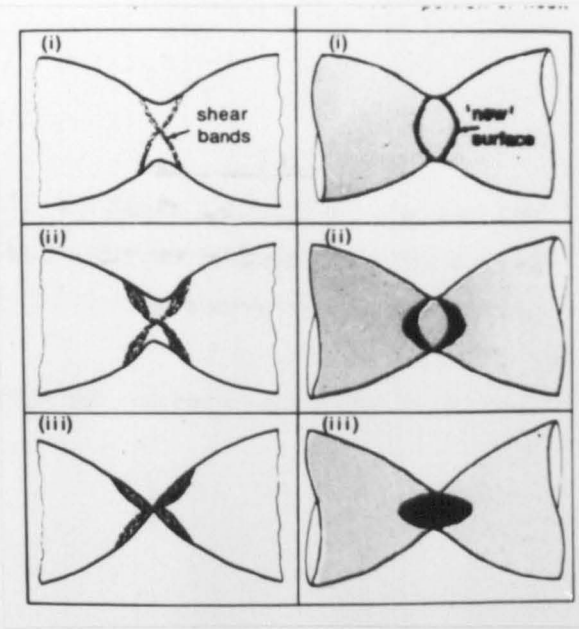

2•6

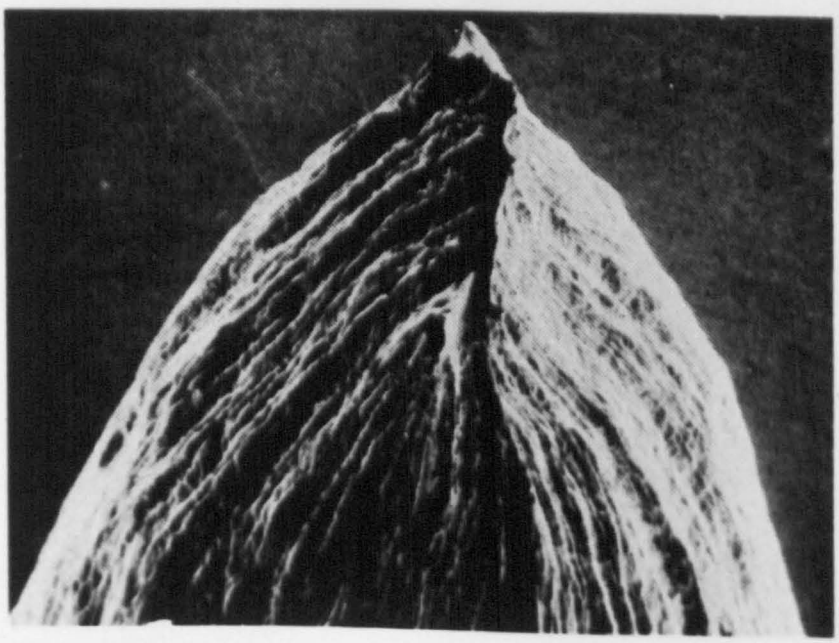

2•7

FIGURE 4.1

Jetting device used in the final thinning of the specimens for straining within the electron microscope.

FIGURE 4.2

The sequence of operations used in the production of the two stage replicas.

FIGURE 4.3

Solvent still, used to disolve the plastic during the making of the two stage replicas.

4•1

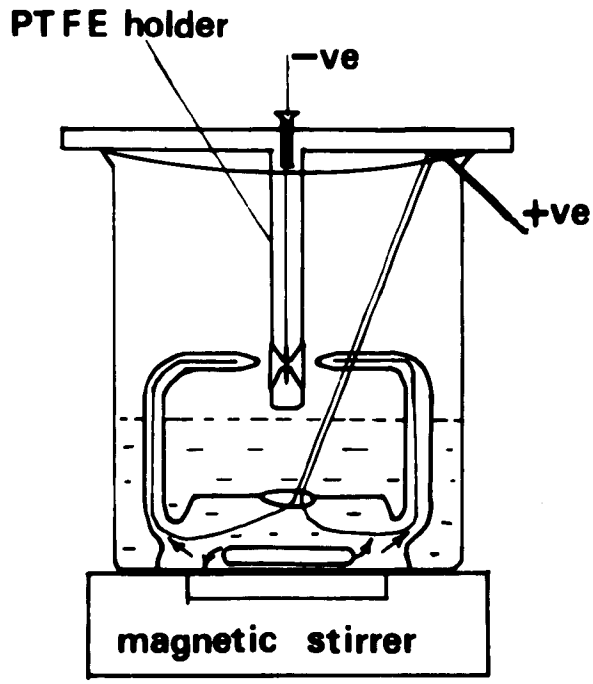
PTFE holder
-ve
+ve
magnetic stirrer

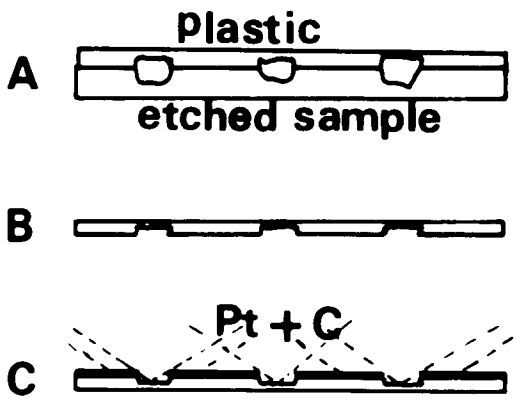
A
Plastic
etched sample
B
C
Pt + C
D
finished replica

4•2

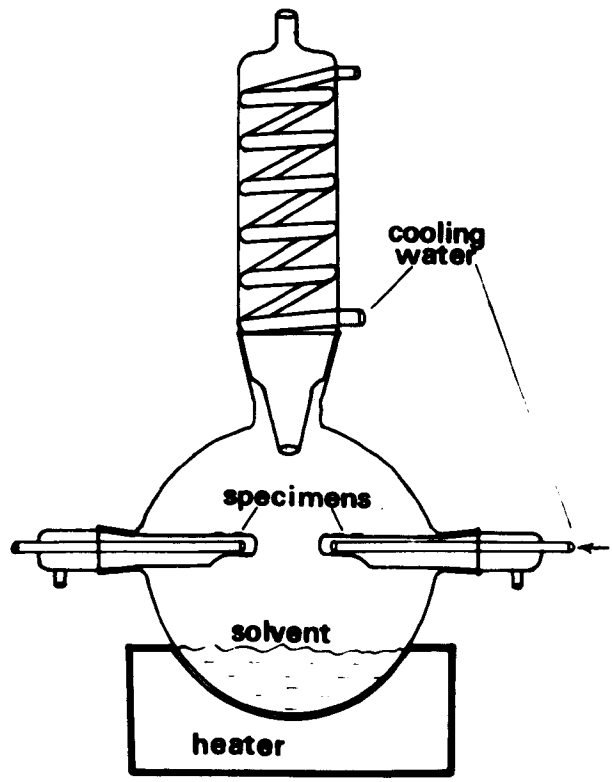
cooling water
specimens
solvent
heater

4•3

FIGURE 5.1

Replica of the starting structure of the 1st steel in the Quenched and Tempered condition.

1μm

FIGURE 5.2

Quenched and tempered steel after 40% reduction. The foil was made from a section transverse to the rolling direction and along the length.

0.5μm

FIGURE 5.3

Transverse section of the quenched and tempered steel after 40% reduction, showing a group of elongated cells and grain boundary carbides in the lower right corner.

1 μm

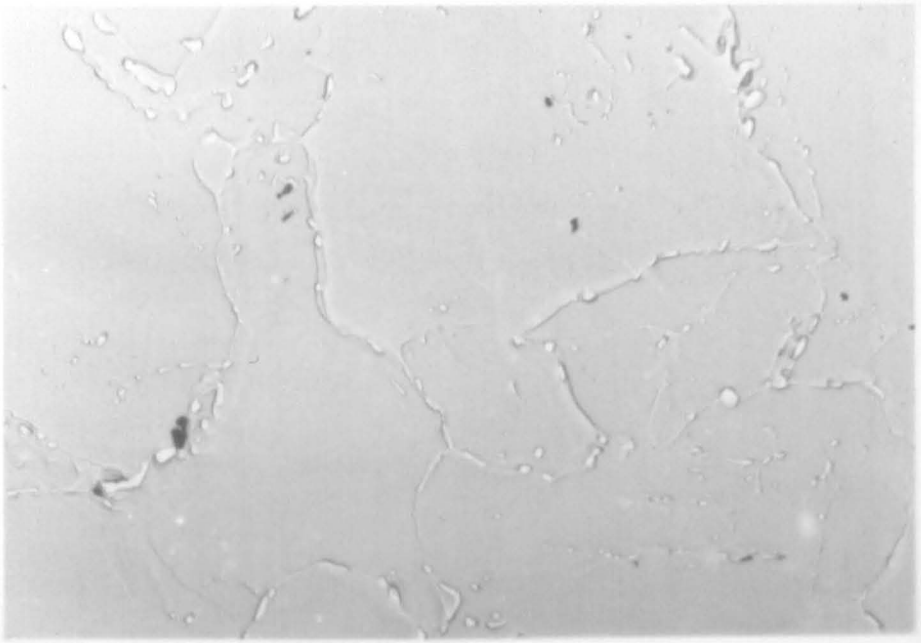

5•1

5•2

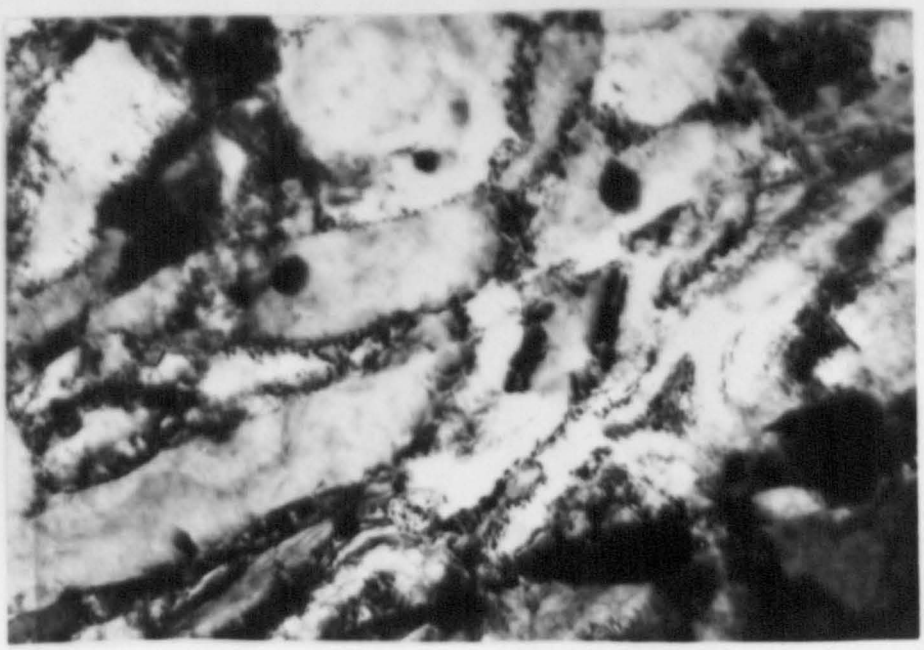

5•3

FIGURE 5.4

Electron diffraction pattern of the area shown in Figure 5.3

FIGURE 5.5

A band of elongated cells in the Quenched and tempered steel after 60% reduction by rolling.

1μm

FIGURE 5.6

Quenched and tempered steel after 60% reduction, showing a stepped grain boundary with elongated bands running from it. The arrow gives the rolling direction.

1μm

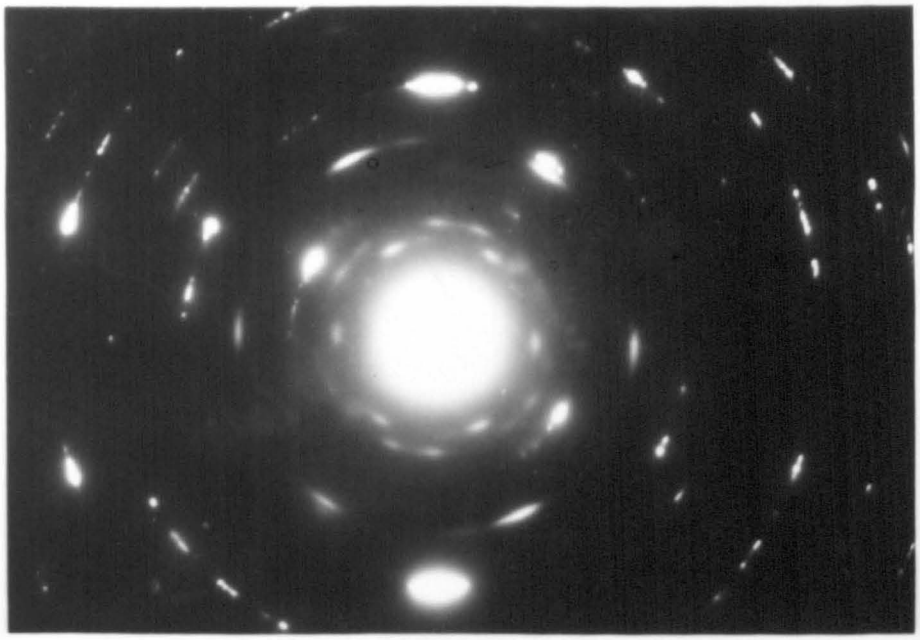

5•4

5•5

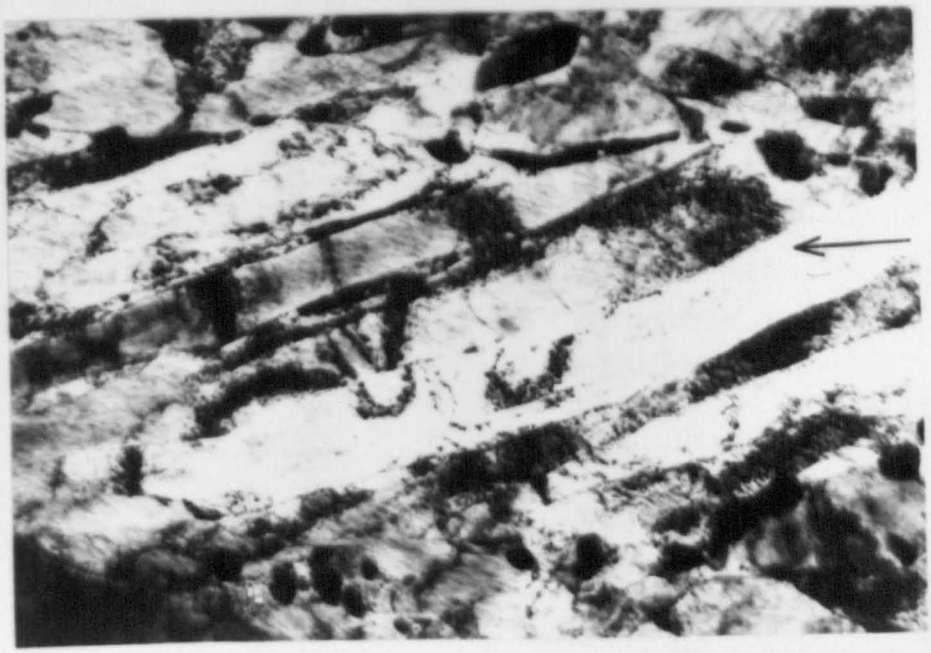

5•6

FIGURE 5.7

Electron diffraction pattern of the lower grain in figure 5.6. The foil surface is a {111} plane. If this is assigned $(\bar{1}\bar{1}1)$ Then $(10\bar{1})$ is perpendicular to the foil and its trace is in the direction of the cell boundaries.

FIGURE 5.8

Rolling plane section of quenched and tempered steel after 80% reduction by rolling

0.5μm

FIGURE 5.9

Electron diffraction pattern of the area shown in figure 5.8

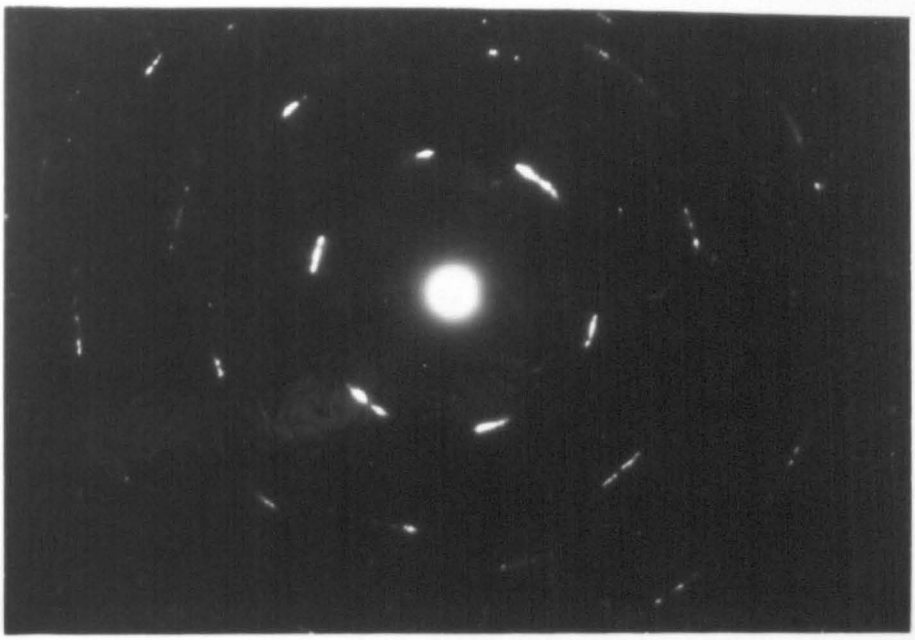

5•7

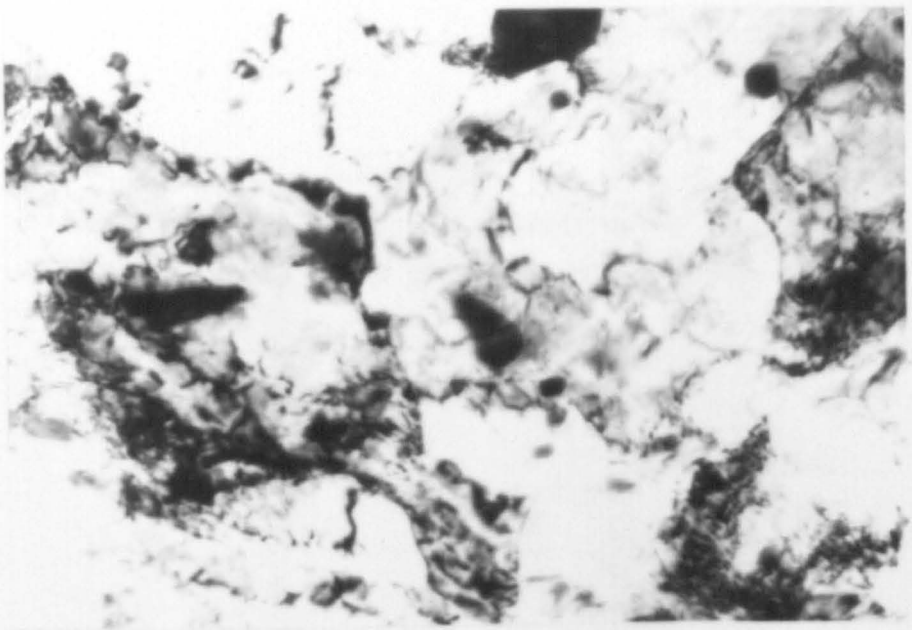

5•8

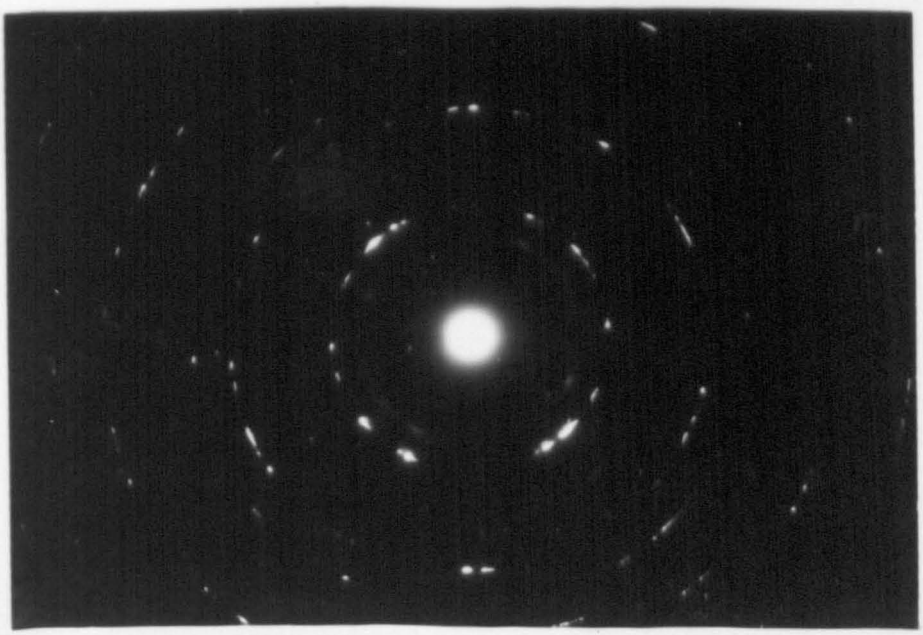

5•9

FIGURE 5.10

Transverse section of quenched and tempered steel after 80% reduction. If the foil surface is assigned (113) then the long cell boundaries are in the direction of the trace of the (211) slip plane.

0.5 μm

FIGURE 5.11

Electron diffraction pattern of the area shown in figure 5.10. The foil plane is {113}

FIGURE 5.12

Rolling plane section of quenched and tempered steel after 98·5% reduction by rolling.

0.5 μm

5•10

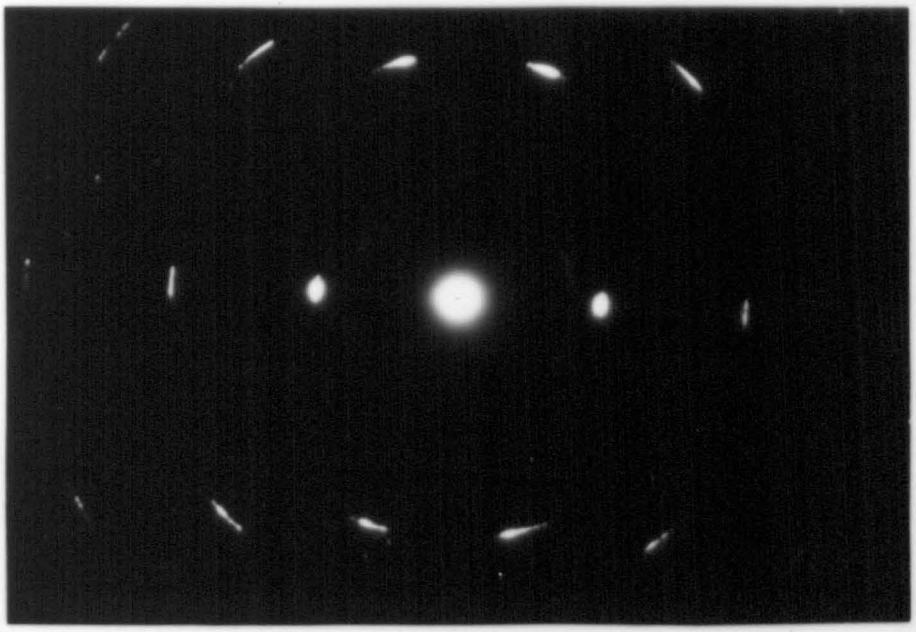

5•11

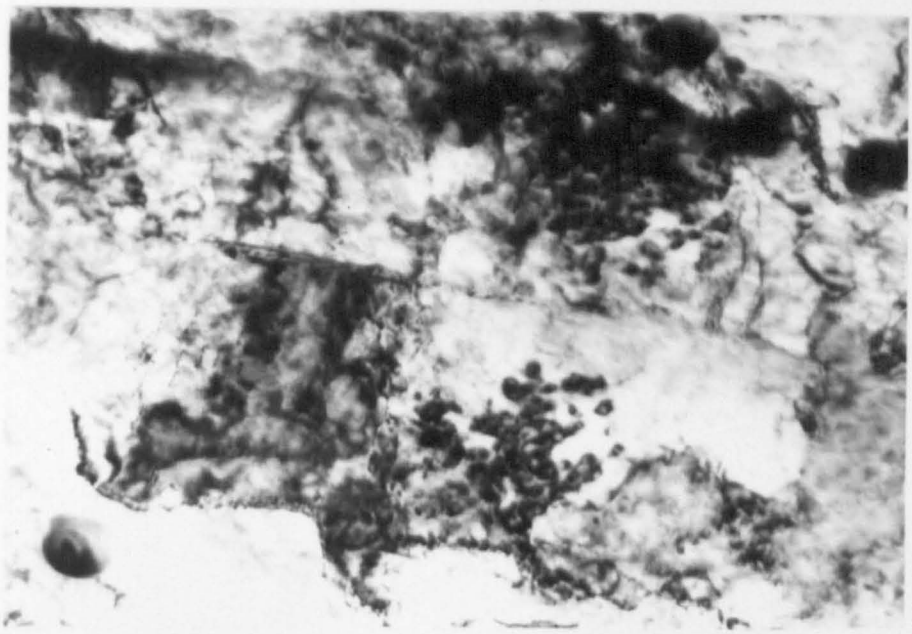

5•12

FIGURE 5.13

Rolling plane section of the quenched and tempered steel after 98.5% reduction by rolling.

0.1 μm

FIGURE 5.14

Electron diffraction pattern of the area shown in figure 5.13

FIGURE 5.15

Transverse section of quenched and tempered steel after 90% reduction by rolling.
The rolling direction is shown by the arrow.

1μm

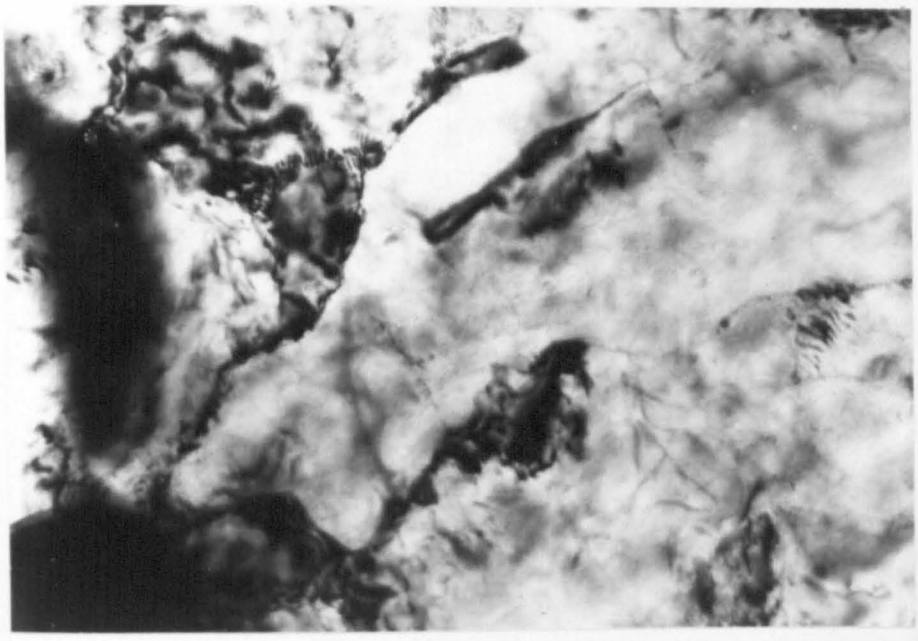

5•13

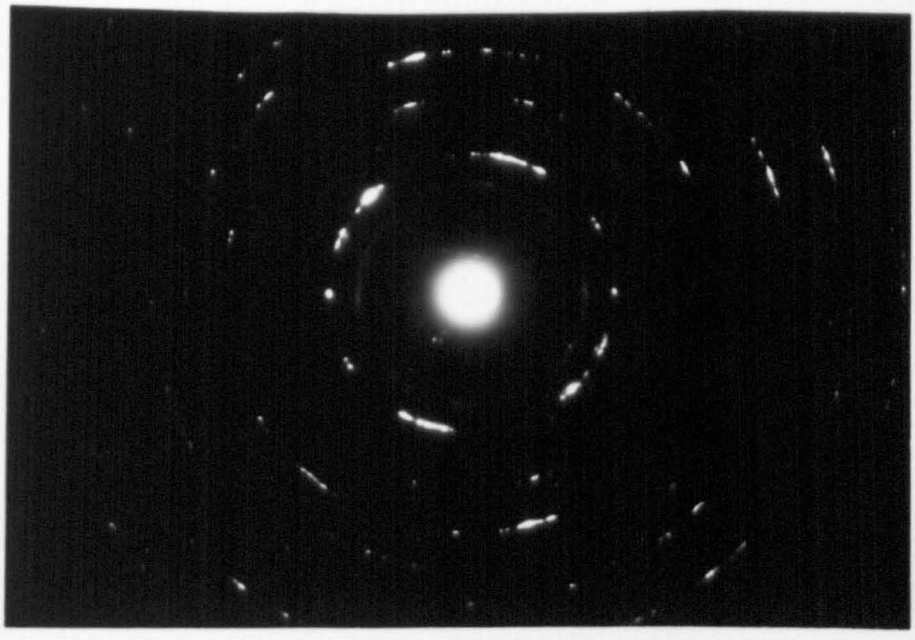

5•14

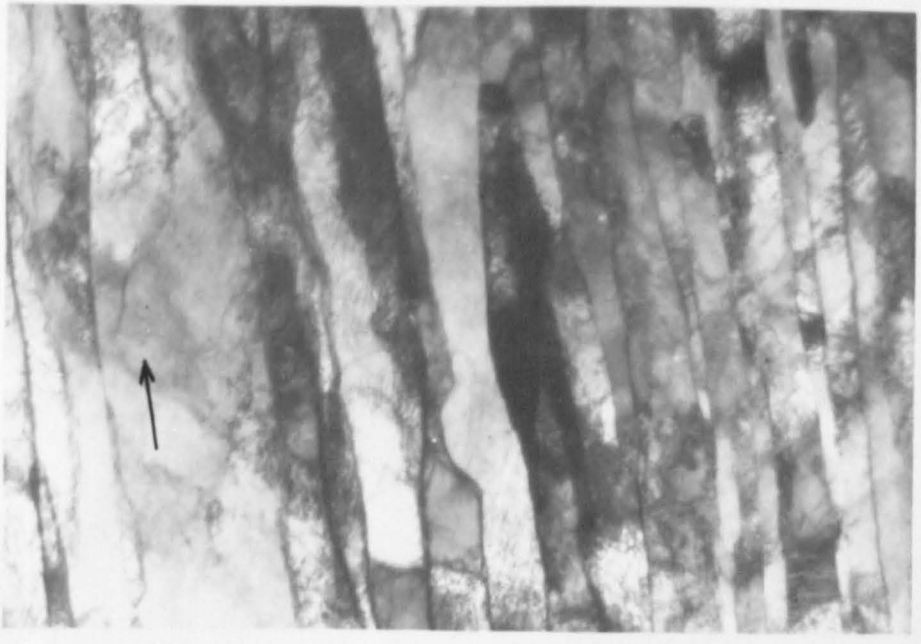

5•15

FIGURE 5.16

Transverse section of quenched and tempered steel after 95% reduction by rolling.

0.5 μm

FIGURE 5.17a

Electron diffraction pattern of a typical elongated band in the quenched and tempered steel after 90% reduction. The first in a series showing the rotation of the diffraction spots as the band is traversed.

FIGURE 5.17b

The second diffraction pattern in a series taken as a typical band of elongated cells was traversed. At this point the pattern has rotated 4° from the point where the series was started.

5•16

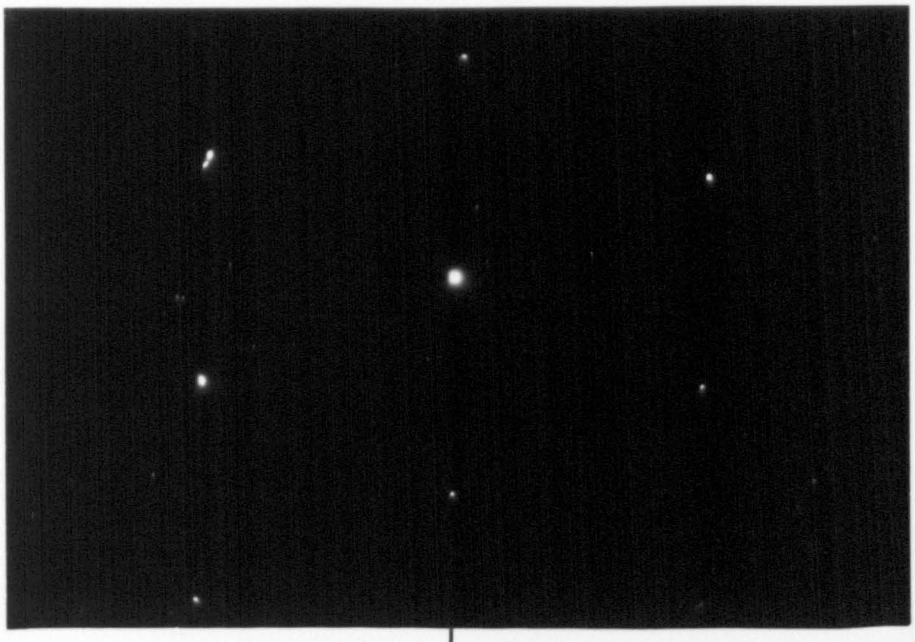

5•17a

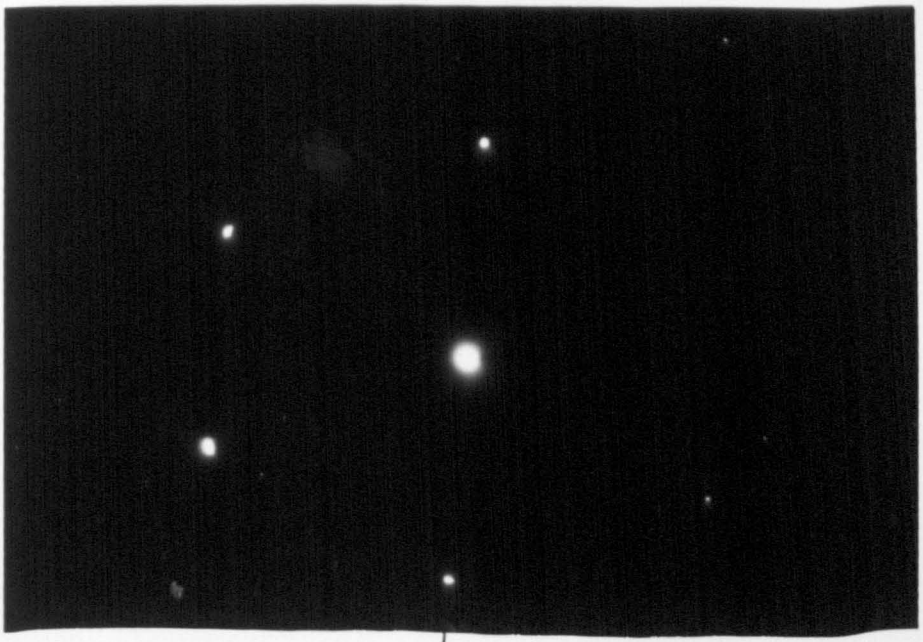

5•17b

FIGURE 5.17c

The third diffraction pattern in a series taken as a typical band of elongated cells was traversed. At this point the pattern has rotated 8^{o} from the starting point.

FIGURE 5.18

High voltage electron micrograph taken of the quenched and tempered steel after 90% reduction by rolling. The foil is a transverse section.

1 µm

FIGURE 5.19

Transverse to rolling direction and across the width. (Rolling direction out of the page) Quenched and tempered steel after 60% reduction by rolling.

1 µm

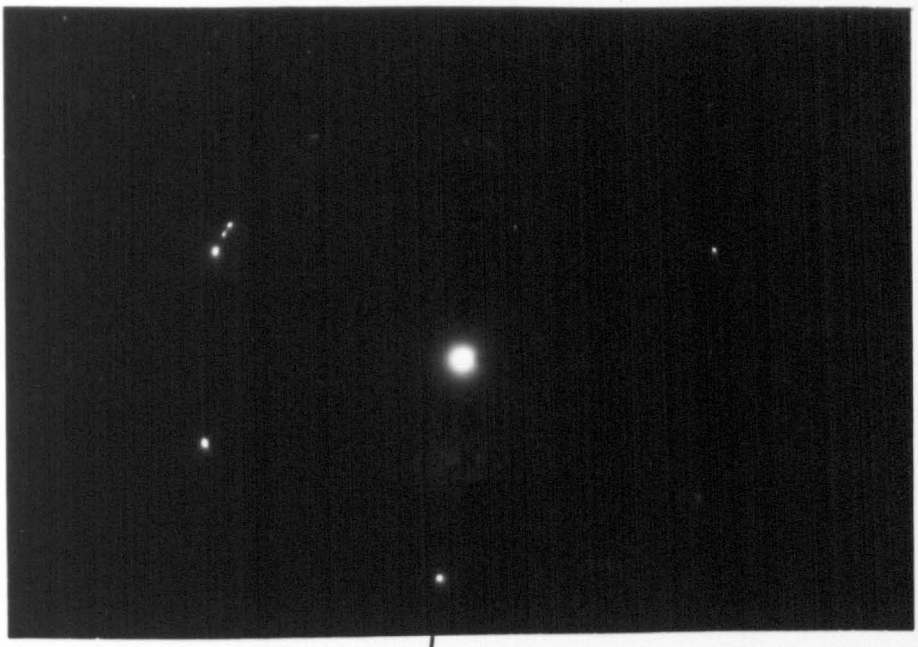

5•17c

5•18

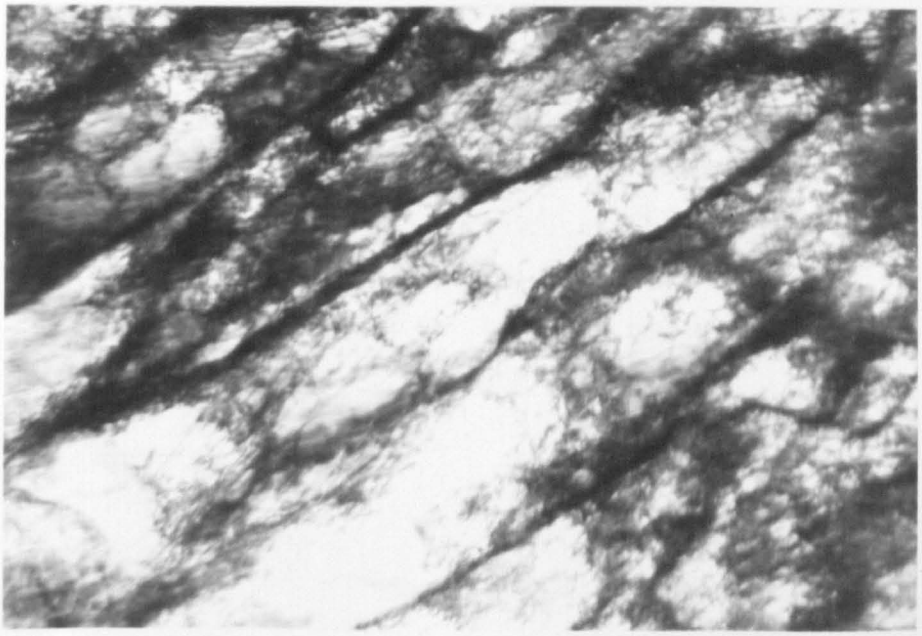

5•19

FIGURE 5.20

Transverse section across the width of the quenched and tempered steel after 60% reduction by rolling.

1μm

FIGURE 5.21

Electron diffraction pattern of the area shown in figure 5.20.

FIGURE 5.22

Two stage replica of etched surface of quenched and tempered steel after 60% reduction by rolling.

10μm

5•20

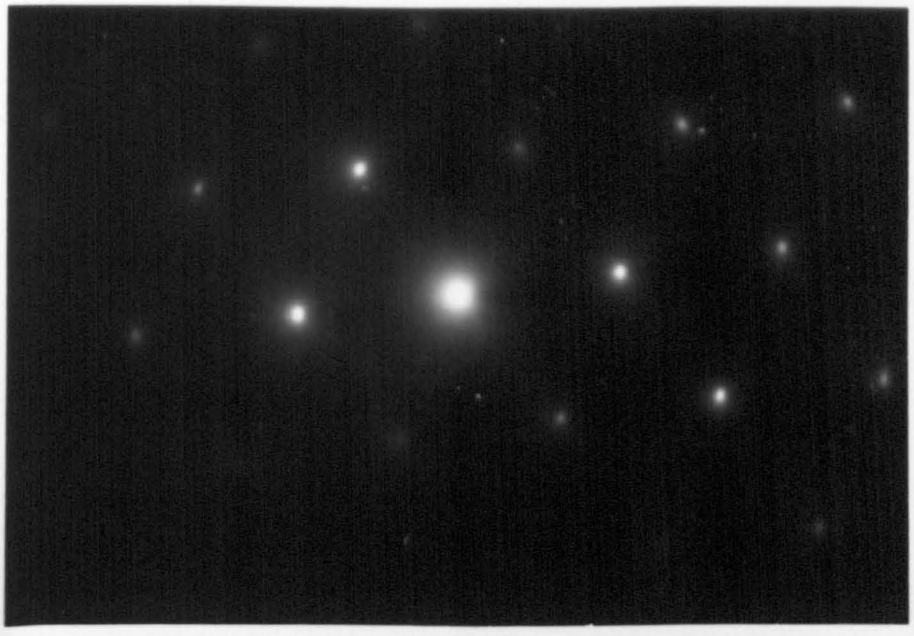

5•21

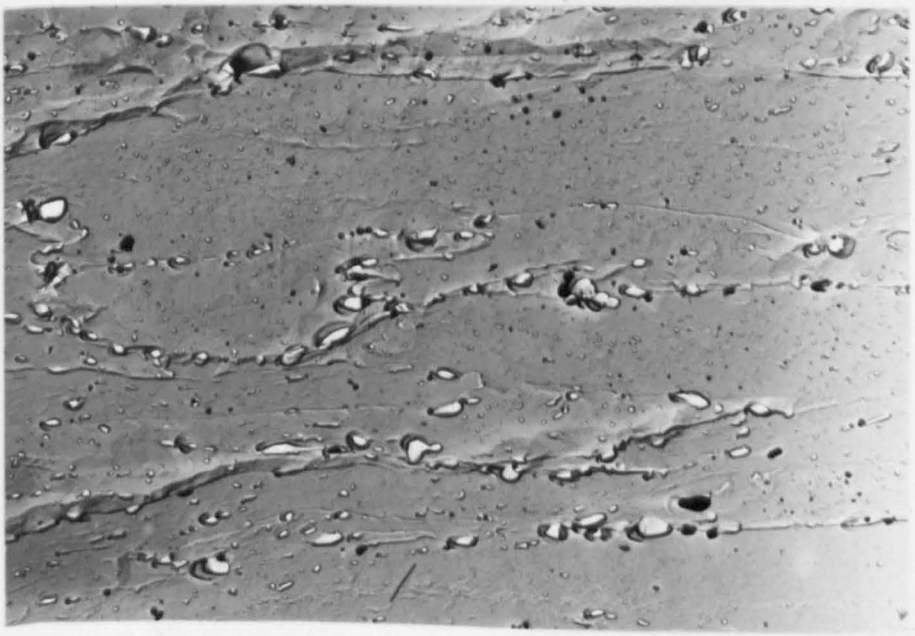

5•22

FIGURE 5.23

Two stage replica of quenched and tempered steel after 80% reduction by rolling, showing trails associated with the larger carbide particles.

10 μm

FIGURE 5.24

Replica of the feature shown in figure 5.23 shadowed at a low angle to show that they are cracks.

1μm

FIGURE 5.25

Optical micrograph of quenched and tempered steel after 80% reduction by rolling.

10 μm

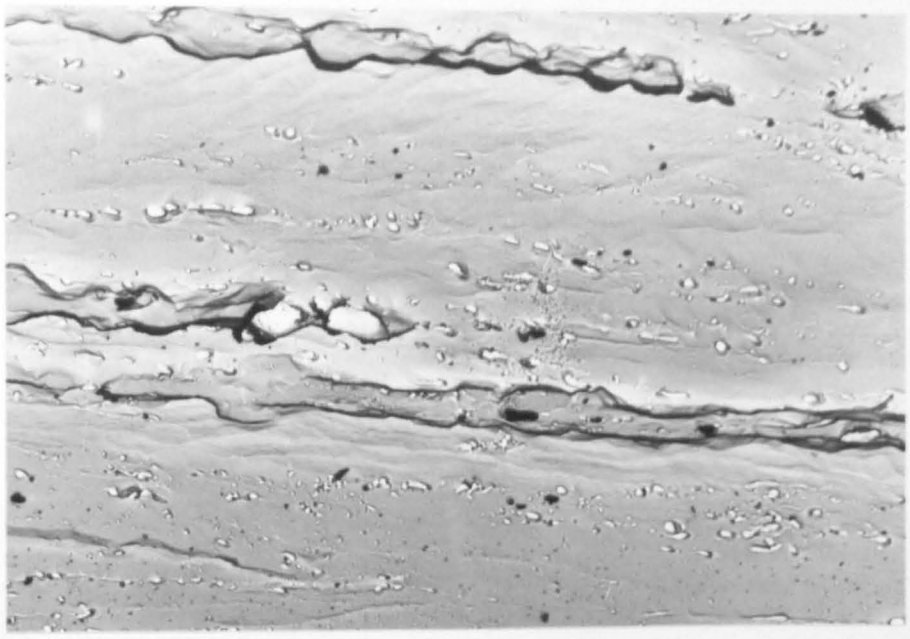

5•23

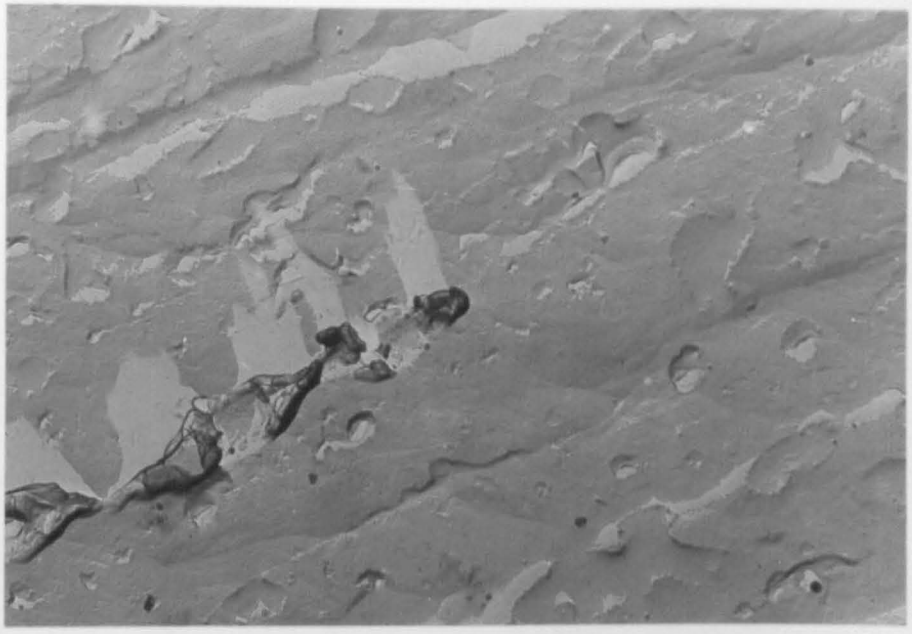

5•24

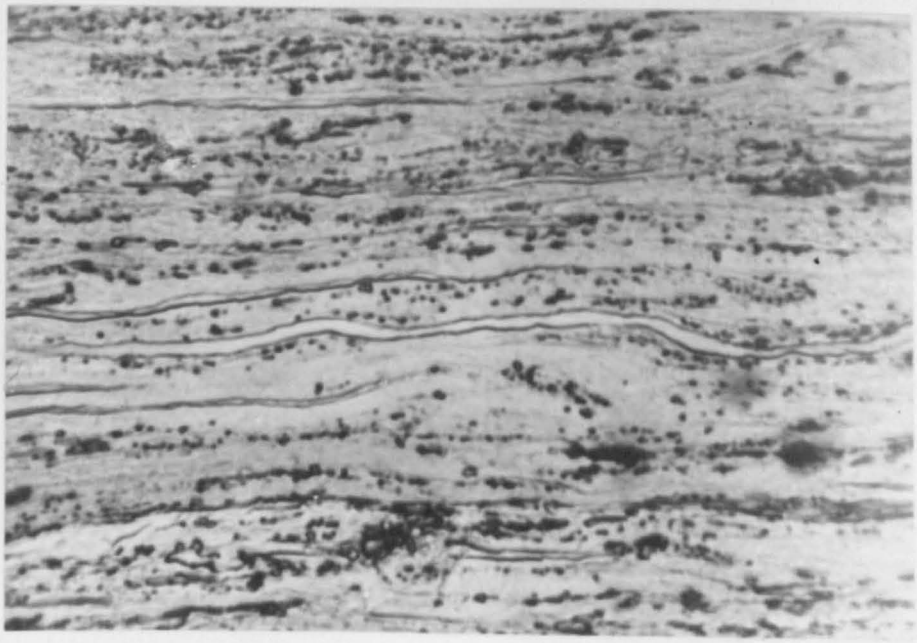

5•25

FIGURE 5.26

Phase contrast optical micrograph of quenched and tempered steel after 60% reduction by rolling

10μm

FIGURE 5.27

Normalised steel. Optical micrograph after 10% reduction by rolling, showing light etching bands and steps in the grain boundaries.

5 μm

FIGURE 5.28

Optical micrograph of the normalised steel showing the typical shape of the grains after 30% reduction by rolling.

5μm

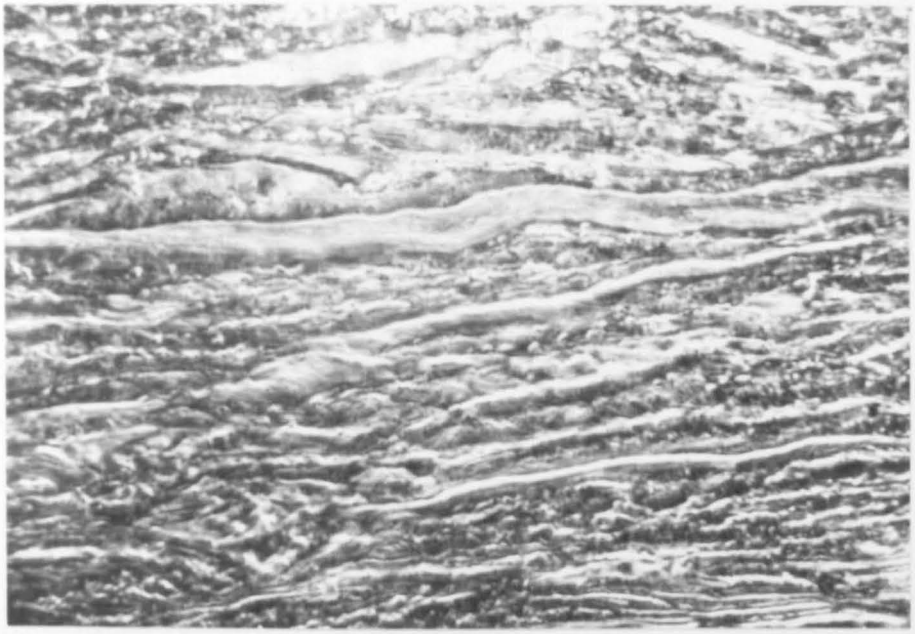

5•26

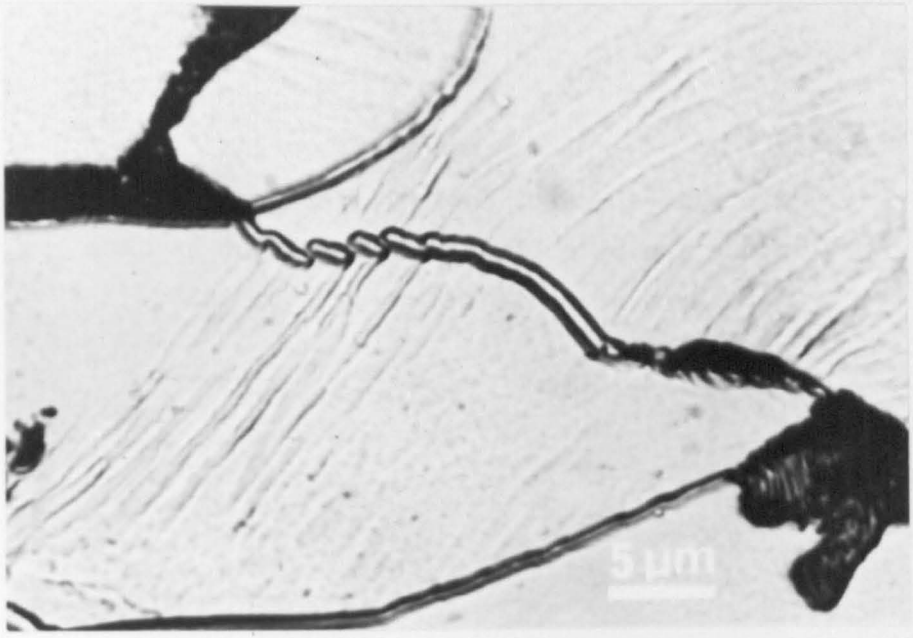

5•27

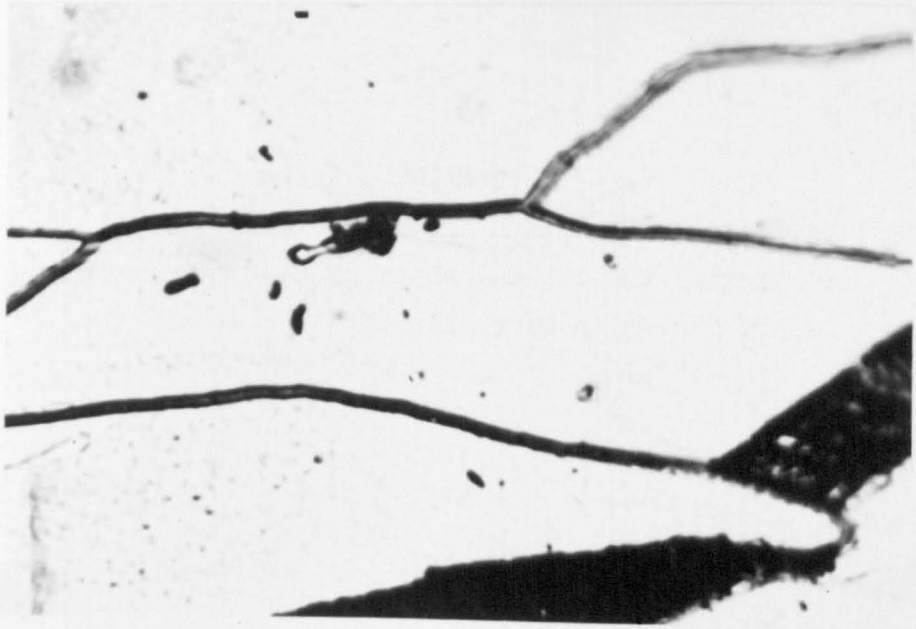

5•28

FIGURE 5.29

Optical micrograph of normalised steel after 60% reduction by rolling, showing the fragmentation of grain boundaries by shear associated with the band structure.

5μm

FIGURE 5.30

The average angle within the grains subtending the rolling direction plotted against rolling strain.

FIGURE 5.31

Photo emission electron micrograph of the normalised steel after 60% reduction by rolling.

10μm

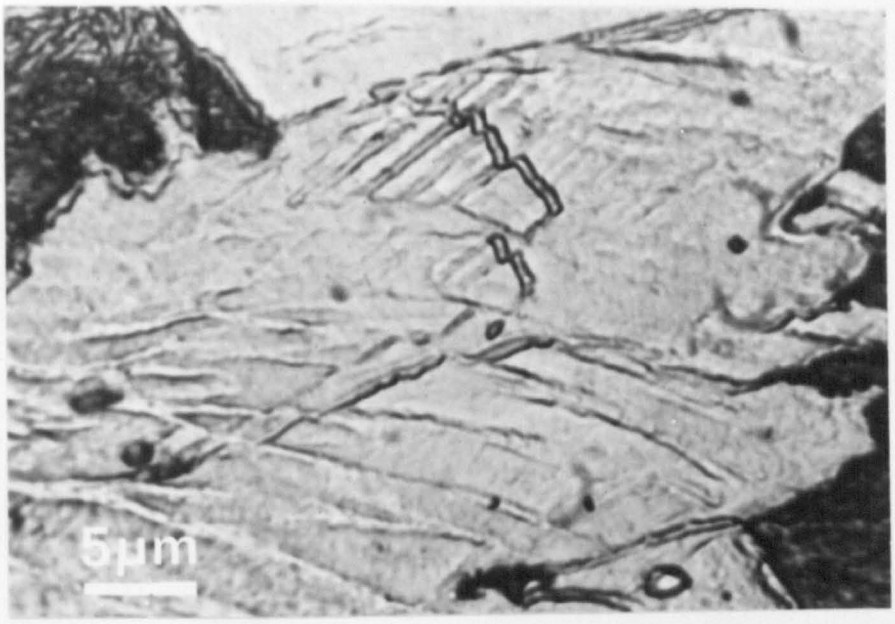
5μm

5•29

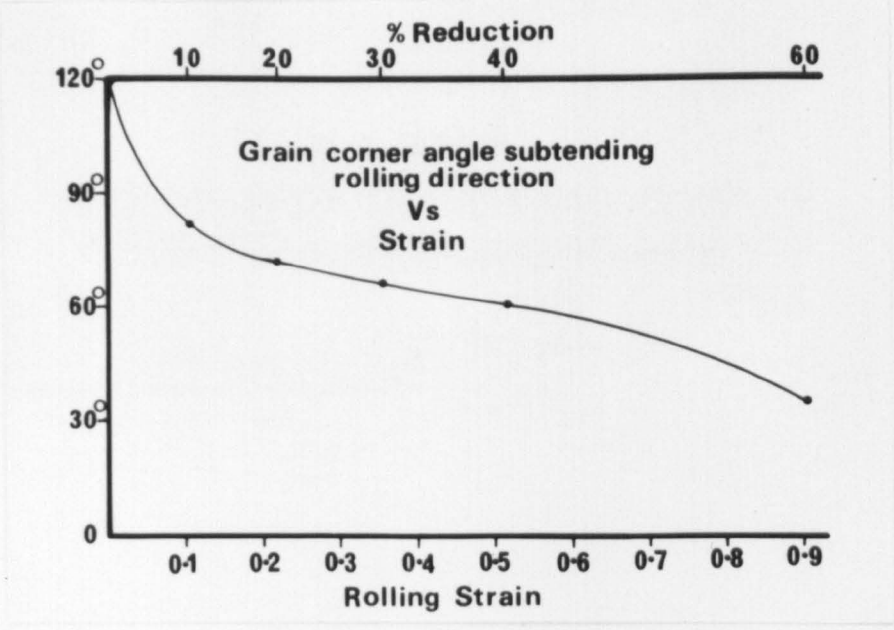
% Reduction
10
20
30
40
60
120°
90°
60°
30°
0
Grain corner angle subtending rolling direction
Vs
Strain
0·1
0·2
0·3
0·4
0·5
0·6
0·7
0·8
0·9
Rolling Strain

5•30


10μm

5•31

FIGURE 5.32

Dislocation dipoles, jogged dislocations and vacancy loops in the normalised steel after 2% reduction by rolling

0.5μm

FIGURE 5.33

Same sample as 5.33 showing some dislocations clustering to form the beginning of a cell wall

1 μm

FIGURE 5.34

Normalised steel after 5% reduction by rolling showing relatively broad cell walls.

1μm

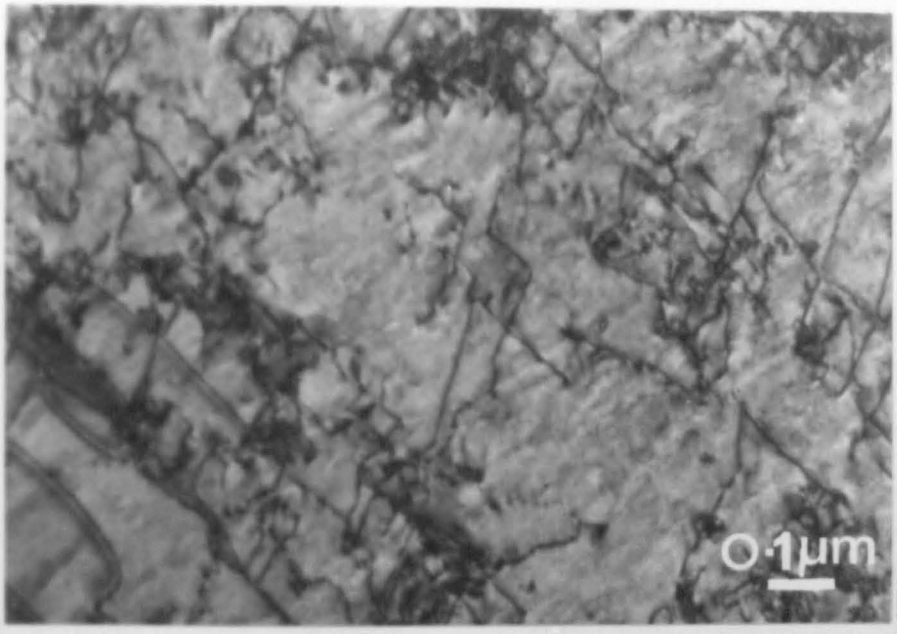

5•32

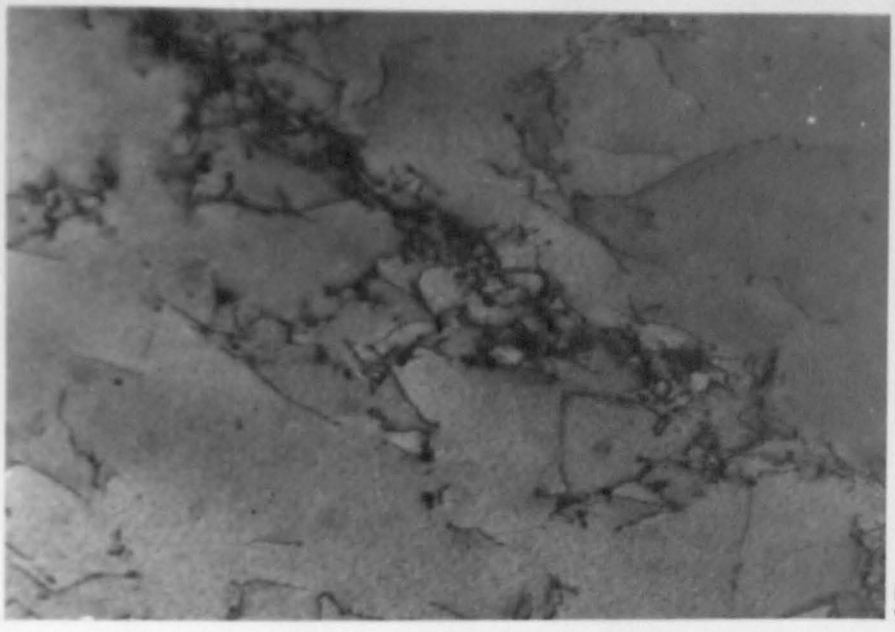

5•33

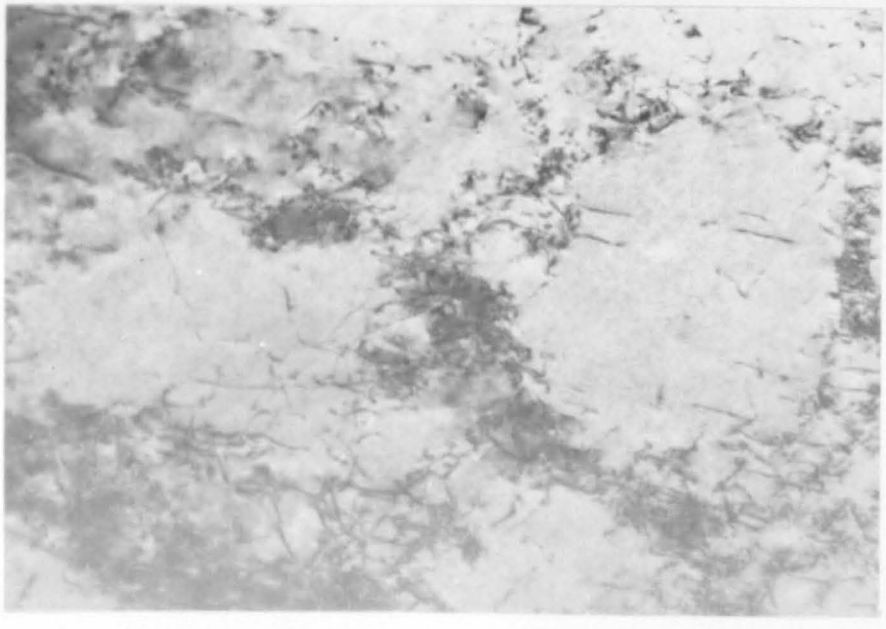

5•34

FIGURE 5.35

Normalised steel after 10% reduction by rolling, showing region where deformation is only light.

1μm

FIGURE 5.36

Another region in the sample of figure 5.35 showing typical grain boundaries and the slightly sharper cell walls.

1μm

FIGURE 5.37

Normalised steel after 10% reduction as in figures 5.35 and 5.36 showing a group of parallel, straight boundaries. The plane of the foil is close to (011) and the boundaries are in the direction of the trace of the $(\bar{0}11)$ plane which is almost perpendicular to the foil furface.

1 μm

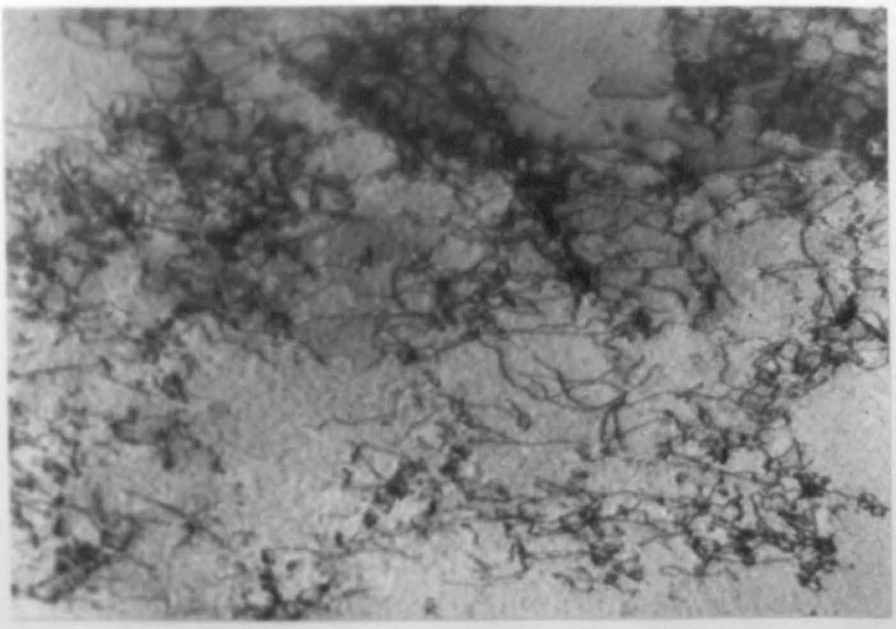

5•35

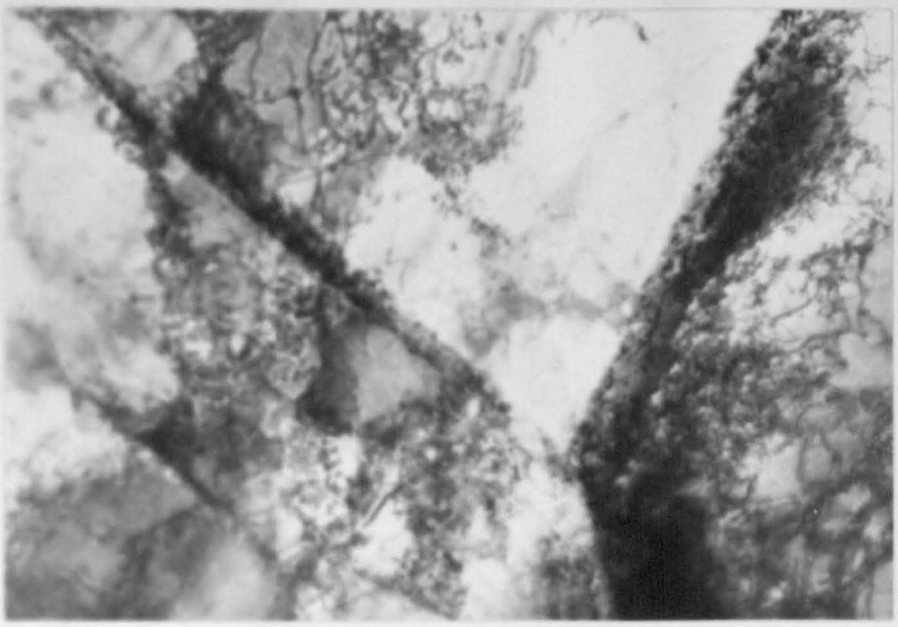

5•36

5•37

FIGURE 5.38

Normalised steel after 10% reduction, showing another area similar to figure 5.37. The boundaries in this case are shown up by the large displacement of the extinction contour along them. The foil surface is again near to (110) and the trace direction of a perpendicular {110} plane is in the direction of the boundaries.

1 μm

FIGURE 5.39

Extinction contours which became displaced along a boundary very abruptly during an in situ straining experiment within the 100 kV electron microscope. In this case the foil plane is (212) and the boundary is in the same direction as the trace of the(011) plane

1μm

FIGURE 5.40

A region of more complex deformation near a grain boundary after 20% reduction by rolling.

1μm

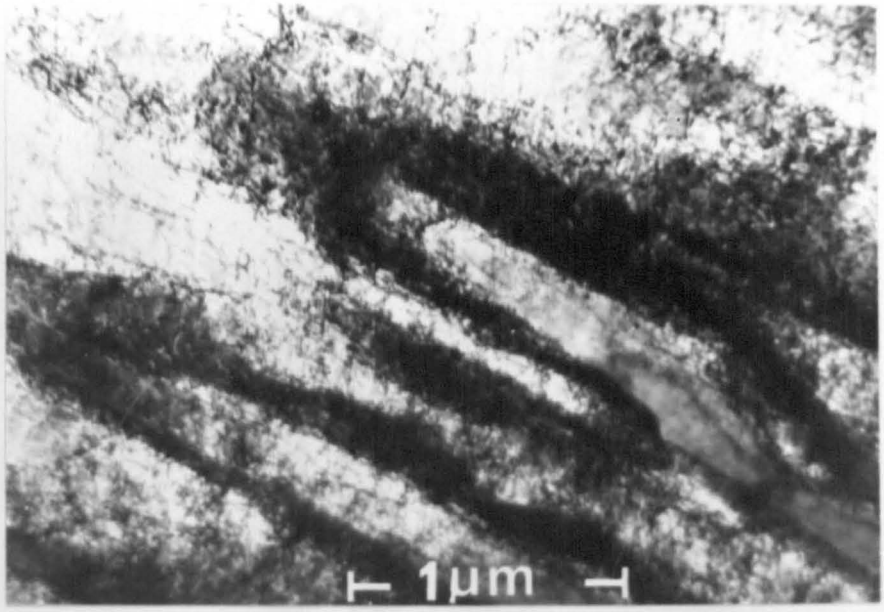

5•38

5•39

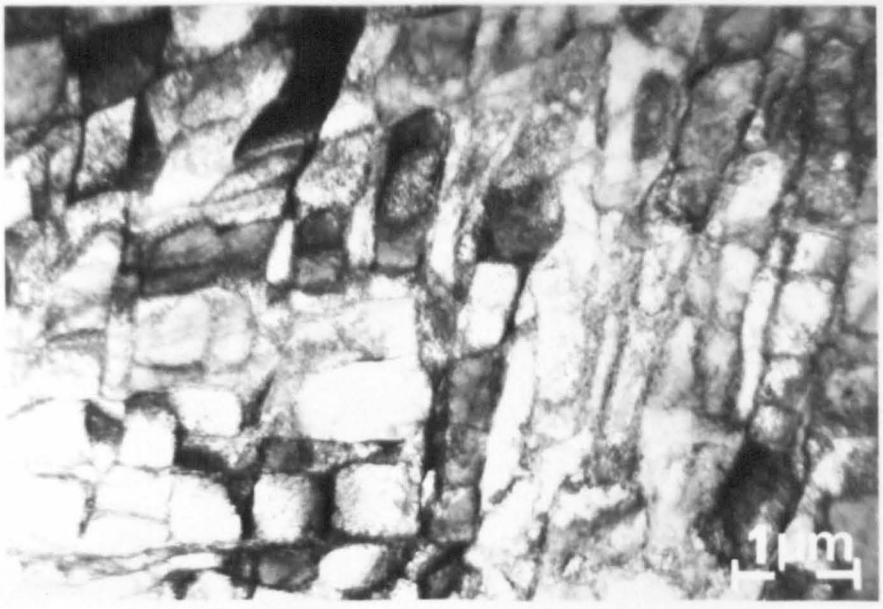

5•40

FIGURE 5.41

Normalised steel after 60% reduction by rolling showing the sideways displacement of a well established band when intersected by a more recently formed one. If the foil is assigned the indices (111) then the broad band and the narrower band can be shown to be in the directions of the traces of $(1\bar{1}0)$ and $(0\bar{1}1)$ planes.

1 μm

FIGURE 5.42

Normalised steel after 50% reduction showing the displacement of band contours at the straight boundaries.

1 μm

FIGURE 5.43

Normalised steel after 90% reduction, taken during an in situ straining experiment.

1 μm

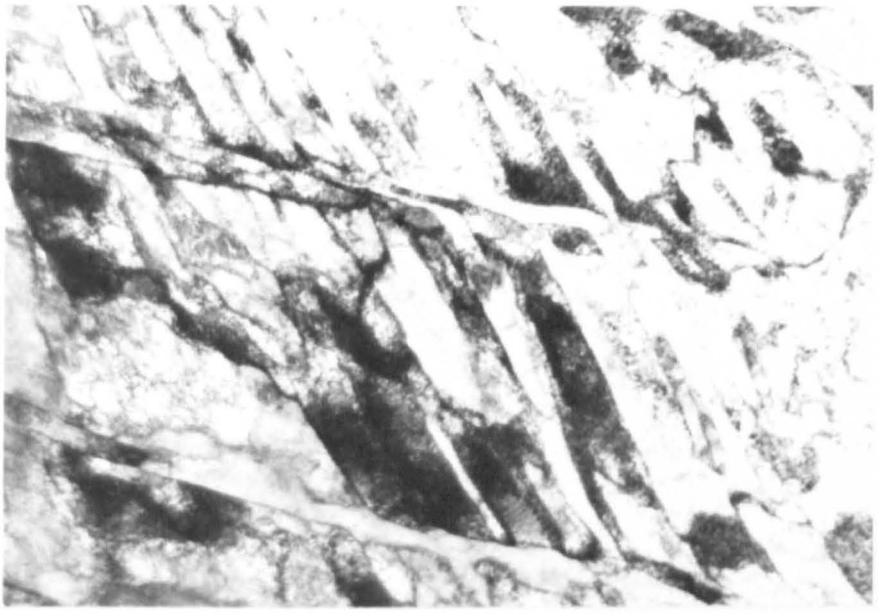

5•41

5•42

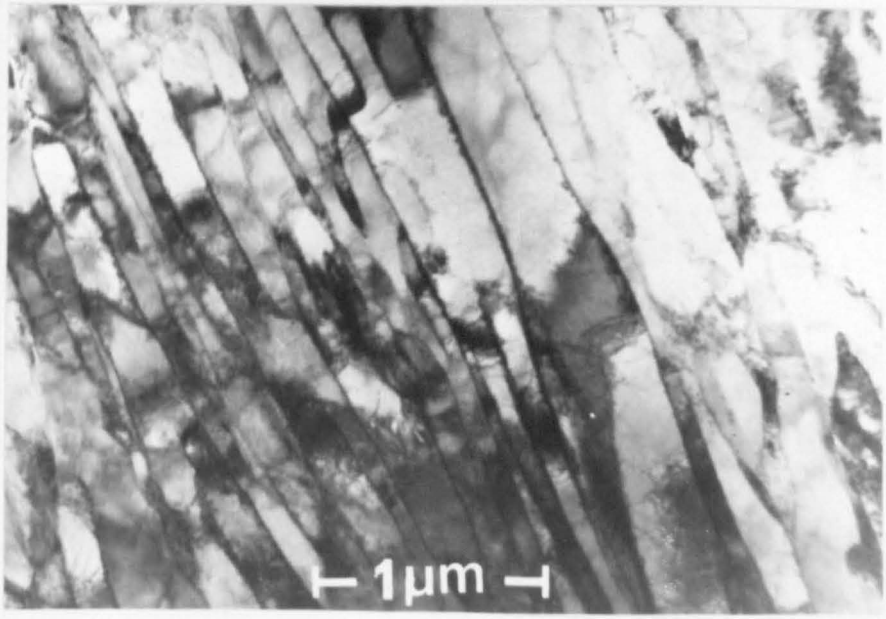

5•43

FIGURE 5.44

Optical micrograph of high sulphur steel after 10% reduction in thickness by rolling.

40 μm

FIGURE 5.45

High sulphur steel after 30% reduction in thickness. Optical micrograph in the unetched condition.

40 μm

FIGURE 5.46

Unetched optical micrograph of the high sulphur steel after 95% rolling reduction.

40 μm

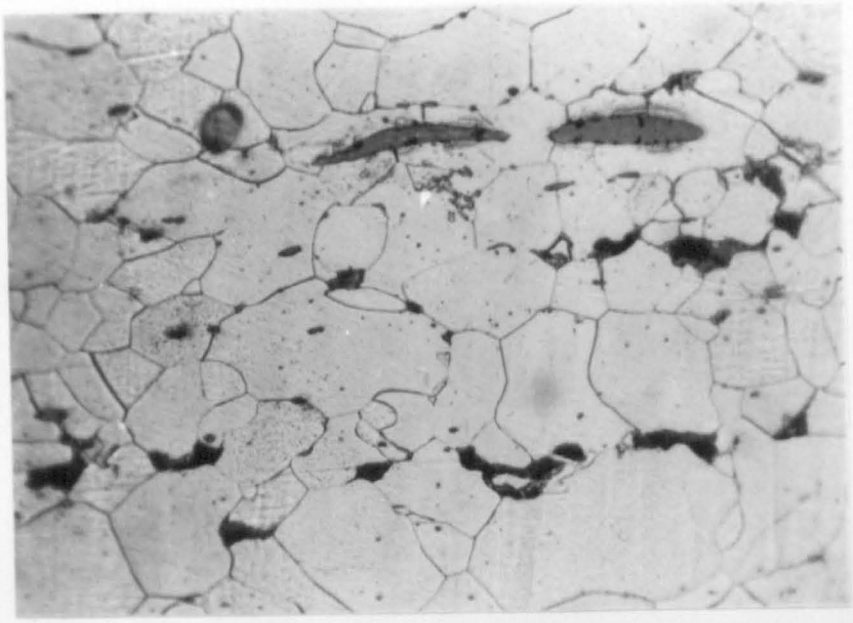

5•44

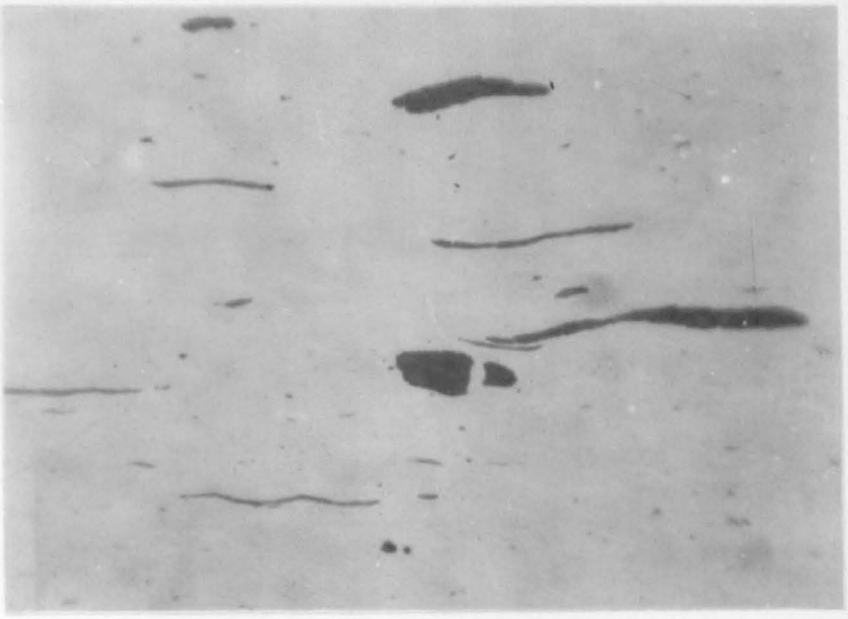

5•45

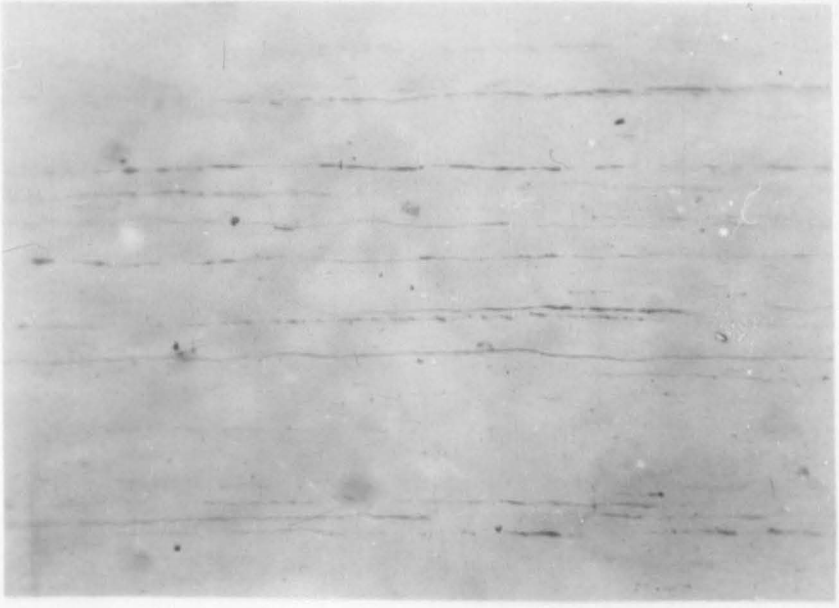

5•46

FIGURE 5.47

As for 5.46 after etching. High sulphur steel after 95% rolling reduction.

10 μm

FIGURE 5.48

High sulphur steel after 10% rolling reduction. Transmission electron micrograph of a foil from a section perpendicular to the rolling plane and parallel to the rolling direction.

0.5 μm

FIGURE 5.49

Transmission electron micrograph of high sulphur steel after 40% rolling reduction.

1 μm

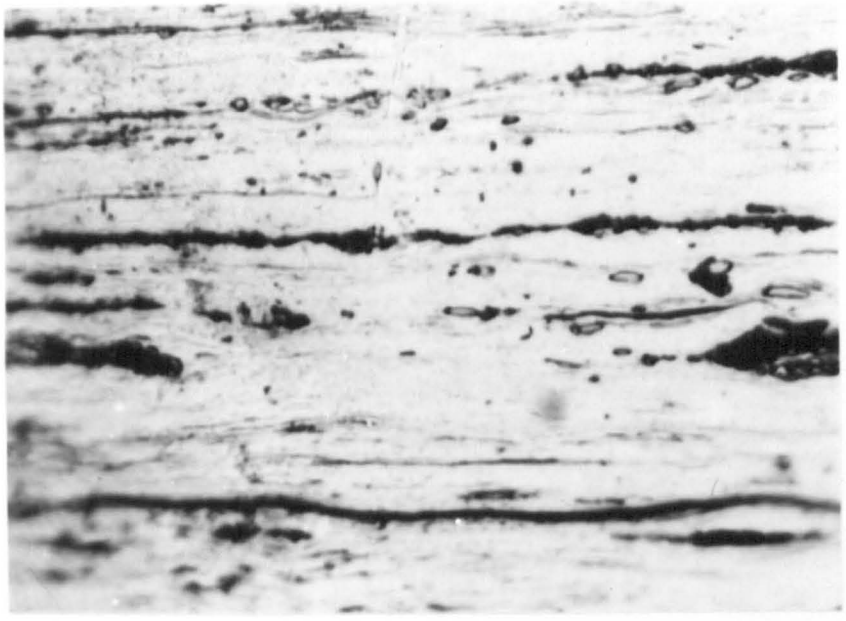

5•47

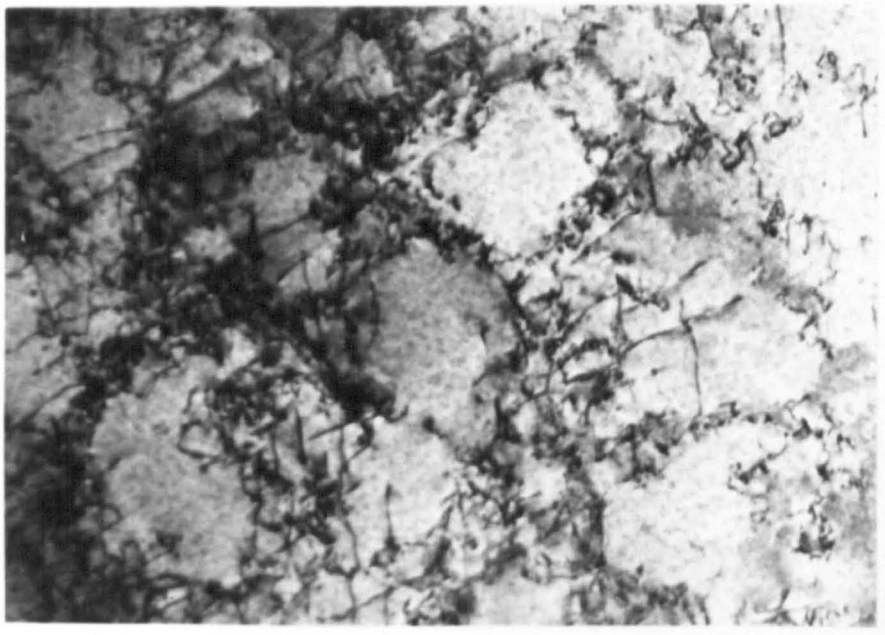

5•48

5•49

FIGURE 5.50

High sulphur steel after 40% rolling reduction. Transmission electron micrograph of foil perpendicular to the rolling plane and parallel to the rolling direction.

1 μm

FIGURE 5.51

Electron diffraction pattern of the area shown in figure 5.50.

FIGURE 5.52

Transmission electron micrograph of the high sulphur steel after 60% rolling reduction.

1 μm

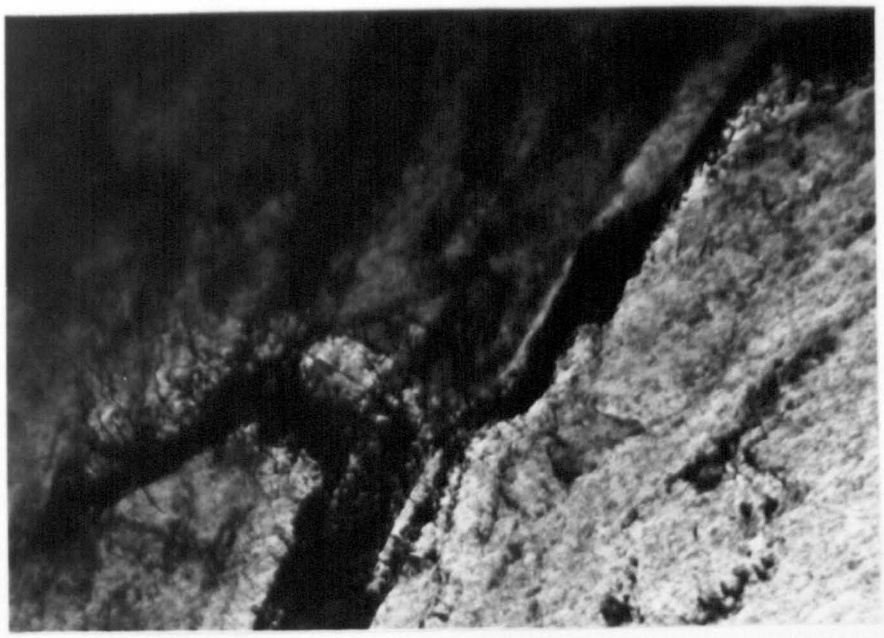

5•50

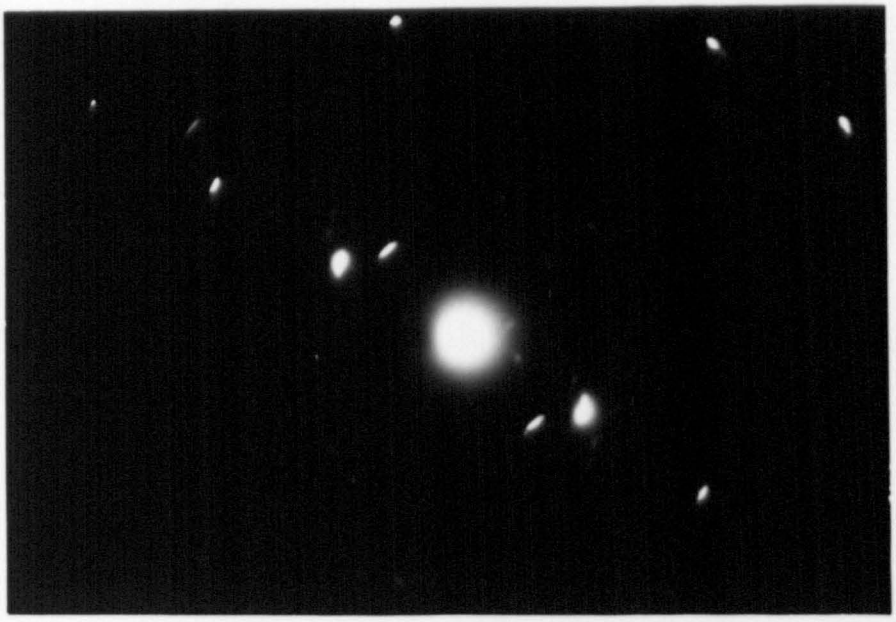

5•51

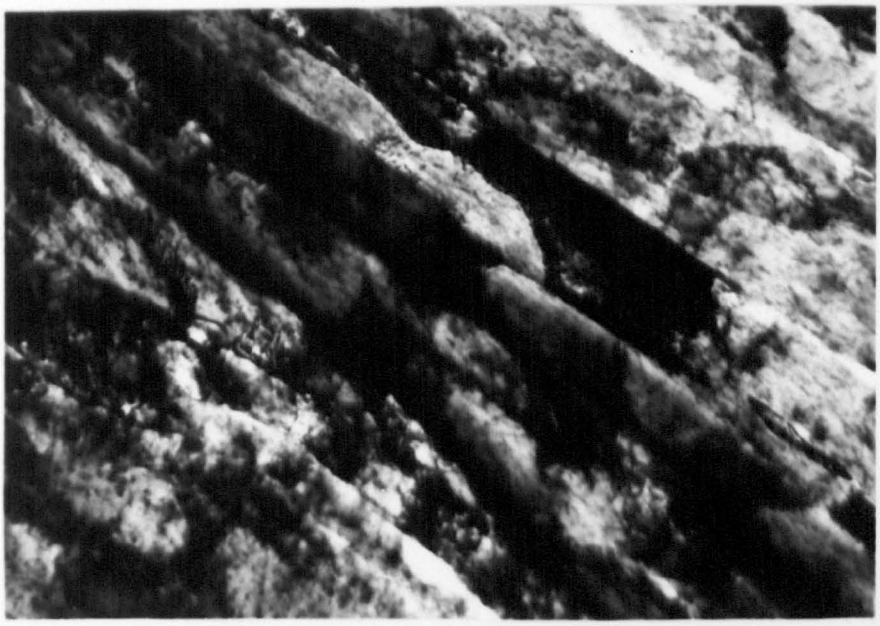

5•52

FIGURE 5.53

Transmission electron micrograph of the high sulphur steel after 40% rolling reduction. If the foil surface is assigned the indices (113), the direction of the bands of dislocations is $[110]$ and possible slip planes with traces in this direction are $(1\bar{1}0)$ which is 65° to the foil surface and $(\bar{1}12)$ which is 60° to the foil surface.

0.5 μm

FIGURE 5.54

Electron diffraction pattern taken across a single band in fig. 5.53 the foil surface is (113).

FIGURE 5.55

High sulphur steel after 85% rolling reduction. The foil is again transverse to the rolling direction.

1 μm

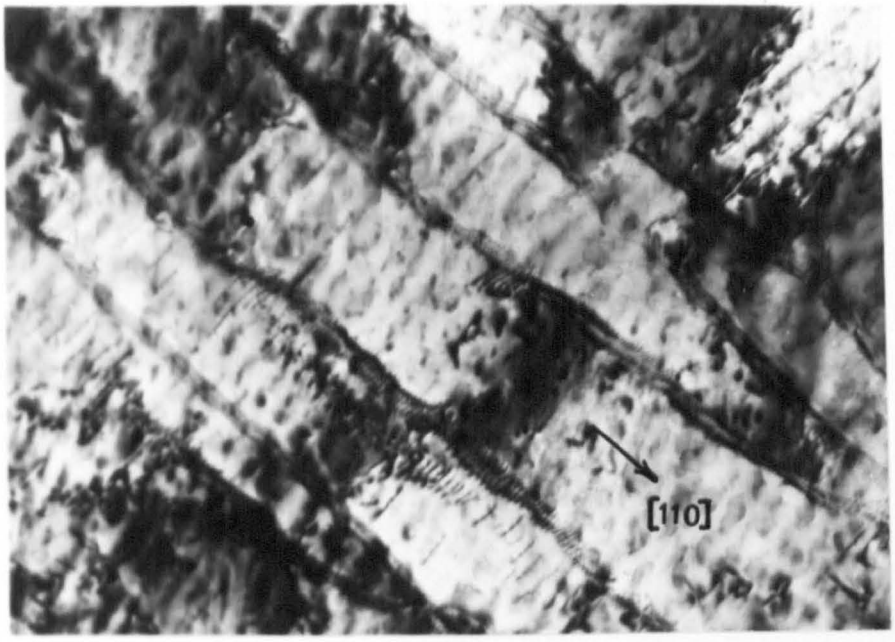

5•53

5•54

5•55

FIGURE 5.56

Long thin manganese sulphide particle, as commonly seen in the high sulphur steel at high strains. This sample had undergone a rolling reduction of 85%.

1 μm

FIGURE 5.57

The same manganese sulphide particle as in fig. 5.56 after straining in the electron microscope.

1 μm

FIGURE 5.58

Optical micrograph of the steel containing sulphur and lead, showing cracking of the sulphide-ferrite interface. This sample had not undergone any rolling.

40 μm

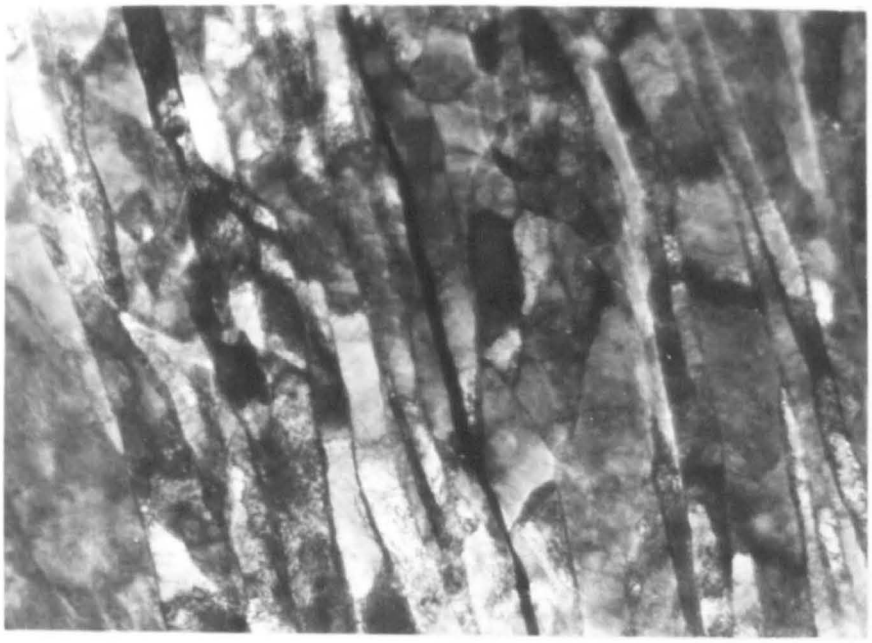

5•56

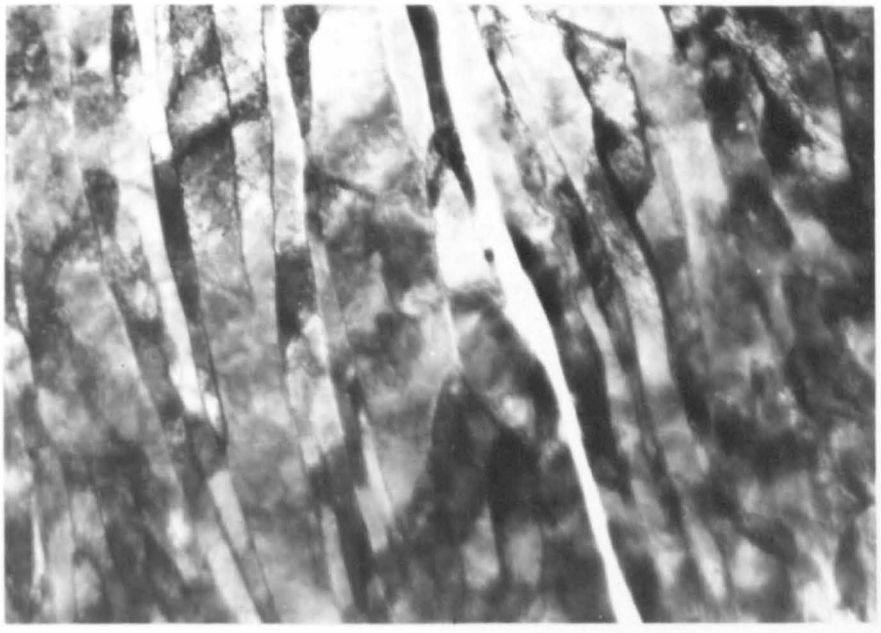

5•57

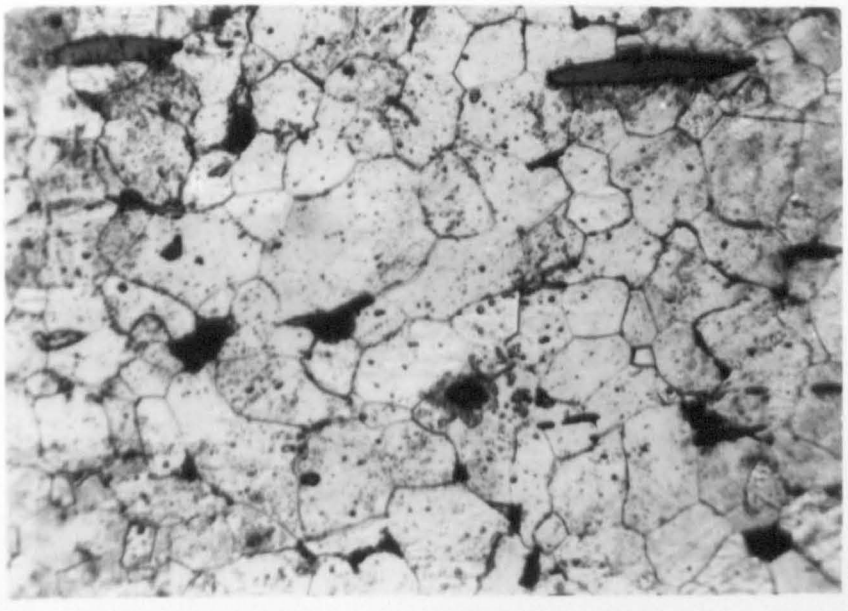

5•58

FIGURE 5.59

Unetched micrograph of the steel with sulphur and lead after 40% rolling reduction.

40 μm

FIGURE 5.60

Unetched micrograph of the steel containing sulphur and lead after 60% reduction by rolling.

40 μm

FIGURE 5.61

Micrograph of the steel containing sulphur and lead when etched, after a rolling reduction of 90%.

10 μm

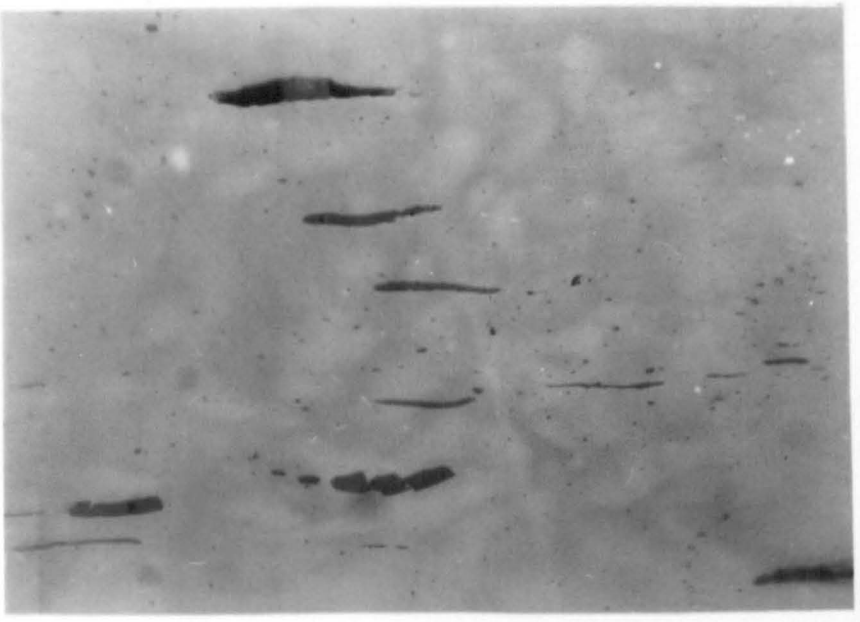

5•59

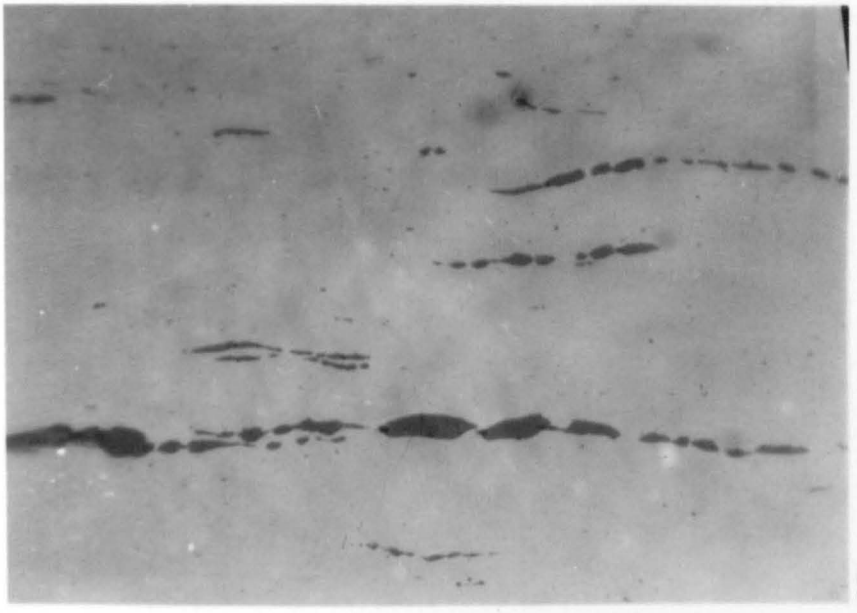

5•60

5•61

FIGURE 5.62

The steel containing sulphur and lead after a rolling reduction of 10%. Transmission electron micrograph from a foil cut perpendicular to the rolling plane and along the rolling direction.

1 μm

FIGURE 5.63

The steel with sulphur and lead after a rolling reduction of 10% as for fig. 5.62

1 μm

FIGURE 5.64

Transmission electron micrograph of the sulphur plus lead steel after a rolling reduction of 60%. The section is again perpendicular to the rolling plane and along the rolling direction.

0.5 μm

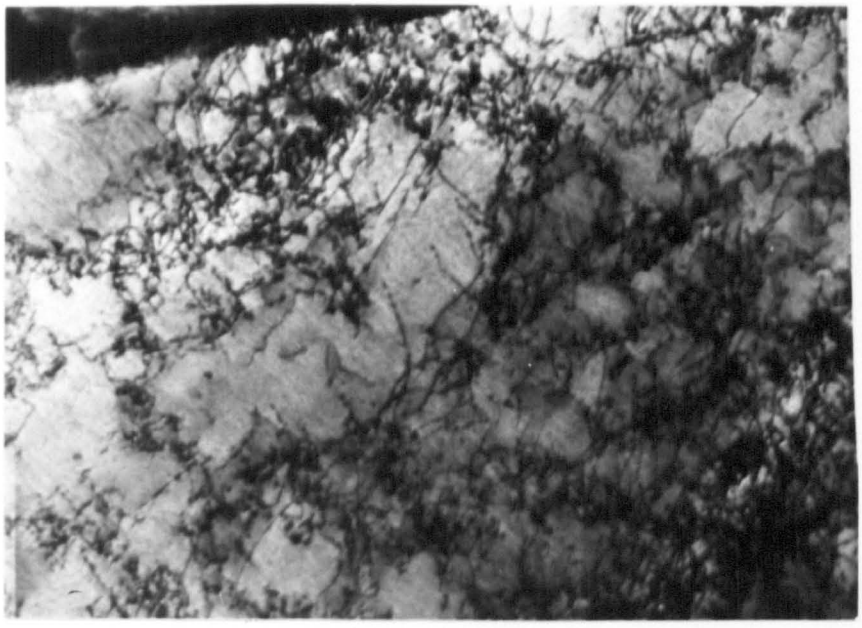

5•62

5•63

5•64

FIGURE 5.65

Electron diffraction pattern of the area shown in figure 5.65.

FIGURE 5.66

The sulphur plus lead steel after 85% reduction by rolling. Transmission electron micrograph of a foil perpendicular to the rolling plane and along the rolling direction.

1 μm

FIGURE 5.67

Optical micrograph of the steel which was heat treated to a structure of fine carbide particles in a ferrite matrix. This micrograph was taken in the as heat treated condition.

40 μm

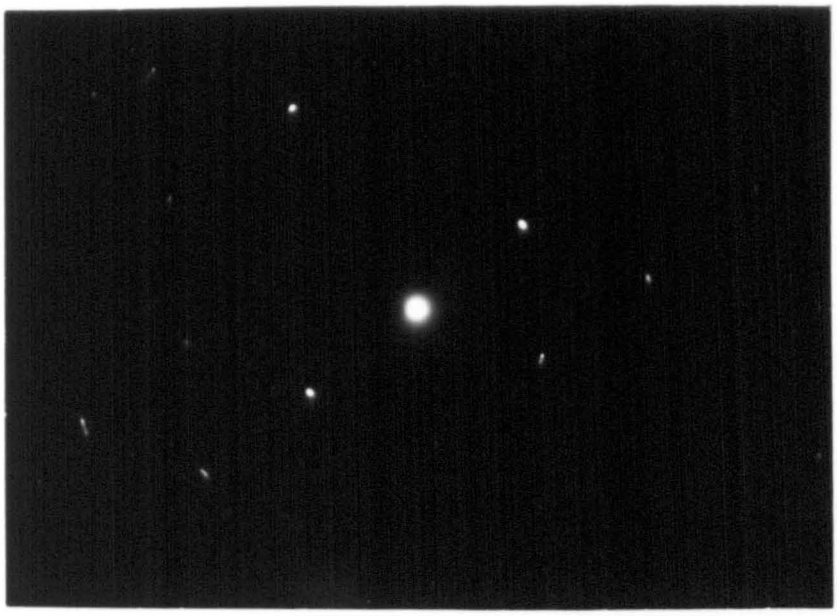

5•65

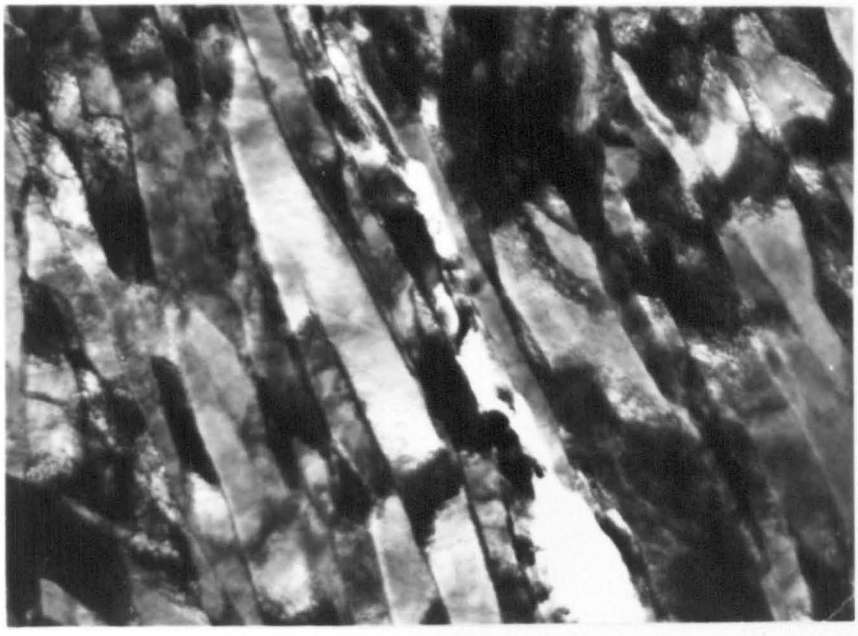

5•66

5•67

FIGURE 5.68

Transmission electron micrograph of the structure shown in fig. 5.67. This is the structure before any rolling strain has been imposed.

1 μm

FIGURE 5.69

The steel containing fine carbide particles after a rolling reduction of 5%. Transmission electron micrograph of a foil cut perpendicular to the rolling plane and along the rolling direction.

0.5 μm

FIGURE 5.70

Optical micrograph of a transverse section of the steel containing fine carbide particles after a rolling reduction of 10%.

40 μm

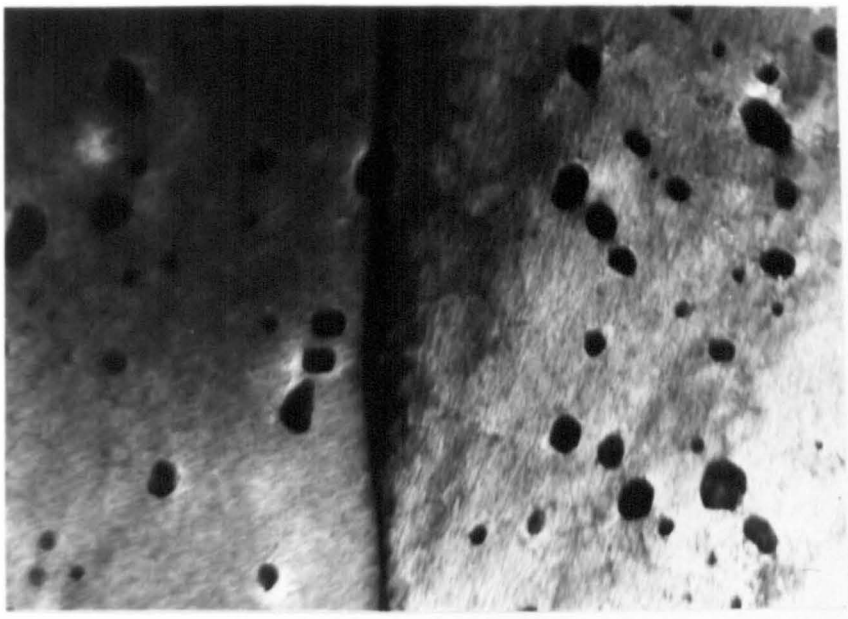

5•68

5•69

5•70

FIGURE 5.71

Optical micrograph of a transverse section of the steel containing fine carbide particles after a rolling reduction of 60%.

40 μm

FIGURE 5.72

Transmission electron micrograph of a replica taken from a transverse section of the steel containing fine carbide particles after a rolling reduction of 80%.

10 μm

FIGURE 5.73

Scanning electron micrograph of a transverse section of the steel containing fine carbide particles after a rolling reduction of 60%

10 μm

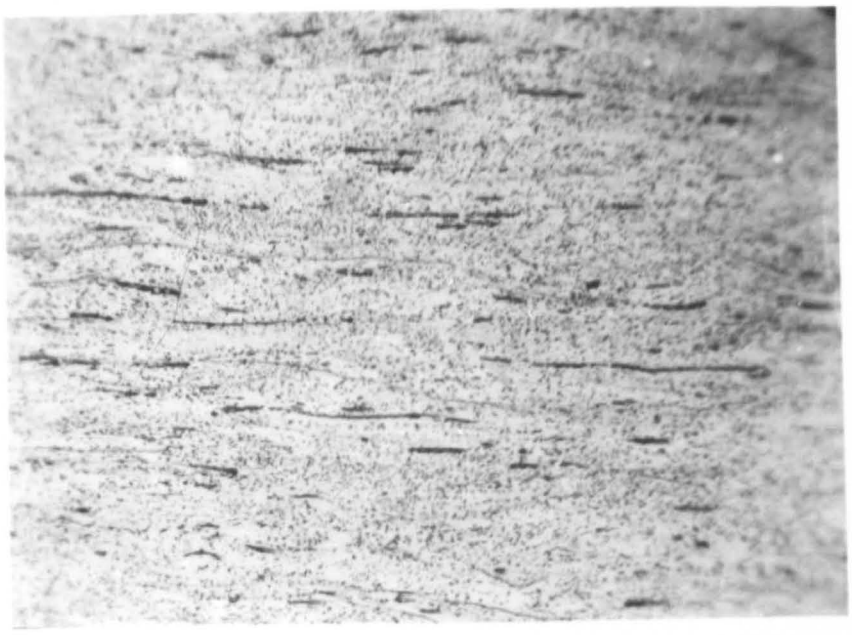

5•71

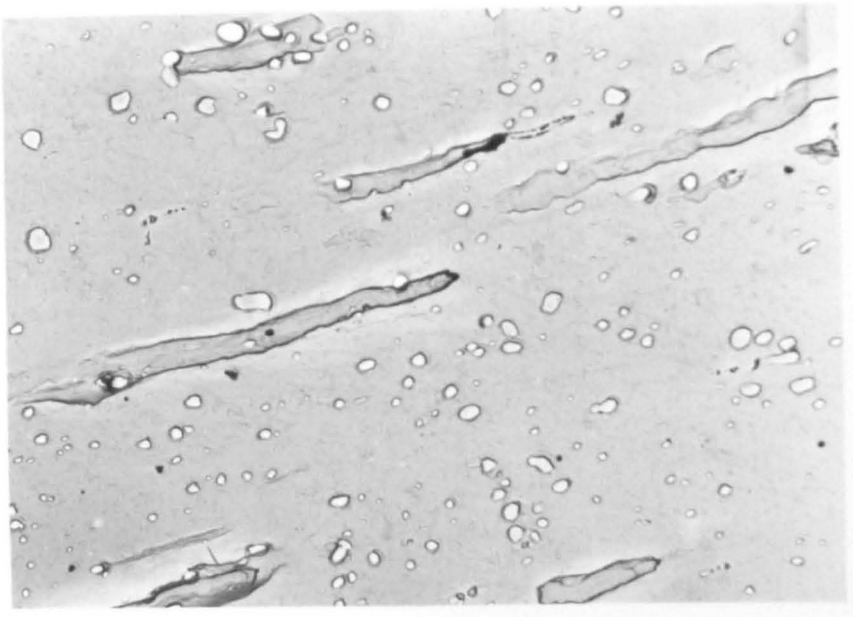

5•72

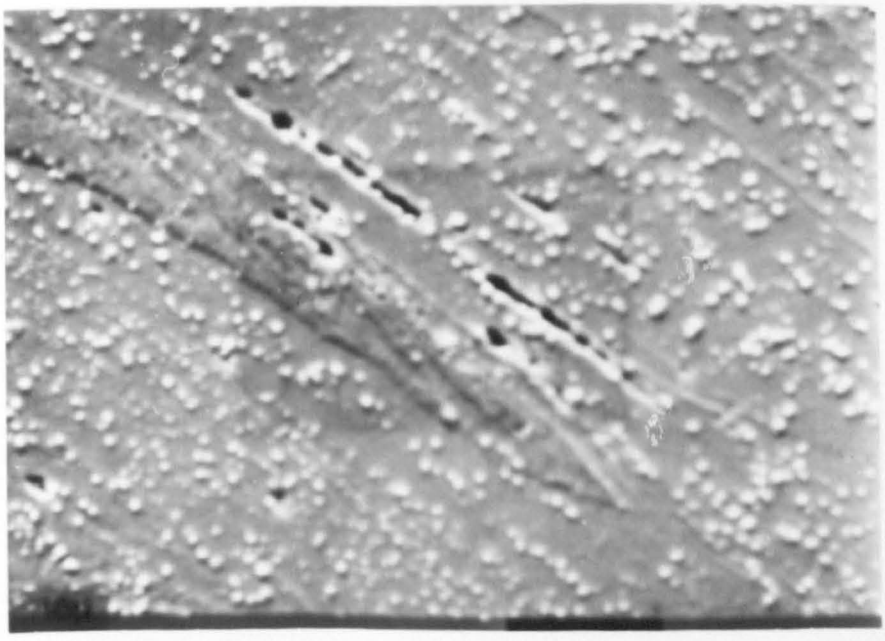

5•73

FIGURE 5.74

Transmission electron micrograph of a transverse section of the steel containing fine carbide particles after a rolling reduction of 10%

1 μm

FIGURE 5.75

As for fig. 5.74 after a rolling reduction of 40%

1 μm

FIGURE 5.76

As for fig. 5.74 after a rolling reduction of 60%

1 μm

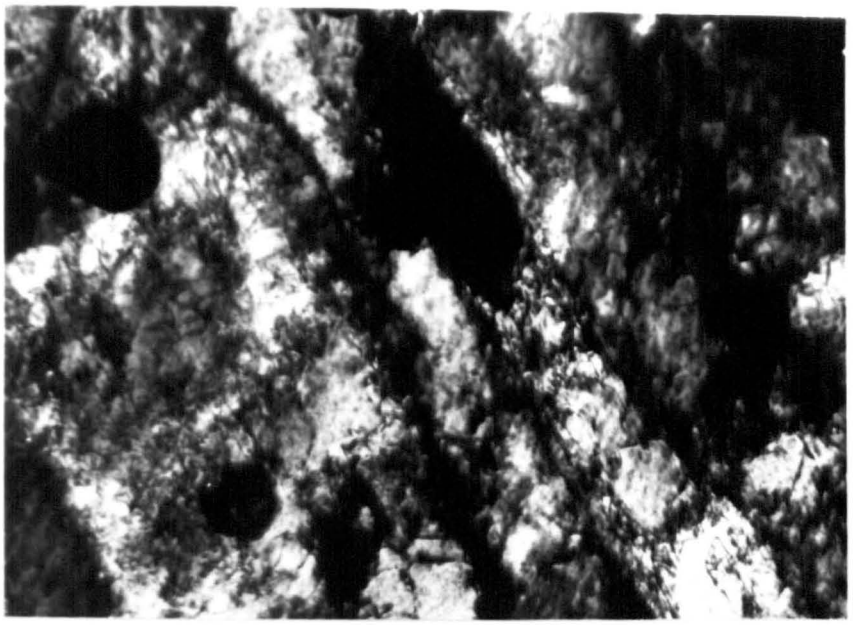

5•74

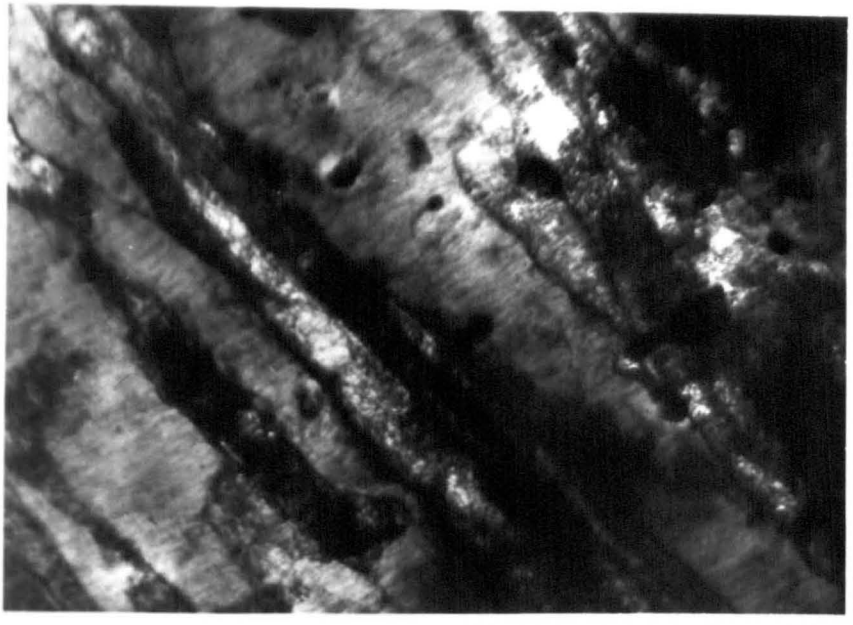

5•75

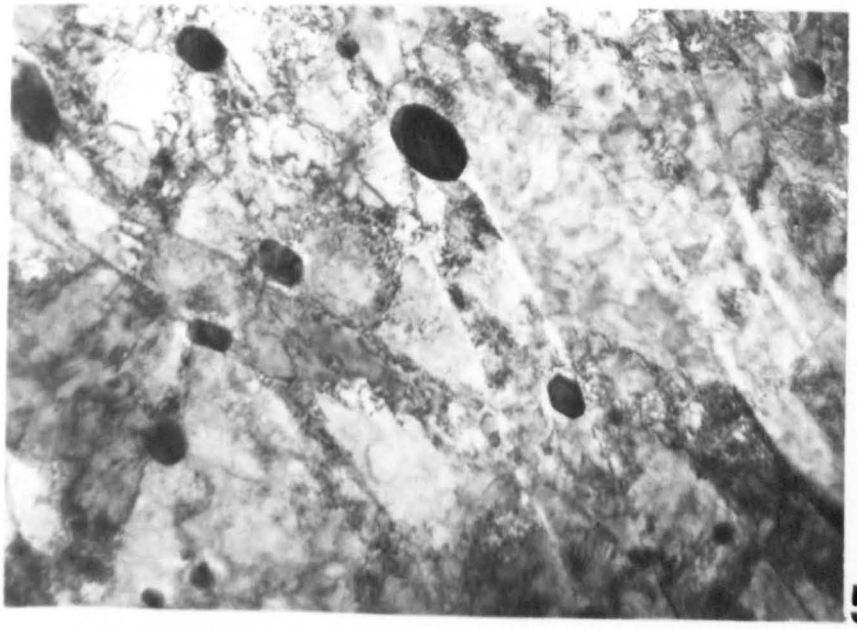

5•76

FIGURE 5.77

Transmission electron micrograph of a transverse section of the steel containing fine particles after a rolling reduction of 40%.

0.5 μm

FIGURE 5.78

Electron diffraction pattern of the area shown in fig. 5.77. The foil orientation is (001) and the trace of the boundary in fig. 5.77 is $[110]$, making the boundary either $(1\bar{1}2)$ or $(\bar{1}12)$.

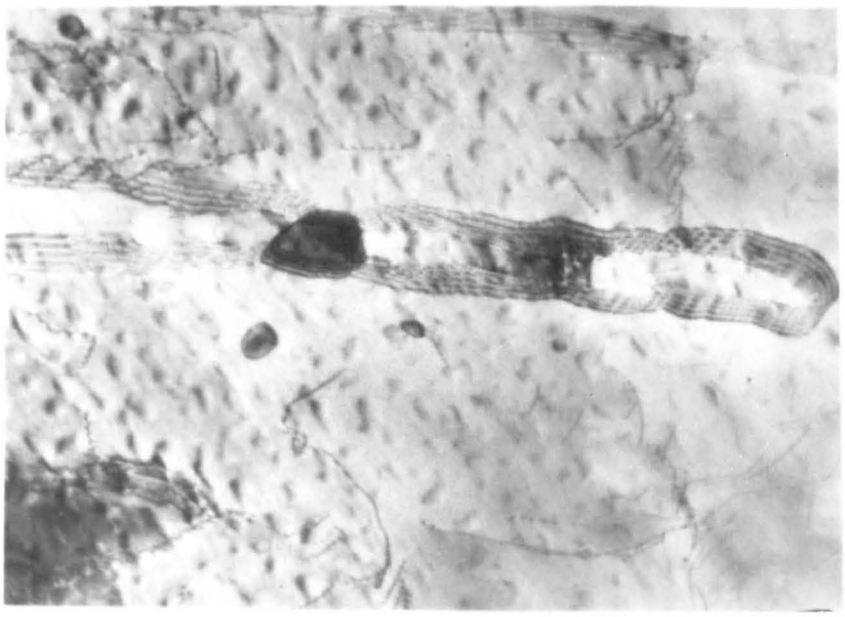

5•77

5•78

FIGURE 6.1

A selection of the load extension curves for the steel (EN 8) in the quenched and tempered condition, showing the variation as rolling strain is increased.

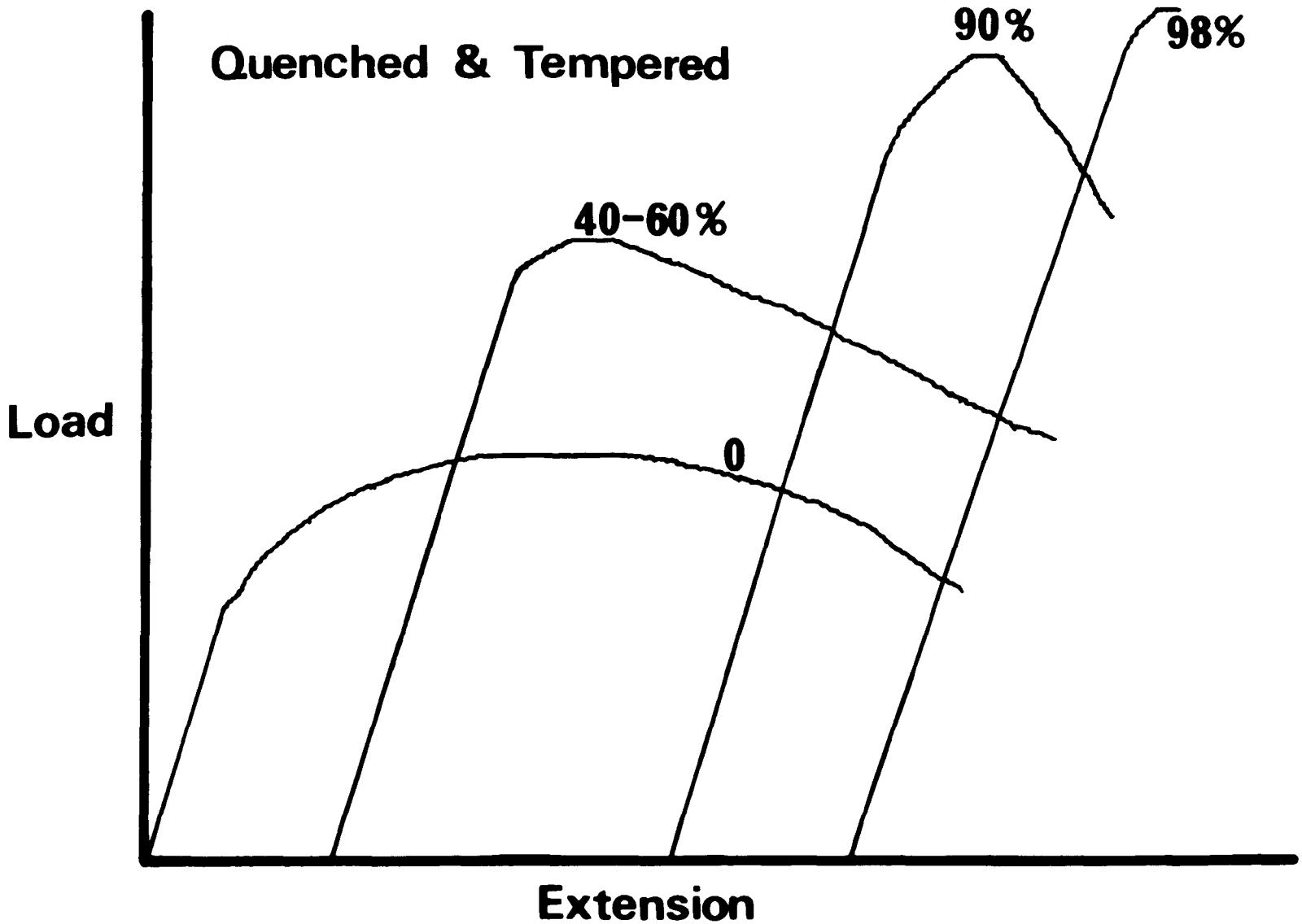
Quenched & Tempered
90%
98%
40-60%
0
Load
Extension

FIGURE 6.2

A selection of load extension curves showing the variation with rolling strain for the steel (EN 8) tested in the normalised condition.

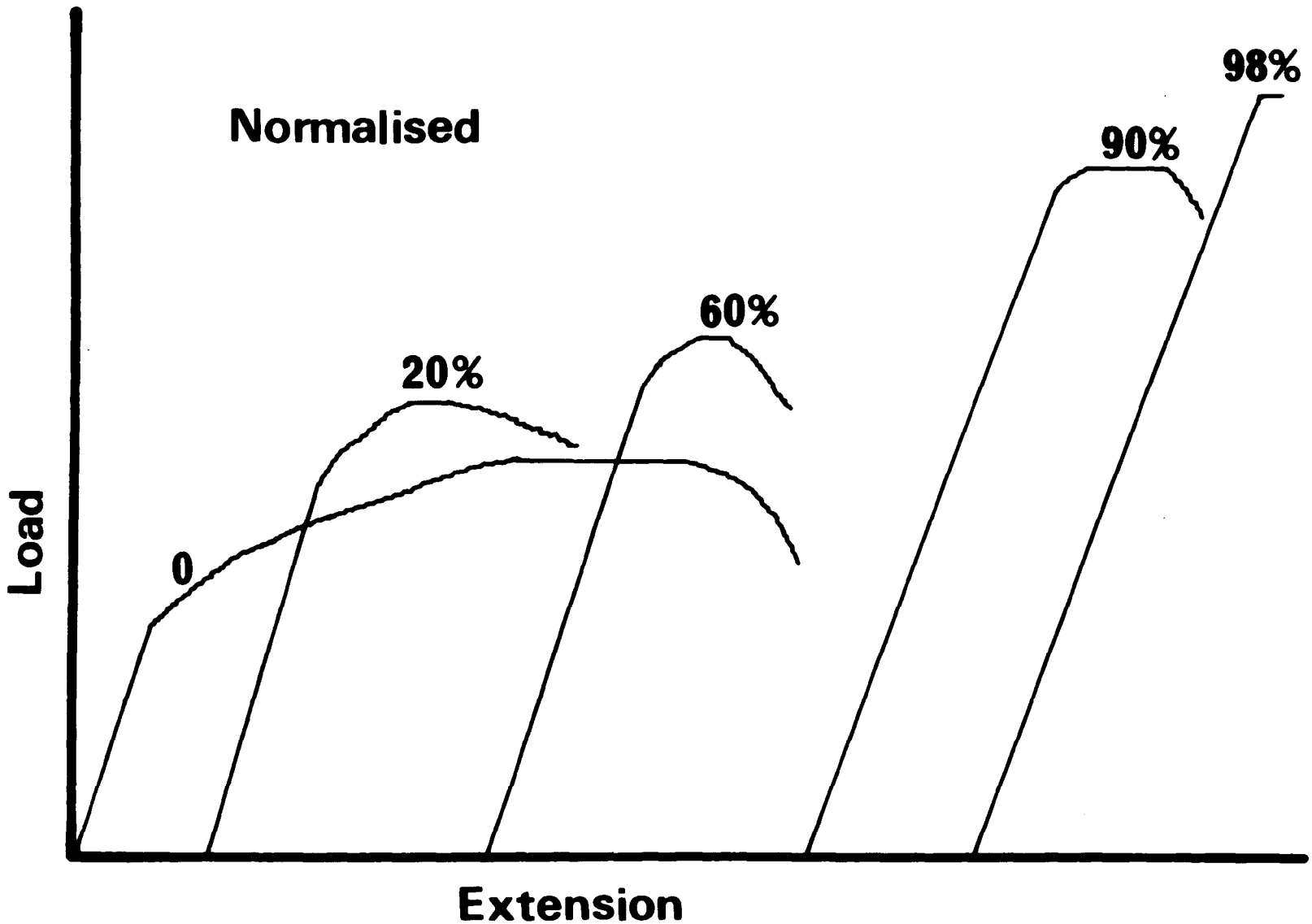
Normalised
98%
90%
60%
20%
0
Load
Extension

FIGURE 6.3

A selection of load extension curves showing the variation with rolling strain for the high sulphur steel.

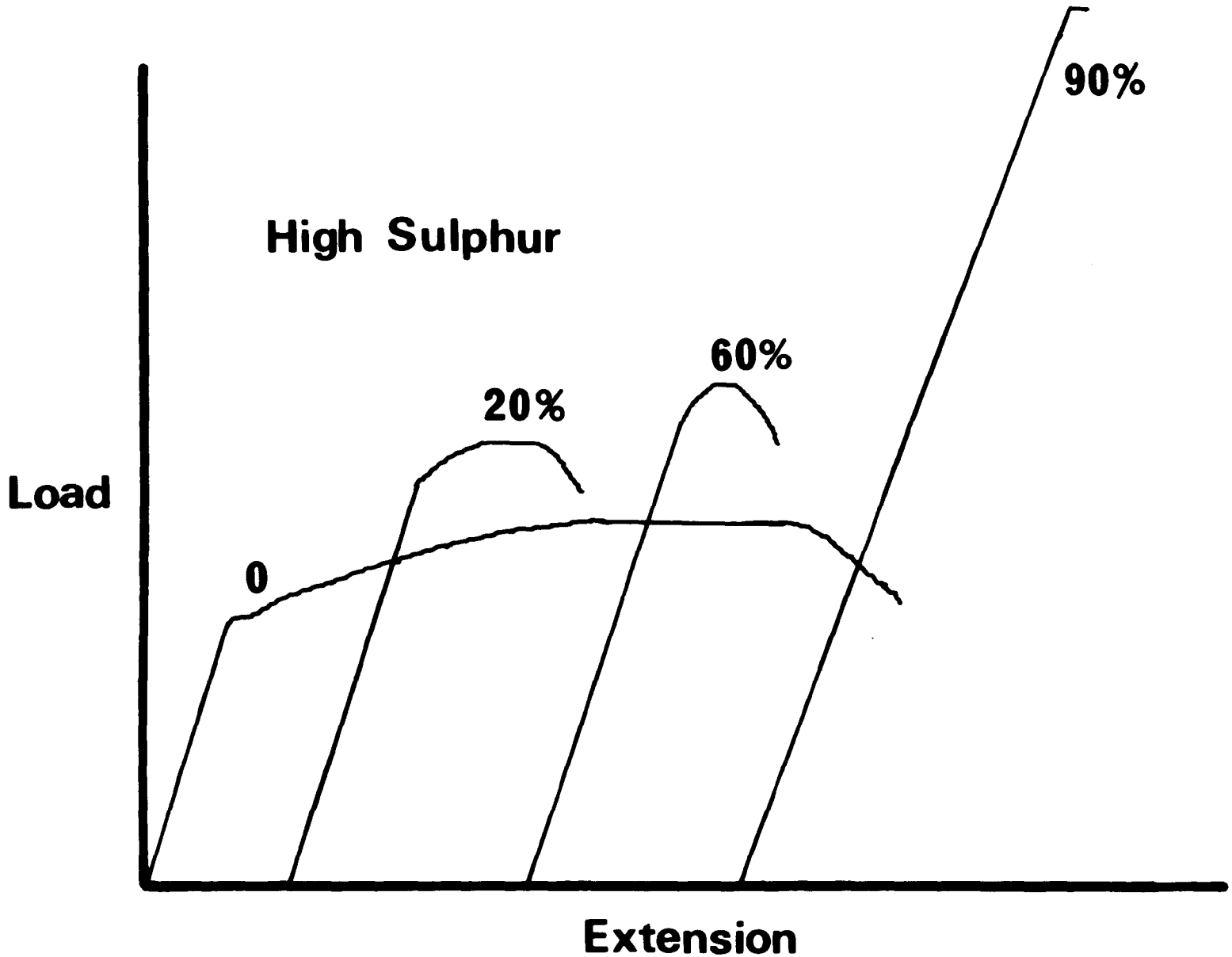
High Sulphur
90%
60%
20%
0
Load
Extension

FIGURE 6.4

A selection of load extension curves showing the variation with rolling strain for the steel containing sulphur and lead.

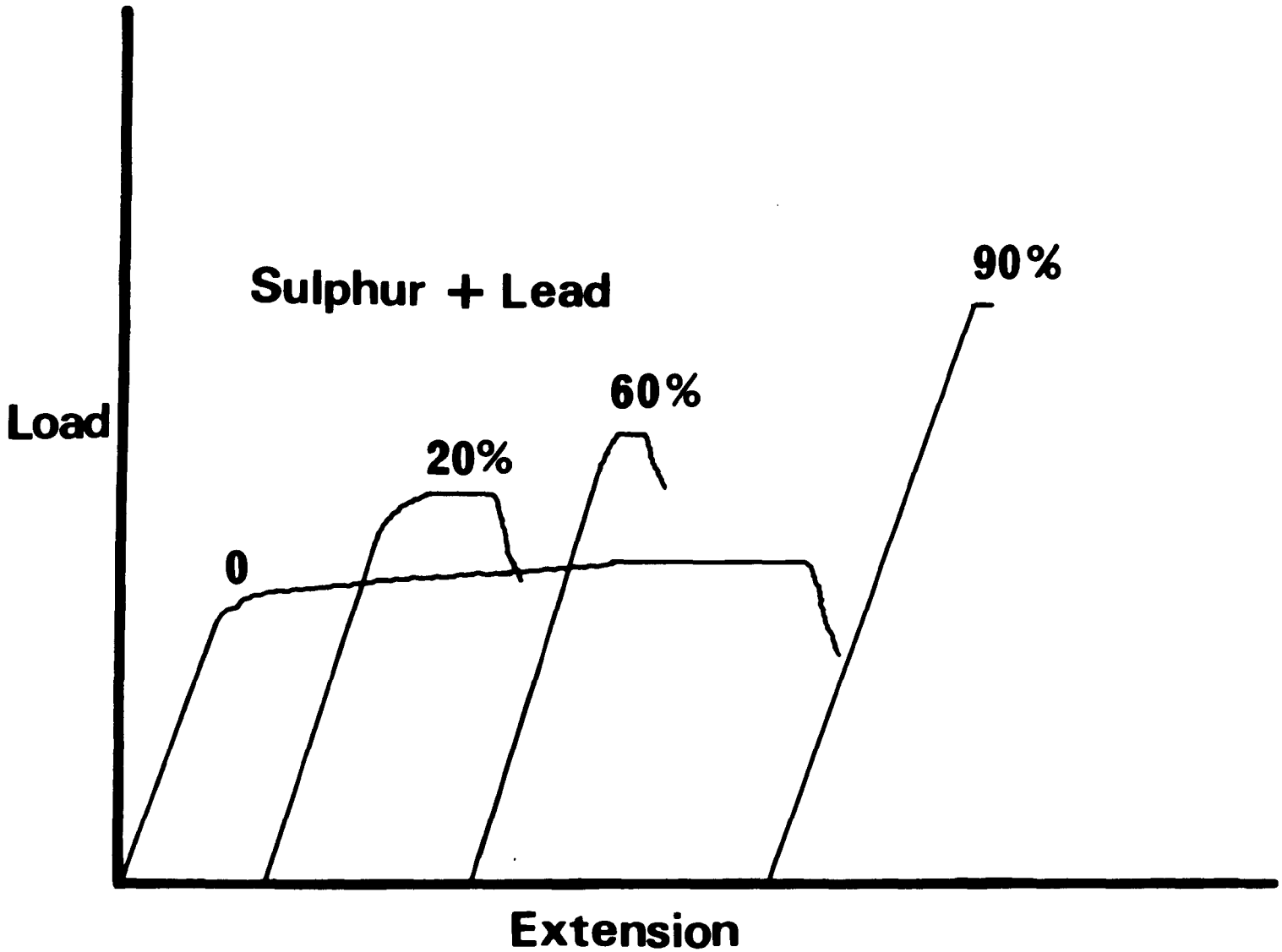
Sulphur + Lead
90%
60%
20%
0
Load
Extension

FIGURE 6.5

A selection of load extension curves showing the variation with rolling strain for the steel (EN 3B) heat treated to give a structure of fine carbide particles in a ferrite matrix.

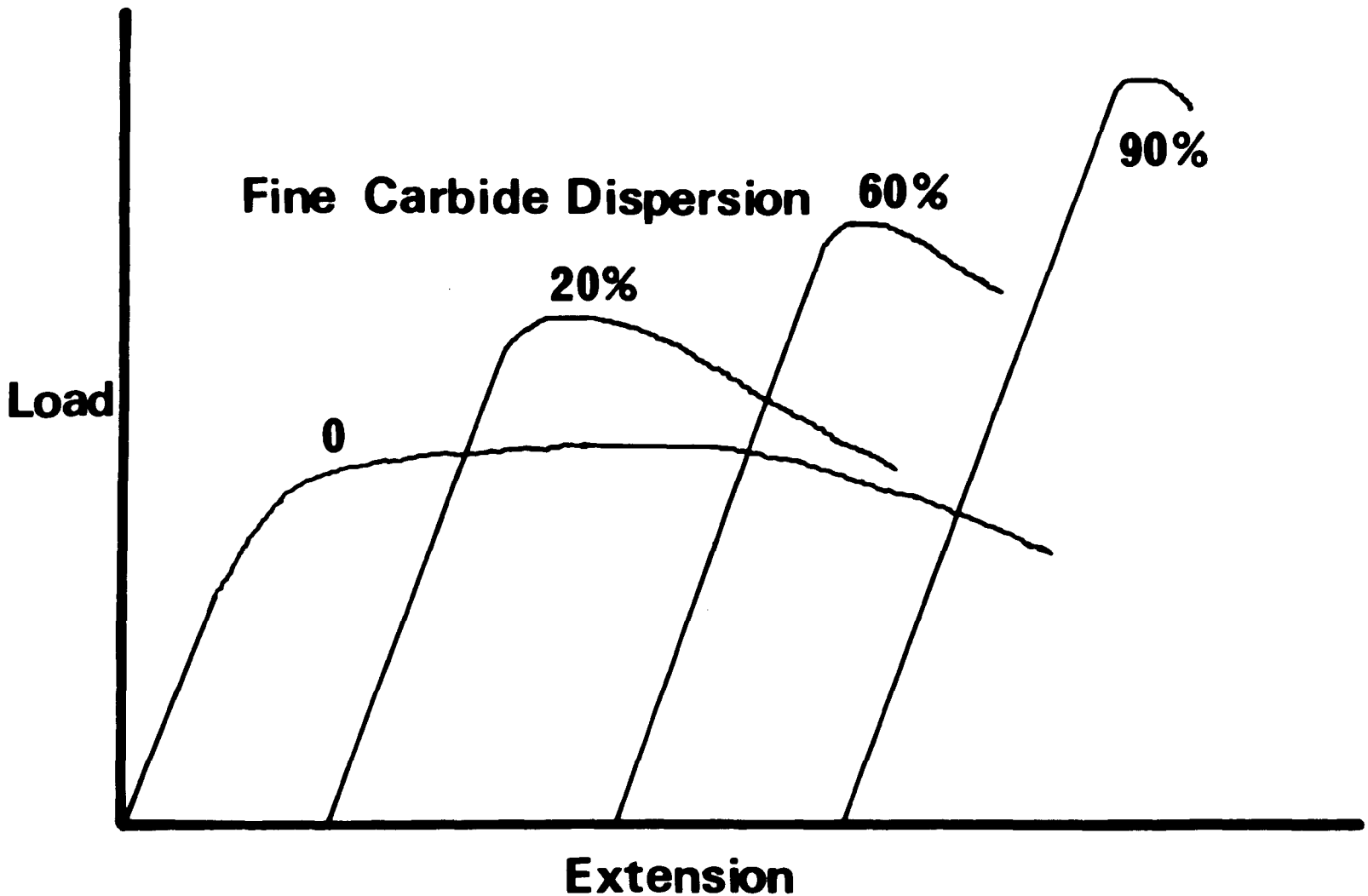
Fine Carbide Dispersion
90%
60%
20%
0
Load
Extension

FIGURE 6.6

The variation in U.T.S. and in uniform strain $\varepsilon_{,u}$ with increasing rolling strain for the steel (EN 8) in the quenched and tempered condition.

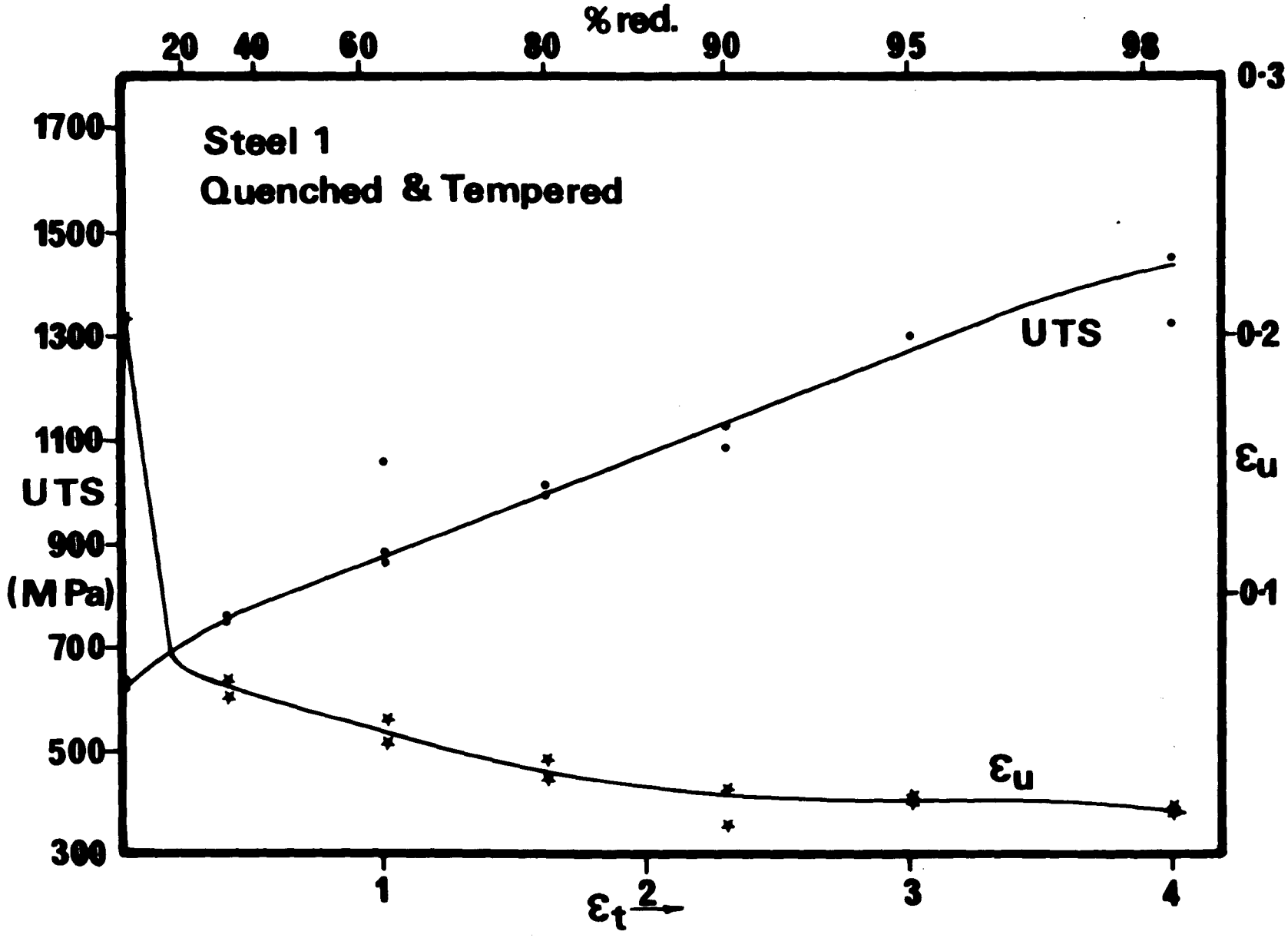
% red.
20
40
60
80
90
95
98
Steel 1
Quenched & Tempered
UTS
ε_u
1700
1500
1300
1100
900
700
500
300
UTS
(MPa)
0·3
0·2
0·1
ε_u
1
2
3
4
ε_t

FIGURE 6.7

The variation in U.T.S. and in uniform strain ε_u with increasing rolling strain for the steel (EN 8) in the normalised condition.

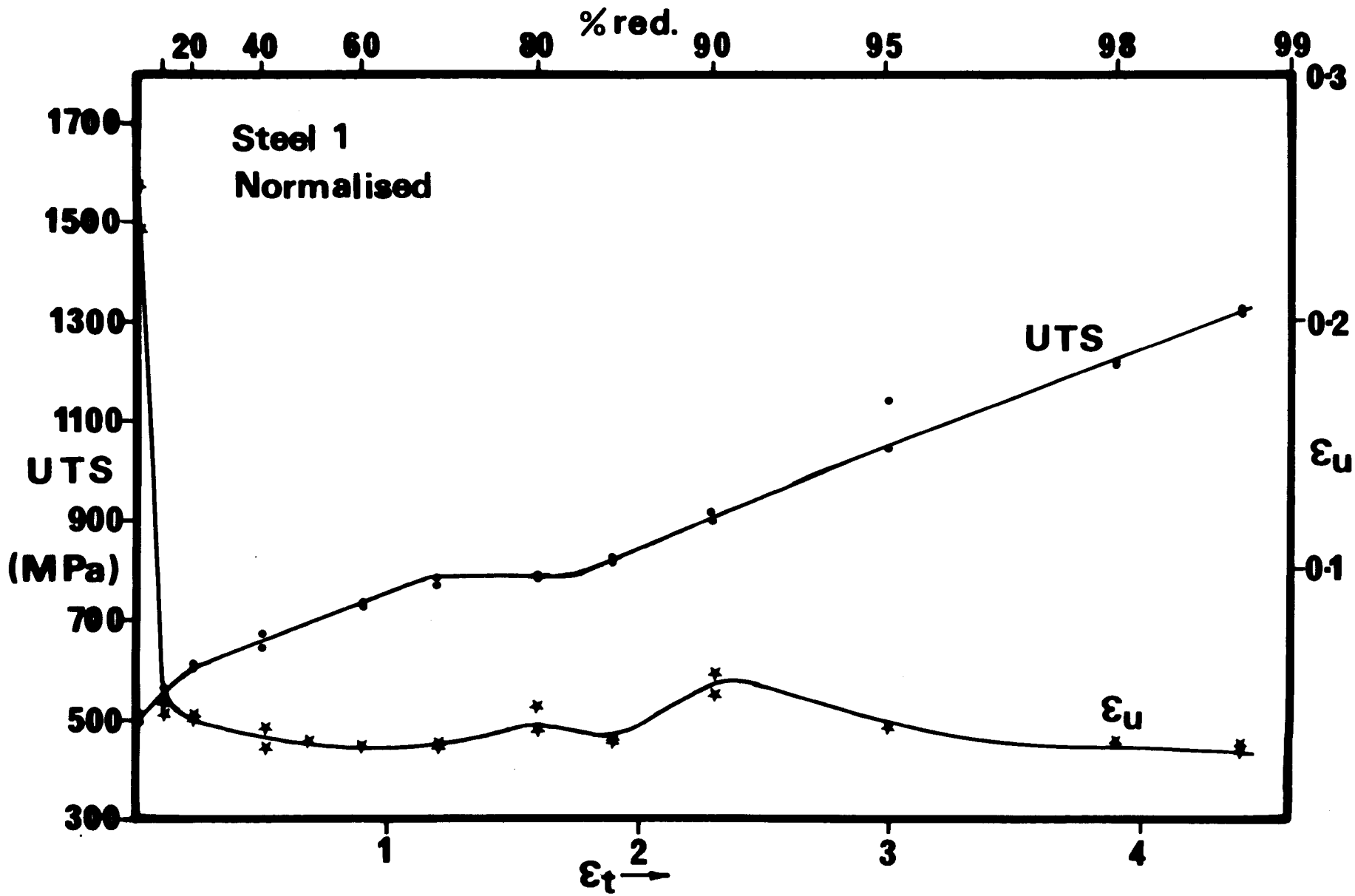
% red.
20
40
60
80
90
95
98
99
Steel 1
Normalised
1700
1500
1300
1100
900
700
500
300
UTS
(MPa)
UTS
ε_u
0·3
0·2
0·1
1
2
3
4
ε_t

FIGURE 6.8

The variation in U.T.S. and in uniform strain ϵ_u with increasing rolling strain for the high sulphur steel.

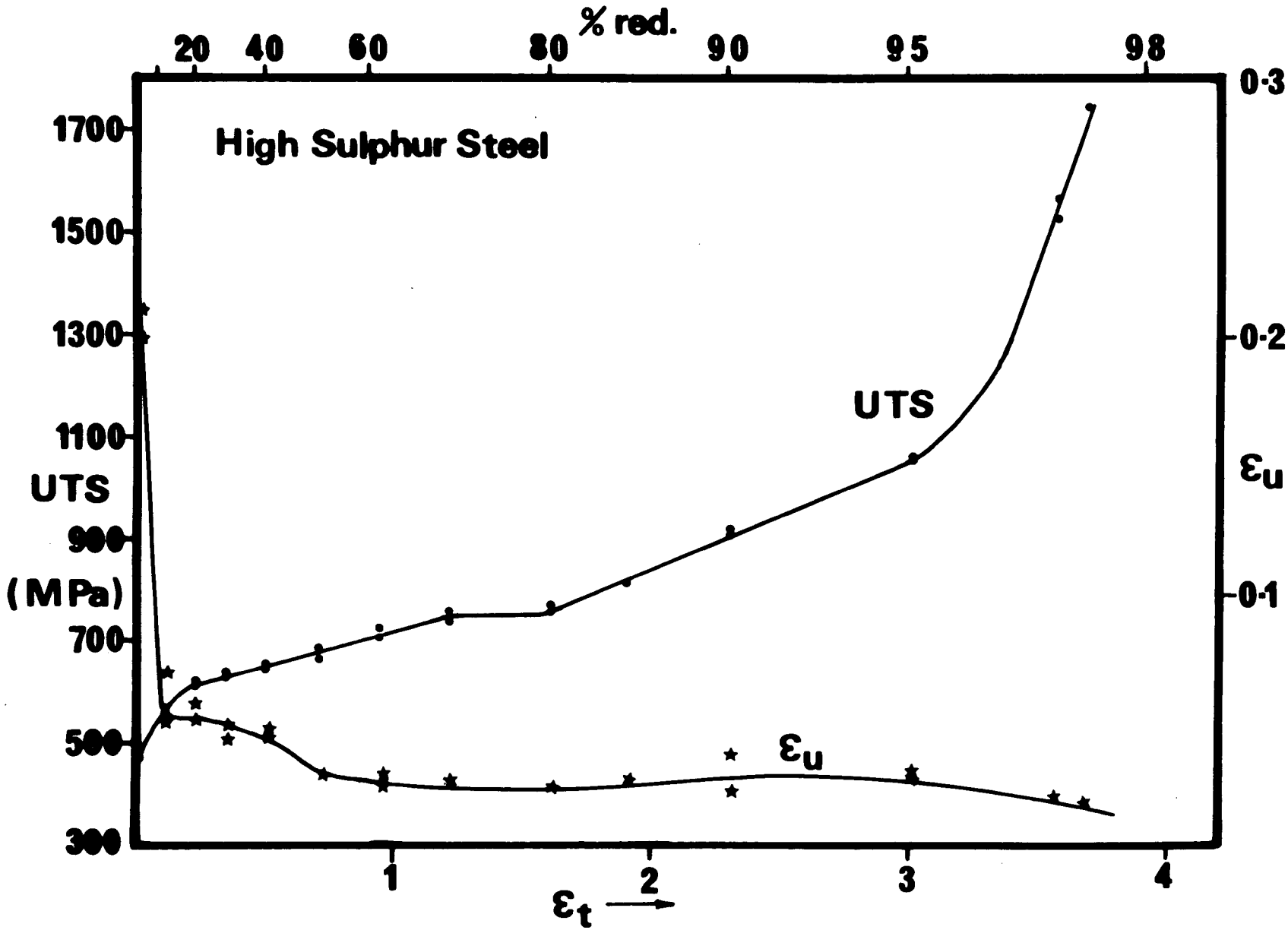
% red.
20
40
60
80
90
95
98
High Sulphur Steel
1700
1500
1300
1100
900
700
500
300
UTS
(MPa)
UTS
ε_u
ε_u
0·3
0·2
0·1
1
2
3
4
ε_t

FIGURE 6.9

The variation in U.T.S. and in uniform strain ε_u with increasing rolling strain for the steel containing sulphur and lead additions.

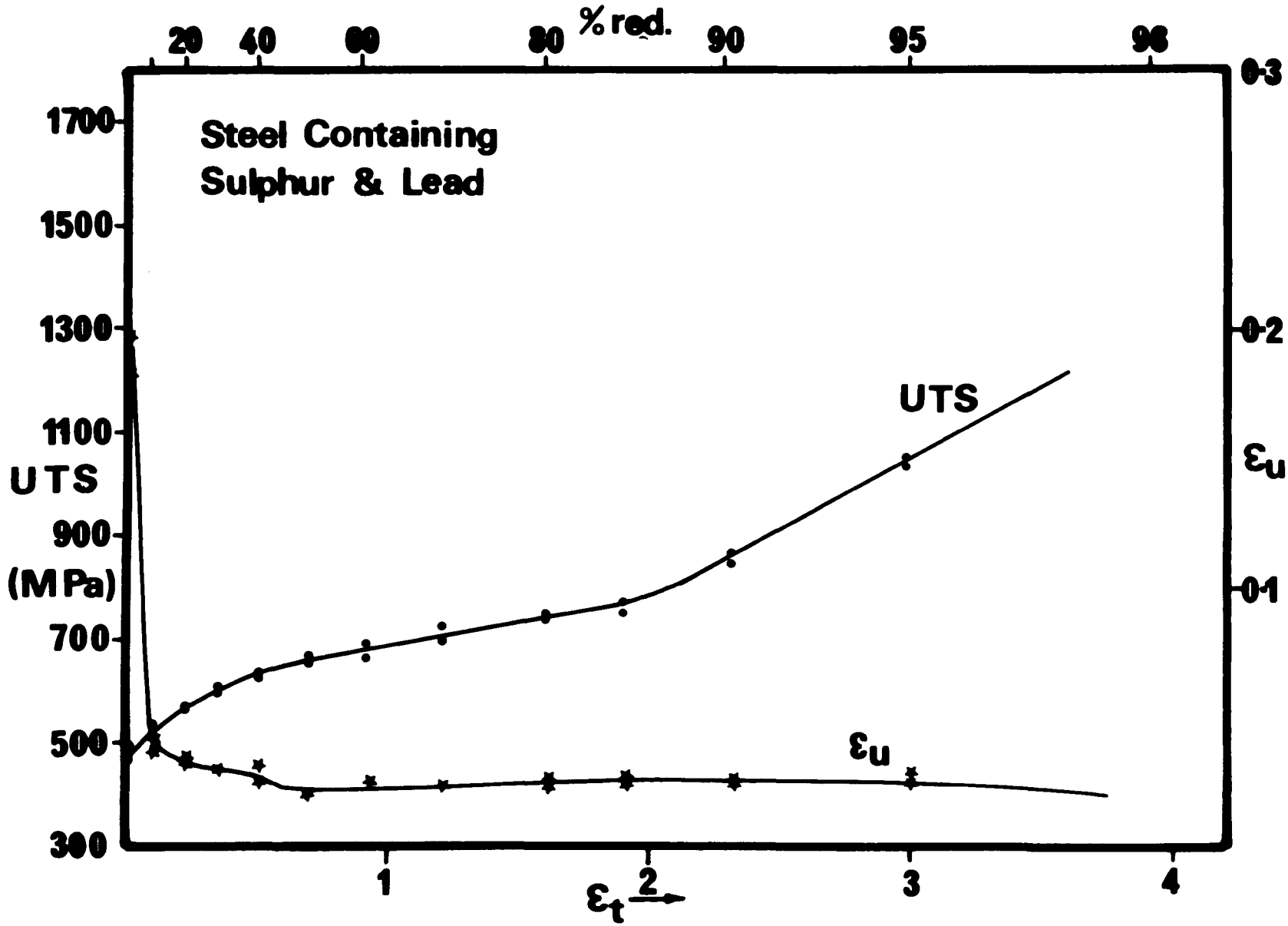
% red.
20
40
60
80
90
95
96
Steel Containing
Sulphur & Lead
UTS
ε_u
UTS
(MPa)
1700
1500
1300
1100
900
700
500
300
0·3
0·2
0·1
1
2
3
4
ε_t

FIGURE 6.10

The variation in U.T.S. and in uniform strain ε_u with increasing rolling strain for the steel (EN 3B) heat treated to give a structure of fine carbide particles in a ferrite matrix.

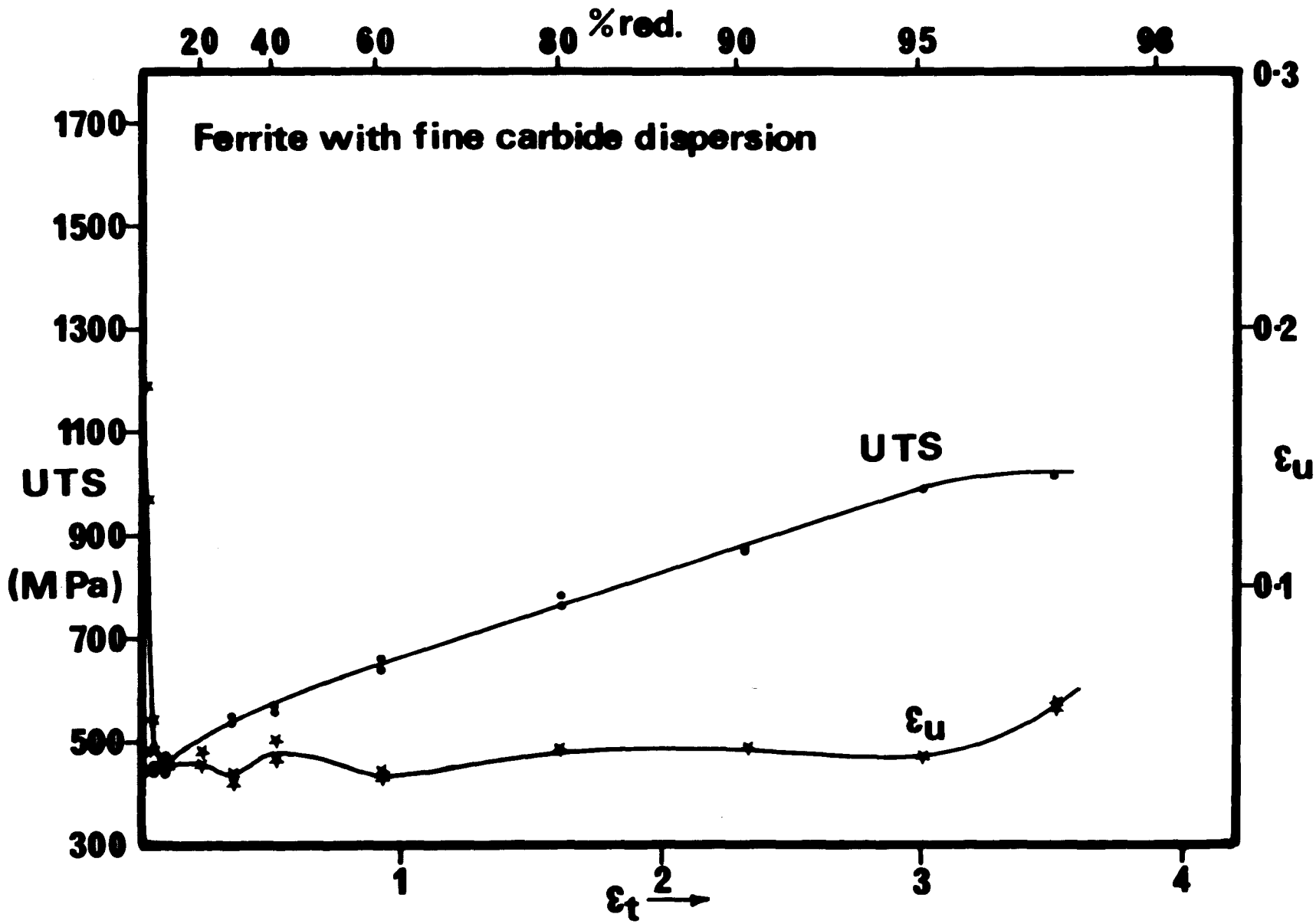
20
40
60
80
% red.
90
95
96
0·3
1700
Ferrite with fine carbide dispersion
1500
1300
0·2
1100
UTS
UTS
ε_u
900
(MPa)
0·1
700
500
ε_u
300
1
2
3
4
ε_t

FIGURE 6.11

Plots of log stress Vs log strain after various rolling strains for the steel (EN 8) in the normalised condition.

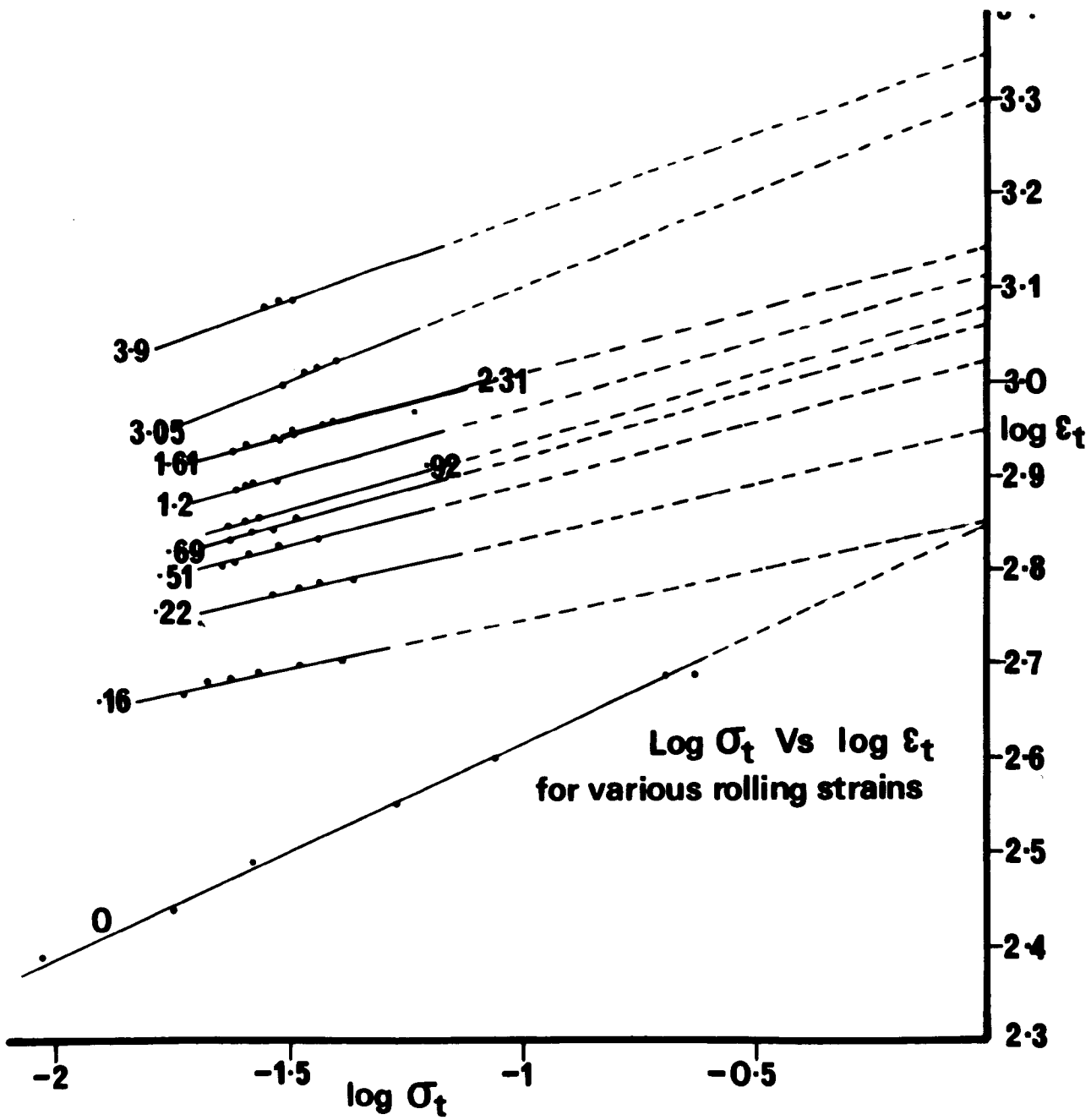
3·9
3·05
2·31
1·61
1·2
·92
·69
·51
·22
·16
0
Log σ_t Vs log ε_t
for various rolling strains
3·3
3·2
3·1
3·0
log ε_t
2·9
2·8
2·7
2·6
2·5
2·4
2·3
−2
−1·5
−1
−0·5
log σ_t

FIGURE 6.12

The variation in strain hardening exponent n with rolling strain for the normalised steel (EN 8), as determined from the slope of the curves in figure 6.11.

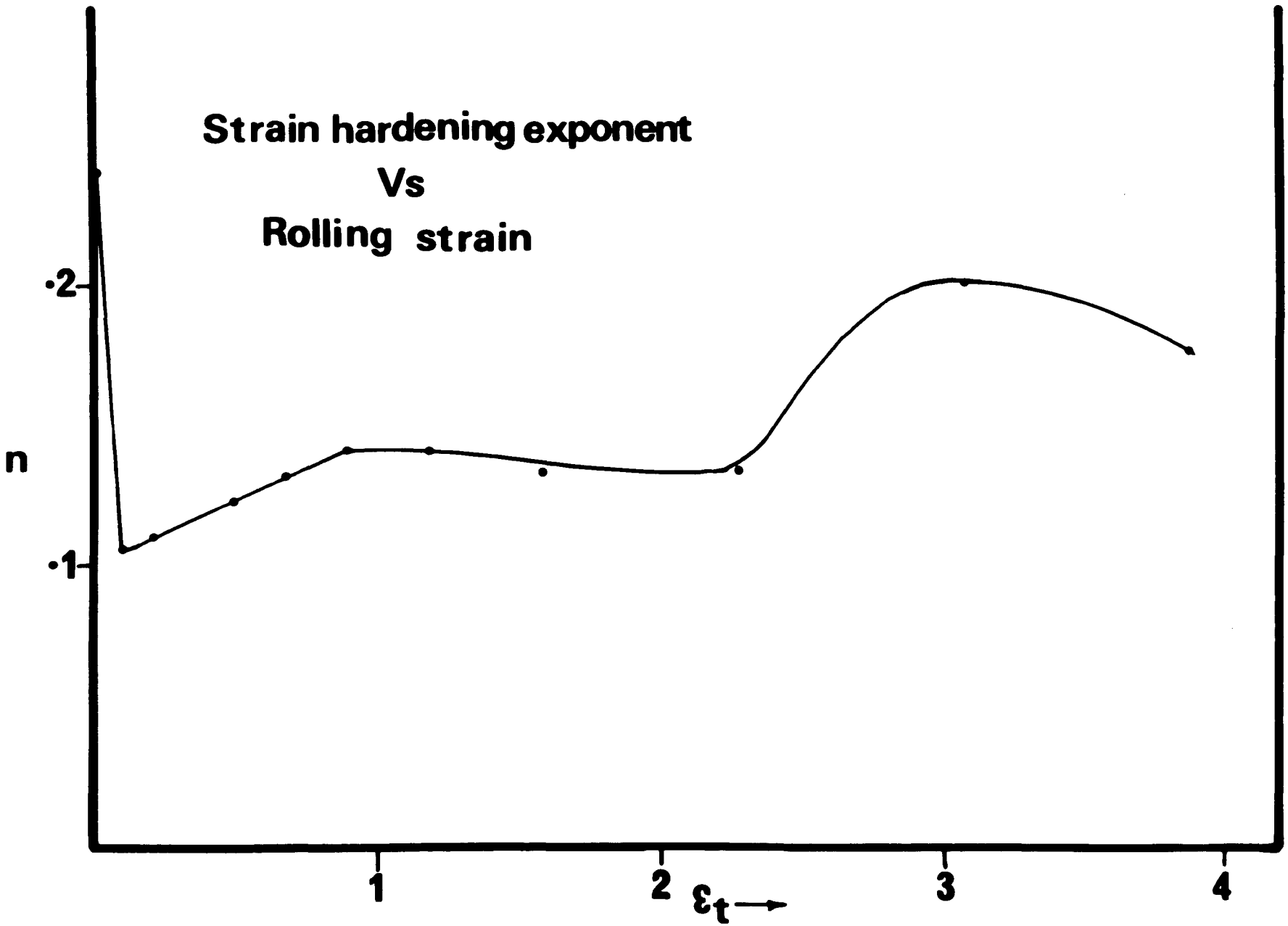
Strain hardening exponent
Vs
Rolling strain
n
·2
·1
1
2
3
4
ε_t

FIGURE 6.13

The variation in strength coefficient k with rolling strain for the normalised steel (EN 8), obtained from the curves of figure 6.11 by extrapolation.

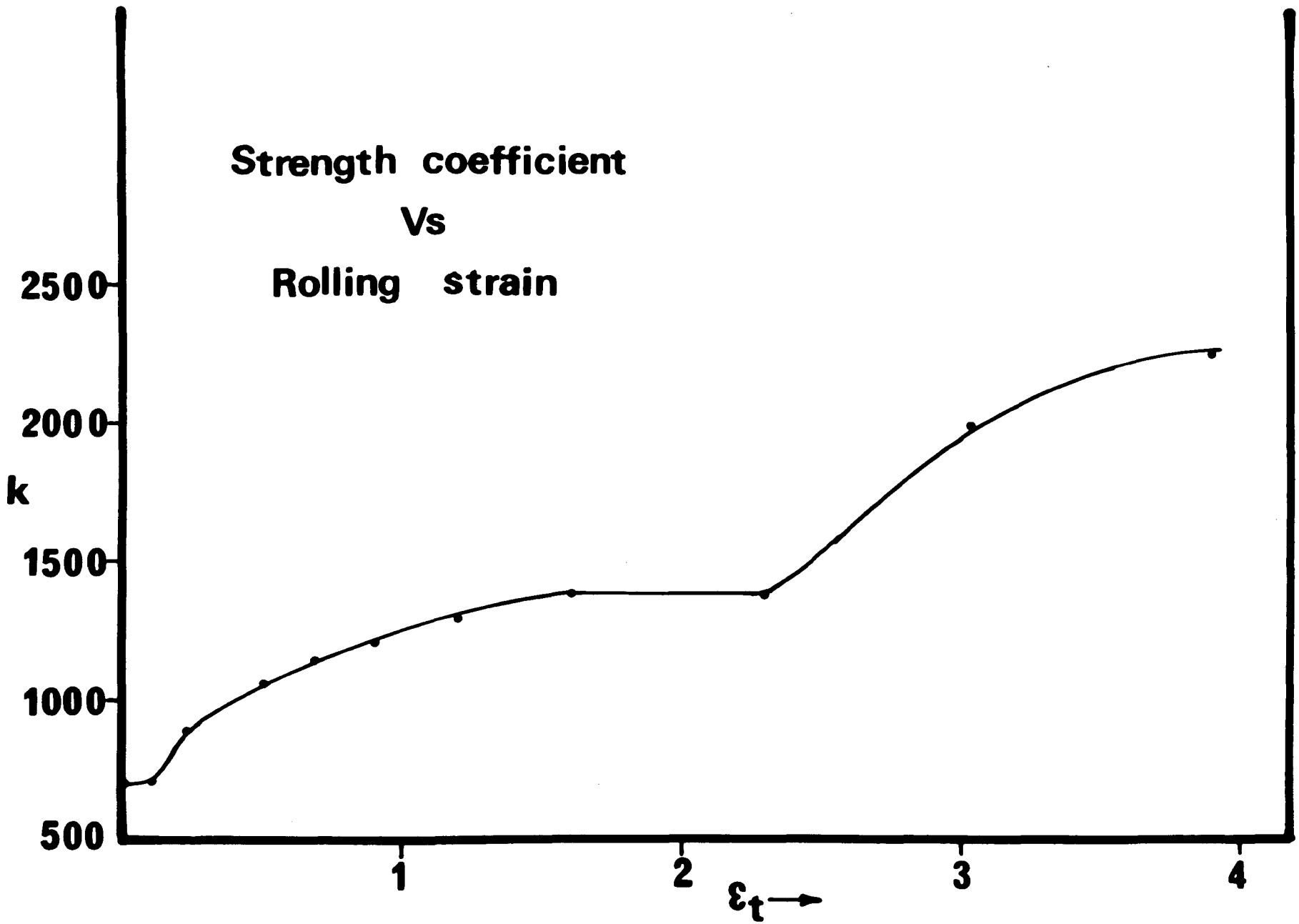
Strength coefficient
Vs
Rolling strain
2500
2000
k
1500
1000
500
1
2
3
4
ε_t

FIGURE 7.1

Fractured tensile specimen of the Quenched and tempered steel after 45% rolling strain.

1 mm

FIGURE 7.2

Equiaxed cavities in the central region of the specimen shown in figure 7.1.

20 μm

FIGURE 7.3

The structure of the sloping shear zones of the specimen shown in figure 7.1.

20 μm

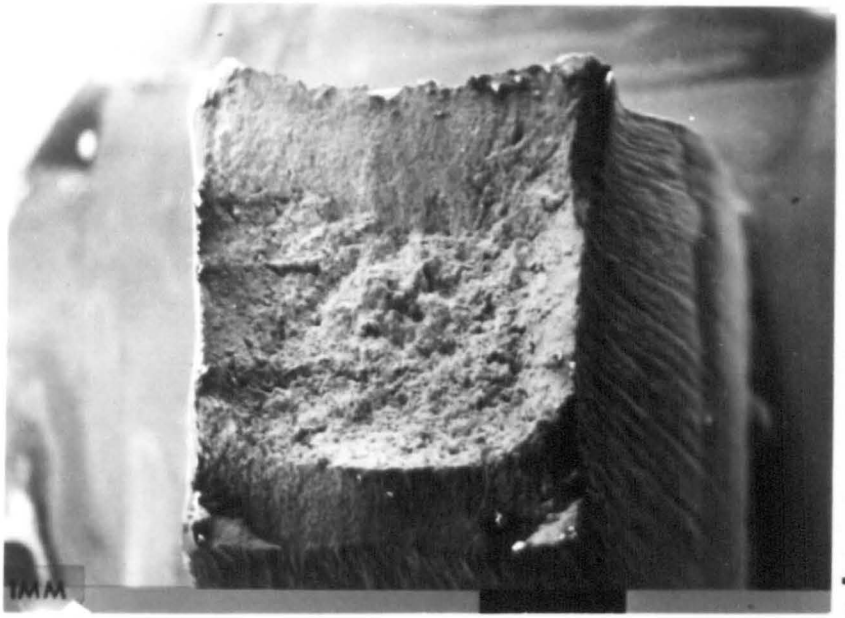

7•1

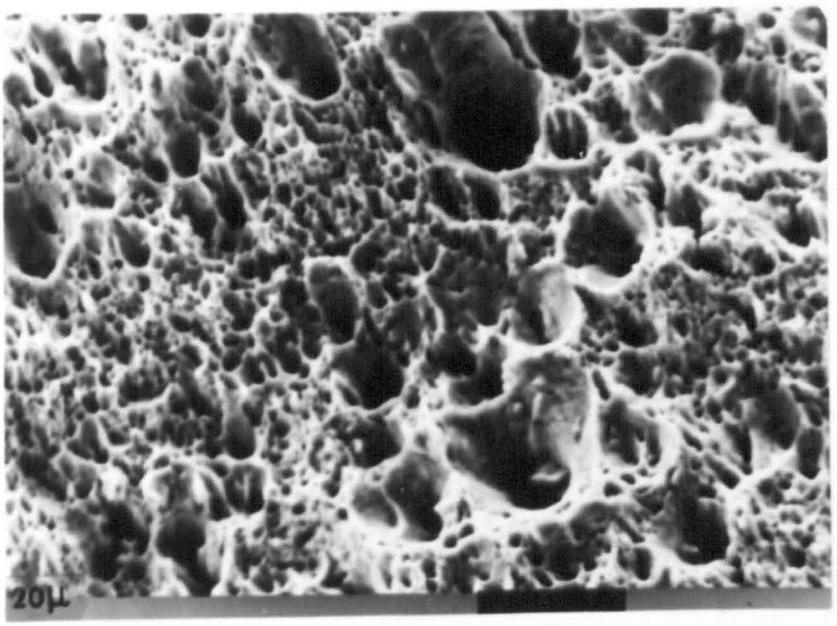

7•2

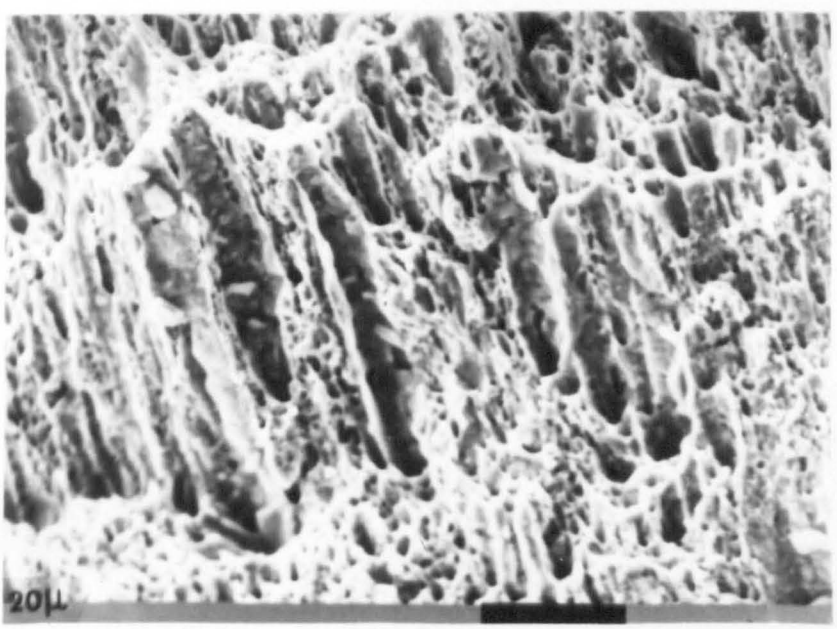

7•3

FIGURE 7.4

Fractured tensile specimen of the quenched and tempered steel after 60% rolling strain.

400 μm

FIGURE 7.5

The central region of the specimen shown in figure 7.4.

20 μm

FIGURE 7.6

The sloping shear face of the specimen shown in figure 7.4.

20 μm

7•4

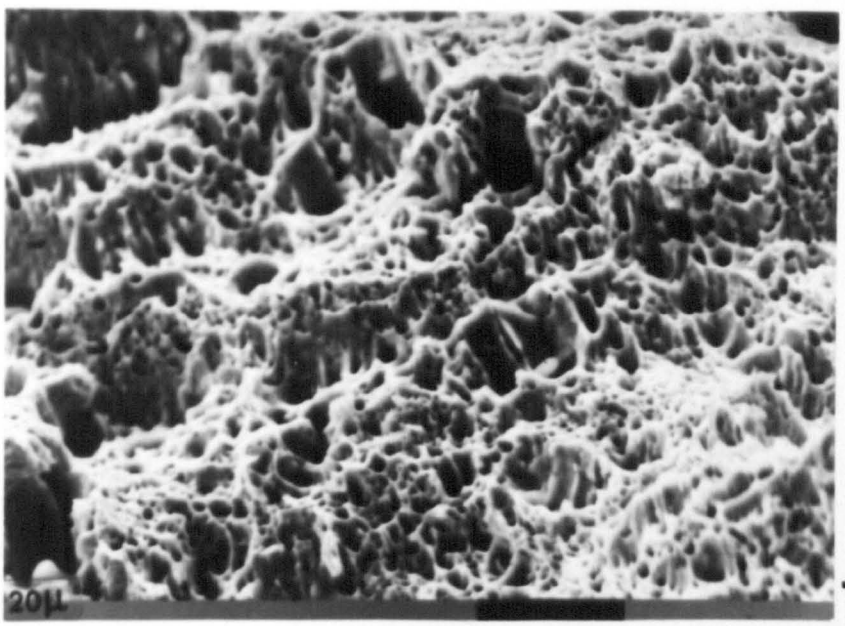

7•5

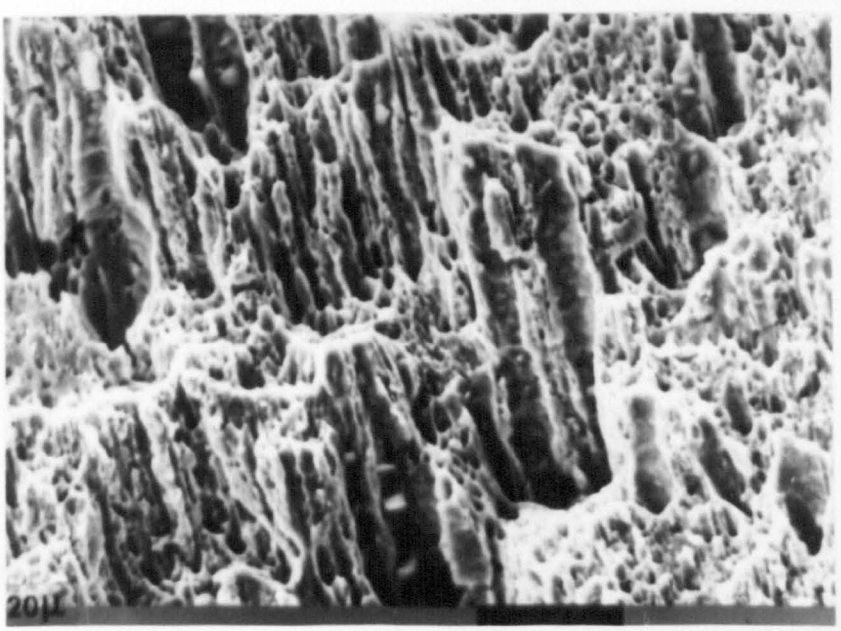

7•6

FIGURE 7.7

Cavities, in the central zone of a double cup fracture, coalescing into cracks. This specimen of the quenched and tempered steel has undergone reduction by rolling.

40 μm

FIGURE 7.8

Fractured tensile specimen of the quenched and tempered steel after 80% rolling reduction, showing a large crack parallel to the rolling direction.

200 μm

FIGURE 7.9

The structure of the surface of the crack shown in figure 7.8.

20 μm

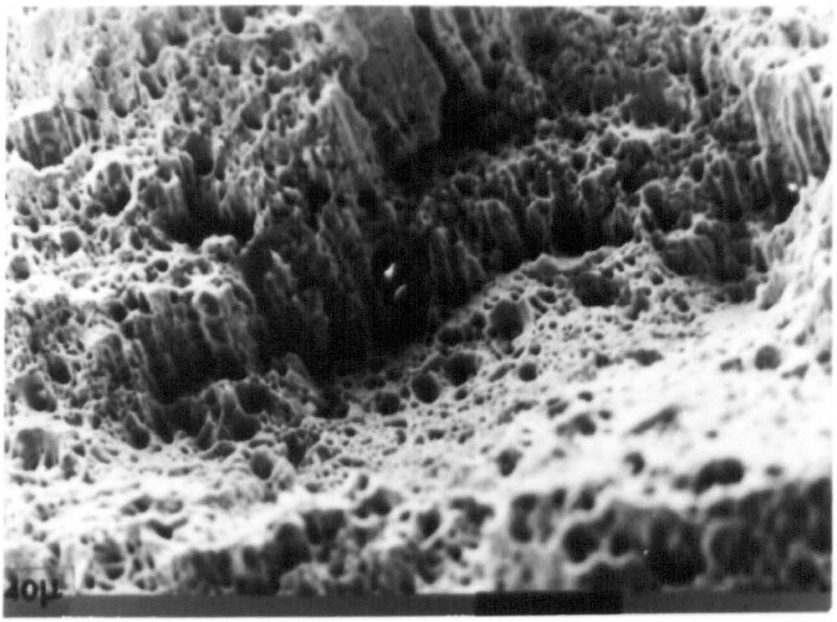

7•7

7•8

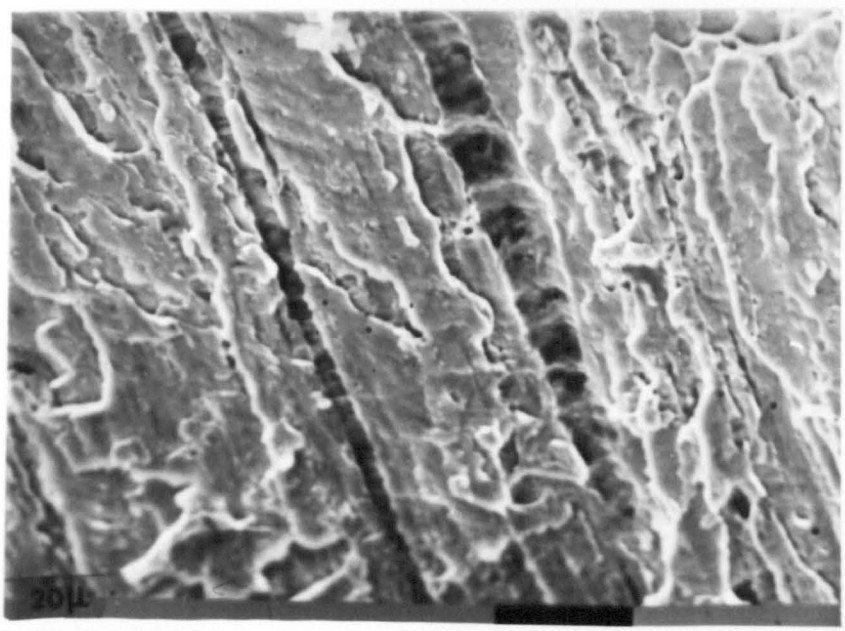

7•9

FIGURE 7.10

The fracture surface of a tensile specimen of the normalised steel which had undergone 60% reduction by rolling.

100 μm

FIGURE 7.11

After 80% rolling reduction, the normalised steel fractures showed only elongated shear dimples.

40 μm

FIGURE 7.12

A specimen of the normalised steel after 80% rolling reduction, showing shear fractures on intersecting planes.

1 mm

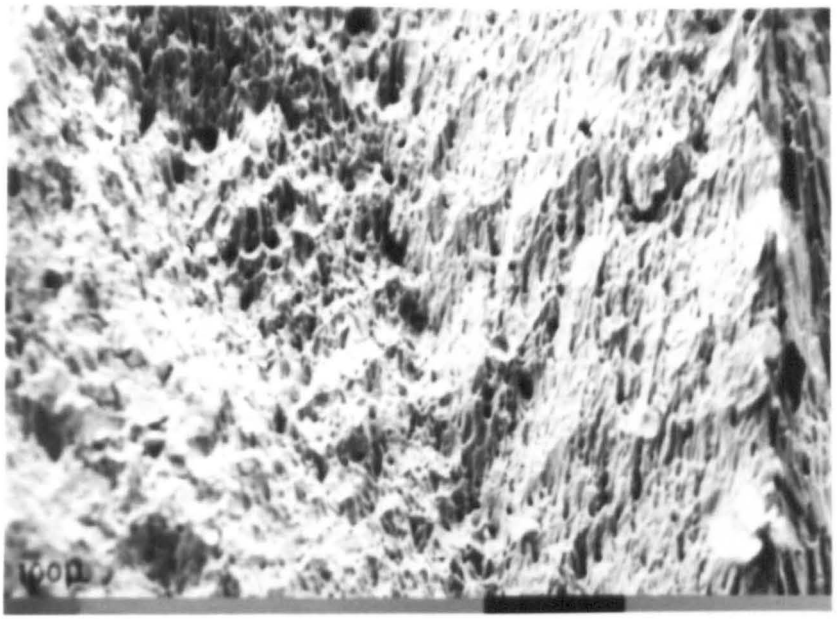

7•10

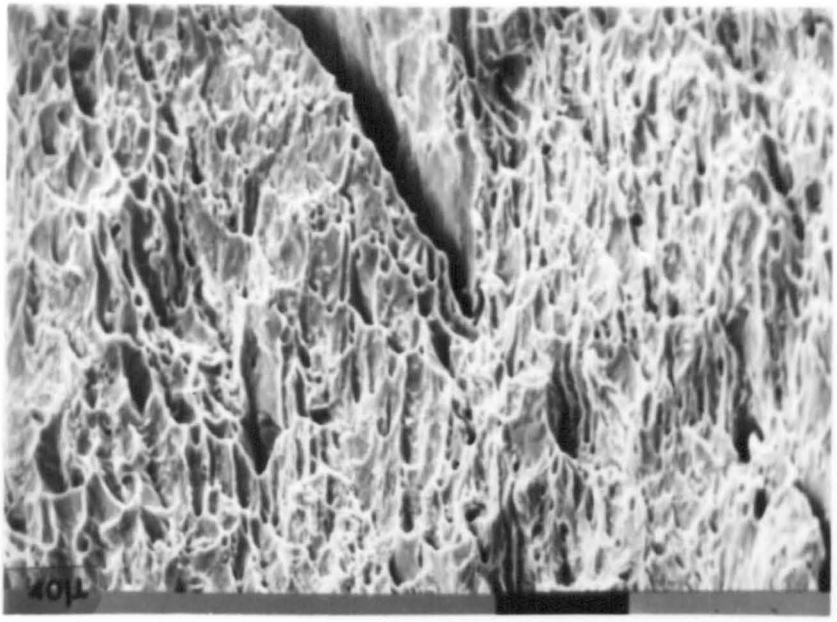

7•11

7•12

FIGURE 7.13

Steps on the fracture surface of a specimen of the normalised steel after 90% rolling reduction.

100 μm

FIGURE 7.14

Another specimen of the normalised steel after 90% rolling reduction, showing intersecting shear fractures.

200 μm

FIGURE 7.15

The structure of the crack faces shown in figures 7.14 and 7.15.

40 μm

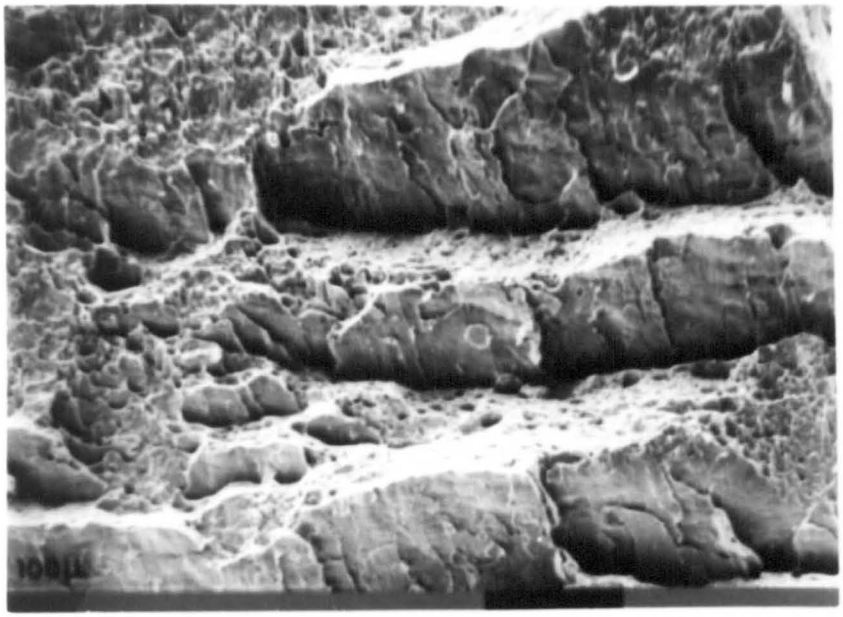

7•13

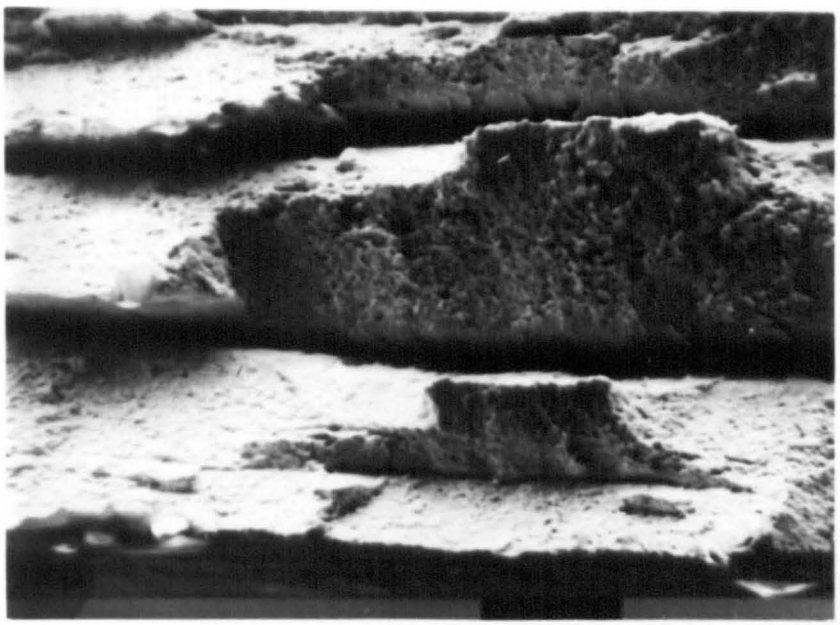

7•14

7•15

FIGURE 7.16

A taper section of the fracture surface shown in figure 7.13, made in order to relate the cracks to features in the etched microstructure.

10 μm

FIGURE 7.17

Another area of the taper section through the fracture surface of the normalised steel specimen after 90% rolling reduction. In this case the depth of the equiaxed cavities can be clearly seen.

10 μm

FIGURE 7.18

The general structure of the fracture surface of a high sulphur steel tensile specimen after 10% rolling reduction.

10 μm

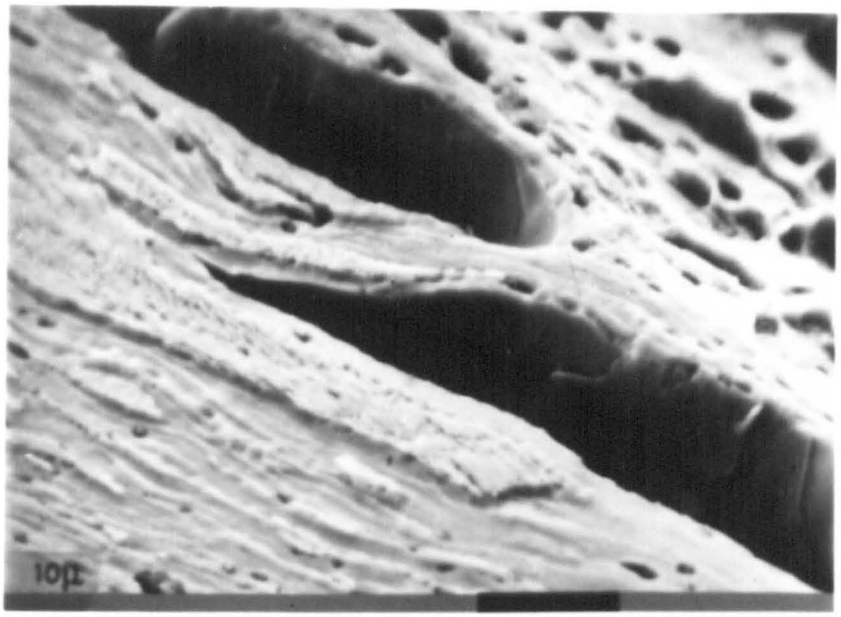

7•16

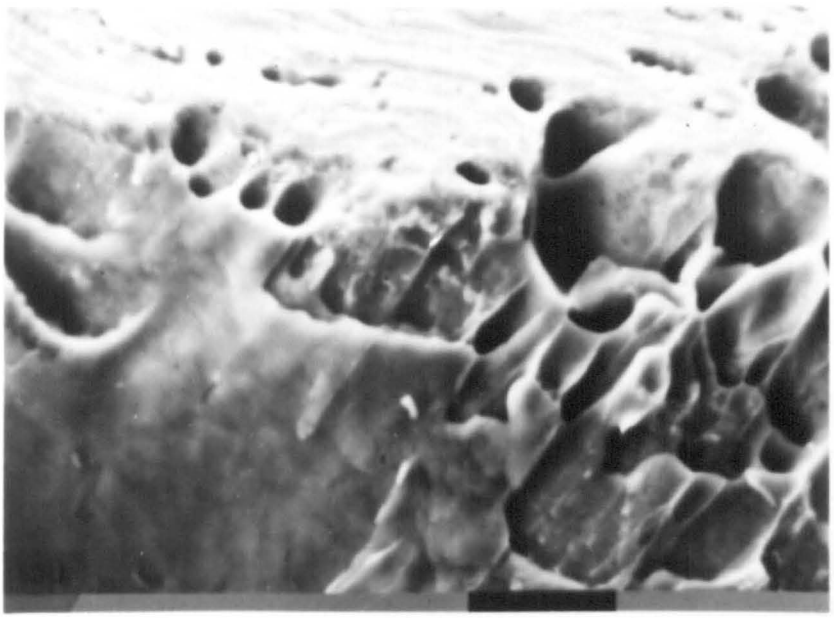

7•17

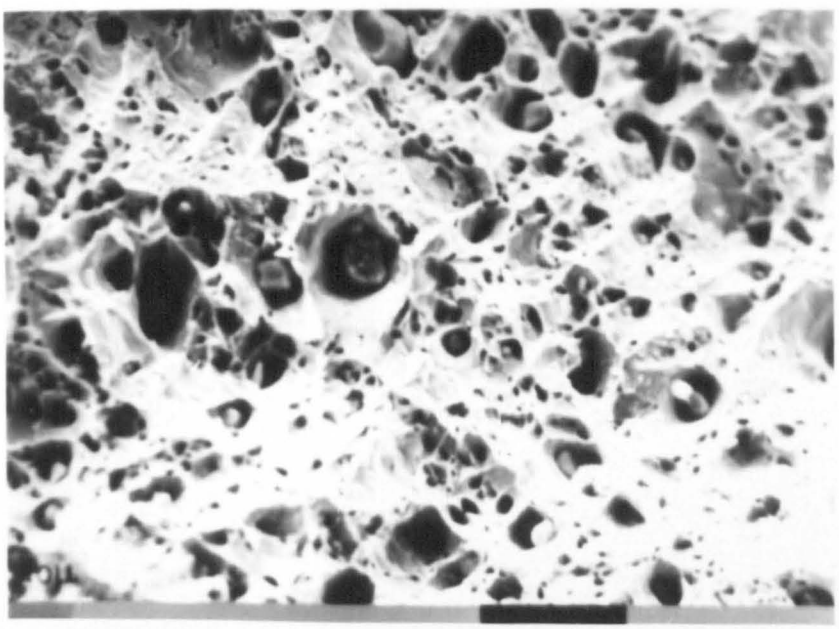

7•18

FIGURE 7.19

Another specimen of the high sulphur steel after a rolling reduction of 10%. In this case the fracture surface sloped at about 30° across the width of the tensile specimen.

40 μm

FIGURE 7.20

The structure of the shear zones in the outer regions of the fracture surface of tensile specimens of the high sulphur steel after 60% rolling reduction.

40 μm

FIGURE 7.21

A general view of the 45° shear fracture surface of specimens of the high sulphur steel which had undergone 90% reduction by rolling.

400 μm

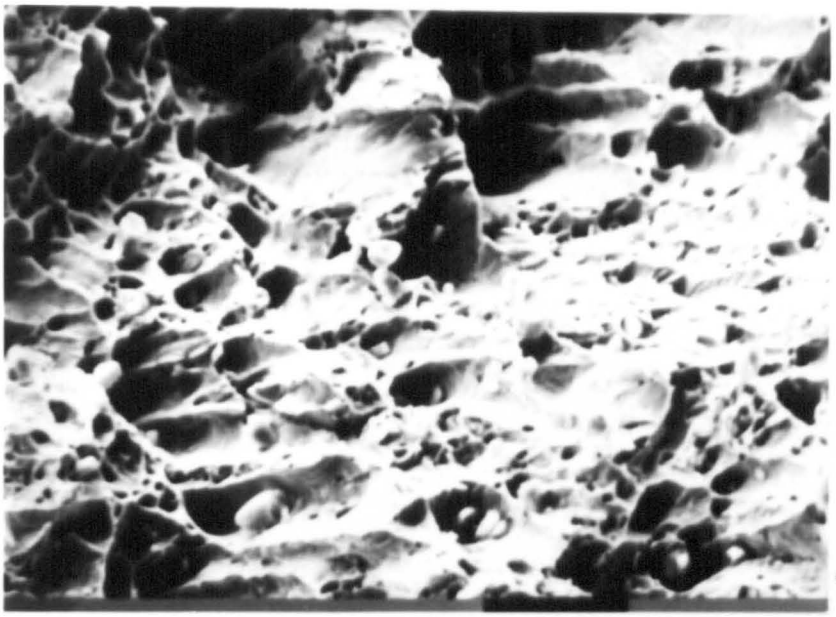

7•19

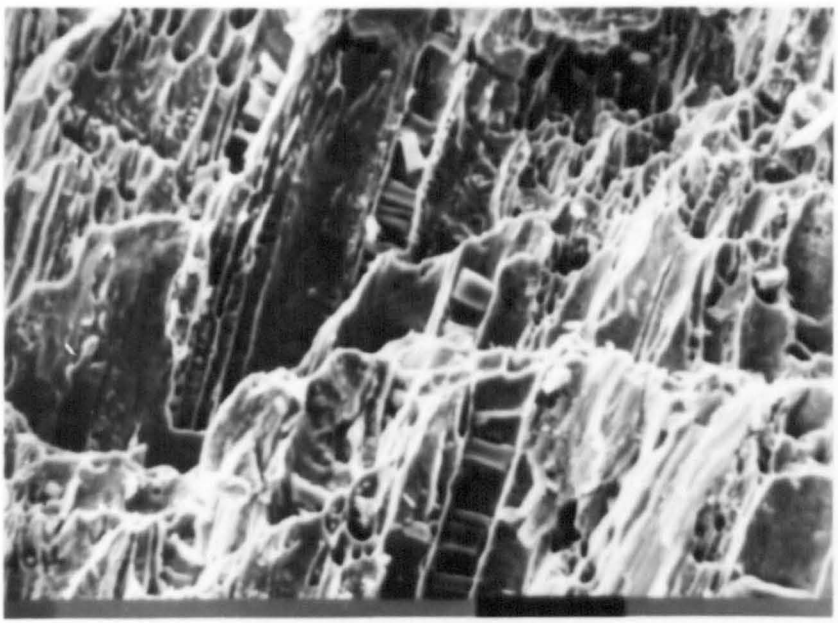

7•20

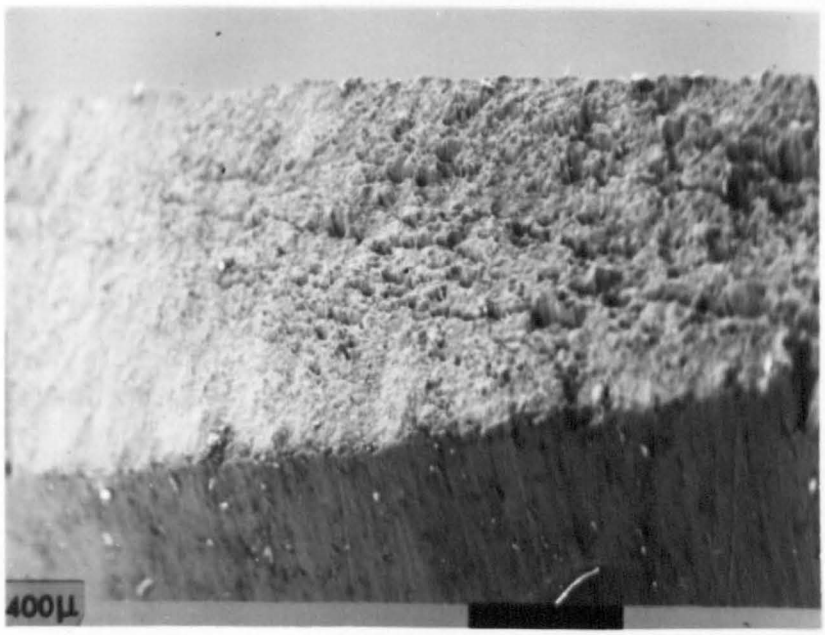

7•21

FIGURE 7.22

An enlarged view of the 90% reduced high sulphur steel specimen shown in figure 7.21.

40 μm

FIGURE 7.23

A shear zone in the fracture surface of a tensile specimen of the steel containing sulphur and lead. This particular specimen has undergone a rolling reduction of 40%.

20 μm

FIGURE 7.24

The central region of the fracture surface of a specimen of the steel with sulphur and lead after only a small rolling reduction.

10 μm

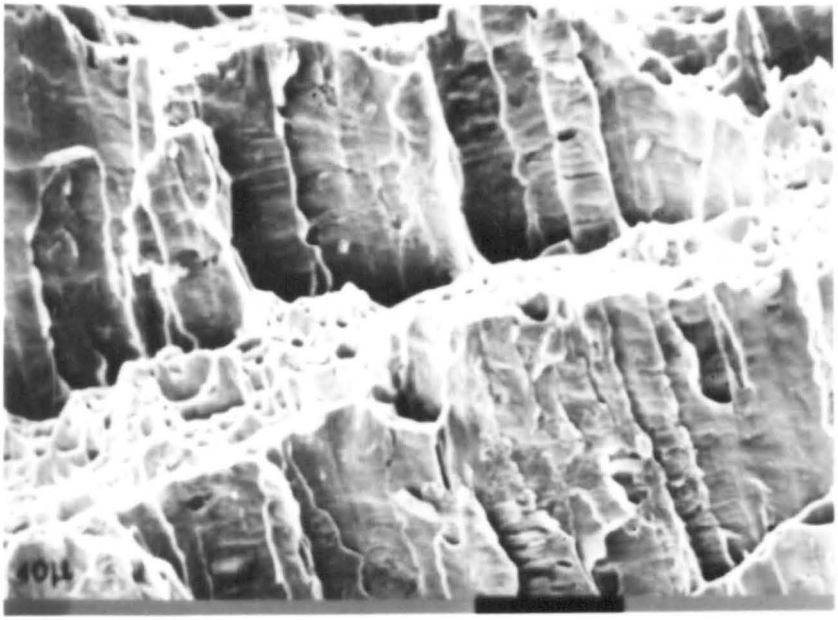

7•22

7•23

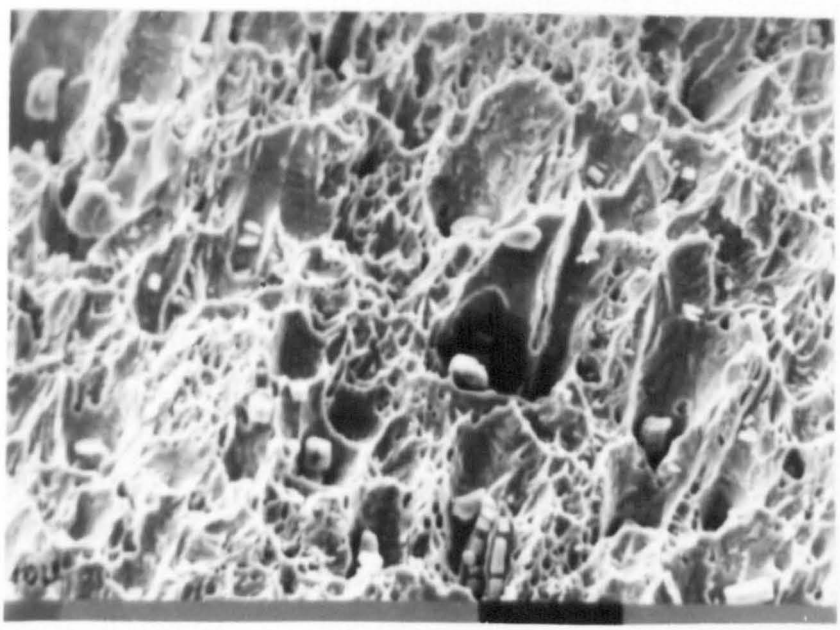

7•24

FIGURE 7.25

Shear fracture surface in the steel containing sulphur and lead after 90% rolling reduction.

20 μm

FIGURE 7.26

The central region of a cup-cone fracture surface in an as heat treated specimen of the steel with a fine dispersion of carbides.

20 μm

FIGURE 7.27

The shear faces of the cup-cone fracture surface shown in figure 7.26 .

10 μm

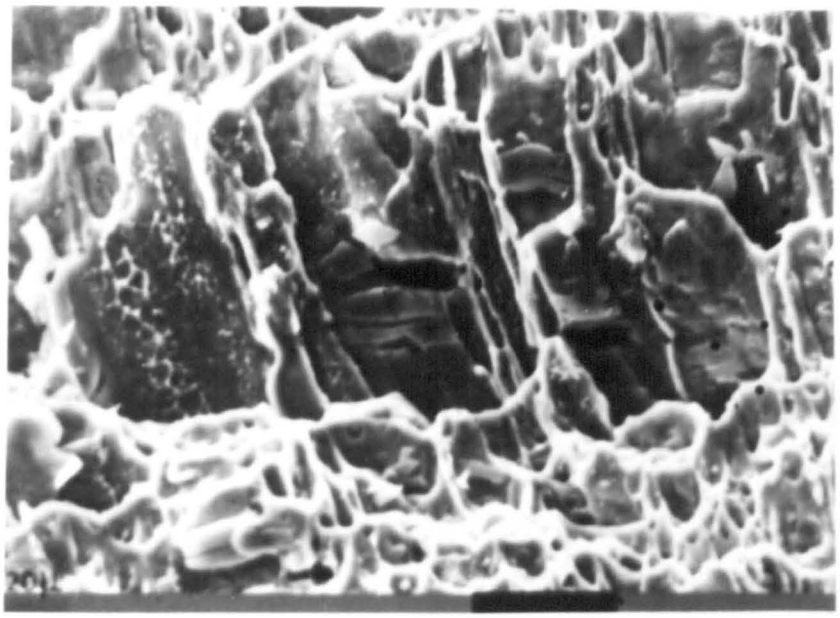

7•25

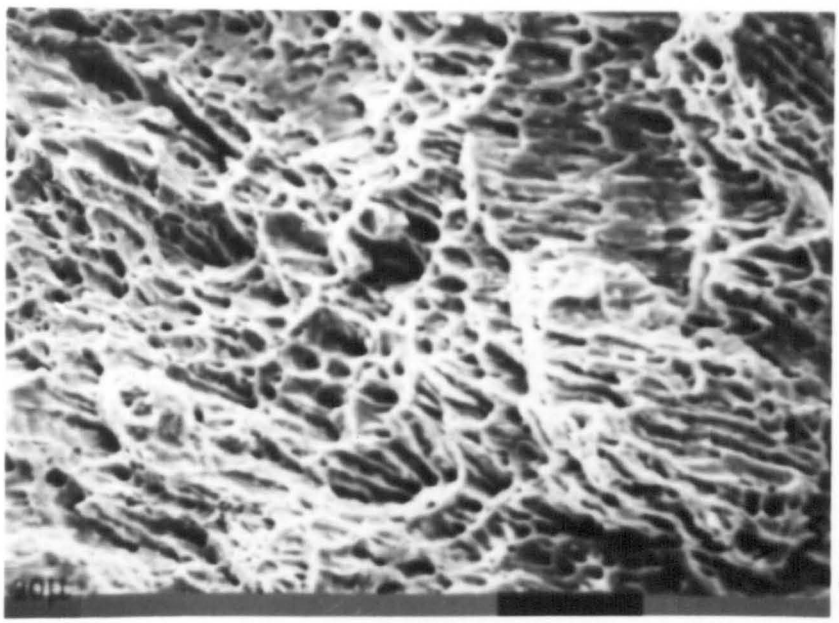

7•26

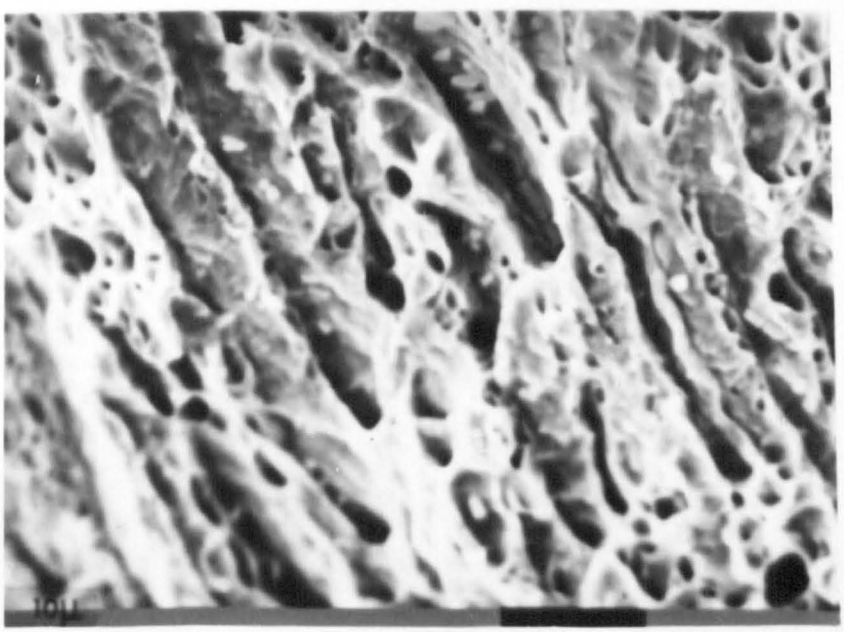

7•27

FIGURE 7.28

The steel with a fine dispersion of carbides after a rolling reduction of 5%, showing coalescence of cavities in the central region of the cup-cone fracture.

10 μm

FIGURE 7.29

Coalescence of the cavities in the shear zone of the fracture shown in figure 7.28.

10 μm

FIGURE 7.30

General view of fracture surface of the steel with a fine dispersion of carbides, after a rolling reduction of 20%.

1 mm

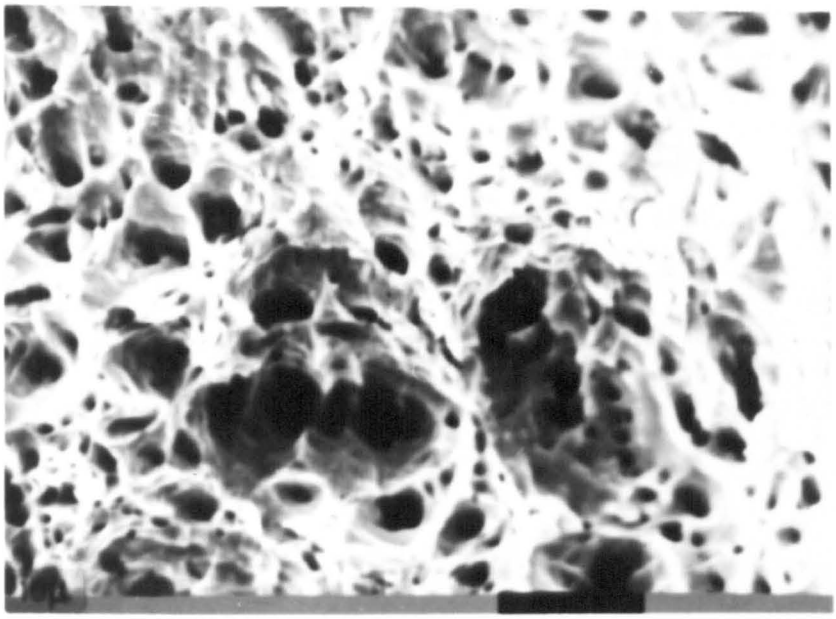

7•28

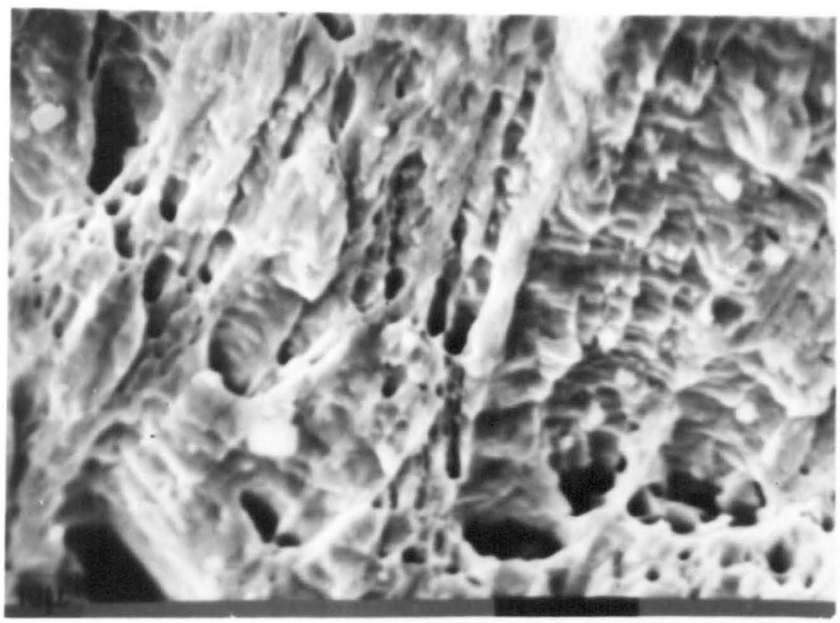

7•29

7•30

FIGURE 7.31

The shear surface of the fracture shown in figure 7.30.

40 μm

FIGURE 7.32

A fracture surface in the steel with a fine carbide dispersion, broken in tension after a rolling reduction of 40%.

100 μm

FIGURE 7.33

Coalesced cavities in the centre of the double cup fracture surface shown in figure 7.33.

20 μm

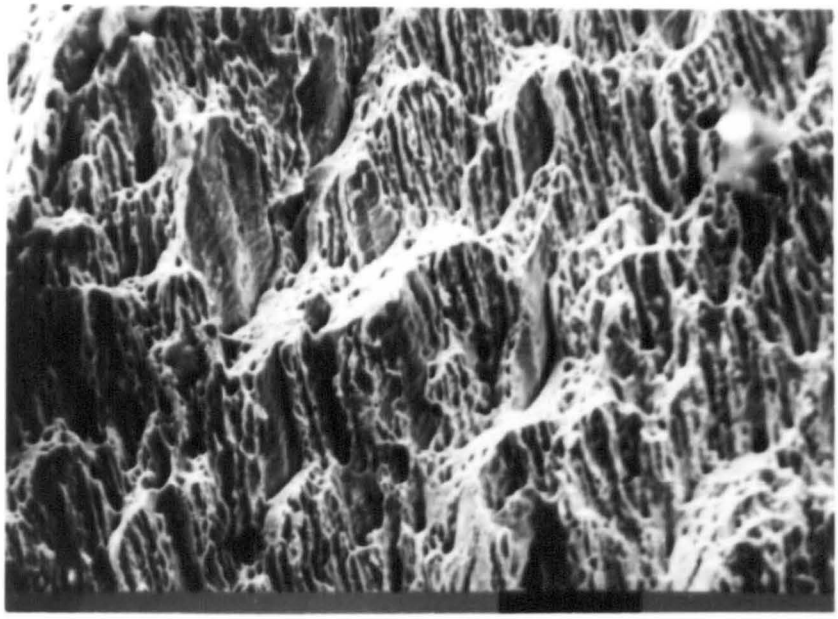

7•31

7•32

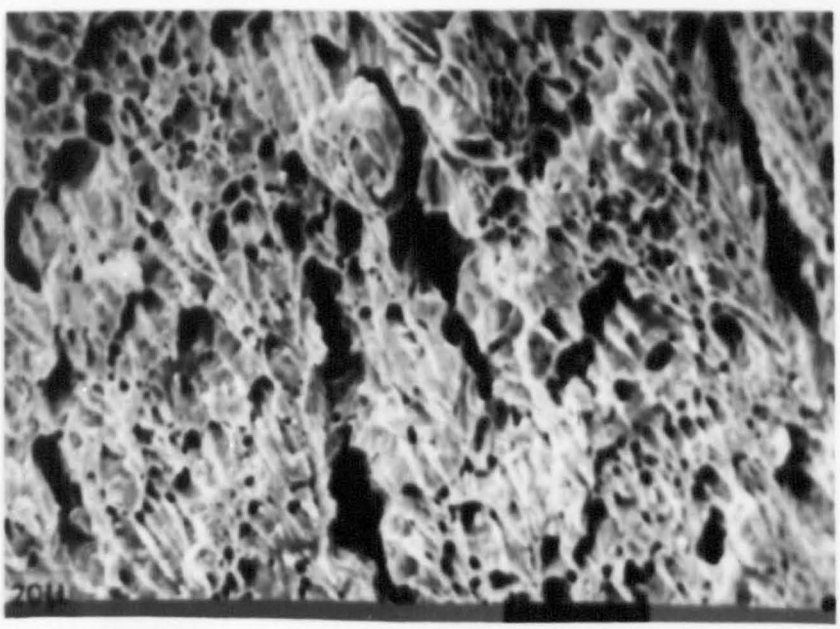

7•33

FIGURE 7.34

A typical non cleavage region of the fracture surface of a machining chip, from the normalised steel in the as heat treated condition. The chip has been fractured at liquid nitrogen temperature.

20 μm

FIGURE 7.35

A region of the fracture surface of a machining chip from the high sulphur steel, after fracturing at liquid nitrogen temperature.

20 μm

FIGURE 7.36

A typical region of fracture surface of a machining chip from the steel with a fine carbide dispersion, after fracturing it at liquid nitrogen temperature.

40 μm

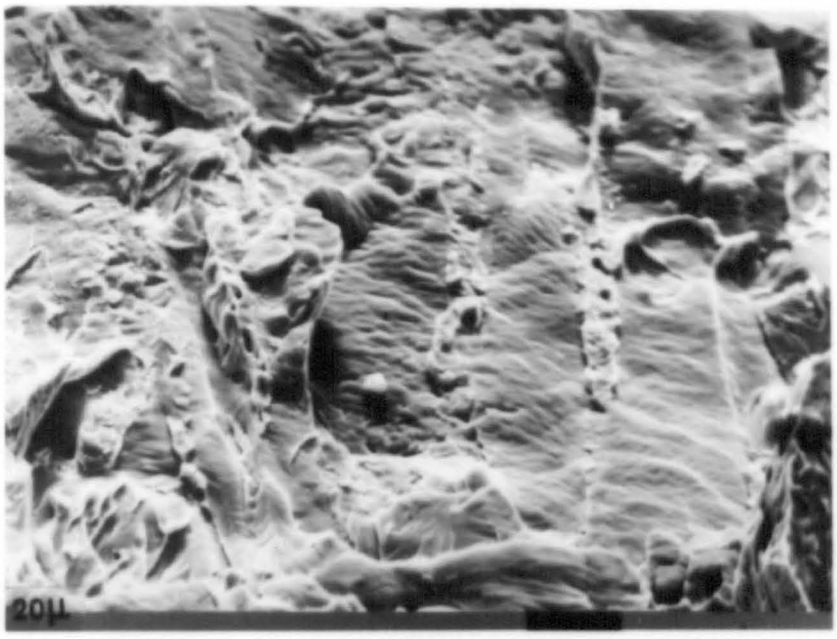

7•34

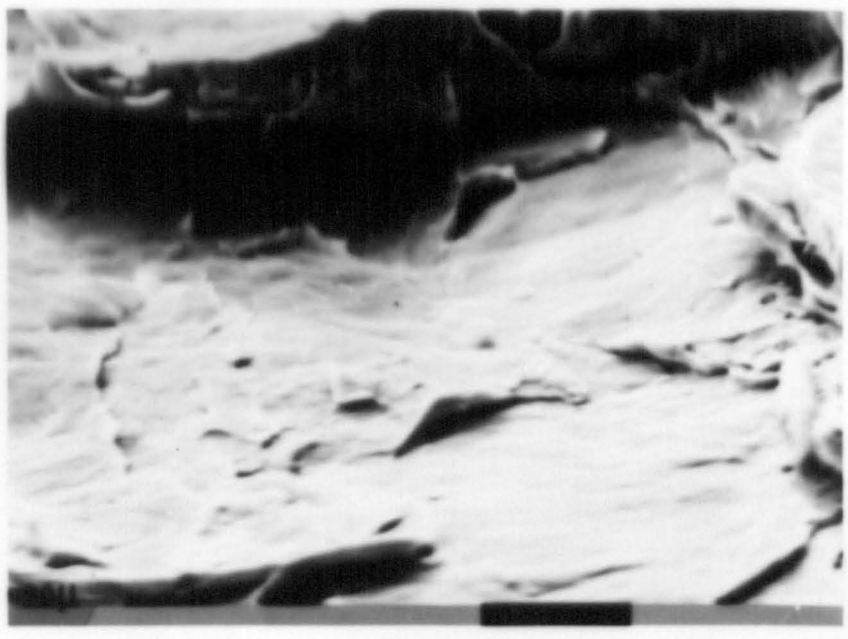

7•35

7•36

FIGURE 7.37

Cavities around manganese sulphide particles in the centre of a cup-cone fracture of the high sulphur steel after 10% rolling reduction.

20 μm

FIGURE 7.38

A tensile fracture, with a shear component across the width of the specimen, in the high sulphur steel after 30% rolling reduction.

20 μm

FIGURE 7.39

A view down a sloping shear face of a tensile fracture, in the quenched and tempered steel after 60% reduction by rolling.

10 μm

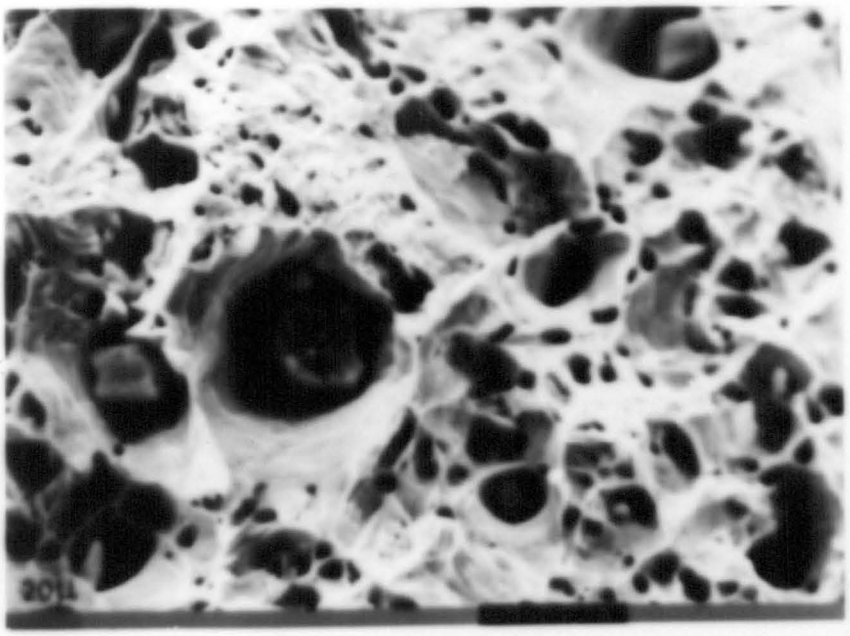

7•37

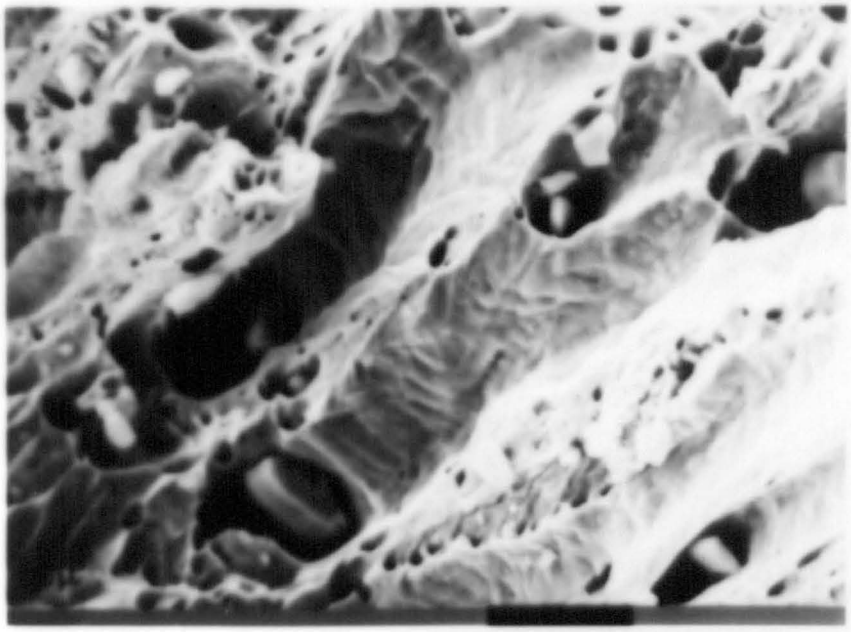

7•38

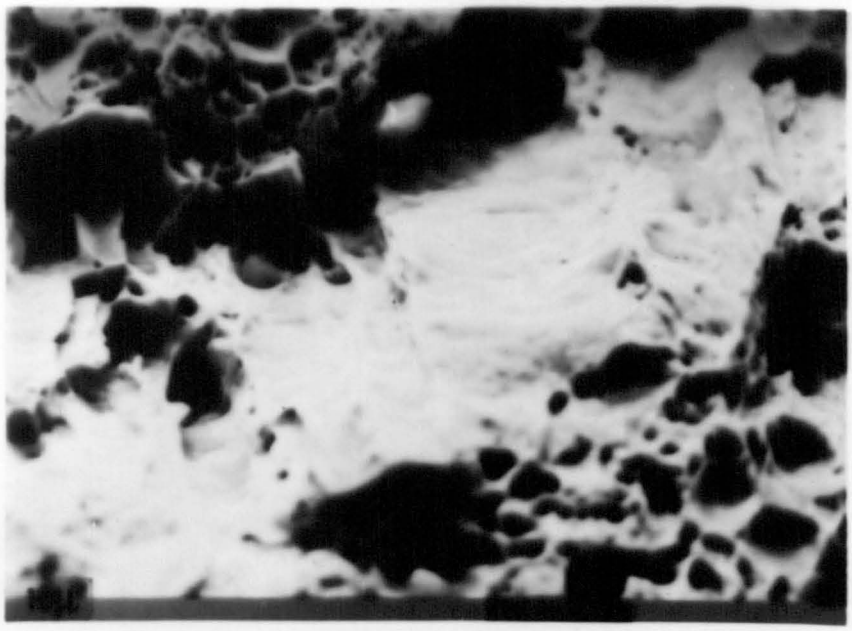

7•39

FIGURE 7.40

A portion of the fracture surface of a high sulphur steel machining chip, which appears to be covered with a thin layer of manganese sulphide.

10 μm

FIGURE 7.41

The front surface of a lathe turning from the high sulphur steel, which has been deeply etched in 20% nitric acid in alcohol to reveal thin particles of manganese sulphide in the shear planes.

10 μm

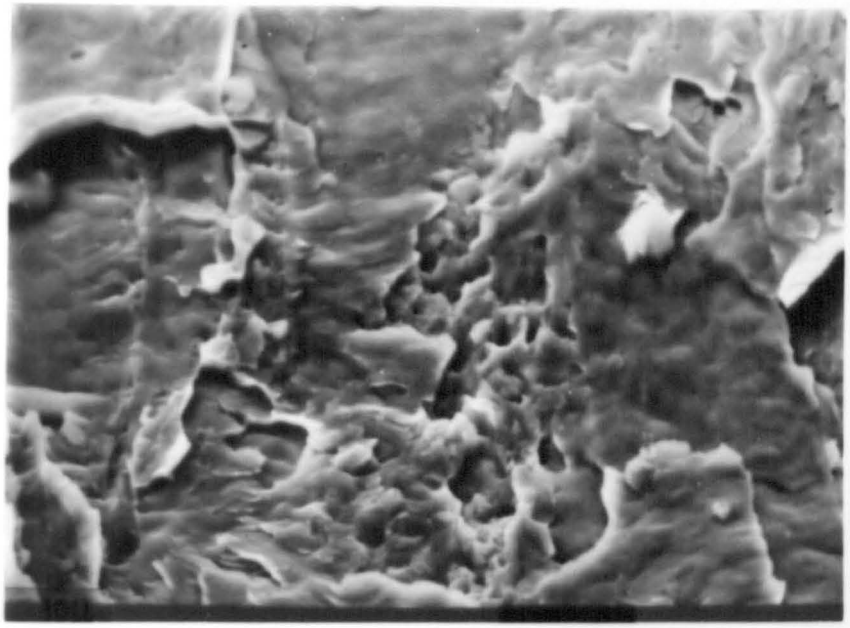

7•40

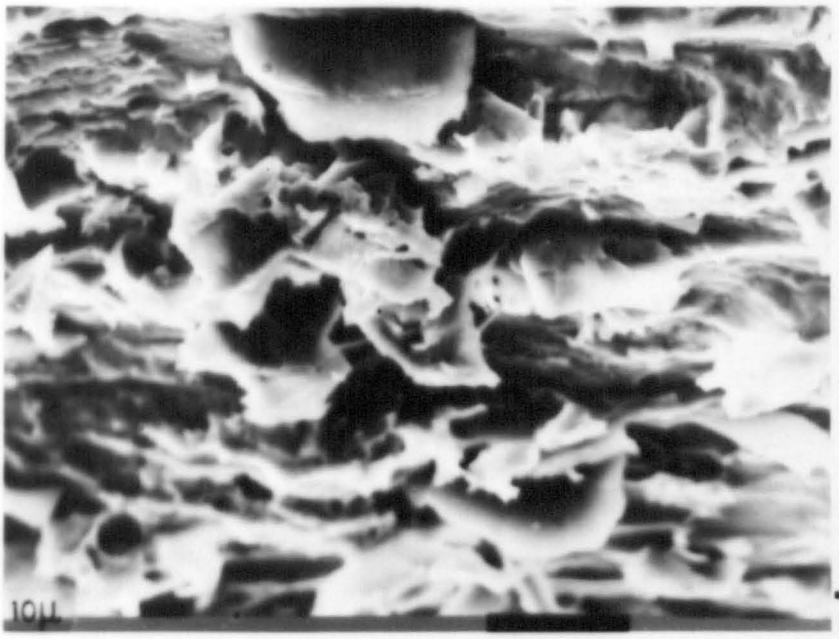

7•41

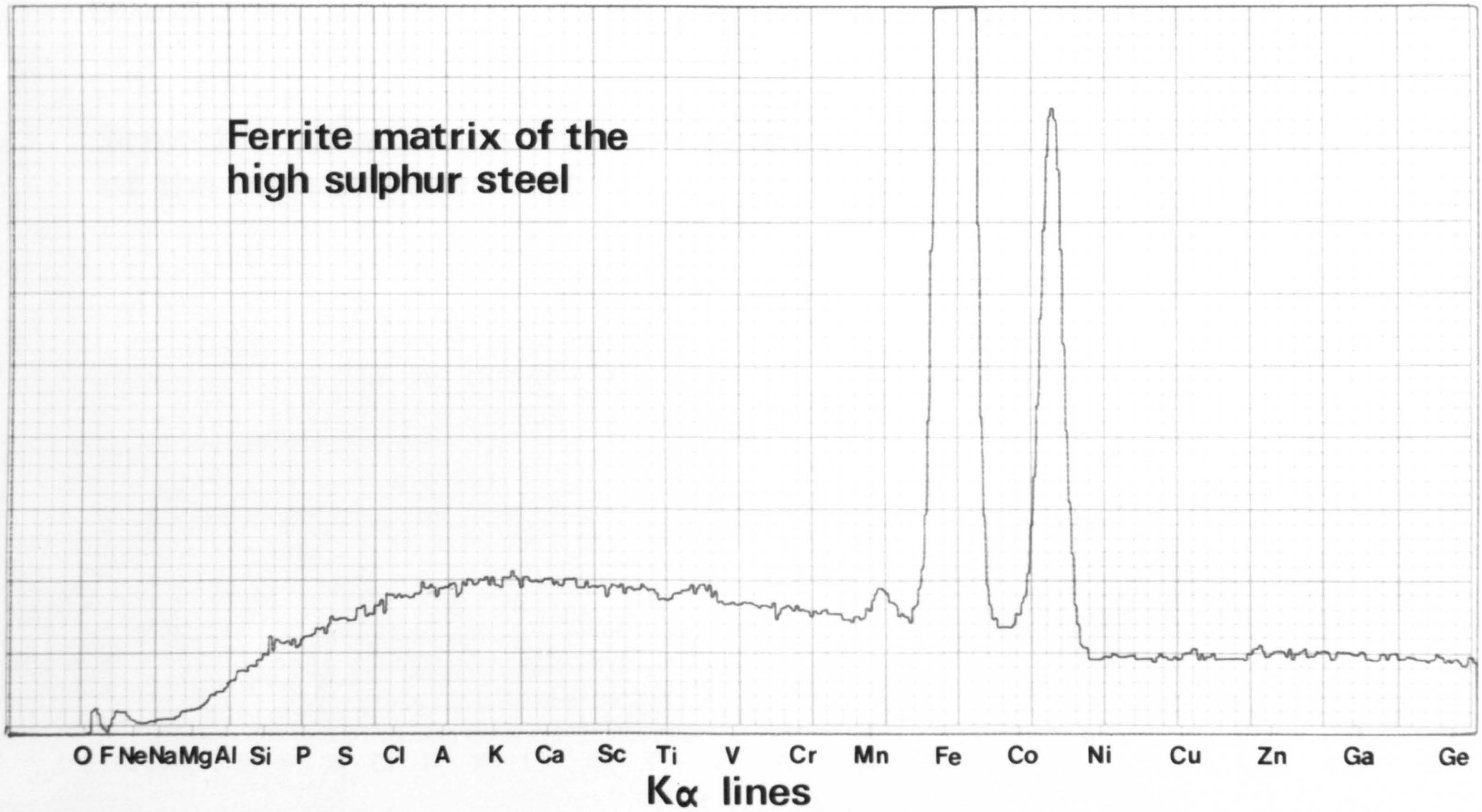
Ferrite matrix of the
high sulphur steel
O F Ne Na Mg Al Si P S Cl A K Ca Sc Ti V Cr Mn Fe Co Ni Cu Zn Ga Ge
Kα lines

Fig. 7•42

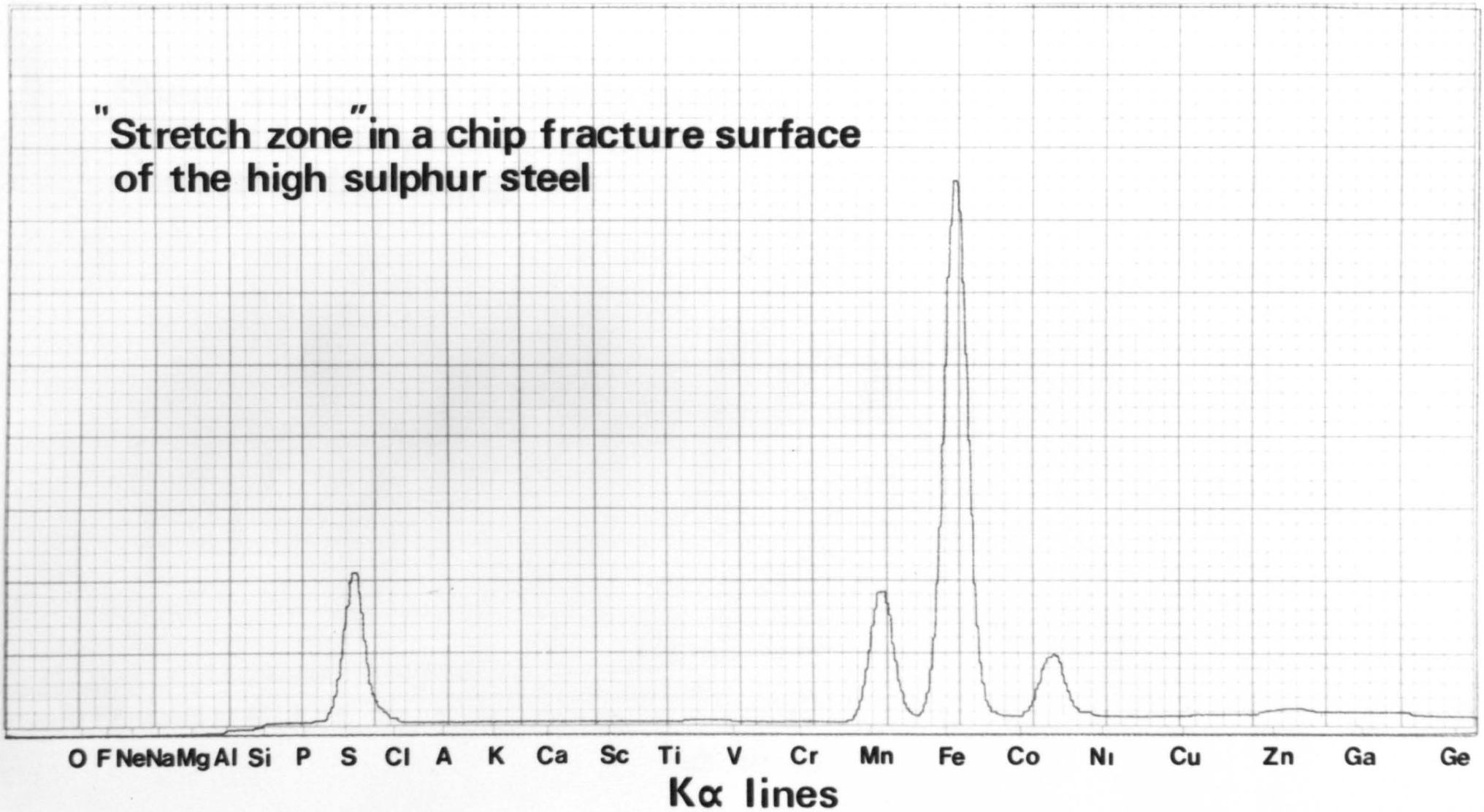
"Stretch zone" in a chip fracture surface
of the high sulphur steel
O F Ne Na Mg Al Si P S Cl A K Ca Sc Ti V Cr Mn Fe Co Ni Cu Zn Ga Ge
Kα lines

Fig. 7•43

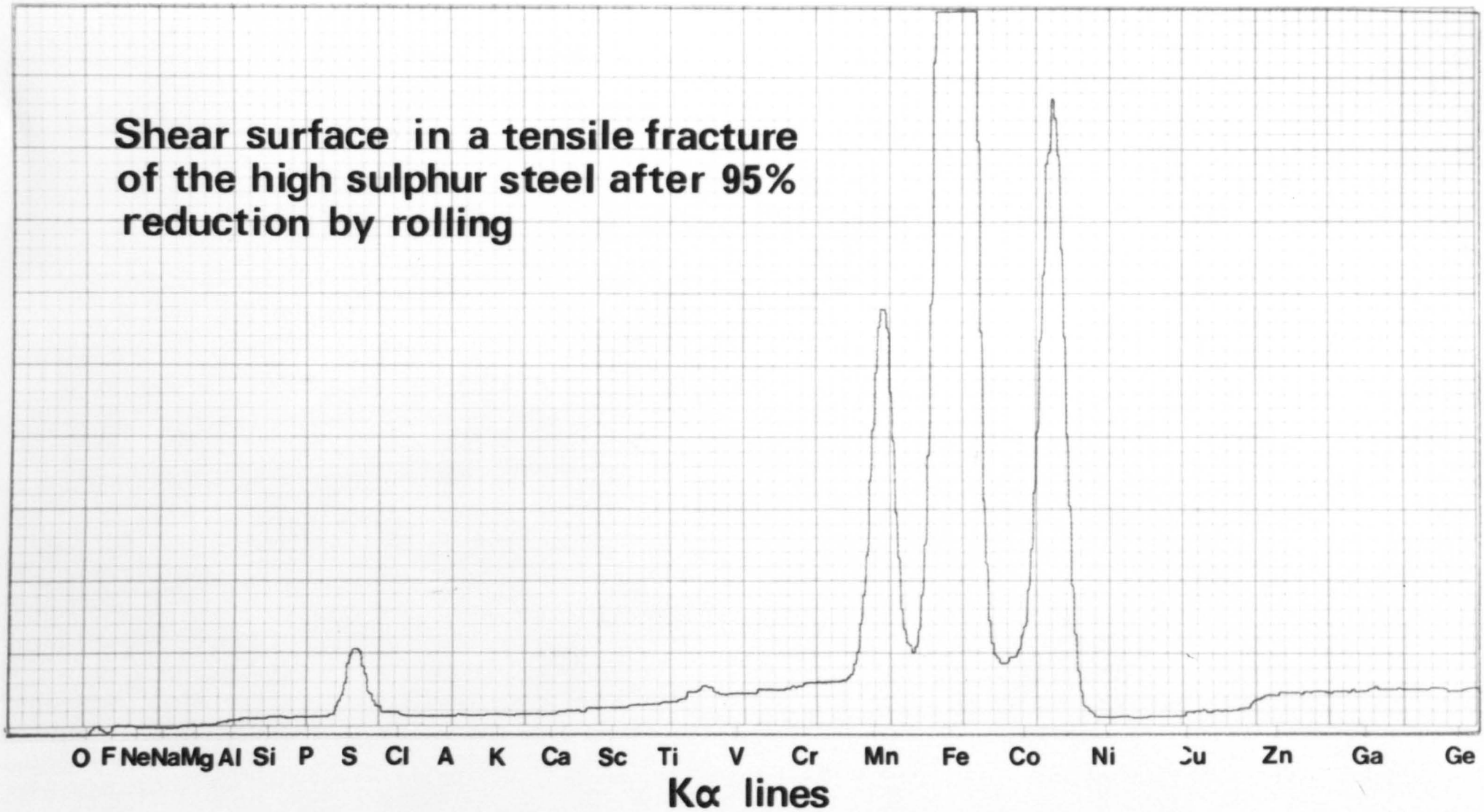
Shear surface in a tensile fracture of the high sulphur steel after 95% reduction by rolling
O F Ne Na Mg Al Si P S Cl A K Ca Sc Ti V Cr Mn Fe Co Ni Cu Zn Ga Ge
Kα lines

Fig. 7•44

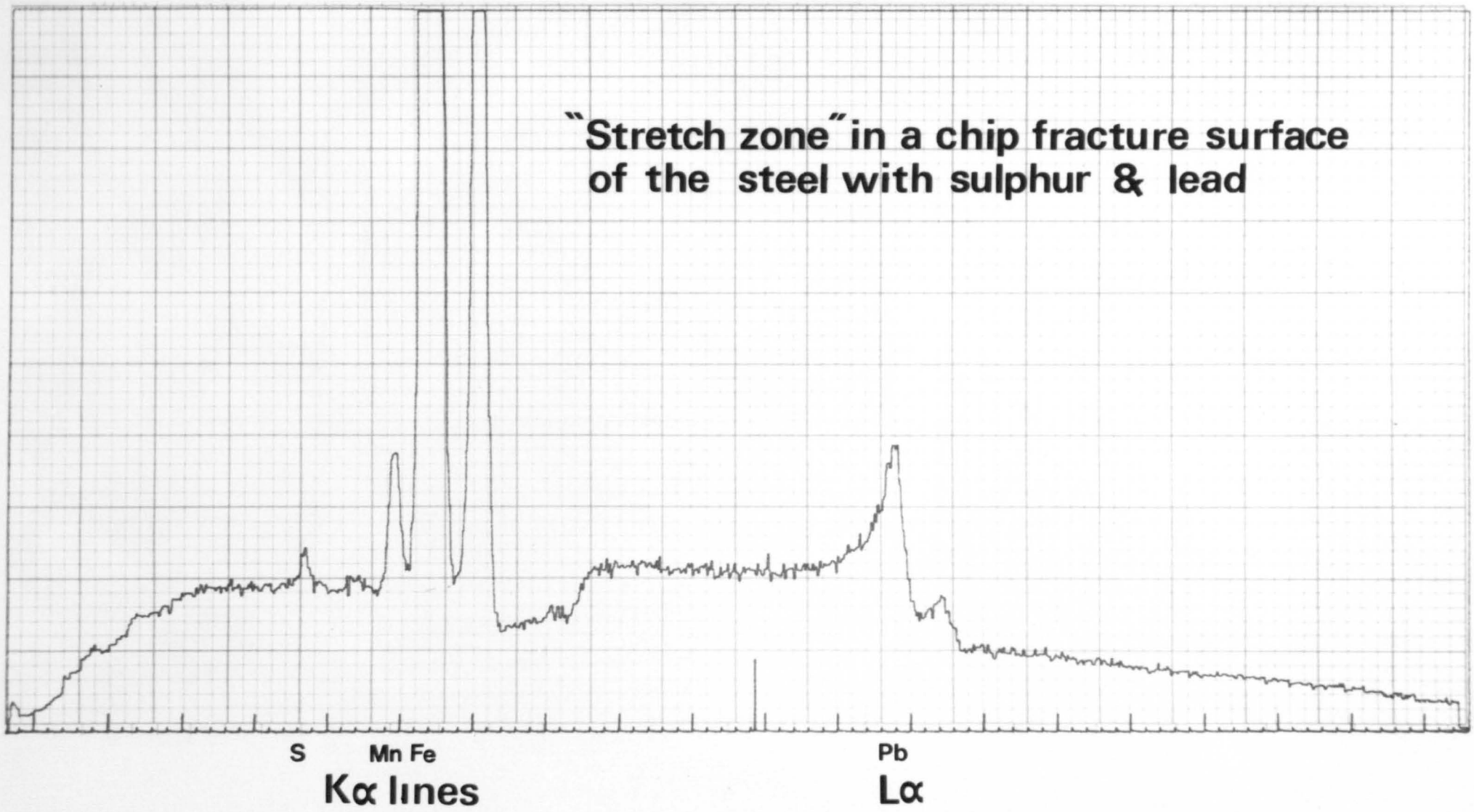
"Stretch zone" in a chip fracture surface
of the steel with sulphur & lead
S
Mn Fe
Kα lines
Pb
Lα

Fig. 7•45

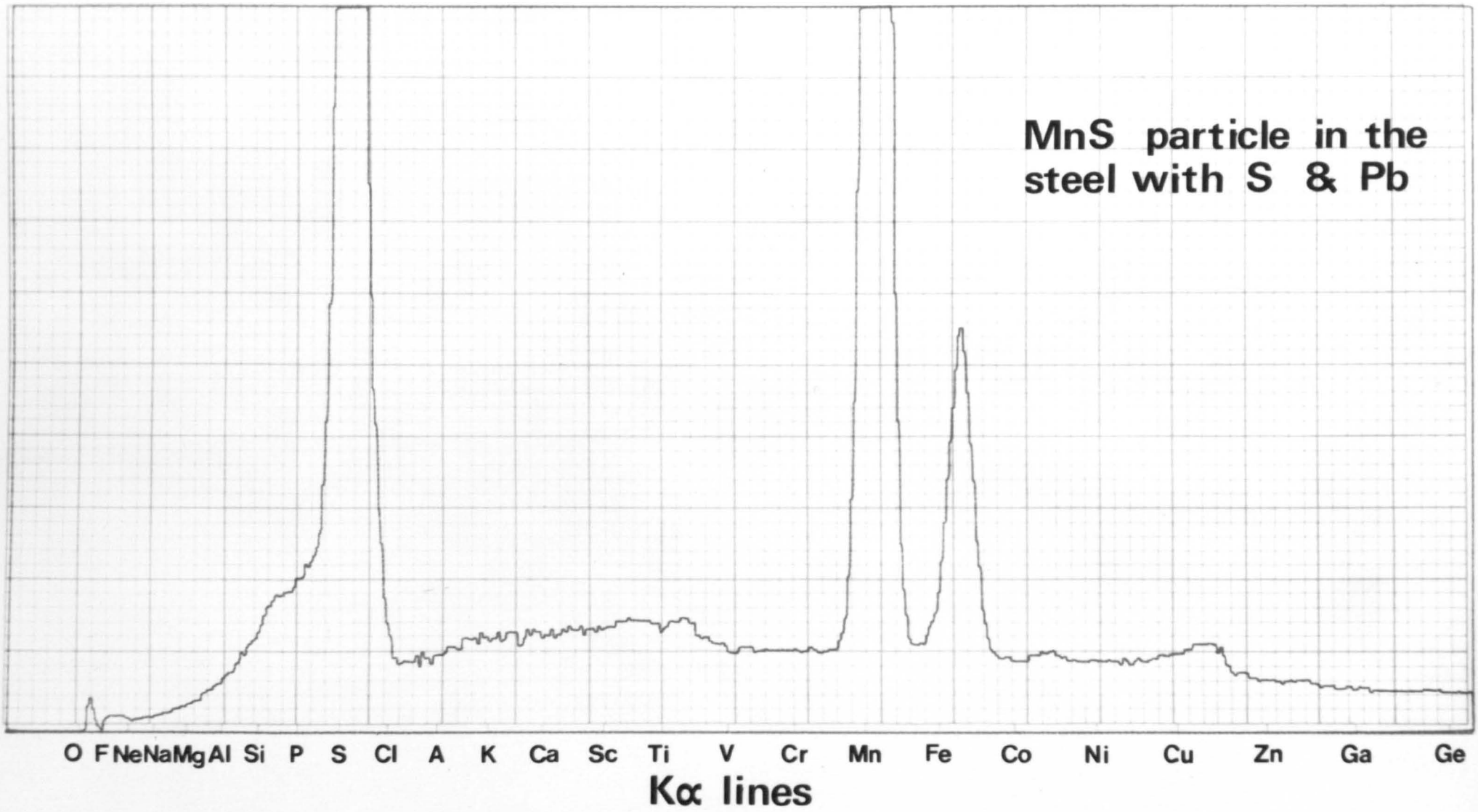
MnS particle in the steel with S & Pb
O F Ne Na Mg Al Si P S Cl A K Ca Sc Ti V Cr Mn Fe Co Ni Cu Zn Ga Ge
Kα lines

Fig. 7•46

FIGURE 8.1

Schematic view of the normal explanation of the formation of 'elongated dimples' on a shear fracture surface.

(After Backofen(262))

FIGURE 8.2

Diagram showing the difference between the central region of a cup cone fracture and the sloping shear regions, in the quenched and tempered steel tested in tension after moderate rolling strains. A central void extending in the direction of the arrow by rupture of cavity walls, suffers a change of direction when the deformation becomes concentrated into shear planes and appears to step longitudinally along the cavities.

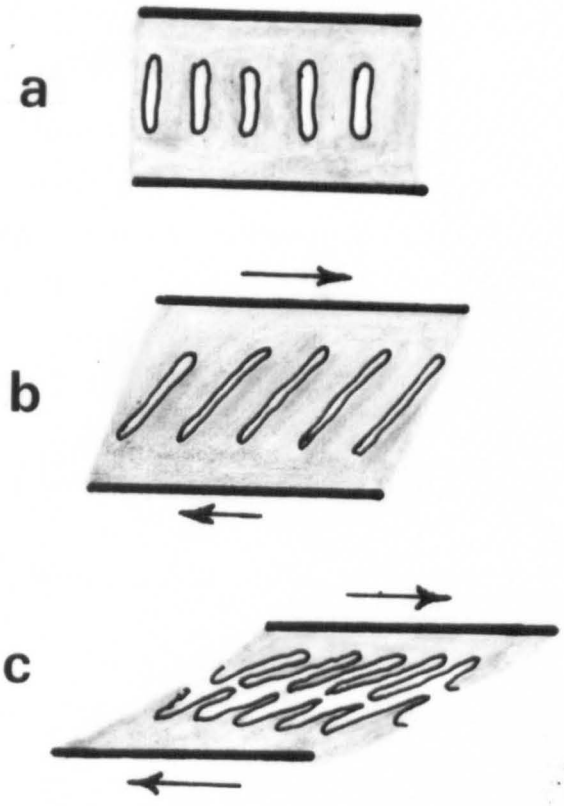

Figure 8•1

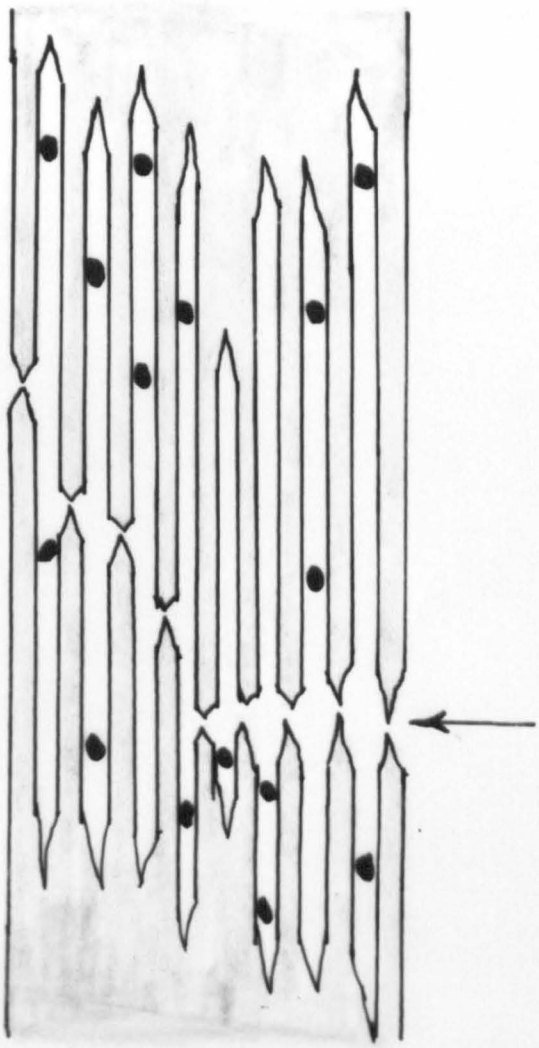

Figure 8•2

FIGURE 8.3

The double cup mechanism of failure in the quenched and tempered steel tested after rolling strains of 60-80% reduction, which shows the opening up of a central void. Before this extends very far laterally, the fracture breaks out in a 45° shear plane. The central void surface and the shear surface both show the same deep cavities as the earlier fractures.

FIGURE 8.4

In the above steel after rolling strains above 80% reduction, one or more large cracks form in the rolling plane by the coalescence of sheets of cavities. Final fracture is by shear through the remaining material in a 45° plane. The shear surface exhibits the same deep cavities as the earlier fractures and has the same stepped appearance.

Figure 8•3

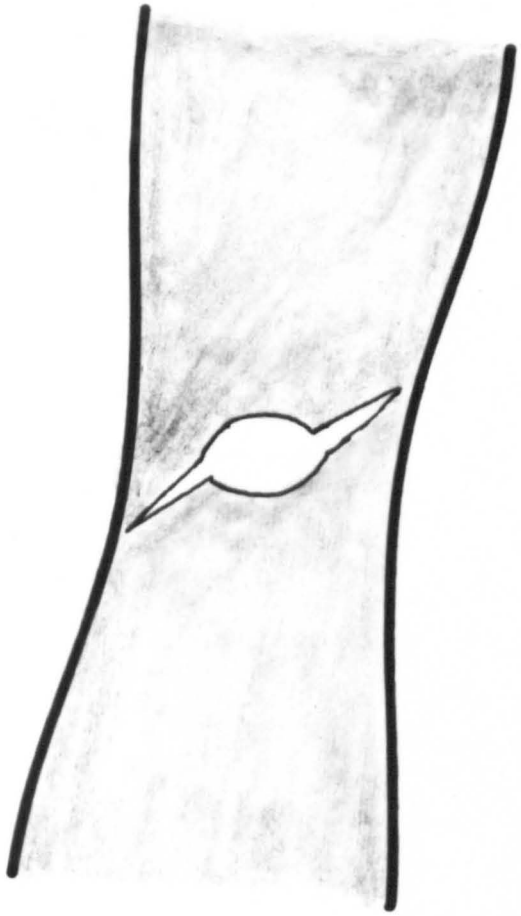

Figure 8•4

FIGURE 8.5

The variation with strain of the fractional change in surface area of a cubic grain which is deformed at constant volume.

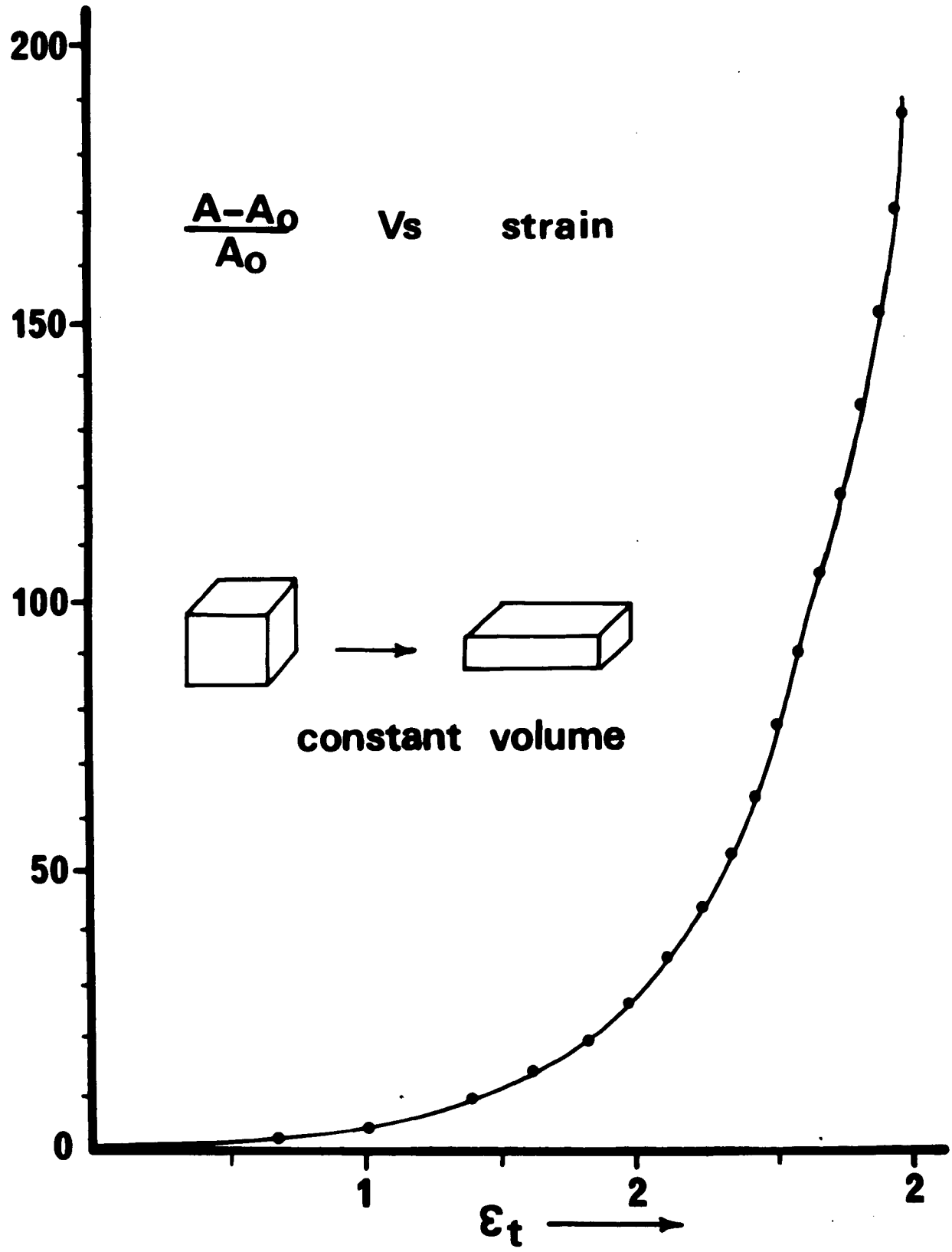
200
150
100
50
0
$\frac{A-A_o}{A_o}$ Vs strain
constant volume
1
2
2
ε_t

FIGURE 8.6

Possible mechanism by which the microbands can rotate into the rolling plane.

a/ A graded glide mechanism of an array of edge dislocations.

b/ A representation of the way in which the rotation may be forced on the bands by the nature of the rolling process.

Fig. 8•6 a

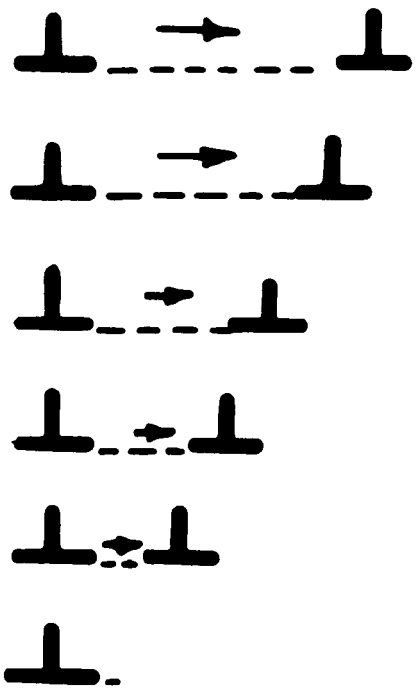

Fig. 8•6 b